NASA Contractor Report 182177

The Advanced Heat Receiver Conceptual Design Study

FINAL REPORT

James B. Kesseli
Roger I. Saunders
Gary Batchelder
Sanders Associates
Nashua, NH

October 1988

Prepared for
Lewis Research Center
Contract NAS3-24858

National Aeronautics and
Space Administration

NASA Contractor Report 182177

The Advanced Heat Receiver Conceptual Design Study

FINAL REPORT

James B. Kesseli
Roger I. Saunders
Gary Batchelder
Sanders Associates
Nashua, NH

October 1988

Prepared for
Lewis Research Center
Contract NAS3-24858

National Aeronautics and
Space Administration

NASA
National Aeronautics and Space Administration

Report Documentation Page

1. Report No.	2. Government Accession No.	3. Recipient's Catalog No.
NASA CR 182177		

4. Title and Subtitle

Advanced Heat Receiver Conceptual Design Study

5. Report Date

7/31/88

6. Performing Organization Code

7. Author(s)

James Kesseli, Roger Saunders, Gary Batchelder

8. Performing Organization Report No.

10. Work Unit No.

9. Performing Organization Name and Address

Sanders Associates
95 Canal Street
Nashua, NH 03060

11. Contract or Grant No.

NAS 3-24858

13. Type of Report and Period Covered

Final 5/86 - 7/88

12. Sponsoring Agency Name and Address

National Aeronautics and Space Administration
Lewis Research Center
Clevelend, Ohio 44135

14. Sponsoring Agency Code

15. Supplementary Notes

Project Manager: Dovie E. Lacy, Solar Dynamics and Thermal Management Branch, NASA Lewis Research Center

16. Abstract

Solar Dynamic space power systems are candidate electrical power generating systems for future NASA missions. One of the key components of the solar dynamic power system is the solar receiver/thermal energy storage (TES) sub-system. Receiver development was conducted by NASA in the late 1960's and since then a very limited amount of work has been done in this area. Consequently the state of the art (SOA) receivers designed for the IOC space station are large and massive. The objective of the Advanced Heat Receiver Conceptual Design Study is to conceive of, and analyze advanced high temperature solar dynamic Brayton and Stirling receivers. The goal is to generate innovative receiver concepts that are half of the mass, smaller, and more efficient than the SOA. It is also necessary that these innovative receivers offer ease of manufacturing, less structural complexity and fewer thermal stress problems. Advanced Brayton and Stirling receiver storage units are proposed and analyzed in this study which can potentially meet these goals.

17. Key Words (Suggested by Author(s))	18. Distribution Statement
Space Auxilary Power Solar Dynamics Solar Heat Storage Brayton Stirling Receiver	Unclassified - Unlimited

19. Security Classif. (of this report)	20. Security Classif. (of this page)	21. No of pages	22. Price*
Unclassified	Unclassified		

NASA FORM 1626 OCT 86

*For sale by the National Technical Information Service, Springfield, Virginia 22161

TABLE OF CONTENTS

LIST OF ILLUSTRATIONS

LIST OF TABLES

APPENDICES

REFERENCES

1. Wallin, W.E., Dustin, M.O., "Advanced Space Solar Dynamic Power Systems Beyond IOC Space Station", Proc. 22rd IECEC, 8/1987.

2. Mendelson, I., "Design and Fabrication of Brayton Cycle Solar Heat Receiver: Final Report," NASA contract NAS 3-10944, July 1971.

3. Cameron, H.M., Mueller, L.A., Namkoong, D., "Preliminary Design of a Solar Heat Receiver for Brayton-Cycle Space Power System," NASA TM X-2552, 1972.

4. Klann, J.L., Staiger, P.J., "Design Tradeoffs for a Space Station Solar-Brayton Power System", NASA PIR no. 106, 1985.

5. Kesseli, J., "Matrix Solar Receiver Research at Sanders," Proceedings of the IEA/SSPS Conference at Sandia National Labs, March 1987.

6. Solar Dynamic Heat Receiver Technology Monthly Progress Reports, Boeing Aerospace Co., Reports 1-6, 1986.

7. Zimmerman, W.F., "Heat Pipe Solar Receiver With Thermal Energy Storage", in Parabolic Dish Solar Thermal Power Annual Program Review Proceedings, DoE Report No. DoE/JPL 1060-46, May 1981.

8. Coombs, M.G. and Strumpf, H.J. Advanced Heat Receiver Conceptual Design Study Garrett AiResearch, 1987.

9. Wichner, R.P., Solomon, A.D., Drake, J.B., Williams, P.T., "Thermal Analysis of Heat Storage Canisters for a Solar Dynamic Space Power System", Martin-Marietta, NASA C-30001-J, 1988.

10. Dustin, M.D., Savino, J.M., Lacy, D.E., Migra, R.P., Juhasz, A.J., Coles, C.E., "Advanced Solar Dynamic Space Power Systems Perspective, Requirements and Technology Needs. NASA Tech Memorandum 88884, 3/87.

1.0 INTRODUCTION

An objective of NASA's Office of Astronautics and Space Technology (OAST) is to develop smaller, lighter solar dynamic space power systems. The solar dynamic power system consists of a large parabolic concentrator which focuses solar power into a receiver which supplies heat to an engine. System studies performed by NASA Lewis reveal that the receiver/thermal storage unit (RSU) is the most massive component of the conservatively designed Initial Operational Capability (IOC) Space Station solar dynamic power systems. Also, unless smaller, lighter power systems are developed, system projections for future technology (Ref. 1) indicate that the RSU will contribute to an even larger percentage of the total mass of future solar dynamic systems.

The program which led to this report was called The Advanced Heat Receiver Conceptual Design Study. The objective of this program was to develop new and advanced receiver storage unit (RSU) concepts which have the potential to provide significant improvements over the Baseline RSU IOC design. Brayton and Stirling engines are candidates for advanced solar dynamic systems. In this report we will present a novel and promising conceptual receiver design for each of these engine cycles. Both designs meet or exceed the following program goals specified by the NASA Lewis Research Center. These designs are scaled within the 1.5 kWe to 35 kWe range with our design point at 7 kWe.

Key challenges associated with this technology are summarized as follows:

- Achieve a 50% mass reduction over the Baseline concept
- Minimize volume
- Increase reliability and operational lifetime
- Minimize fabrication complexity
- Maximize efficiency

To measure our progress towards these goals, we establish a point of reference as the space station Brayton RSU. Sanders proposes RSU designs with masses less than half that of the Baseline, efficiencies greater than the Baseline, and a ten year operational lifetime. The Baseline Space Station heat receiver and Sanders Advanced Receivers are described in Sections 2 and 4 respectively.

The final phase of this program (Task IV) was designed to address the critical technology issues which arose during the design of the two RSU's. This work, primarily presented in Section 5, produced an experimental plan which is intended to address and resolve the critical technical issues associated with both the Stirling Advanced Cavity Heat Pipe (CHP) and Brayton Advanced Direct Absorption Receiver (DAR) designs.

1.1 OPERATIONAL CONCEPT

The receiver accepts focused solar energy from a parabolic concentrator and provides a zone where the Brayton or Stirling engine working fluid is heated. The engine then thermodynamically converts the thermal energy to shaft power, and a permanent magnet alternator converts the power to electricity to meet satellite demands.

The particular space application defined for this program is a low earth orbital system. Since the equatorial orbit, referred to as the "Space Station" orbit, is at a nominal altitude of 494 Km, the solar cycle has a day of nominally 56 minutes and a night eclipse of about 34 minutes. The RSU must store enough thermal energy to power the space platform for the night eclipse.

The proposed Sanders RSU design stores this energy in the latent heat of fusion of alkali metal - fluoride phase change materials. The Brayton receiver utilizes lithium fluoride (LiF) while the Stirling receiver stores energy in an eutectic mixture of lithium fluoride and calcium fluoride (79 LiF - 21 CaF_2). In concept, the phase change material (PCM) medium becomes predominantly liquefied at the end of the solar charge period and solidifies as energy is extracted during the night period.

Alkali metal - fluoride latent heat storage has positive and negative aspects which strongly influence the design concept. Of all materials which melt at a temperature appropriate for the Brayton cycle, LiF has the highest latent heat of fusion. Other key advantages of LiF unique exploited by the Sanders Brayton design are high surface tension and high optical transmissivity in the solar spectrum. As for the Stirling, the mixture has a melting point consistent with the state-of-the art heater head technology and a high heat of fusion relative to other candidates in its temperature range. The disadvantages of these PCMs are their high volumetric change upon phase change (DV/V), low thermal conductivity, and high reactivity.

In this program a substantial effort was directed towards defining and understanding the current state-of-the-art in solar dynamic power systems, which we refer to as the Baseline technology. The Baseline space solar dynamics technology (Ref. 2) results from NASA/General Electric (GE) programs during the 1960's and early 1970's. A similar version of these earlier designs is presently under development by Garret AiResearch Co. for the IOC space station Brayton RSU.

The Brayton Direct Absorption Receiver (DAR) achieves the advancements that NASA seeks by incorporating two features not considered in the Baseline or other RSU designs. First, the micro-gravity environment and the high LiF surface tension enhance liquid control, allowing the heat exchanger corrugations in the RSU cavity to control and contain the liquid LiF. Secondly, by direct solar irradiation of the PCM through a windowed cavity it takes advantage of the sun's spectral content to obtain a parallel conductive and radiated energy transport through the LiF. The detailed description of this design is presented in Section 4.1.

The Advanced Stirling Cavity Heat Pipe (CHP) Receiver utilizes a single sodium heat pipe to couple the solar absorber with the PCM and engine heater head heat exchangers. Also, as a basis for our design work, we devoted a high priority to the engine integration issues. The versatile and high power density characteristics of a single-cavity type heat pipe and the ultra-high flux tolerance of an evaporative surface minimize the solar cavity dimensions. The high transport capacity of condensing sodium vapor provides the

ultimate in heat exchanger geometry flexibility necessary to satisfy the demanding requirements of the heater head and the thermal energy storage unit. A detailed description of this RSU design is presented in Section 4.4.

2.0 BASELINE HEAT RECEIVER OVERVIEW (TASK I)

In this section we discuss the baseline NASA Brayton RSU, and analyze the problems inherent in the design such as:

- o low solar flux tolerance which increases mass and size
- o PCM void formation which decreases RSU efficiency
- o thermal ratcheting which degrades system reliability

Following the Brayton history, the state-of-the art in Stirling receivers will then be presented.

2.1 BASELINE BRAYTON RSU DESIGNS FOR LOW EARTH ORBIT

GE conducted a substantial design effort followed by component testing of a Brayton receiver for NASA in the 1960's (Ref. 2,3,4). This technology, in principle, is still the standard for today's space station designs. The concept involves storing LiF in the annular envelope between an internal gas tube and the exterior solar absorber wall. The five schemes illustrated in Figure 2.1 were proposed in the early NASA programs. In the originally selected NASA/GE design, (Figure 2.1a), these tubes are arranged to form a conical solar cavity with torroidal gas manifolds at both ends of the cone. Recent space station designs have employed concepts illustrated in Figures 2.1a and 2.1b.

The specific masses of these RSU designs are in the 66 to 78 Kg/KWe range. When examining the contributors to these relatively high masses, it can be seen that only a small percentage (12-16%) of the mass is attributable to the PCM storage media. Rather, it is the PCM containment vessels, structure, gas piping, manifolding and insulated exterior housing that contribute to most of the receiver weight.

The size of the receiver cavity is dictated by matching the incident solar flux to the maximum allowable heating rate of the PCM. This maximum allowable flux influences the overall system weight in that a low flux tolerance results in a larger receiver. Efficiency is also affected by the flux tolerance, since large cavities imply large overall housings which radiate more energy to the environment. Therefore, a principle objective of this program is to develop methods to increase the tolerable peak flux within the receiver.

In the Baseline receiver, since the solar power must conduct through a layer of low thermal conductivity PCM as well as two or three containment walls, flux tolerance is about a factor of 20 lower than Sanders terrestrial Brayton receiver designs (Ref. 5). This high thermal impedance is further worsened by a distribution of voids within the PCM totaling as much as 30% (for LiF) of the envelope volume. These voids form as a result of the increase in PCM density upon solidification.

In a confined PCM container of the Baseline type, in micro-gravity, the interfacial surface energies (surface tension) of the system drive the liquid migration which causes contraction voids. A design that eliminates these voids, or at least their thermal impedance, is critical to meeting all three of NASA's goals. To understand this phenomenon, first consider the state where the PCM is fully charged at sundown. In this condition, the molten medium will occupy the maximum volume within its container. Figure 2.2 illustrates this condition for one of the several possible configurations presented in Figure 2.1. As energy is

Baseline Solar Dynamic Receivers have a Common Theme–

and a Common Set of Problems

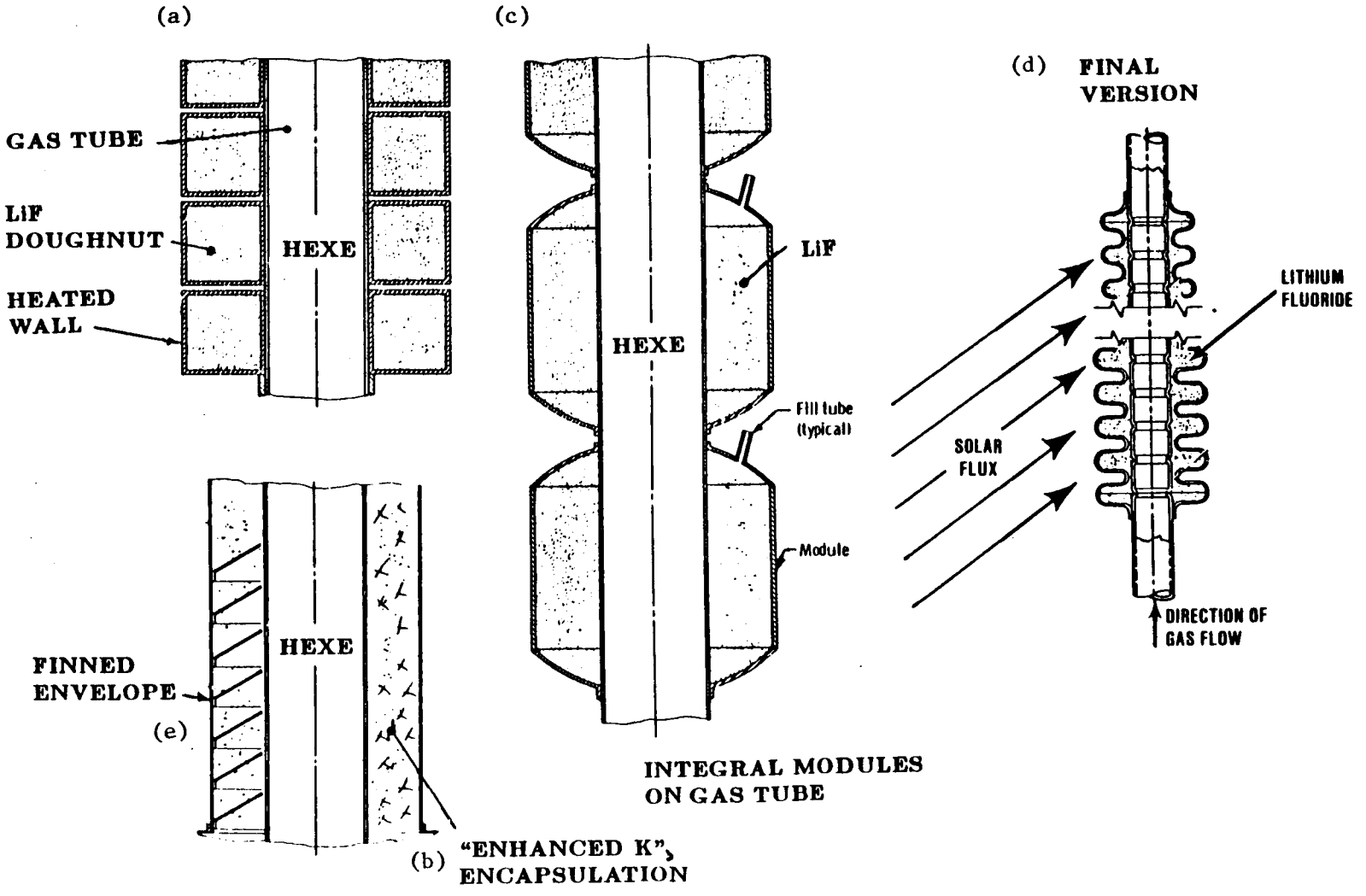

Figure 2.1 Five Integrated Gas Tube/Storage Module Schemes

From Early NASA Programs

ΔV/V Characteristics of PCM in μ G is a Key Problem which Limits Size and Efficiency of the Baseline Design

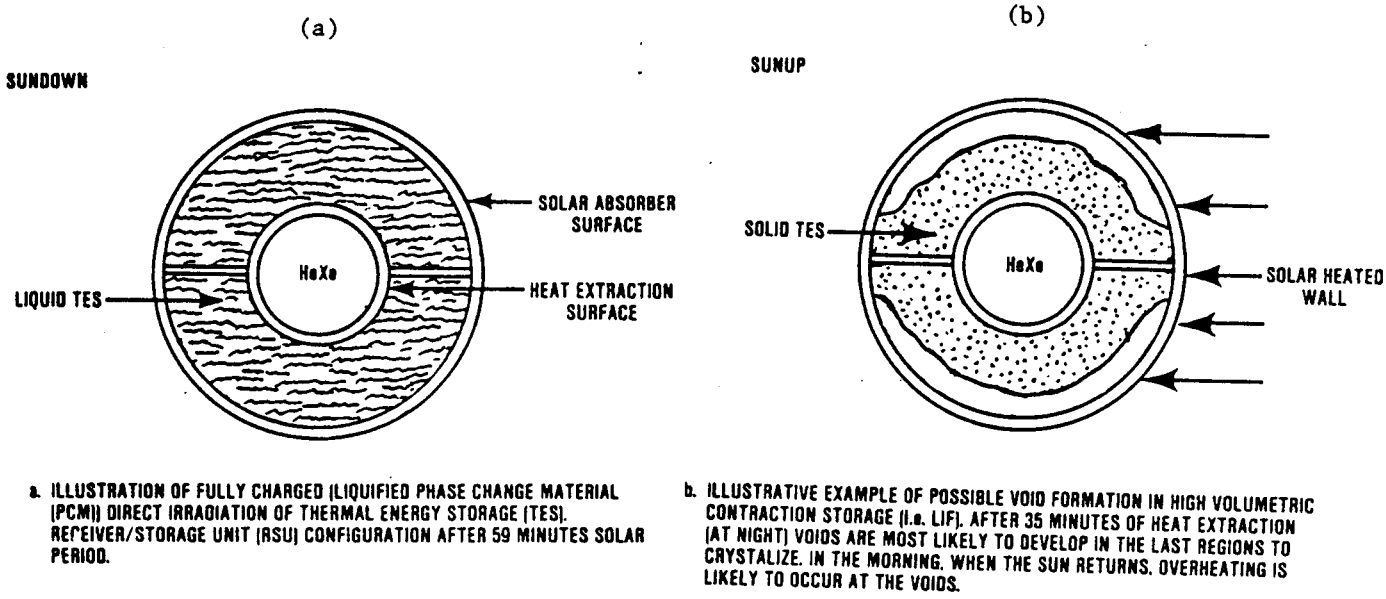

a. ILLUSTRATION OF FULLY CHARGED (LIQUIFIED PHASE CHANGE MATERIAL (PCM)) DIRECT IRRADIATION OF THERMAL ENERGY STORAGE (TES). RECEIVER/STORAGE UNIT (RSU) CONFIGURATION AFTER 59 MINUTES SOLAR PERIOD.

b. ILLUSTRATIVE EXAMPLE OF POSSIBLE VOID FORMATION IN HIGH VOLUMETRIC CONTRACTION STORAGE (i.e. LiF). AFTER 35 MINUTES OF HEAT EXTRACTION (AT NIGHT) VOIDS ARE MOST LIKELY TO DEVELOP IN THE LAST REGIONS TO CRYSTALIZE. IN THE MORNING, WHEN THE SUN RETURNS, OVERHEATING IS LIKELY TO OCCUR AT THE VOIDS.

Very low Solar Flux Tolerance Due to Impedance of the Void and Low Thermal Conductivity

Figure 2.2

transferred from the molten PCM through the gas tube wall at night, a layer of crust (solid) forms on the gas tube wall. During this period of heat extraction, the crystallizing front propagates outward from the gas tube and to a lesser extent, the fins. Energy extraction from the storage medium is, therefore, accompanied by the creation of a void within the vessel adjacent to the outer PCM container wall. Because the surface energy of the crystal is higher than the liquid-vapor surface tension, the residual liquid will "wet" the solid interface. The liquid will also wet the metal container, making the prediction of the exact void location very difficult. In a near zero gravity condition, however, the residual liquid will not migrate to the "bottom" of the container to fill in the voids as it would in Earth-based testing.

In the Baseline design, a portion of the exterior PCM containment wall serves as the solar absorber. If indeed the freezing process occurs in the manner described above, a substantial contraction void will develop behind the solar absorber surface. With the PCM frozen in this position, as indicated in Figure 2.2b, solar energy incident on the absorber would not be conductively coupled to the storage medium. In this condition, the dominant mechanism for energy exchange between the absorber wall and the PCM is radiation. Therefore, excessive absorber wall temperatures are expected in these regions throughout most of the solar period.

More realistically, for this case, one should expect a small layer of the PCM to freeze on the inner wall of the absorber because of the cavity radiation losses at night. This layer would then be heated to temperatures significantly above its melting point. This condition was analyzed for the 1960's GE configuration and on our current NASA program and was shown to yield peak wall temperatures of 1480^{0}K. Oak Ridge National Labs conducted a more thorough analysis which indicated that the containment wall of the space station RSU would reach peak temperatures in the 1250 degree K range for a LiF system. In either case, such a condition will lead to accelerated corrosion rates, excessive thermal stresses, and poor thermal efficiency.

The issues of verification through Earth-based (1-g) testing adds to the controversy of this subject. It can be argued that test data from simulated operation of the GE receiver did not show such elevated temperatures, thus disproving this hypothesis. However, in an Earth environment, the gravitational effects from the orientation of the assembly will dominate the surface tension effects. In the NASA/GE experiment, the gravitational influence on the liquid caused it to flow into voids on the absorber wall. For this reason, we do not believe that the test results present an accurate representation of the space operating environment.

It is generally believed that the NASA/GE receiver test exhibited the condition of thermal ratcheting as a result of gravity-induced longitudinal liquid redistribution. Thermal ratcheting is a cyclic process where the expanding liquid is bound on all sides by the container wall and a displacement-resisting section of solid PCM. The modification to this concept adopted for the IOC space station minimized the stress severity by confining the PCM in rugged torroidal containers around the central gas tube (Figure 2.1a). This longitudinal partitioning greatly reduces the force applied by the expanding PCM to the container walls. However, since the thermal impedance of the voids is not affected, little is gained in terms of increasing the solar flux tolerance. Therefore, this approach is at least as large and is likely to be heavier (due to the added container mass) than the original NASA/GE baseline.

To mitigate the effects of PCM void formation, the use of metal fins or felt metal as illustrated in Figures 2.1b and 2.1e can be considered. Although fins provide discrete higher conductivity connections between

the absorber surface and the gas tube, voids still occur between the fins. Moreover, it is likely that such discontinuities in the absorber surface temperature profile during the solar period will aggravate the thermal stress problems. Thermally induced fatigue stresses in the fin area are also likely since the fin may expand upon heating more than the container wall. Finally, in the illustrated configuration, the high aspect ratio fins are not sufficient to appreciably raise the flux tolerance of the envelope. The high fin density required would significantly increase weight and PCM container volume.

High porosity metal felt or foams immersed in the PCM can be considered as a limiting case for the internal finning approach. This mesh passively controls the migration of the liquid PCM with surface tension (capillary) forces. Typically, designers have recommended 18 to 30% of the mesh by volume (Ref. 6) which adds weight to an already heavy system. Also, due to the large surface area of the fibers, corrosion is much more of an issue. This, and wire fatigue due to the cyclic movement of the expanding/contracting salt, are distinct limitations.

The issue of conductivity enhancement also remains to be experimentally verified. Since, upon freezing, the solid/mesh matrix must also contain a distribution of pore size voids which accounts for 30% of the volume of the envelope (with LiF), the bulk conductivity of the system is in question. These voids, acting as they would for example in urethane foam, would serve to form a series of insulating barriers. In addition, the conductive path length between the solar absorption surface and the gas tube must be increased to accommodate the additional volume of the mesh.

Despite the potentially higher bulk conductivity of the liquid phase, we do not see a significant potential for an increase in the flux tolerance exhibited within the cavity using this approach because the power for engine operation must always be conducted through this low conductivity solid during both heat addition and extraction periods.

2.2 BASELINE STIRLING RECEIVER TECHNOLOGY

Baseline technology involving solar activated Stirling engines has centered primarily around the DoE and the Air Force Wright Aeronautics Laboratories (AFWAL) sponsored terrestrial systems of the late 1970's. This technology has evolved from the original concepts of directly irradiating a bundle of tubes containing the engine working fluid, to multiple linear heat pipe cavities, and most recently to the single cavity-type heat pipe. Illustrations of this evolutionary trend are presented in Figure 2.3. Each of these concepts was for a 20 to 25 kWe Dish-Electric Module. The following paragraphs will briefly describe some of the issues associated with the past and present receiver designs.

2.2.1 ADVANCO/USS TERRESTRIAL STIRLING RECEIVER

Three receiver test programs have been conducted with the United Stirling 20 kWe 4-95 engine (Figure 2.3a). These receivers use an array of U-tubes to form the receiver cavity absorber connecting the regenerator and displacer manifolds. Full scale testing was plagued with numerous tube failures. Solar flux non-uniformities or so-called hot spots within the compact cavity yielded excessive local temperature and stresses. The complexities associated with simultaneously satisfying performance and stress/life criteria of the tube bundle have proved to be unmanageable. The joint conclusion of the DoE and their prime contractor responsible for the testing, Advanco, was that this concept could not meet the necessary life cycle cost goals of the solar program.

ORIGINAL PAGE IS
OF POOR QUALITY

(a) UNITED STIRLING ESOR-IIB HEATER HEAD

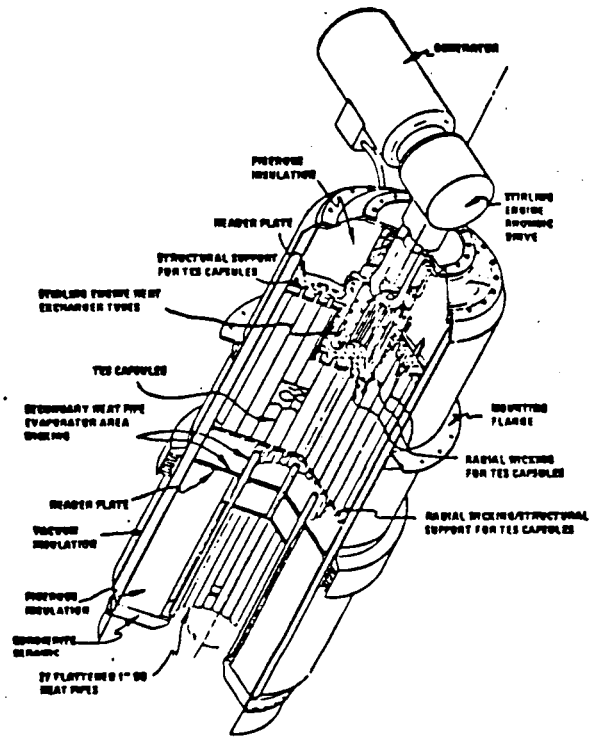

(b) JPL/GE STIRLING RECEIVER CONCEPT

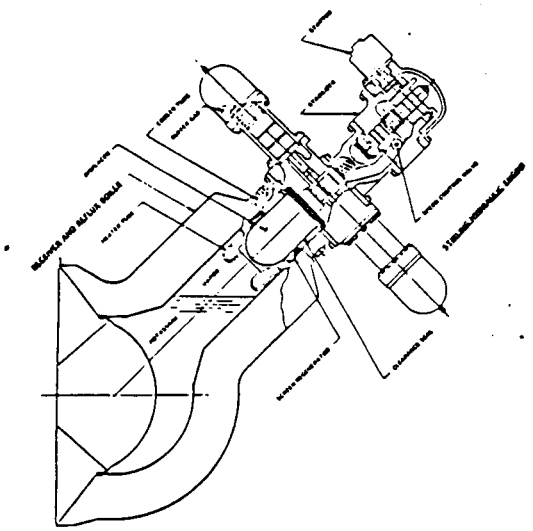

(d) STC/SANDERS/SAASKI ASSOCIATES
REFLUX POOL BOILER SOLAR RECEIVER

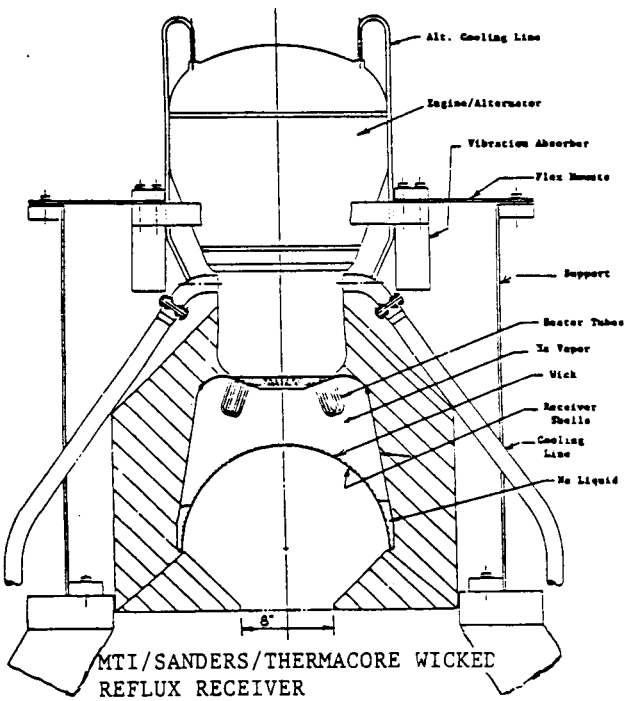

MTI/SANDERS/THERMACORE WICKED
REFLUX RECEIVER
(c)

Figure 2.3. Evolutionary Trends in Terrestrial Stirling Receivers

In the same time frame as this work, two other Stirling related design programs looked at the use of heat pipes for the solar receiver applications. The Jet Propulsion Laboratory (JPL) sponsored through GE (Ref. 7) the design of a 20 kWe receiver for a kinematic Stirling engine in the late 1970's. AFWAL, while also supporting some of the United Stirling research discussed previously, has a long standing interest in solar activated Vuilleumier (Vm) cycle cryocoolers. Both of these systems also incorporated PCM thermal storage. The Vm and JPL receivers are described in the following section.

2.2.2 AFWAL VM RSU

In that 1970's, AFWAL sponsored the development of an RSU for their Vm cryocooler. This work is pertinent to this program because their design embodied many of the features of Sanders' CHP. The Vm cryocooler is essentially a Stirling cycle wherein the mechanically driven compressor has been replaced by a thermal compressor section. Only a small amount of electromechanical input is required to shuttle the two displacers back and forth. The design of the heat addition section therefore resembles that of an annular Free Piston Stirling Engine (FPSE). Although the thermal input, less than 2 kWt, is well below this program's requirements, many of the design issues are similar. An integrated thermal storage module was encapsulated within the small heat pipe chamber.

This solar activated system utilized a single heat pipe to form the receiver cavity much like the CHP concept. Because of the size of the cryocooler assembly relative to the concentrator, it was necessary to locate it outside the aperture region of the concentrator. A single long heat pipe transports the received solar power from the focal plane to the cryocooler assembly. The secondary heat pipe encloses nine wicked canisters of LiF for storage and contacts the heated cylinder space. The design accomplished CHP features such as the flux levelization within the cavity while striving to minimize the fabrication complexities.

2.2.3 JPL TERRESTRIAL HEAT PIPE RSU

The JPL terrestrial concept (Figure 2.3b) utilizes three separate groups of heat pipes. The cylindrical cavity is lined with an array of 27 one inch diameter tubular heat pipes. A pancake-type heat pipe forms the back of the cavity and acts to redistribute the solar flux non-uniformities transported by each of the primary heat pipes. These primary heat pipes and the pancake unit contact a single large secondary heat pipe. The secondary heat pipe, enclosing numerous wicked PCM containers, was designed to contact a tubular engine heater assembly. Although stress levels of this concept are likely to be much lower than those of the directly irradiated tube in the Avanco design, the fabrication cost and complexity were perceived to be prohibitive. Fabrication and testing of this unit were never initiated.

Figure 2.3b illustrates the relative size of this unit as compared to a kinematic engine. Also, one can see the numerous components which will compromise reliability. It is pertinent to note that the designers acknowledged the importance of homogenizing the solar flux non-uniformities within the cavity. However, the multiple staged heat pipe is not the most practical means for accomplishing this from weight and reliability standpoints.

2.2.4 DoE REFLUX BOILER RECEIVERS

A culmination of the DoE sponsored work is under way in the current development of a 25 kWe Free Piston Stirling Engine/Receiver module. Experts at the DoE have chosen a receiver concept which they

believe to have significant reliability, cost, and performance advantages over previous receivers. The two competing designs both utilize a single liquid metal evaporator surface within the receiver cavity. The concept developed for Mechanical Technology Inc.'s (MTI) engine utilizes a 20 inch diameter wicked evaporator dome. The competing approach for Stirling Technology Co.'s (STC) engine utilizes a similar diameter pool boiler. These designs are illustrated in Figure 2.3c and d.

A third DoE sponsored reflux boiler concept is presently under development for the Stirling Thermal Motor (STM) 25 kWe engine. This reflux boiler, designed as a fuel fired heater head interface, energizes the four separate heater heads of the four cylinder kinematic engine. Due to some early problems, this design is currently undergoing extensive rework. The DoE/Sandia National Labs - Albuquerque (SNLA) staff has provided most of the technical guidance for this effort. This design is gravity sensitive, but nevertheless illustrates the versatility of the two-phase boiler concept.

The DoE at SNLA must be considered as the technical leader in solar terrestrial receiver technology. They, and their contractors, have developed an acute awareness of the practical aspects of receiver designs through numerous field tests. They favor the cavity heat pipe concept because it can optimally accommodate the realistic conditions of a high flux, high temperature solar cavity while maintaining a fundamental simplicity. In the course of initial design and trade studies for the DoE under the MTI and STC subcontracts, multiple tubular heat pipe arrangements including that of the earlier GE concept, were considered in detail. The overwhelming result of these comparisons was that the cavity heat pipe was the only viable approach for meeting the stringent life, performance and cost goals.

3.0 ADVANCED HEAT RECEIVER CONCEPTS (TASK II)

The advancement of the heat receiver technology, requires that both an in depth knowledge of the current obstacles as well as the latitude to innovate. The objective of this programs Task II was to define the "Advanced" goals and generate a number of new concepts which can potentially meet them. In light of serious technological limitations of the Baseline concepts and the ambitious NASA goals, new ideas, not variations on current themes, are needed. In response to this need, four "Advanced" concepts for the Brayton and three for the Stirling cycle were generated. In the process of expanding solar dynamic receiver technology, theories not previously applied to the problem were considered.

This section opens with a review of NASA's goals and a discussion on how they impact the conceptual design process. The Baseline design and its limitations with respect to these goals is referenced. Both Brayton and Stirling goals and requirements are addressed. After the discussion on the Advanced goals, a description of the new concepts is presented for the first Brayton and then the Stirling. The presentation of these concepts is predominantly graphical. In the following sections, 4.0 and 5.0, the most promising Brayton and Stirling concepts selected for further evaluation are described in detail.

3.1 ADVANCED GOALS FOR BRAYTON AND STIRLING HEAT RECEIVERS

The following subsections provide a brief overview of the challenges inherent in advancing the state-of-the-art for the low earth orbit space environment. This section contains a definition of the four critical parameters by which competing RSU's must be evaluated. These are:

- Size (Mass and Volume)
- Performance (Thermodynamic efficiency)
- Reliability (Life and failure modes)
- Cost (Fabricability, complexity)

3.1.1 MASS AND VOLUME

NASA's system studies have projected that the RSU is the most massive component of the conservatively designed space station solar dynamic system. Mass is important because it affects the cost for transportation into space. Volume, generally correlated with mass, similarly affects cost by consuming valuable cargo space on the Space Shuttle.

Since the energy storage requirement dictates that all RSU designs have approximately the same PCM mass, reductions must occur in the balance of the RSU elements. Since only about 15% of the Baseline RSU mass is directly attributed to PCM ($LiF\text{-}CaF_2$) mass, it can be stated that RSUs are not inherently massive due to the energy storage requirement. Likewise, the PCM volume is extremely small (1-2%) relative to the RSU envelope.

The Baseline RSU is a cavity-type configuration according to DoE solar terminology, a hollow shell where concentrated solar power passes through an aperture and illuminates the relatively large interior cavity wall. The mass of the integral receiver storage unit is therefore predominantly located in the relatively thin annular volume between the concentric shells.

The interior cavity diameter is determined by the maximum tolerable solar flux on the absorber surface. Therefore, a critical parameter affecting both the RSU volume and mass is the safe flux threshold, which is dictated by performance and stress limits. Since the narrow list of absorber material candidates is shared by all competitors, the specific scheme for energizing the PCM and working fluid becomes the discriminating factor between design concepts. The higher the flux tolerance within the cavity, the greater the potential for size and mass reduction. Non integral RSU concepts where the PCM is not located in the cavity can potentially operate at high fluxes but pay the mass penalty in the additional heat exchanger.

3.1.2 RSU EFFICIENCY

RSU efficiency, defined as the ratio of useful energy provided to the engine to available energy at the receiver aperture plane during an equilibrated orbit cycle, is of importance for two reasons. First, the receiver efficiency as a component of the overall module efficiency affects the required concentrator collection aperture and hence the orbital drag on the satellite. Increased drag drives the costly requirement for expendable thrust propellent. Secondly, since losses incurred within the receiver must be compensated for in size of the concentrator, overall system mass and volume are affected.

Table 3.1 lists key RSU energy losses. As illustrated in the table, first order losses include thermal, fluid mechanic and thermodynamic mechanisms.

Table 3.1. RSU ENERGY LOSS MECHANISMS

Thermal Energy Losses	-	Cavity reradiation
	-	Reflection
	-	External shell conduction
	-	Shading
	-	Intercept factor (spillage)
Brayton Momentum energy Losses	-	Frictional pressure drop in working fluid
	-	Form or fluid separation pressure drop
Stirling Engine Integration Losses	-	Excess heater head volume
	-	Excess heater head pressure drop
	-	Entropy mixing losses (non-uniform gas path heating)
Carnot Cycle Energy Losses	-	Time dependent exhaust temperature (relative to PCM melting point)

In this task, certain assumptions are necessary to perform a comparative assessment of thermal losses between alternate RSU designs. Since the concentrator configuration is somewhat unidentified, we have selected the performance characteristics shown in Table 3.2. A description of Sanders' optical model is provided in Appendix A. To precisely determine the optimum receiver aperture, it is necessary to trade the competing energy loss effects of varying the aperture diameter. This study, however, deals with the relatively small magnitudes of energy quantities and requires an extremely detailed knowledge of the specific concentrator. Our concentrator model design is based on information in Table 3.2 and our correlations with the DoE/Sandia National Labs, Albuquerque (SNLA) Test Bed Concentrator. For reference, the Harris

IOC concentrator will yield, at design performance, a concentration ratio of about 1200. At a concentration ratio of 2139, our model predicts a spillage (non-collected aperture plane power) of less than 2%.

Table 3.2. CONCENTRATOR CHARACTERISTICS FOR BRAYTON RSU

PARAMETER	VALUE	REFERENCE
Reflectivity	93	NASA RFP 3-109561
Rim Angle	60^{o}	Ref. 1, 3, 4
Dish Diameter	7.40m	Baseline assumption
Insolation	1.37 kW/m^2	Ref. 5
Intercept factor in 16.0 cm	0.98	Derived
Standard Deviation of Surface Specularity Error	2 mrad	Same value used to correlate with DoE TBC
Standard Deviation of Surface Normal Error	2 mrad	Same value used to correlate with DoE TBC
RSU Aperture Diameter	16 cm 14.5 cm	(Brayton) (Stirling)

Having established this RSU aperture, cavity reradiation losses through that area can be analyzed. These losses are highly dependent upon the characteristics of a window, if present, as well as the temperature of the various surfaces within the cavity. Decreasing the receiver aperture would reduce radiation losses at the expense of increased spillage. Ultimately such an optimization process will be conducted, but at this time sufficient specifications for the concentrator do not exist.

Exterior loss of energy conducted through the insulated envelope is the greatest single thermal loss in the Baseline Brayton RSU and the area with the greatest potential for improvement. Assuming similar insulation materials and techniques, this loss is essentially related to the exterior surface area of the RSU. Therefore, our efforts to reduce the overall size will produce efficiency benefits as well.

Pressure drop, or momentum loss, within the Brayton RSU gas side heat exchanger typically produces cycle power losses of nominally 10% (see Appendix B). Since this is roughly comparable to the thermal losses, we have addressed techniques for improvement in our RSU design. The two sub-categories listed in Table 3.1 are design issues associated with the ducting and distribution manifold, and the Reynolds analogy-type losses occurring on the heat transfer surfaces.

Stirling engine integration losses are divided into three categories in Table 3.1. Gas mixing or entropy losses arise when the many parallel gas paths within the heater head are not maintained at a uniform temperature. This situation can occur if the typically non-uniform solar flux distribution within the cavity

is not properly homogenized within the RSU. An example of this condition was evaluated on Avanco/United Stirling dish-electric module tested in the early 1980's for the DoE (Ref. 8). Their receiver configuration was such that the heater head tubes were directly irradiated by the sun within the cavity. By their estimations, tube temperature variations on the order of 30°C resulted in an efficiency penalty of approximately two percentage points. This same penalty is expected from RSU designs that attempt to use an array of unconnected heat pipes extending into the receiver cavity.

In all thermodynamic engine cycles the peak operating temperature affects the potential system efficiency. With the PCM melting point as a datum, the cycle efficiency decreases with the thermal drops within the RSU. These temperature drops can arise if PCM voids impede heat transfer from the thermal storage system. Also, if the PCM heat exchanger area is insufficient, a transient temperature droop will occur over the orbital period.

3.1.3 RELIABILITY

The reliability of the RSU is predominantly determined by the working life of the hot cavity elements. Creep, fatigue and PCM corrosion at elevated temperatures present the fundamental design limits. These conditions are further aggravated by the long term degradation in material integrity due to space environmental effects, including reaction of the high temperature metals with atomic oxygen, and vacuum volatility of trace amounts of alloy constituents.

Other factors affecting reliability relate to the specific fabrication requirements. The total length of welds in contact with the PCM is important because highly corrosive, high surface tension salts are extremely difficult to contain over long periods of time. These concerns originate from DoE's experience in molten nitrate and carbonate salt transport loops and the data base on liquid metal cooled nuclear reactors.

Corrosion within heat pipes is an area of intense research. To minimize the risk on this program, we have chosen materials which have already demonstrated extremely long working life. The Incoly 800 with a nickel wick is under test at Thermacore and is entering its fourth year of continuous operation without incident. For RSU applications, however, low thermal and pressure stresses are required to make it possible to use this proven combination of materials. There is a strong motivation for using these materials because the alternative appears to involve costly and more developmental refractory metal alloys.

To guard against the potential for accelerated corrosion rates in crevices, we have adopted rigorous joint and weld standards developed on the NASA/DoE terrestrial Stirling program on which Sanders performed two sub-contracts. On the continuation of this program, Sanders and researchers at Thermacore and Sandia National Labs will be further analyzing this phenomenon and developing fabrication procedures.

The Advanced Brayton RSUs utilizing LiF require the additional strength offered by the refractory metal alloys to meet the combined corrosion and creep requirements. Niobium alloys such as Cb-1Zr, PWC III, C103, and FS-85 were considered.

Another area of the Baseline technology where we feel improvements are warranted is the start-up capability. The inherently high heat capacity of the PCM-lined cavity is likely to place serious requirements

on the starting system. Motoring the permanent magnet alternator for extended periods is not attractive because of the excessive power requirements. Also, excessive thermal gradients and local temperatures could result due to the high thermal inertia and unpredictabilities of the PCM voids (46% contraction of LiF from liquid to room temperature).

3.1.4 COST ISSUES

Another critical goal is to avoid increasing cost and fabrication complexity while advancing the state-of-the-art. In fact, we believe that the Baseline exhibits several areas in which fabrication complexity can be reduced, particularly in the areas of weld length, number of welds and number of components. Since a requirement for refractory metal components will increase fabrication complexity and significantly affect cost, we will select alternative materials whenever possible.

3.2 NEW BRAYTON CONCEPTUAL DESIGNS

Schematic representations of the four Brayton Advanced Concepts evaluated in Task II are illustrated in Figure 3.1. The following subsections contain a description of of each of these concepts. Table 3.3 presents a review of the critical technology issues associated with the Baseline design and states the advanced theory for solving these problems. A summary of the performance characteristics of each concept is provided in Section 3.2.5.

3.2.1 CONCEPT I: QUARTZ DOME

The theory behind concept I is to achieve parallel heating of the working fluid and the PCM container. In the Baseline concept compared in Figure 3.2, all of the solar power must be conducted in series through the PCM envelope prior to affecting the working fluid. This approach referred to as parallel heating, employs a common solar irradiated wall which separates the two heat sinks. Where as the peak flux tolerance for series heated receiver criteria is on the order of 3 to 5 w/cm^2, forced convection of the absorber surface allows this to be raised from 10 to 15 w/cm^2, in concept I. This increase in flux will result in a more compact RSU. Figure 3.2 also illustrates the potential for a higher cycle efficiency for a given PCM by raising the achievable exit temperature by 40 to 60°C.

The layout of the Concept I is presented in Figure 3.3. A large quartz dome lines the receiver cavity. The working fluid of HeXe is sealed within the system with metal "C" rings located at the relatively cool gas inlet end. The PCM is contained within a corrugated metal shell. The corrugations serve to increase the heat exchanger primary heat transfer area.

Figure 3.4 presents the thermal analysis results generated by the lumped nodal analysis of SINDA. Although the heat exchanger geometry was not optimized, the analysis yielded a viable geometry demonstrating the potential for a highly compact receiver design.

3.2.2 CONCEPT II: DIRECT ABSORPTION

The DAR Brayton RSU design is illustrated in Figure 3.5. A corrugated cone forms the inner cavity wall, and serves as the PCM to engine working fluid (HeXe) heat exchanger. The Brayton working fluid flows

FOUR CATEGORIES OF BRAYTON RSUs CONFIGURED FOR TASK II

CONCEPT I: Quartz Dome

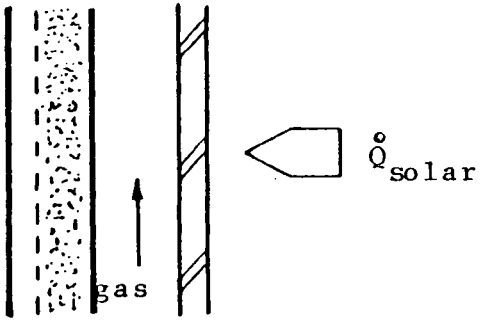

CONCEPT II: Direct Absorption

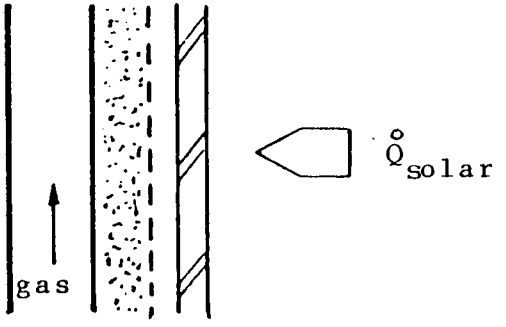

CONCEPT III: MATRIX ABSORBER WITH TES

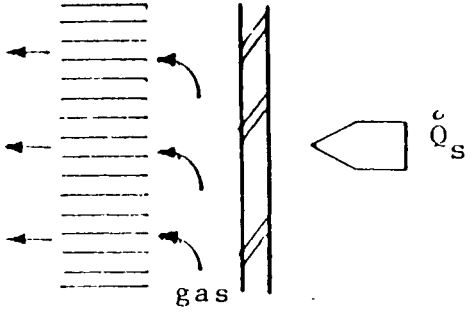

CONCEPT IV: PUMPED LIQUID SENSIBLE STORAGE LOOP

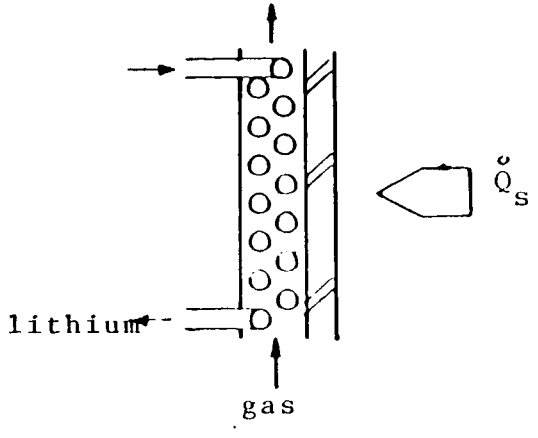

Figure 3.1

BASELINE BRAYTON RSU KEY ISSUES:

HOW WERE THEY ADDRESSED?

ISSUE	CONCEPT I	CONCEPT II	CONCEPT III	CONCEPT IV
PCM Δ V/V IMPEDIANCE	COMMON HEAT ADDITION/ EXTRACTION SURFACE (1)	DIRECT SOLAR ABSORPTION (1)	MICRO ENCAPSULATION (2)	ELIMINATE PCM (1)
"THERMAL RACHETING"	1) GEOMETRY 2) WEEKENING AGENTS 3) GRADED PCMS (2)	NON CONFINING (1)	MICRO ENCAPSULATION (2)	ELIMINATE PCM (1)
VOLUME	RAISE FLUX CAPACITY WITH PARALLEL HEATING OF TES AND WORKING FLUID			
MASS	REDUCE GAS/PCM CONTAINMENT METAL AND GAS MANIFOLDING			
COMPLEXITY	REDUCE PARTS COUNT AND NUMBER OF WELDS			

Table 3.3

QUARTZ DOME CONCEPT I THERMAL RESPONSE

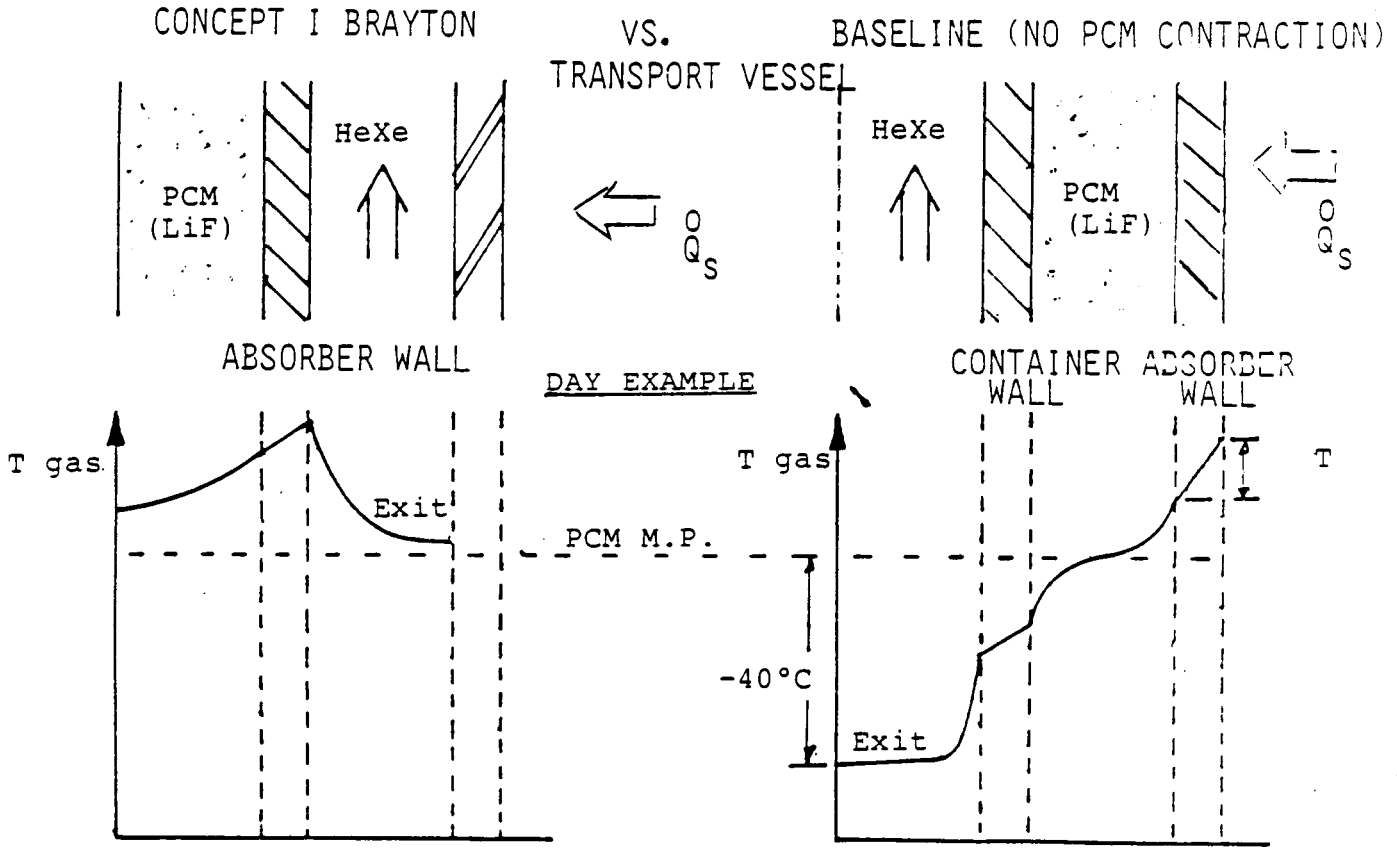

Figure 3.2

BRAYTON CONCEPT I

QUARTZ DOME WITH CORRUGATED TES CONTAINMENT

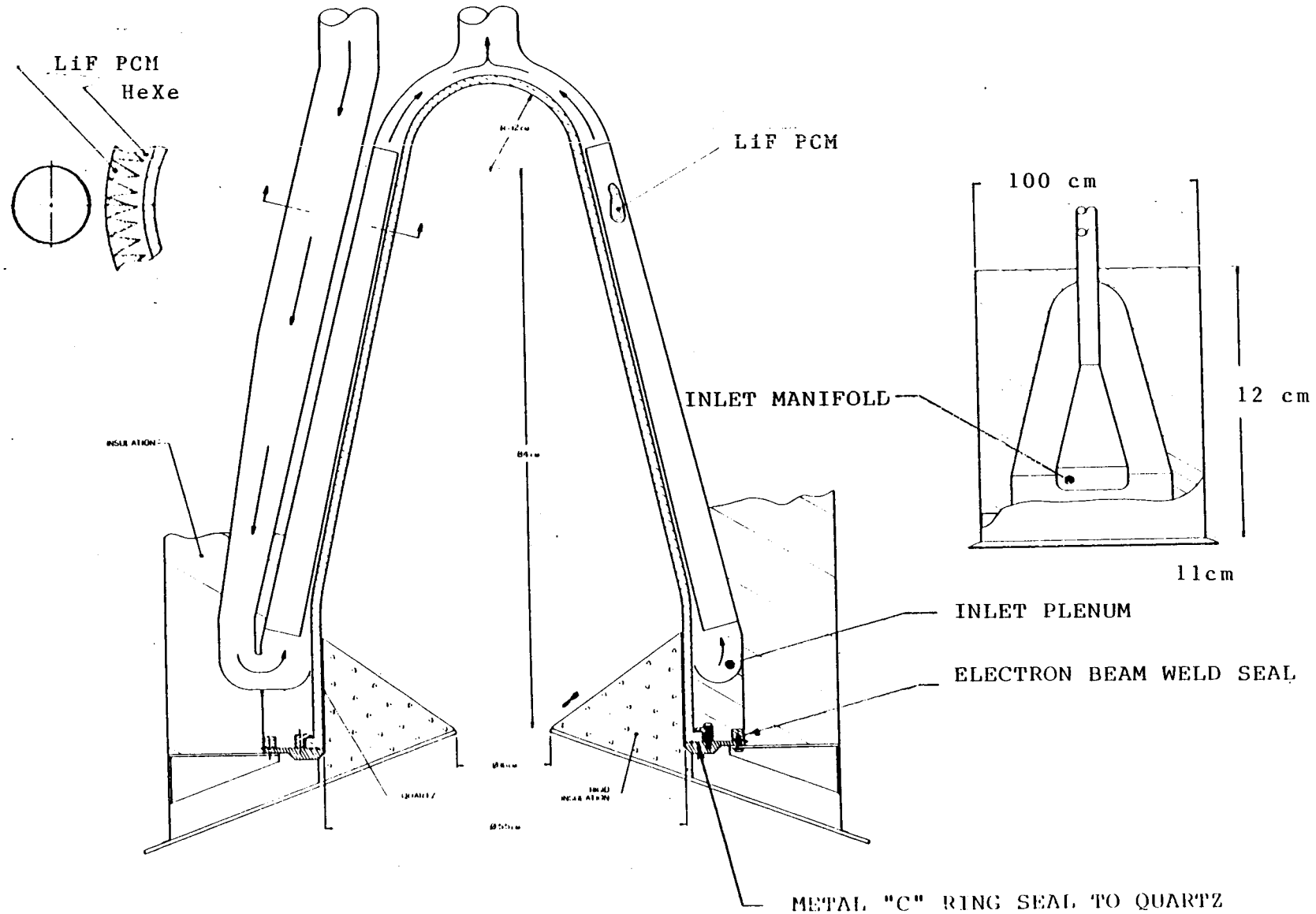

Figure 3.3 20

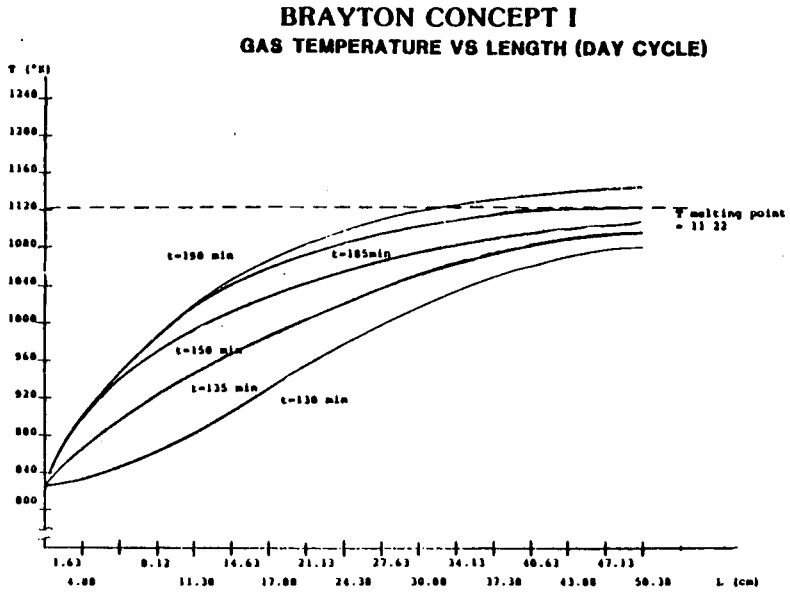

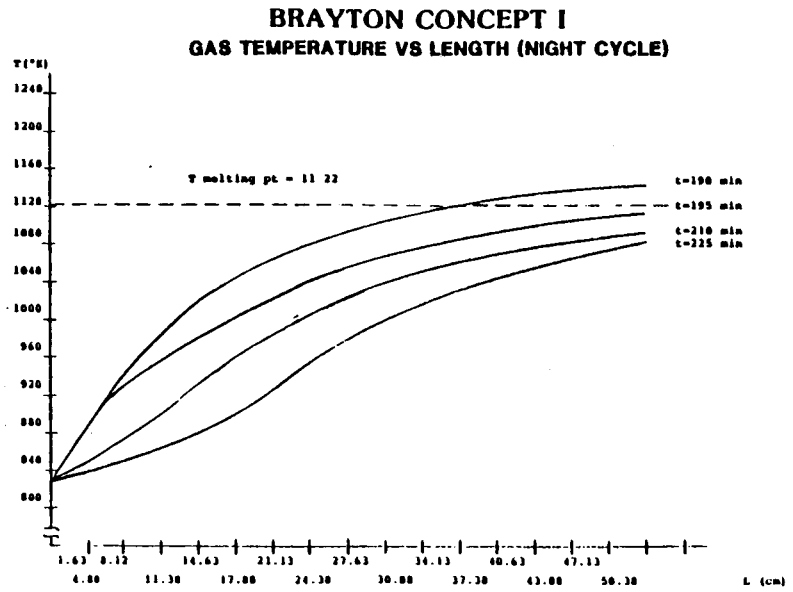

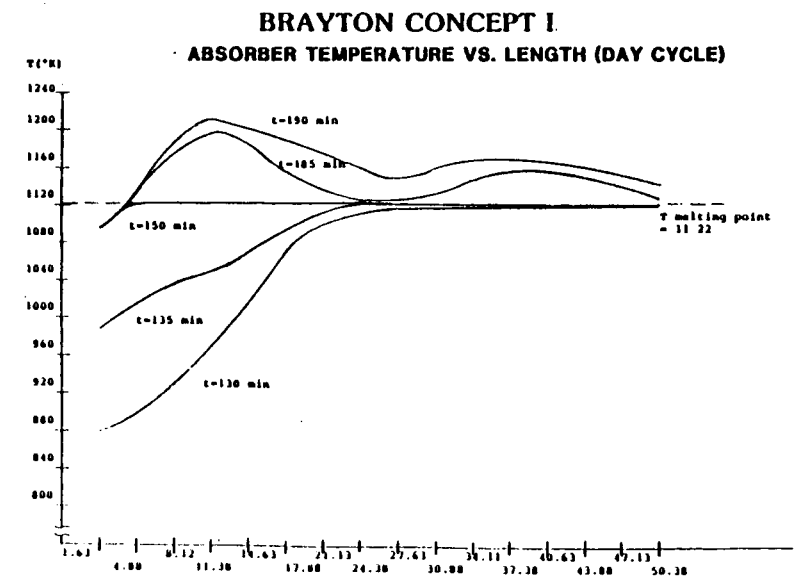

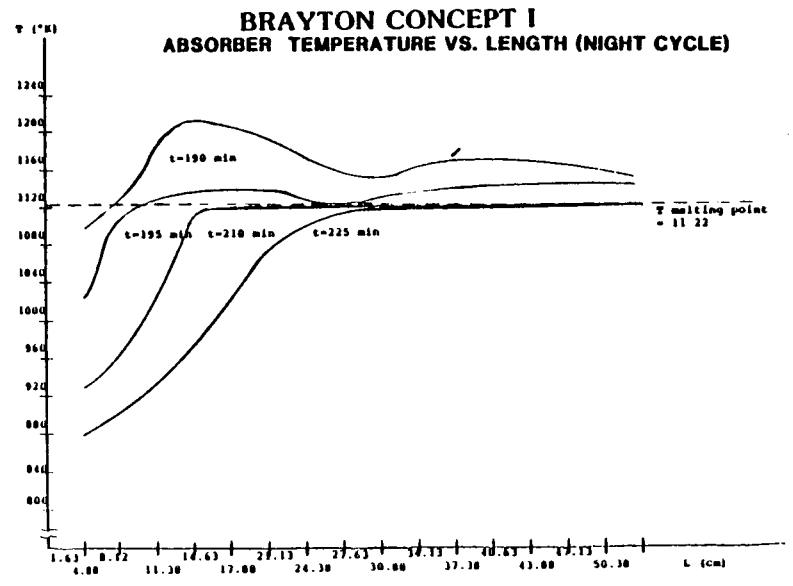

Figure 3.4

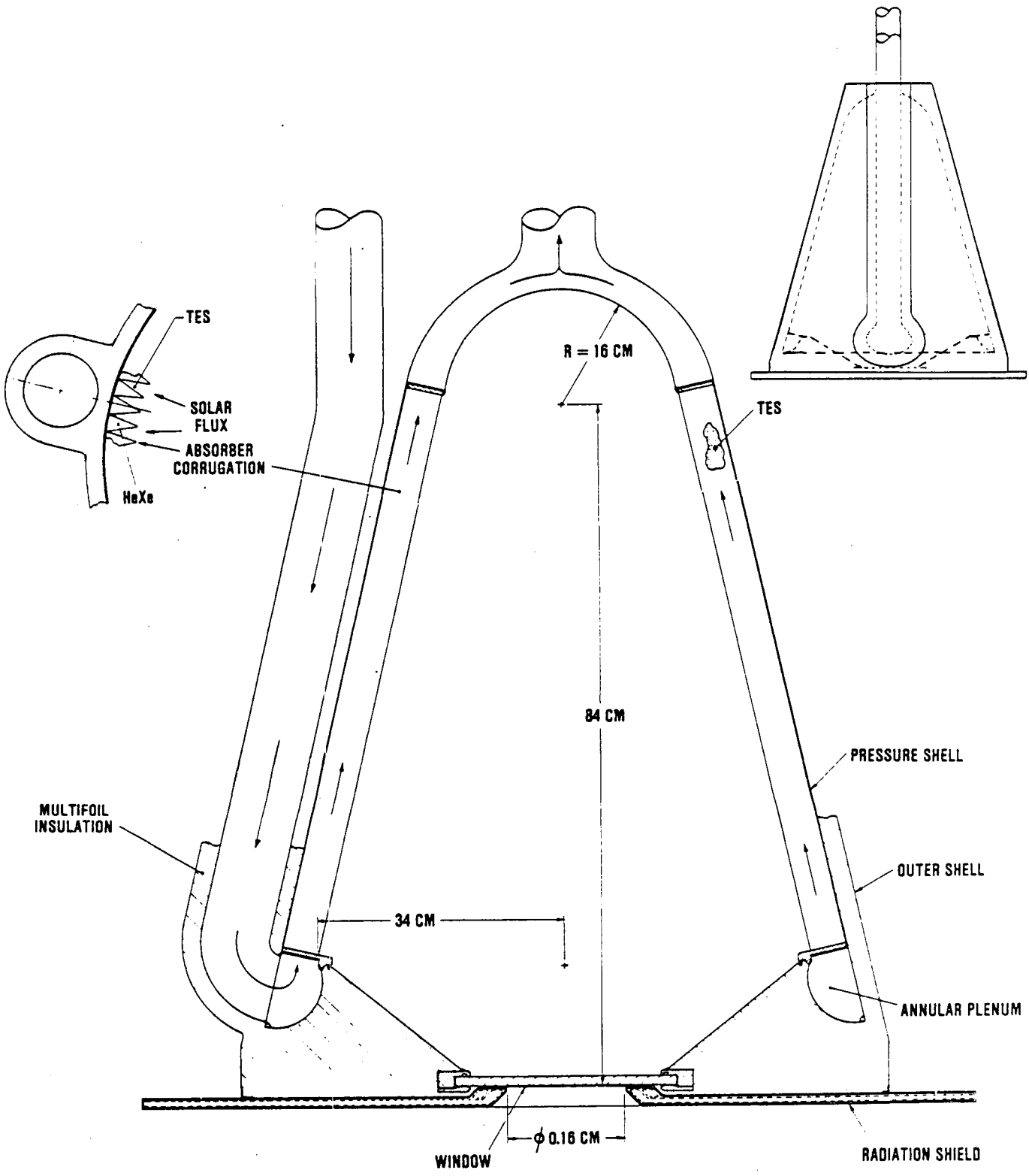

Figure 3.5 DAR Layout Drawing

from an annular plenum at the cavity aperture end, across the outside of the corrugated heat exchanger and exits through an axial discharge duct. Concentrated solar energy enters the receiver through a windowed aperture and strikes the LiF filled corrugations on the cavity interior. Although pure LiF is almost entirely transparent to the solar spectrum, by selectively doping the LIF with small percentages of rare earth or transition metals we can tailor its absorption coefficient to achieve optimum thermal charging. By absorbing a portion of the solar energy directly into the PCM without the impedance of the opaque envelope present in other designs, parallel heating of the PCM and heat exchanger wall is achieved. This direct and simultaneous heating permits greatly increased operating solar flux levels absorbed on the cavity interior. This in turn permits a smaller RSU cavity which yields better performance and significantly lower overall RSU volume and mass compared to the Baseline Space Station RSU projections.

The near zero gravity environment, combined with the high surface tension of LiF, allows the coarse corrugations to act as a "wick" to control and contain the PCM. Since the LiF is contained by the open corrugations rather than within confining walls, the melting PCM is free to expand, and is less likely to impose DV/V stresses on the heat exchanger wall. This feature, combined with reducing by two orders of magnitude the length of weld exposed to the corrosive LiF will significantly increase the RSUs operational lifetime relative to that of the IOC designs. The detailed analysis of this concept is contained in Section 4.

3.2.3 CONCEPT III: PACKED BED MATRIX RSU

The principle of this concept is to transfer energy to a Brayton working fluid by forcing the gas through a matrix of small channels or a packed bed of pellets. The size and packing density of the pellets are two of many variables which can be selected for a specific application. Many industrial heat transfer applications, such as flue gas regenerators and process heat storage already employ this concept. Typically in these applications the bed is charged by forcing the hot waste gas through the cool matrix. The major advantage of this approach over more conventional indirect heat exchangers is the attainability of a large surface area exposed to the working fluid. Sanders has exploited this design principal for high temperature terrestrial receivers, solar energy storage, and periodic Brayton regenerators.

One packed bed concept initially investigated attempted to take advantage of these attractive heat exchanger features by enclosing numerous pellets within a bank of tubes. The bank of tubes (10 to 20) arranged in a cylindrical cage, formed the irradiated portion of the receiver cavity. However our analysis indicated that the solar integration could not effectively utilize the enhanced gas-solid convection mechanisms. Since the concentrated solar flux is incident on the opaque cylinder wall, heat transfer radially into the bed limited the tolerable fluxes affecting the operating stresses and the performance. Charging the bed in this manner requires that energy be transferred radially through the tubes. However, the poor thermal contact of the pellets and axial gas flow naturally resists the radial heat flow. Also, even under relatively uniform inlet conditions, the gas will have a tendency to "channel" through the matrix. Channeling is a quasi-stable condition which results in a significant variation between theory and the actual heat transfer and pressure drop characteristics of the design. This condition would serve to further limit the acceptable incident flux levels on the solar absorbing surface. For effective utilization of the thermal mass as well as efficient performance, it is important to achieve a small radial temperature gradient.

After considering these limitations a more practical concept was generated which utilized the packed bed principles and could meet the program goals. The Brayton Concept III improved upon the concept of an indirectly heated opaque container of pellets by again incorporating a quartz window. Absorption of the

BRAYTON CONCEPT III

CONCEPTUAL REPRESENTATION OF PACKED BED OR MATRIX RSU

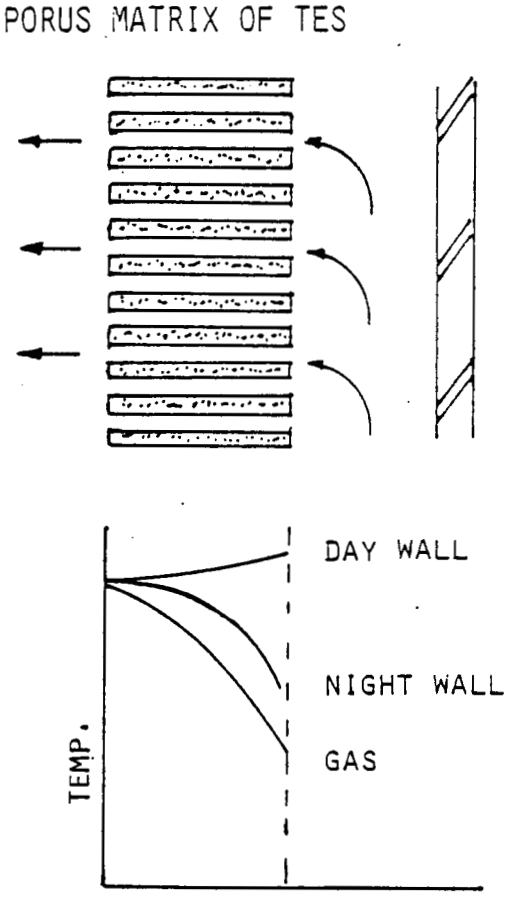

- PCM ENCAPSULATED IN SUBSTRATE, SOME SENSIBLE STORAGE
- ΔV/V CONTROL OVER PCM
- VERY HIGH SURFACE AREA/VOLUME FOR HEAT TRANSFER
- VERY HIGH HEAT TRANSFER COEFFICIENTS ESPECIALLY ON IRRADIATED FACE

Figure 3.6

BRAYTON CONCEPT III

DIRECT IRRADIATION OF COMPHASE MATRIX TES

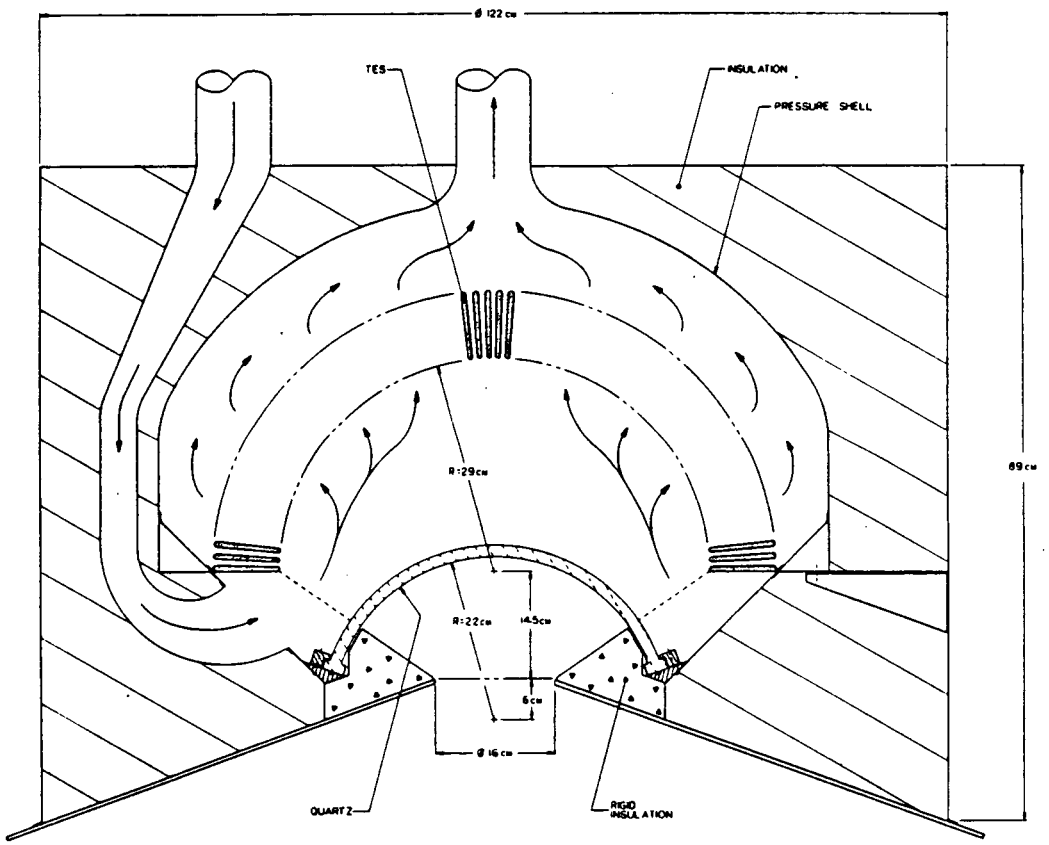

Figure 3.7

STEADY STATE MATRIX TEMPERATURE PROFILE FOR BRAYTON CONCEPT III

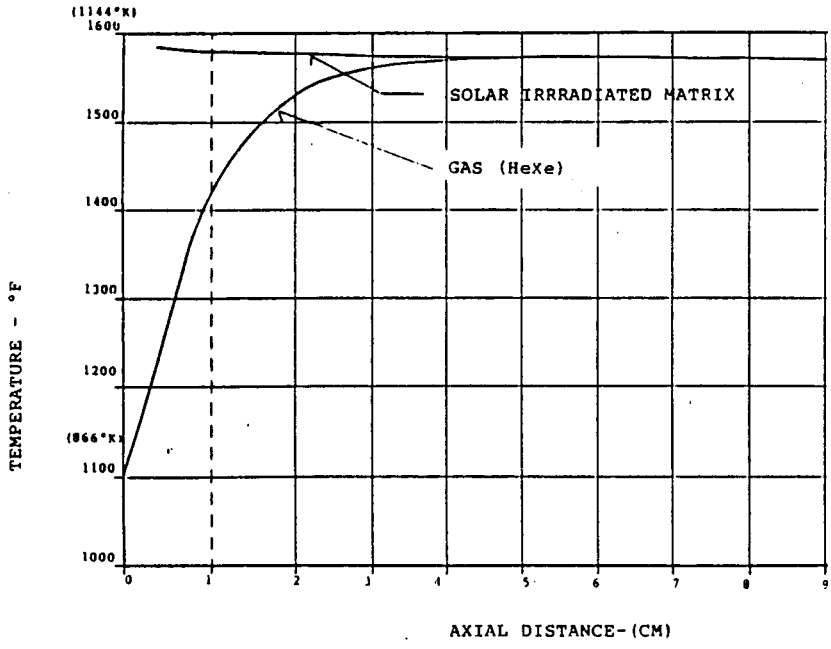

The First Analysis for Establishing the Bed Thickness Required for The Heat Extraction Period (night) made the following assumptions:

- 1/4" Spheres
- 50% LiF, 50% MgO
- 50% Porosity
- Neglected Sensible Storage in MgO

Figure 3.8

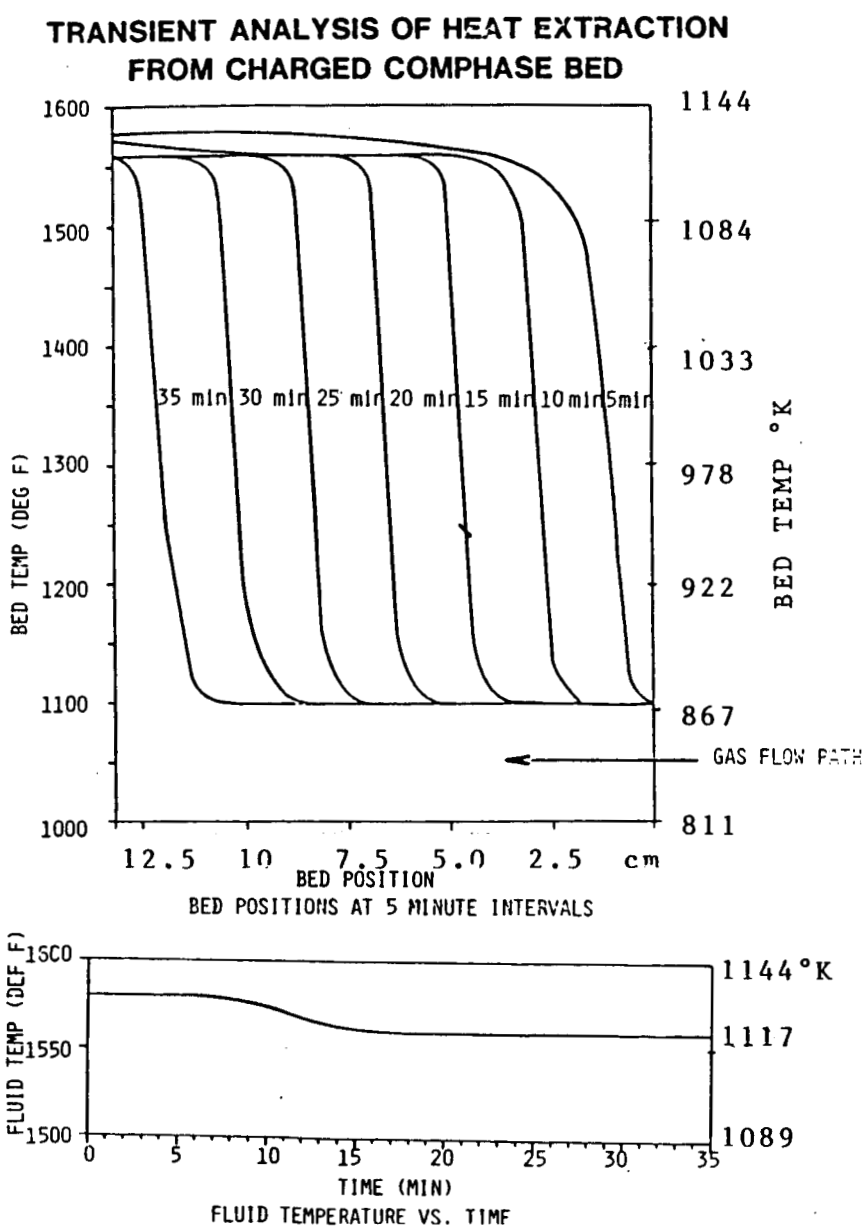

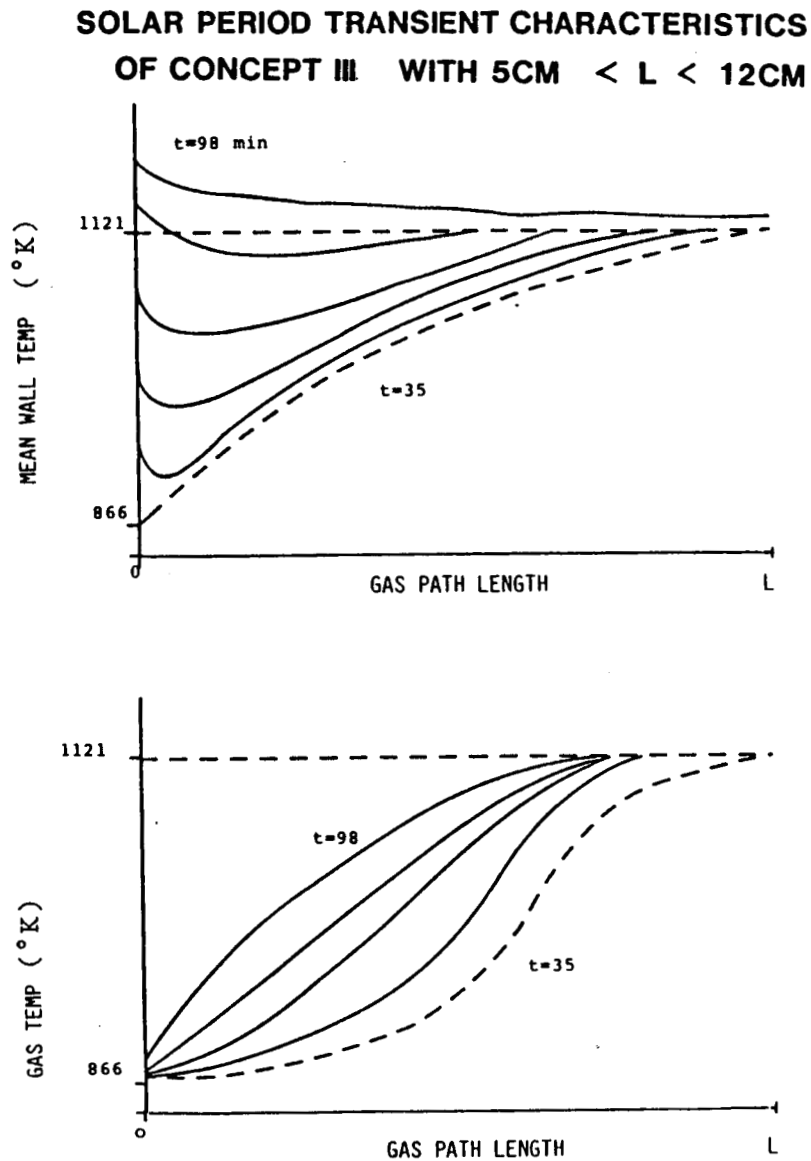

Figure 3.9

Thermal Charging and Discharging
of Solar Irradiated Packed Bed, Concept III

solar energy directly on the matrix as illustrated in Figure 3.6 would not only save the weight of the pressurized containment tubes and manifolds, but it would provide a more efficient means of charging the PCM. Also by orienting the flow direction with the thermal charging gradient, convection aides in reducing temperature variations in the relatively short bed.

Figure 3.7 illustrates the final design concept where the very high surface area of the bed is exposed to the sun. The porous matrix allows sunlight to penetrate 2 or 3 pore diameters. The inlet gas is distributed over the absorber matrix surface as it enters the large cavity plenum. This avoids the weight and pressure drops associated with conventional manifolds. The domed quartz window, loaded in compression, contains the working gas in a manner similar to Sanders' line of terrestrial receivers.

The absorber matrix was envisioned to be either a bed of pellets or a composite matrix encapsulating the PCM. The numerous pellets would be suspended by a screen to produce the desired absorber geometry. The matrix concept would employ the Institute of Gas Technology's (IGT) developmental Comphase (trademark). Comphase is a ceramic "sponge" which encapsulates the PCM in 2 to 5 um interstitial voids. A pellet or extrusion of Comphase could have sufficient structural integrity so that only a very thin exterior coating would be required to seal the PCM. Since the ceramic substrate candidates in Table 3.4 are considerably lower density than the metal container materials, there is a potential for lower weight than the pure metallic pellets. Additionally, since surface tension semi-immobilizes the liquid phase within the micropores, they may prove to be more stable against the thermal ratcheting stress.

Table 3.4 Promising Candidate Substrate Materials for IGT Comphase

- MgO
- B_4C, or WC
- Nb or Ta
- Graphite

Approximately 50% substrate, 50% LiF

The concept for Comphase microencapsulation can be applied in a range of degrees. The volume fraction of PCM affects the strength of the composite structure. Typically, the PCM fraction can not exceed about 50% to generate a close-celled product. If pellets fracture they would slowly release PCM to the working fluid. Greater PCM fractions are possible, however the open-celled product is more analogous to liquid saturated sand. To accommodate this lack of strength, pellets of this material would require a thicker overcoat.

A major drawback of the Comphase concept at this time is the expense required to advance the technology. IGT has not yet performed experimentation with fluoride PCMs. Under subcontract to Sanders in our Task II, we took the first step in identifying a few possible substrate candidates from the literature. Admittedly, there are a great number of unknowns yet to be addressed.

The Sanders direct absorption packed bed was analyzed (Figure 3.8 and 3.9) to the extent necessary to show that a more significant weight reduction is possible with equal or better thermal performance than the Baseline. However, due to the risks and lack of experimental experience with the high temperature fluoride PCMs it does not appear to be feasible at this time to take the next costly step. Simply stated, there are other areas of potentially greater payoff where excellent progress can be made with a more realistic budget.

3.2.4 CONCEPT IV: LITHIUM SENSIBLE STORAGE LOOP

In a departure from previously discussed concepts, the fourth new concept utilizes the sensible heat content of liquid lithium for thermal storage. The operating temperature of sensible heat storage is not fixed to the melting point of the PCM. As indicated by Figure 3.10, the lithium sensible temperature rise and the lithium reservoir mass are inversely related to one another for a given thermal storage capacity. For the 7 kWe system an operating point was chosen where the thermal storage was only about 60% of the conventional PCM mass. This was accomplished at the expense of raising the cavity temperature 124^0K above the nominal HeXe turbine inlet temperature. The 320^0K working range is established between the recuperator exit of 1209^0K and the peak lithium temperature..

The final concept (schematic in Figure 3.11) again employs a window to achieve the most compact RSU. During the heat extraction period the liquid lithium and engine working fluid flow countercurrently. Figure 3.12 shows the design details where the solar energy is directly incident on the tubular heat exchanger containing the lithium. The 1/4" diameter lithium tubes are connected on both ends to the helical storage reservoir. The heat exchanger design details are illustarted in Figure 3.13. The temperature excursions of the reservoir are shown in Figure 3.14. Other non-windowed versions of this concept were also studied and results indicated only a modest weight escalation in this case.

The concept relies on the use of an electromagnetic pump to circulate the hot lithium. These pumps have no moving parts and one sized for this application would have the following characteristics. Although a final design has not been made, these specifications have been provided with high assurance from an experienced manufacturer.

Input Power	=	2.5 Watts
Volume	=	400 cm^3
Weight	=	1 kg
Life	=	10 years

3.2.5 BRAYTON COMPARISON STUDY

A summary of the critical performance and size characteristics of the four new Brayton concepts is provided in Table 3.5. This comparison shows substantial improvements for each of the four new concepts over the Baseline. In balancing the developmental risks against the potential gains shown in Table 3.5, the Direct Absorption Concept II was selected for further analysis in the program's Task III. This work is presented in Section 4.0.

CONCEPT IV BRAYTON: SENSIBLE LOOP STORAGE MASS TRADES

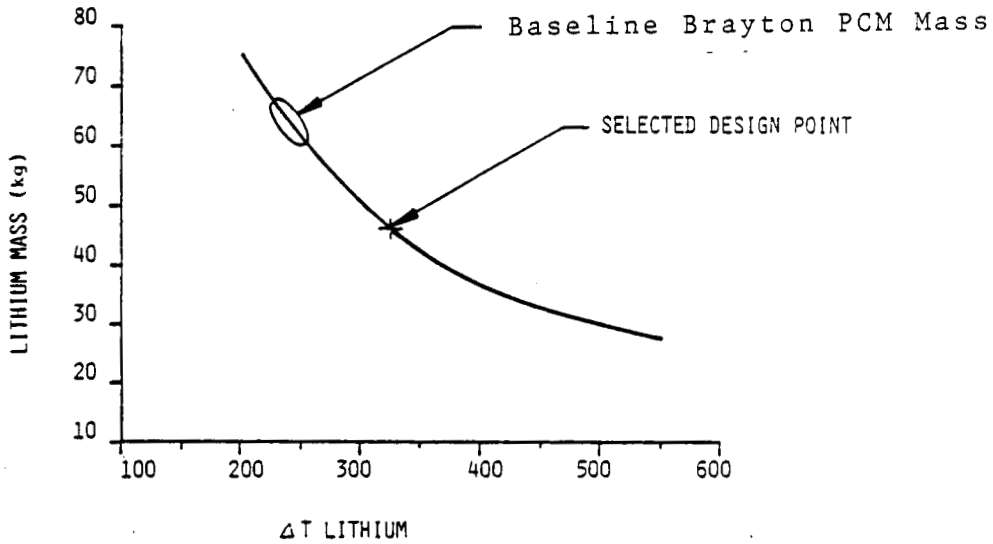

- SELECTED LOOP TEMPERATURES YEILD LOWER TES MASS THAN LiF BASELINE
- AVERAGE CAVITY RADIATING TEMPERATURES ARE STILL LOWER THAN BASELINE BRAYTON PROJECTIONS

Figure 3.10

CONCEPT IV BRAYTON SENSIBLE PUMPED LOOP

CONCEPTUAL REPRESENTATION OF PUMPED LOOP CIRCUIT

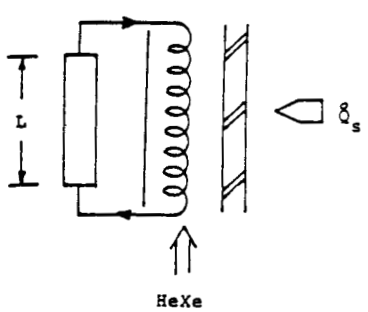

- ELIMINATE ΔV/V ISSUES
- ELIMINATE PCM COMPATABILITY
- VERY HIGH FLUX CAPACITY, THUS SMALL CAVITY DESIGN
- NO TIT CONSTRAINTS IN RSU

Figure 3.11

BRAYTON CONCEPT IV

QUARTZ DOME WITH PUMPED LITHIUM THERMAL ENERGY TRANSPORT AND STORAGE

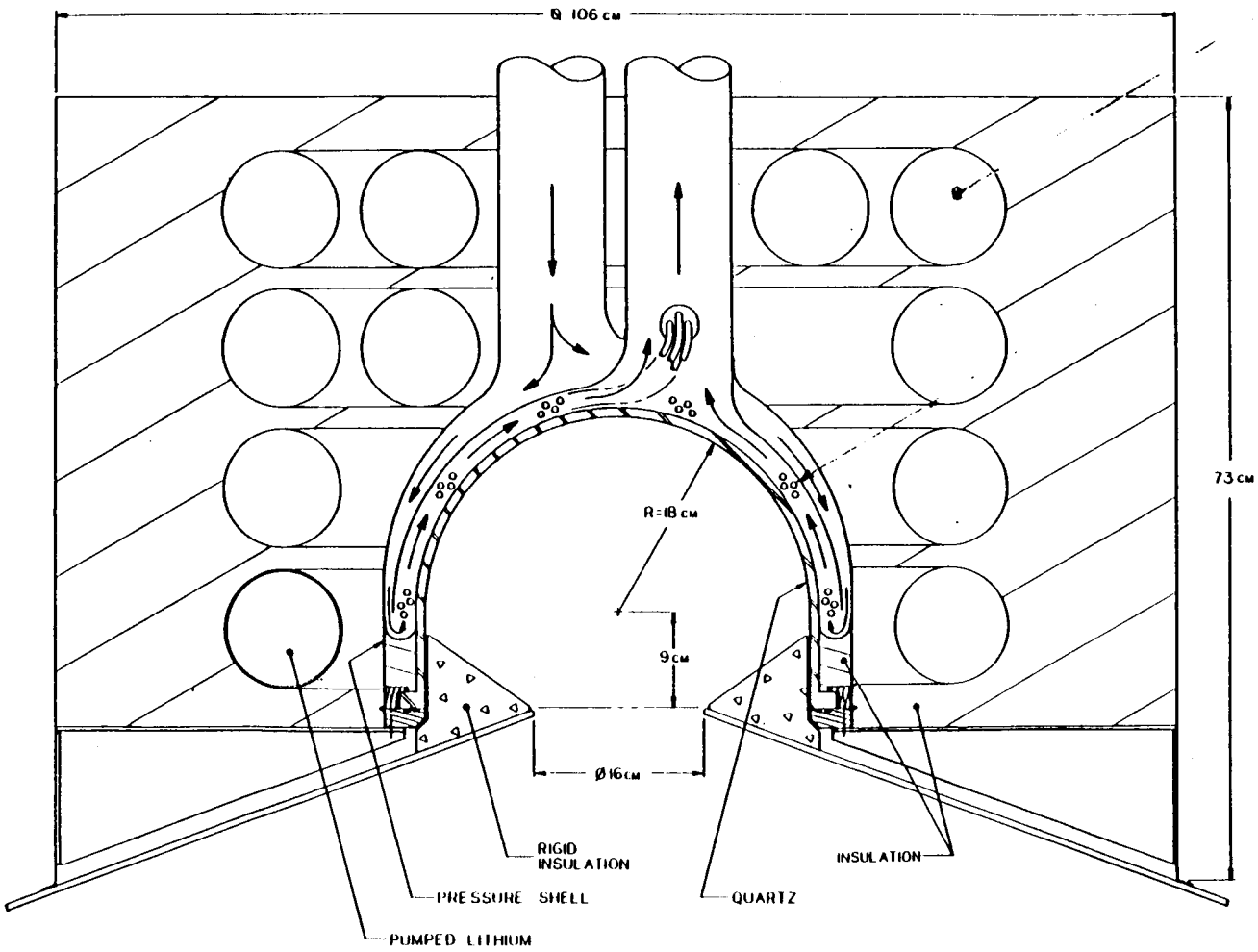

THERMAL ENERGY STORAGE TUBES

HEAT TRANSFER TUBES

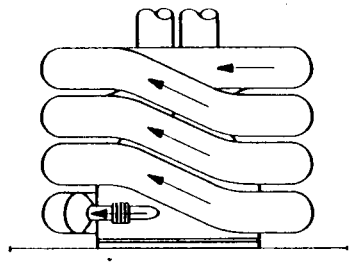

LITHIUM IS CIRCULATED BY LINEAR INDUCTION PUMP

Figure 3.12

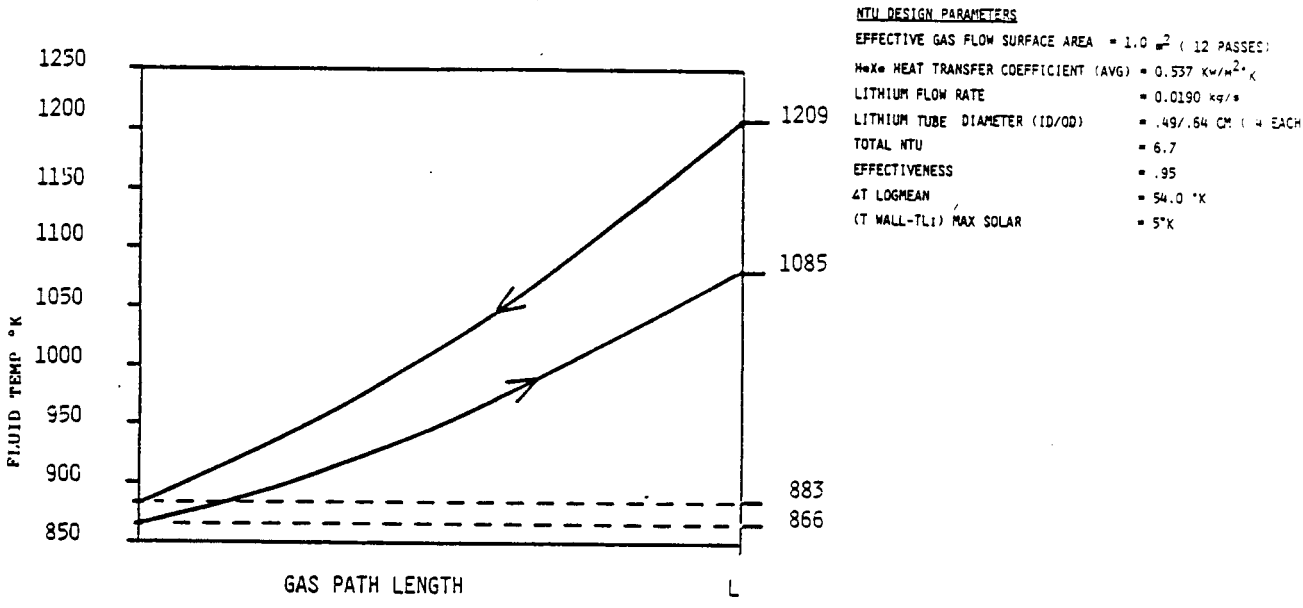

Figure 3.13

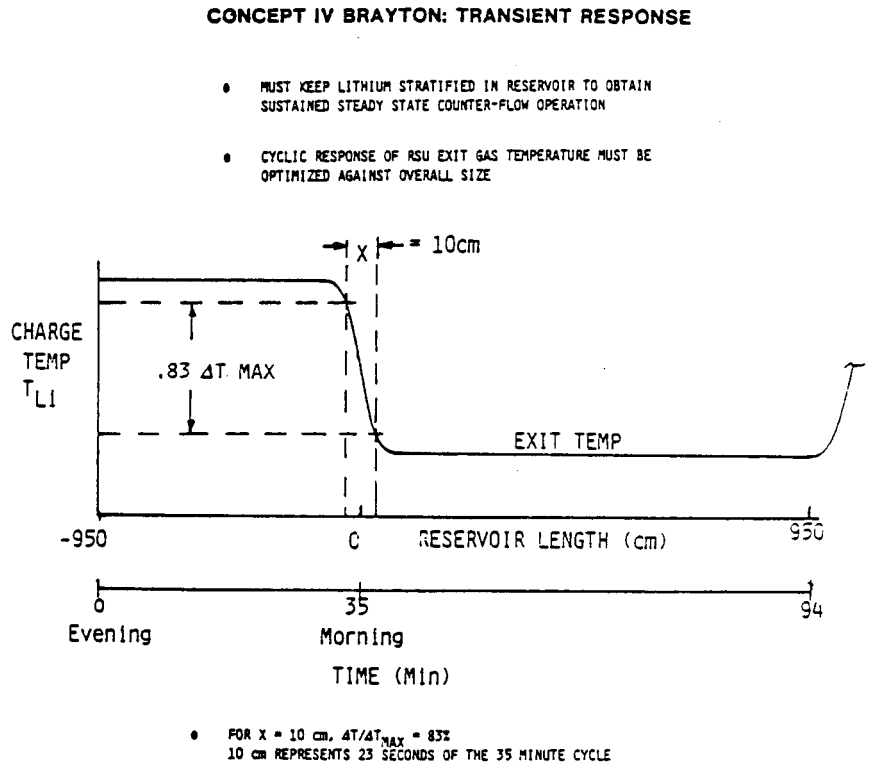

Figure 3.14

Table 3.5 Performance Summary of New Brayton Concepts

Parameter	Concept I	II	III	IV	Baseline
Cavity Diameter (M)	0.55	0.60	0.58	0.36	1.35
Overall Diameter (M)	1.0	0.84	1.22	1.06'	1.65
Overall Length (M)	1.05	1.08	0.67	0.48	1.54
Exterior Surface Area (M^2)	4.87	2.84	4.91	3.38	12.2
Insulation Losses (kW)	1.31	0.76	1.33	0.91	3.3
Day Cavity Losses (kW)	1.50	1.37	1.24	1.18	1.89 (4.78)*
Mean Cavity Temp (^0K)	1160	1120	1135	1084	1142 (1440)
Night Cavity Losses (kW)	1.17	1.17	0.37	1.17	1.86
Mean Cavity Temp (^0K)	1080	1080	870	1079	1138
Reflective Loss (kW)	1.52	2.5	0.48	1.52	1.52
RSU Thermal Efficiency (%)	85.7	86.0	88.0	87.2	76.5 (71.2)
Total RSU Losses(Thermal $_{KJ}$)	24,351	23,800	20,032	21,427	44,960 (55191)
RSU Shading Losses (kW)	1.08	0.95	1.60	1.21	2.43
Mean Working Fluid Temp (^0K)	1110	1110	1110	1089	1089
Mean Brayton Efficiency (%)	27.5	27.5	27.5	27.0	27.0
RSU Pressure Drop (%)	1.0	1.0	1.0	1.0	2.0
Brayton P Losses (kW)	1.35	1.35	1.35	1.35	2.69
RSU Specific Mass (KG/kW)	29.1	30.0	27.1	16.6	76

* Figure in parentheses indicates the potential effects resulting from an adverse void location in the PCM container. Baseline losses derived from Reference 3.

3.3 NEW STIRLING CONCEPTUAL DESIGNS

In the absence of a true Stirling Baseline RSU three advanced concepts were proposed which specifically addressed the integration requirements of the Stirling engine. Accommodation of the Stirling engine heater head thermodynamic and fluid mechanic requirements is a high priority in the receiver designs. The first two concepts in Figure 3.16 illustrate schematic attempts to directly irradiate the working fluid (He) convection surfaces. In order to evaluate such designs it was necessary to consider the effects of heater head parameters such as volume, pressure, pressure drop, and heat transfer coefficient. To accomplish a preliminary design and evaluation of these new concepts it was therefore necessary to configure a receiver/engine model capable of conducting these trades. This engine model, developed by Gedeon Associates, is illustrated in Figure 3.17. Two sets of characteristics for a 8kWe and 25kWe free piston Stirling engine are displayed in Table 3.6. Since the 8kWe model previously used by NASA on another program was relatively close to our 7kWe design point, we have adopted this configuration as the basis of the RSU parametric analysis.

NEW STIRLING RSU CONCEPTS

CONCEPT I: CONNECTIVE ABSORBER

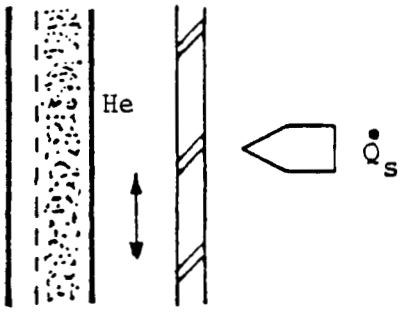

- INTEGRAL WORKING FLUID HEATER HEAD WITH TES IN CAVITY
- PERIODIC FLOW IN DIRECTLY IRRADIATED PASSAGE
- REQUIRES INTERACTION WITH ENGINE DESIGN PARAMETERS

CONCEPT II: MATRIX ABSORBER WITH TES

- INTEGRAL CAVITY DESIGN
- DIRECTLY IRRADIATED MATRIX
- REQUIRES INTERACTION WITH ENGINE PARAMETERS

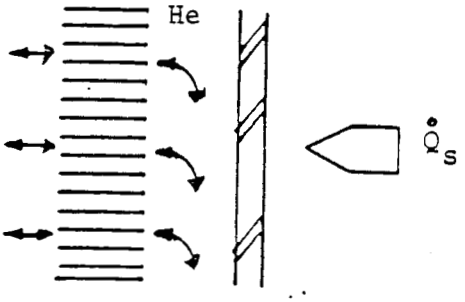

CONCEPT III: CONVENTIONAL HEAT PIPE ARRANGEMENT

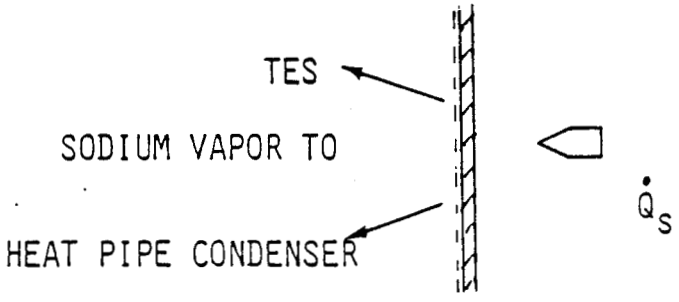

- ALLOWS DECOUPLING OF ENGINE HEATER HEAD DESIGN FROM CAVITY AND TES DESIGN
- SEVERAL COMBINATIONS OF EVAPORATOR, TES AND CONDENSER VARIATIONS

Figure 3.16

BASELINE STIRLING ENGINE USED IN PREVIOUS NASA 8-25 KW STUDY

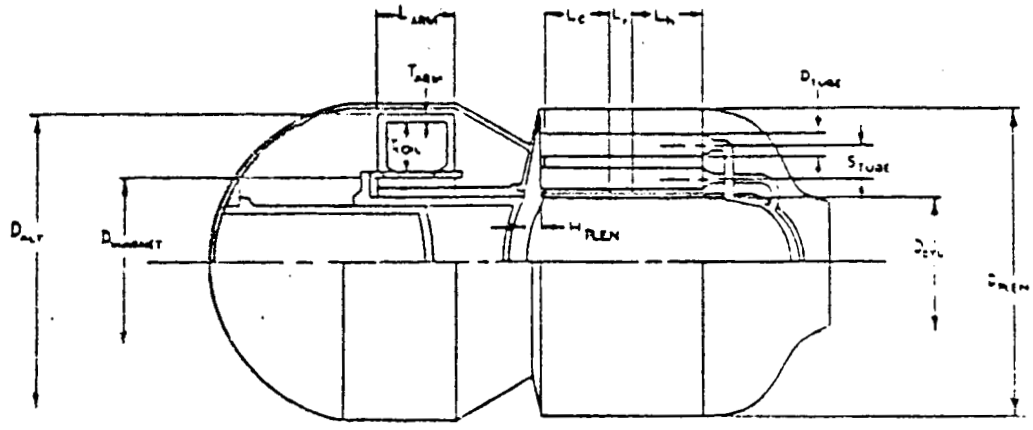

Figure 3.17

Table 3.6 Baseline Stirling Engine Characteristics Assumed for this Study

General		
Electrical Power Output (kW)	8	25
Pressure (N/m^2)	82.E5	177.E5
Frequency (Hz)	152	95
Heater Wall Temperature (K)	1080	1080
Cooler Wall Temperature (K)	540	540
Coordinates		
Piston Amplitude; 1/2 Stroke (mm)	7.8	15
Displacer Amplitude (mm)	5.7	11
Displacer Phase Referenced to Piston (rad)	0.785	0.785
Major Diameters		
Piston Cylinder ID (mm)	145	160
Alternator Pressure Vessel ID (mm)	342	401
Alternator Magnet Ring OD (mm)	205	253
Cooler Plenum Diameter (mm)	337	423
Alternators		
Armature Length (mm)	83	160
Magnet Thickness (mm)	6.3	12
Coil Thickness (mm)	53	44
Armature Thickness (mm)	7.8	15
Heat Exchangers		
Entrance Height of Cooler Plenum (mm)	14	29
Tube OD for C, R and H (mm)	25	16
Tube Spacing BC (mm)	34	26
Number of Tube Assemblies (mm)	62	178
Cooler Length (mm)	75	120
Total Number of Cooler Channels (mm)	248	712
Cooler Channel Gap (mm)	1.7	1.6
Cooler Channel Height (mm)	4.4	2.4
Regenerator Length (mm)	24	38
Regenerator Wire Diameter (mm)	0.025	0.025
Regenerator Matrix Porosity; void/total volume(mm)	0.0822	0.875
Heater Length (mm)	75	120
Total Number of Heater Channels (mm)	372	1068
Heater Channel Gap (mm)	1.7	1.6
Heater Channel Height (mm)	4.4	2.4
Masses		
Alternator Stationary Mass (kg)	21	46
Piston Mass Including Alternator Magnets (kg)	5	13
Displacer Mass (kg)	3	4
Total Mass of all Pressure Vessels (kg)	9	38
Cooler Area (kg)	5	10
Regenerator Mass (kg)	2	6
Heater Mass (kg)	8	20
Balance Unit Piston Mass (kg)	3	7
Total Module Mass (kg)	56	144

Volumes		
Alternator/bounce Space Pressure Vessel Volume (liters)	33	54
Balance Unit Volume External to Valt (liters)	0	3
Heat Exchanger Shroud Volume (liters)	23	59
Total Module Volume (liters)	56	116

Under the category of Concept III, several other RSU concepts were generated which apply the principles of heat pipes. Over the course of the study various arrangements were evaluated which resemble the earlier multi-heat pipe configuration pursued by the JPL (Figure 2.3b) as well as a single larger heat pipe vessel. The sodium heat pipes of the multi-pipe JPL receiver accounted for a large percentage of its total mass. Moreover, our studies indicated that as the number of individual pipes was reduced to one it became possible to meet the NASA mass goal.

The performance and size of these three concepts is summarized in Table 3.9. The Baseline Brayton is presented for comparison in lieu of a relevant Stirling design. The Stirling receivers use the 21 CaF_2 + 79 LiF eutectic PCM for thermal storage rather than LiF as planned for Advanced Brayton RSUs. This implies a Stirling cycle peak temperature of 980°K at which the engine should achieve a thermal to electric efficiency of 29%. However, the attempts to integrate the heater head, thermal storage, and receiver cavity resulted in adverse affects on engine efficiency in Concepts I and II. Only the Cavity Heatpipe Concept III avoided tampering with the 29% Baseline Stirling engine. For this and other reasons described in the following subsections, Concept III was elected for further analysis in the programs Task III (Section 5).

3.3.1 CONCEPT I: INTEGRAL WINDOWED HEATERHEAD

The Concept I attempts to integrate the Stirling heaterhead and PCM thermal storage within the receiver cavity. In Figure 3.18 the engine helium directly contacts the thermal storage container. The PCM heat exchanger wall is irradiated through a window. Stirling cycle analysis in conjunction with the heat exchanger design yielded the preliminary geometry shown in this figure. Despite numerous design iterations a set of satisfactory engine dimensions were not obtained.

Modeling data presented in Table 3.7 lists two sets of conditions which illustrate the short-comings of the concept. Unacceptable losses arose in trading the volume of the gas within the heaterhead against the frictional pressure losses in that heated space. Attempts were made to compensate for the excessive dead volume to swept volume ratio by enlarging the displacer diameter and lowering the nominal cycle pressure. In progressive increments in this direction described in Table 3.7 a low engine thermal efficiency of 21.5% resulted with considerably more engine mass than our Stirling Baseline Engine.

Due to the unacceptable impact of the RSU interface on the engine, the receiver performance issues are somewhat academic. However, it's worth mentioning that the absorber heat transfer characteristics could tolerate solar fluxes in excess of 50 w/cm^2 by design and window stresses at an engine pressure of 2000 psi (13.8 M Pa) were less than 10% of its yield strength.

STIRLING CONCEPT I

QUARTZ DOME WITH DOMED TES

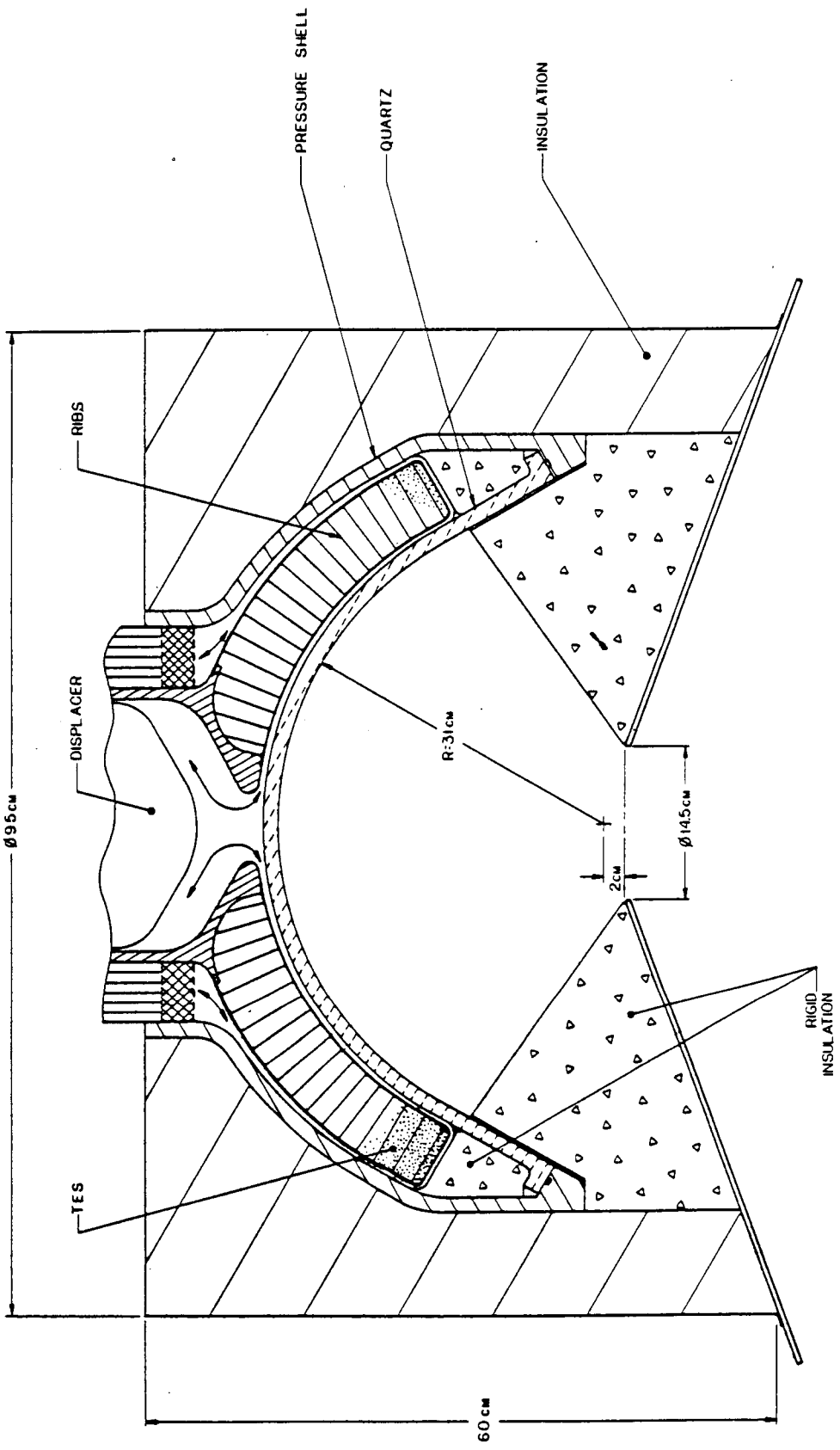

Figure 3.18

STIRLING CONCEPT II
CONCEPTUAL REPRESENTATION OF HONEYCOMB HEATER HEAD

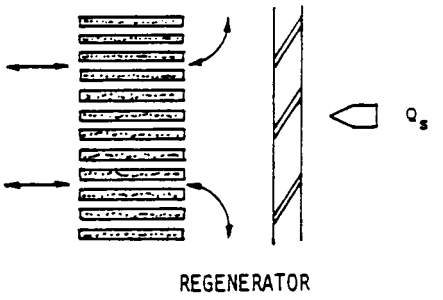

Figure 3.19

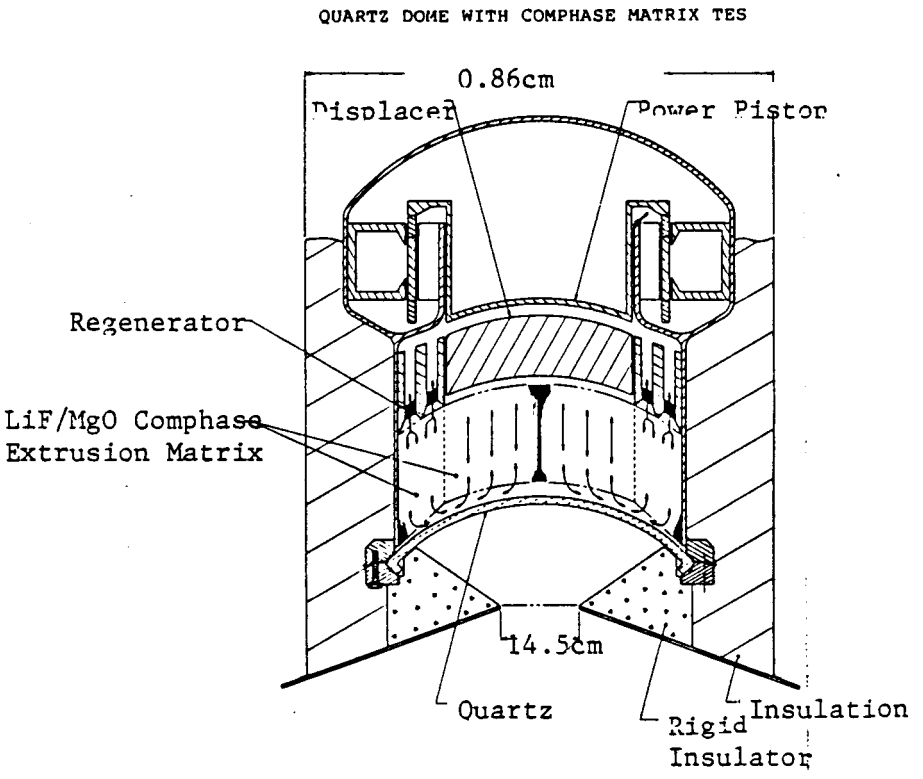

Figure 3.20

Table 3.7 Baseline and Modified Concept I Configuration

	Baseline	Concept I.1	Concept I.2
General			
Electrical Power Outlet (kW)	8	8	8
Pressure (N/m^2)	82.E5	7.5E6	4.5E6
Frequency (Hz)	152	118	90
Heater Wall Temperature (K)	1080	1080	1080
Cooler Wall Temperature (K)	540	540	540
Coordinates			
Piston Amplitude; 1/2 Stroke (mm)	7.8	7.2	6.8
Displacer Amplitude (mm)	5.7	5.3	5.0
Displacer Phase Referenced to Piston (rad)	0.785	0.785	0.785
Major Diameters			
Piston Cylinder ID (mm)	145	240	390
Alternator Pressure Vessel ID (mm)	342	490	720
Alternator Magnet Ring OD (mm)	205	315	490
Cooler Plenum Diameter (mm)	337	500	740
Heat Exchangers			
Entrance Height of Cooler Plenum (mm)	14	20	25
Tube OD for C, R and H (mm)	25	25	25
Tube Spacing BC (mm)	34	34	34
Number of Tube Assemblies (mm)	62	124	248
Cooler Length (mm)	75	95	120
Total Number of Cooler Channels (mm)	248	248	496
Cooler Channel Gap (mm)	1.7	2.3	2.9
Cooler Channel Height (mm)	4.4	6.8	5.0
Regenerator Length (mm)	24	29	38
Regenerator Wire Diameter (mm)	0.025	0.025	0.025
Regenerator Matrix Porosity; void/total volume (mm)	0.822	0.89	0.96
Heater Length (mm)	750	750	750
Total Number of Heater Channels (mm)	372	1	1
Heater Channel Gap (mm)	1.7	1270	1270
Heater Channel Height (mm)	4.4	4.0	6.0
Masses			
Alternator Stationary Mass (kg)	21	34	60
Piston Mass Including Alternator Magnets (kg)	5	17	66
Displacer Mass (kg)	3	12	50
Total Mass of all Pressure Vessels (kg)	9	14	26
Cooler Area (kg)	5	12	31
Regenerator Mass (kg)	2	5	9
Heater Mass (kg)	8	N/A	N/A
Balance Unit Piston Mass (kg)	3	8	33
Total Module Mass (kg)	56	N/A	N/A
Volumes			
Alternator/bounce Space Pressure Vessel Volume (liters)	33	100	320

Balance Unit Volume External to Alternator Volume (liters)	0	10	43
Heat Exchanger Shroud Volume (liters)	23	N/A	N/A
Total Module Volume (liters)	56	N/A	N/A

3.3.2 CONCEPT II: STIRLING COMPOSITE MATRIX HEATERHEAD RSU

Another novel integrated receiver/heaterhead concept is schematically illustrated in Figure 3.19. This concept is analogous to the previously described Brayton Concept III and builds from the successfully demonstrated principles of Sanders line of terrestrial receivers. The challenge is to incorporate the necessary quantity of PCM in the heaterhead and adequately expose it to the working gas. The small pressure, high contact area of a matrix appeared to be more conducive to the heaterhead integration than the Stirling Concept I.

The design shown in Figure 3.20 illustrates how difficult integration of the heaterhead, thermal storage, and solar receiver truly is. The volume of PCM mass is so large compared to the swept volume of the displacer that losses are inevitable. The final concept design illustrates a displacer enlarged to the diameter of the receiver cavity. This was done in attempt to improve the flow distribution and lower the critical dead volume/swept volume ratio. As in the the Stirling Concept I trade studies, the engine mass increased as the efficiency dropped. Table 3.8 presents the engine and heaterhead data obtained in the final iterations. Efficiency projections are listed in Table 3.9.

Table 3.8 Preliminary Stirling Engine Design Modifications Required for Concept II

	Baseline	Concept II
General		
Electrical Power Outlet (kW)	8	8
Pressure (N/m^2)	82.E5	20.E5
Frequency (Hz)	152	60
Heater Wall Temperature (K)	1080	1080
Cooler Wall Temperature (K)	540	540
Coordinates		
Piston Amplitude; 1/2 Stroke (mm)	7.8	10
Displacer Amplitude (mm)	5.7	10
Displacer Phase Referenced to Piston (rad)	0.785	0.785
Major Diameters		
Piston Cylinder ID (mm)	145	360
Alternator Pressure Vessel ID (mm)	342	720
Alternator Magnet Ring OD (mm)	205	470
Cooler Plenum Diameter (mm)	337	510
Heat Exchangers		
Entrance Height of Cooler Plenum (mm)	14	50
Tube OD for C, R and H (mm)	25	25
Tube Spacing BC (mm)	34	34
Number of Tube Assemblies (mm)	62	90
Cooler Length (mm)	75	95

Total Number of Cooler Channels (mm)	248	130
Cooler Channel Gap (mm)	1.7	5.0
Cooler Channel Height (mm)	4.4	5.0
Regenerator Length (mm)	24	20
Regenerator Wire Diameter (mm)	0.025	0.025
Regenerator Matrix Porosity; void/total volume (mm)	0.822	0.97
Heater Length (mm)	75	400
Total Number of Heater Channels (mm)	372	150
Heater Channel Gap (mm)	1.7	7.0
Heater Channel Height (mm)	4.4	10.0
Masses		
Alternator Stationary Mass (kg)	21	85
Piston Mass Including Alternator Magnets (kg)	5	56
Displacer Mass (kg)	3	38
Total Mass of all Pressure Vessels (kg)	9	8
Cooler Area (kg)	5	9
Regenerator Mass (kg)	2	2
Heater Mass (kg)	8	N/A
Balance Unit Piston Mass (kg)	3	28
Total Module Mass (kg)	56	N/A
Volumes		
Alternator/bounce Space Pressure Vessel Volume (liters)	33	300
Balance Unit Volume External to Valt (liters)	0	34
Heat Exchanger Shroud Volume (liters)	23	N/A
Total Module Volume (liters)	56	N/A

3.3.3 CONCEPT III: STIRLING CAVITY HEAT PIPE

During the investigation of Stirling RSUs many configurations founded on the principals of heat pipes were postulated. Multitubular configurations such as that proposed by GE (Ref 7, Figure 2.3) were ruled out from weight and volume considerations in initial trade studies. With the goal of minimizing size and weight, this study focused on the application of a single large heat pipe. Some of the forms analyzed are presented in Appendix G. Among these were cylindrical and conical receiver cavities where the sodium working fluid was contained in an annular volume behind the solar absorber.

The final concept shown in Figure 3.21 incorporates a near hemispherical dome functioning on the solar absorber and the sodium-wicked evaporator. Vapor generated from this surface will simultaneously condense on PCM modules and the heater head heat exchanger elements located within the sealed vessel. This concept effectively decouples the stringent thermodynamic and stress requirements of the absorber, PCM containers, and heater head. In the previously discussed Stirling concepts I and II, it was this integration which placed unacceptable design constraints on each of the three heat exchangers. A detailed discussion of the final CHP design is presented in Section 5.0.

3.3.4 SUMMARY OF THE NEW STIRLING RSU CONCEPTS

Cavity Heat Pipe Stirling Receiver

WITH FINNED TUBE/SHELL HEATER HEAD

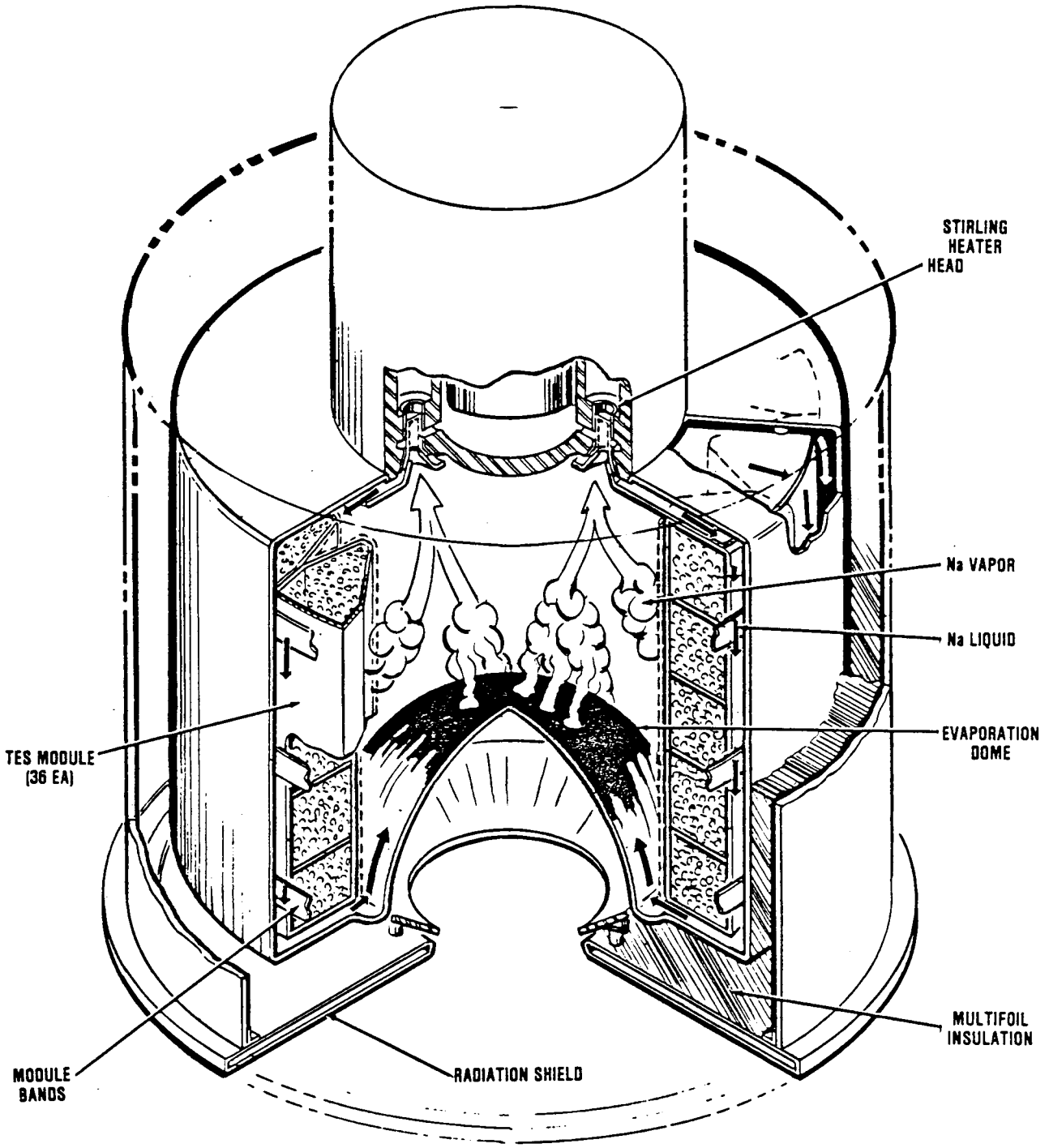

ORIGINAL PAGE IS OF POOR QUALITY

Figure 3.21

The new Stirling RSU concepts studied in Task II of this program can be divided into two categories: those which attempted to integrate the heater head and RSU and those which employed a heatpipe. When considering integration of the heater head with the RSU it is necessary to model the engine cycle in conjunction with the heaterhead design. This combined Stirling cycle RSU analysis was accomplished for two concepts. The conclusion of this work is that 7 kWe (or greater) LEO integrated Concepts I and II are not feasible. Receiver efficiencies as shown in Table 3.9 are in an acceptable range, however, the engine efficiency was shown to drop 7 or more percentage points. In comparison, the CHP concept produced no detrimental engine effects. Also as shown in Table 3.9 the complete engine/ RSU package is smaller despite the separation of the heater head and receiver.

Table 3.9 Performance Summary of Stirling Concepts

Parameter	Concept I	II	III	Baseline
Cavity Diameter (M)	.62	.60	.28	1.35
Overall Diameter (M)	.95	.86	.546	1.65
Overall Length (M)	.60	.44	.457	1.54
Exterior Surface Area (M^2)	3.21	2.35	1.25	12.2
Insulation Losses (kW)	0.65	0.47	.25	3.3
Day Cavity Losses (kW)	0.845	0.783	1.13	1.89(4.78)
Mean Cavity Temp (^0K)	1058	1048	1049	1142(1440)
Night Cavity Losses (kW)	.726	.756	1.09	1.86
Mean Cavity Temp (^0K)	1030	1038	1039	1138
Reflection Losses (kW)	1.3	1.3	0.90	1.52
Shading Losses (kW)	0.97	0.80	0.41	2.43
Total RSU Losses(Thermal) (KJ)	16,222	14446	12,370	44,960(55191)
Total RSU Efficiency (%)	89.5	90.5	91.7	76.5(71.2)
Mean Working Fluid Temp (^0K)	980	980	980	1089
Engine P/P Losses (%)	16.8	3.9	0	2.0
Engine Efficiency	21.5	16.2	29	27.0
RSU Specific Mass (kgm/kW)	15.4LiF	21.6LiF	26.7	76.6

* Figures in parentheses indicate the potential effects resulting from an adverse void location PCM container. Baseline losses derived for Reference 3.

4.0 ANALYSIS OF SELECTED BRAYTON CONCEPTS (TASK III)

NASA's Advanced Heat Receiver Conceptual Design Study (AHRCDS) Program and several Sanders Internal Research and Development (IR&D) projects have evaluated many RSU design candidates, and have developed an innovative RSU design concept for Brayton and Stirling engines that will meet or exceed NASA's program goals. Sanders proposes the Direct Absorption Receiver (DAR) described in Section 4.1 for the Brayton and the Cavity Heat Pipe (CHP) receiver storage unit for the Stirling as described in Section 4.4. Sections 4.2 and 4.5 present comparisons of each of these advanced designs with the Baseline.

4.1 SANDERS DIRECT ABSORPTION RECEIVER (DAR) DESIGN

This section describes our proposed receiver design. Key features are summarized as follows:

- Achieves a total volume one-sixth that of Baseline
- Achieves a total mass less than one-half that of Baseline
- Eliminates thermal ratcheting problems since the PCM is unconfined by heat transfer walls, thus improving system reliability
- Eliminates formation of PCM voids which can reduce efficiency
- Achieves parallel heating of PCM and engine working fluid to maximize flux tolerance
- Achieves efficient charging of PCM through selective doping to tailor its solar absorption.
- Reduces the length of weld exposed to the LiF to 0.6% of Baseline to reduce cost and increase reliability.

In the preceding description of Baseline receiver technology, the distinction was made between series and parallel heating of the engine working fluid and the PCM. The low thermal conductivity of the PCM, further reduced by void formations, severely limits the solar flux that the series heating configuration can absorb. The thermal circuit in Figure 4.1 illustrates a parallel conductive/not diathermy heating arrangement. This concept significantly reduces the thermal impedance of the PCM by exploiting the radiating absorption characteristics of LiF. Simultaneously, a portion of the incident solar power is absorbed on the working-fluid-cooled heat exchanger wall.

Figure 4.2 illustrates the DAR configuration. A corrugated cone forms the inner cavity wall and serves as the PCM to working fluid (HeXe) heat exchanger. Capillary forces suspend the LiF in these corrugated channels on the inside cavity surface. The Brayton working fluid flows from a torroidal plenum at the aperture end of the cavity over the outside of the corrugated heat exchanger and exits through an axial discharge duct.

The solar energy enters the cavity through a windowed aperture and is partially absorbed in the LiF. Although pure LiF is almost entirely transparent to the solar spectrum, by doping the LiF with small

Parallel Heating of PCM Has Advantages Over Series Heating

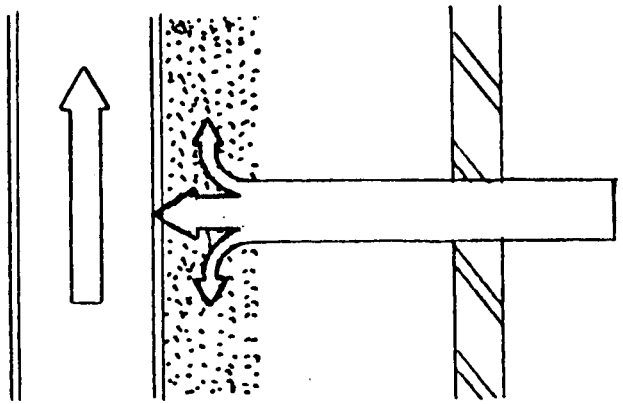

PARALLEL HEATING IN DAR

- Very High Flux Capacity 12 to 15 W/cm^2 Due to direct absorption
- Potentially Eliminates Thermal Racheting Problems as PCM is Unconfined
- Δ V/V Voids Cannot Inhibit Solar Heat Heat Transfer to the HeXe and the PCM

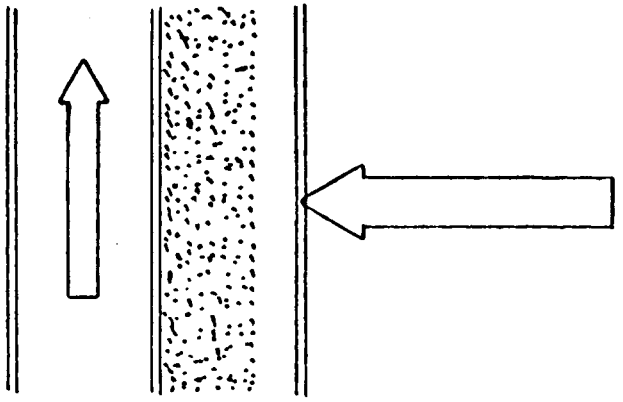

SERIES HEATING IN BASELINE

- Low Flux Capacity 3 to 5 w/cm^2 Due to Low Conductivity PCM
- Thermal Racheting Stresses Imposed on Container
- Voids Impede Heat Transmission to Working Fluid

Figure 4.1 Brayton Direct Absorption Receiver (DAR) Concept

Direct Absorption Brayton Receiver

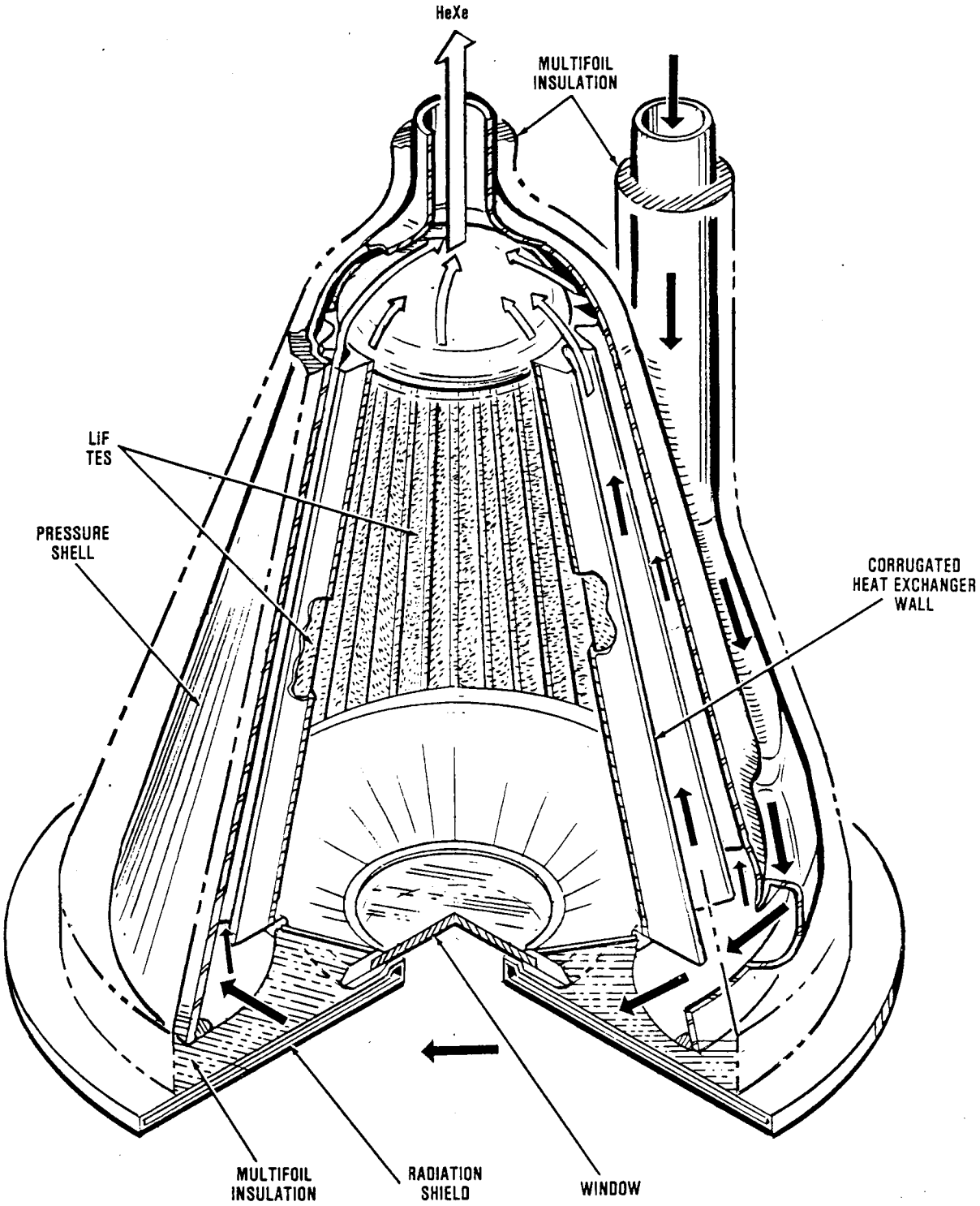

Figure 4.2a Direct Absorption Brayton Receiver

Direct Absorption Brayton Receiver

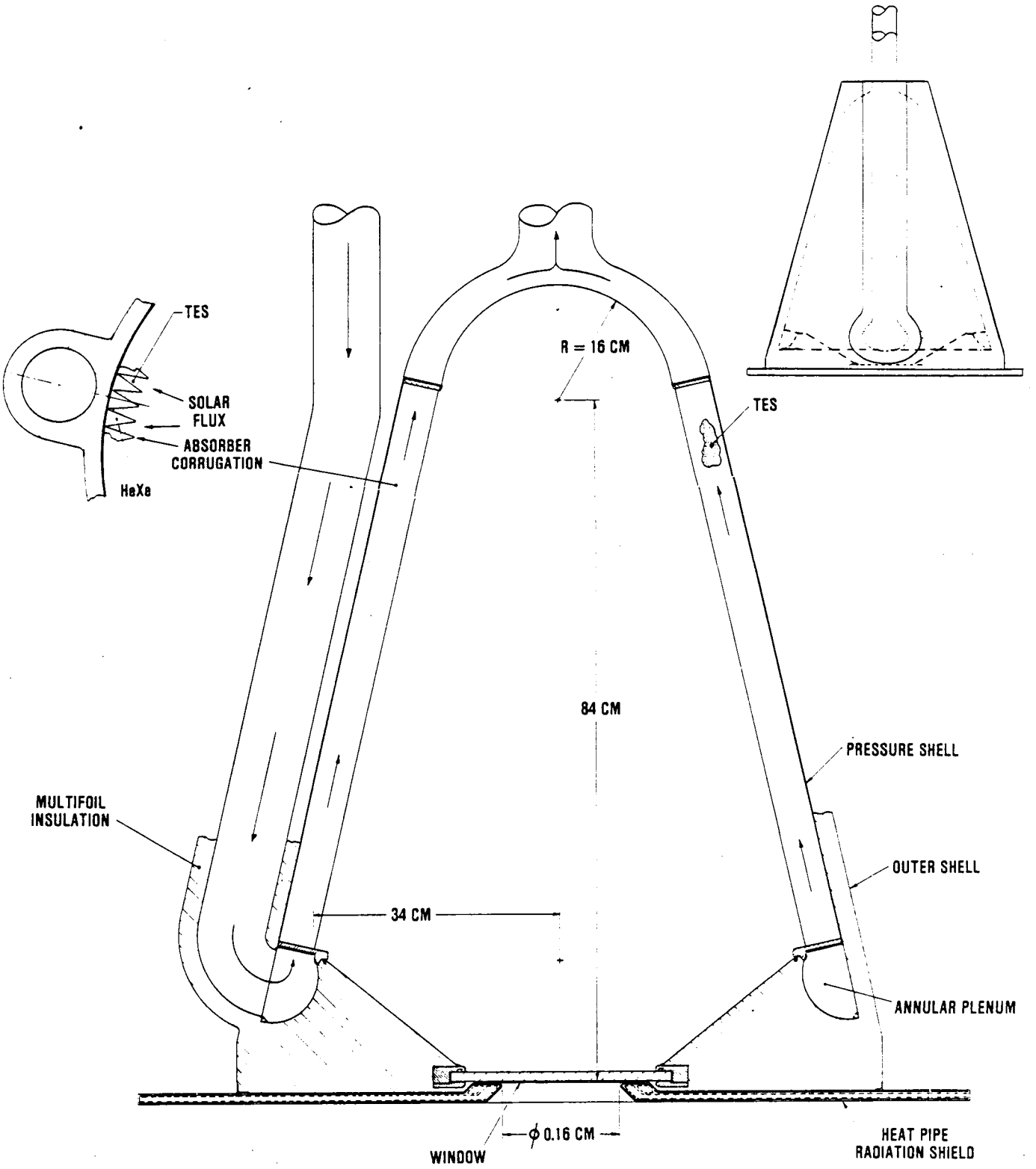

Figure 4.2b DAR Layout Drawing

percentages of rare earth or transition metals, it is possible to tailor the absorption coefficient for optimum thermal charging conditions. A list of candidate doping agents is categorized in Figure 4.3 relative to the spectral bands affected. Nearly complete absorption in these wavelengths can be obtained with less than 2% doping. Ideally, the PCM may be melted volumetrically by nominally 40% of the solar flux while the remaining 60% penetrates directly to the corrugated heat exchanger wall. Absorbing the solar energy directly into the PCM, without the impedance of an opaque envelope, has several important advantages as outlined in Table 4.1 and described in the following paragraphs.

Parallel heating of the heat exchanger wall and the PCM provides the potential to greatly increase the operating solar flux levels. Since both the Sanders DAR and GE Baseline designs utilize conical cavities, it is possible to compare the flux levels on the imaginary conical surface of the nominal cavity dimensions. In this comparison, the 2 to 3.5 W/cm^2 peak incident Baseline flux levels are increased by about a factor of 6 in the Sanders DAR design. This results in a decrease in cavity diameter by a factor of 2.4 and hence a much smaller RSU.

Table 4.1. KEY DESIGN FEATURES OF DAR

	NASA GOALS			
DESIGN FEATURES OF DAR	LOWER SIZE AND MASS	HIGHER EFFICIENCY	LESS DV/V STRESS	RELIABILITY
Increased Operating Flux Levels to Shrink Cavity/RSU	X	X		
Eliminates Opaque Absorber Wall in Baseline	X		X	X
Eliminates Need for Metal Mesh Conductivity Enhancement	X			X
Uses Annular Plate-Fin HX to Eliminate Tube Shell Manifold	X	X		
Decreases Absorber Wall Temp		X		X

Significant efficiency improvements in the DAR are achieved by reducing the receiver exterior surface area. This has been determined to be less than 30% of the surface area of the Baseline receiver assuming the same insulation thickness. We have also calculated the average radiating temperature of the cavity to be very nearly that of the LiF melting point. Baseline cavity temperature, at best, is about 20°C higher, and

ABSORPTION BANDS OF CANDIDATE TRANSITION METALS IN LiF

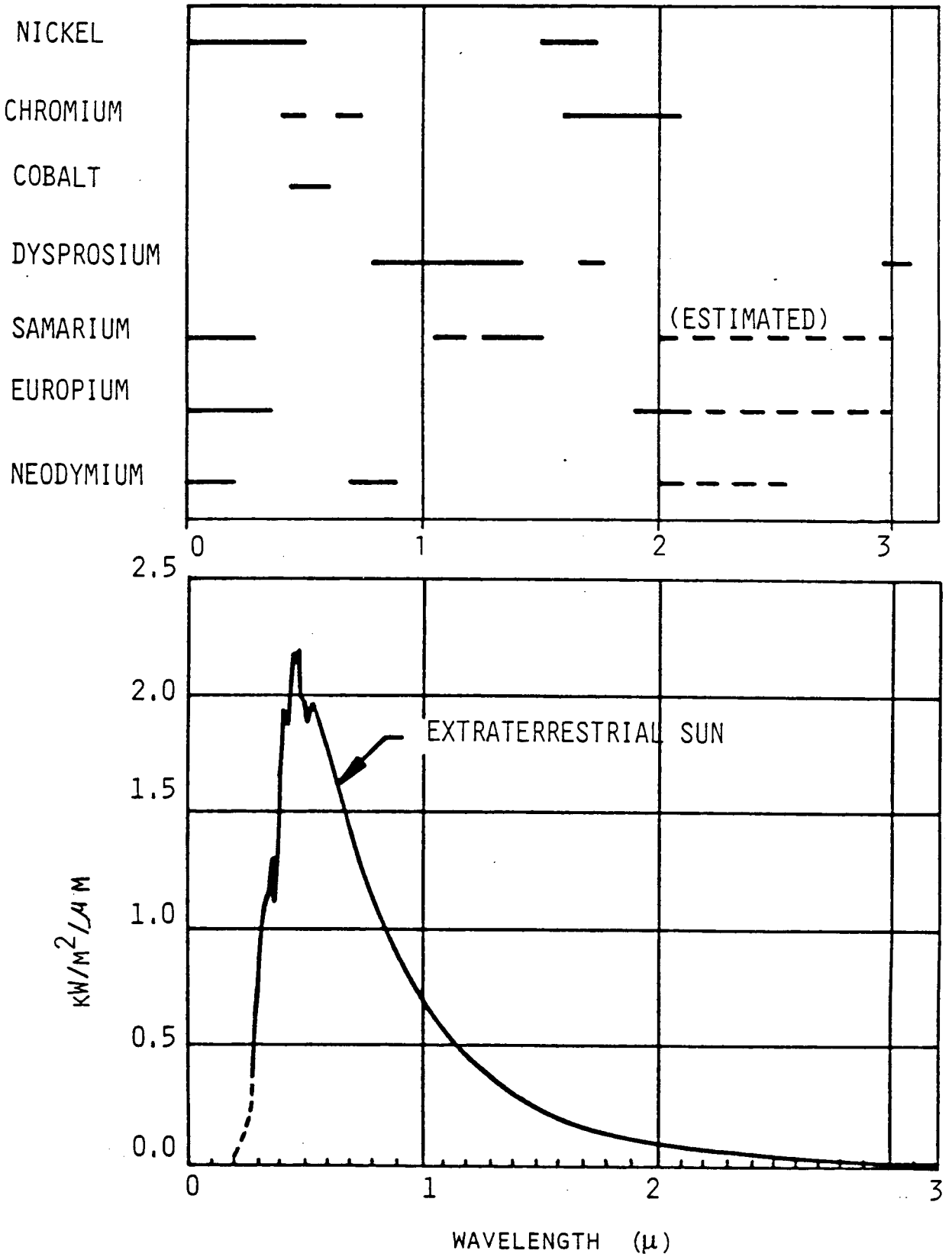

Figure 4.3 Candidate Doping Agents

with a maldistribution of voids could peak at as high as 320°C above the LiF melting point resulting in higher re-radiation cavity losses. Moreover, the Baseline produces a lower mean working fluid discharge temperature which also penalizes the engine. These comparisons are discussed more thoroughly in the following sub section.

4.2 COMPARISON OF ADVANCED DAR AND BASELINE RSU's

Having presented descriptions of both the Baseline Brayton and the DAR, it was the requirement of our program to perform a detailed comparison of these competing designs. At this point in the program the Baseline design has been slightly altered to conform with recent information made available on the Space Station Receiver (Reference 8). The previous comparison was based on the NASA GE receiver (Reference 2,3). The following subsections address the key technical issues that represent NASA's highest priorities.

4.2.1 MASS AND SIZE COMPARISONS OF BRAYTON RSUs

Figure 4.4 illustrates the envelope dimensions of these designs and Table 4.2 lists their envelope dimensions. Two differences between the Sanders DAR and the other designs are immediately evident. Not only is the Sanders DAR one-sixth the Baseline volume, but it utilizes a conical rather than a cylindrical cavity. The cylindrical cavity of the Baseline was likely motivated by a concern to reduce the fabrication complexity. With the cylindrical configuration it is possible to have all 5852 PCM canisters alike.

However, the choice of a cylindrical cavity is not optimal from a size or performance standpoint. The conical cavity allows for the storage mass to be proportionated throughout the cavity in a manner more consistent with the flux distribution. With the cylindrical PCM distribution it is necessary to include

Table 4.2. RECEIVER ENVELOPE DIMENSIONS

RECEIVER DIMENSION	BASELINE	SANDERS DAR
Diameter (m)	1.146	0.840 (.358 top)
Length (m)	2.08	1.080
Surface Area (m^2)	9.55	2.84
Volume (m^3)	2.15	0.354

excess PCM at the upper end of the Baseline cavity which, coupled with series heating, results in a a requirement for approximately 15% more PCM than the DAR.

As presented in Table 4.3, the DAR concept achieves most of its weight advantage from the reduction of PCM containment metal. This is attributable to the elimination of the absorber surface and the inherent compactness of the plate-fin heat exchanger.

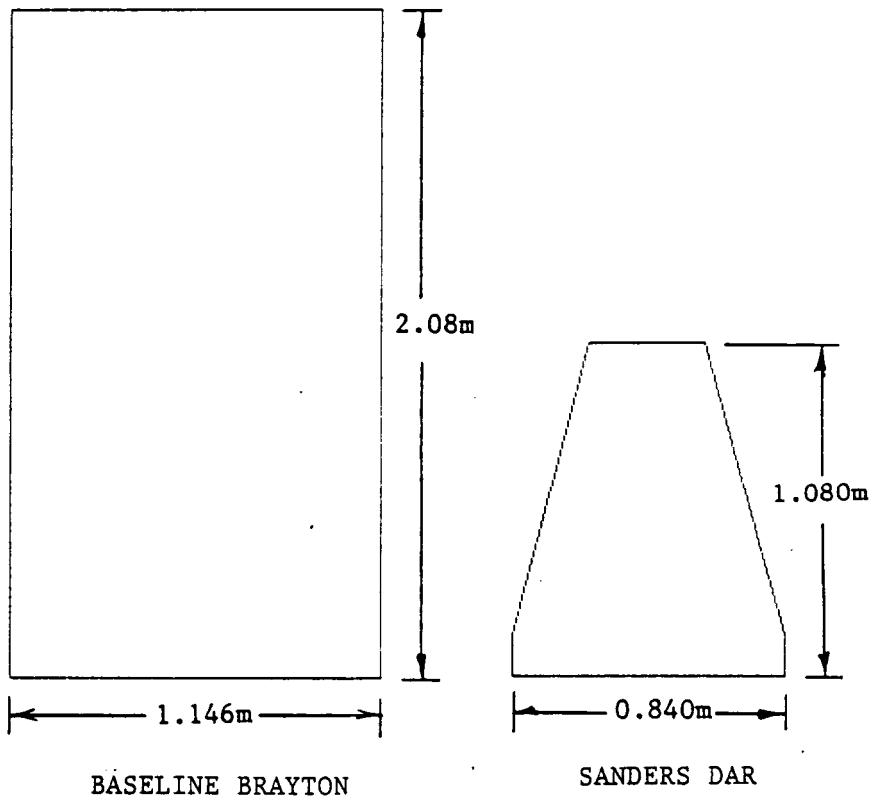

Figure 4 . 4 Brayton Receiver Size Comparisons

Table 4.3. BRAYTON RECEIVER MASS COMPARISONS

RECEIVER COMPONENTS	BASELINE (Kg)	SANDERS DAR (Kg)
PCM	70	60
Absorber/ PCM Containment	150	73
Aperture Shield		22
Manifolds		12
Multifoil Insulation		11
Outer Shell		16
Baffles/Supports		14
Misc	242	4
Total	461	212

Finally, as part of this discussion on mass and size, it should be pointed out that the final figures presented for the DAR are believed to be conservative. In performing our stress analysis, we have considered a set of worst case conditions which results in a thicker, more massive corrugated heat exchanger to achieve 10 year creep life for Cb-1Zr. For example, we design for peak solar absorption that is twice the theoretical level. Realistically, the peak zones will be significantly reduced by internal cavity reflections. In performing the more detailed final thermal and stress analysis, we expect to optimize the geometry to achieve an even lower mass.

4.2.2 EFFICIENCY COMPARISONS OF BRAYTON RSUs

Projections for the various energy losses within the RSU are listed in Table 4.4. Efficiency improvements are achieved by reducing thermal, fluid mechanic, and thermodynamic energy loss mechanisms.

Table 4.4. COMPARISON OF RSU EFFICIENCY FACTORS

PARAMETER	SANDERS DAR	BASELINE BRAYTON
Insulation Losses (kW)	0.76	2.57
Day Cavity Losses (kW)	1.37	1.89
Mean Cavity Temp (^{o}K)	1120	1142

Night Cavity Losses (kW)	1.17	1.86
Mean Cavity Temp (^{o}K)	1080	1118
Reflective Losses (kW)	2.50	1.1
RSU Shading Losses (kW)	0.95	1.41
Total RSU Thermal Losses (MJ)	23.8	34.0
Receiver Thermal Efficiency (%)	86.0	81.1
Mean Working Fluid Temp (^{o}K)	1120	1089
Carnot Efficiency Gain (%)	2.8	0
RSU Pressure Drop (%)	1.0	2.0
Brayton DP Losses (kW)	1.35	2.69
Cycle Efficiency Gain (%)	5.2	0

Thermal efficiency improvements occur primarily due to the large reduction in exterior surface areas, so that the greatest source of thermal loss in the Baseline is reduced by 70% in the DAR. To obtain consistency between these values, we have assumed the same insulation thickness and thus simply scaled the exterior surfaces to acquire our heat loss estimate.

The same relative scaling approach is employed to estimate cavity losses on a consistent basis. In this case, we had to scale up the Baseline value based on what we considered to be a more realistic aperture diameter. The windowed DAR cavity, however, performs quite differently than the open Baseline aperture. The window impedes the exiting cavity radiation while also reflecting away a small percentage of the incident solar energy. For this reason, the night time performance of the cavity is better for the DAR, while the day performance is somewhat worse. Overall, the combined radiation-reflection losses do not provide significant advantage to either configuration.

It should also be noted that there is considerable controversy over the approach used to predict the Baseline cavity temperatures. Independent researchers at Oak Ridge National Labs (ORNL) (Ref. 9) have estimated higher absorber surface temperatures than used in Table 4.4. The principal discrepancy involves the prediction of the PCM void location.

The Carnot efficiency effect referenced in Table 4.4 presents an additional advantage of the direct absorption concept. Parallel heating of the PCM and absorber wall as achieved by Sanders' DAR design results in immediate thermal response of the working gas at sunrise. The Baseline approach, however, suffers from a prolonged thermal droop at this time because of the large impedance between the absorber wall and the working gas. This droop results in a further degradation of the engine performance, not accounted for as an RSU inefficiency in Table 4.4. This table is based on our analytical prediction that the working gas temperature of the DAR will oscillate within $\pm 15^{o}$K about the LiF melting point (1121^{o}K). In contrast, the Baseline receiver, at best, operates between 20 and 50^{o}K below the LiF melting point. Therefore, a 2.8% improvement in the Carnot efficiency of the cycle is achievable with our proposed approach.

Improvements in RSU pressure losses are shown in Table 4.4 to be relatively significant. Our calculations are based on reducing the pressure drop from 2% (of the total pressure) to 1%. This is not simply an arbitrary goal, but reflects a typical advantage of the plate-fin heat exchanger over a tube-shell configuration. A plate-fin configuration, in general, will exhibit a higher number of transfer units (NTU) per unit pressure drop than a tubular heat exchanger, particularly when manifolds are included. The DAR achieves one additional advantage by utilizing the conical convergence of the corrugations to accelerate the hot gas into a common axial discharge plenum. Alternatively, the cylindrical tubular configurations must include a torroidal discharge manifold, which complicates the circumferencial flow distribution problem while adding pressure drop.

4.2.3 RELIABILITY FACTOR COMPARISONS OF BRAYTON RSUs

The major factors affecting reliability of the Brayton solar receiver are stress and corrosion effects. To achieve the ten-year design, both RSU's are proposed to use a niobium alloy for the hot containment vessel material. These alloys, which typically contain 1% Zr, provide adequate resistance to the embrittlement caused by trace oxygen contamination.

Welding, however, can adversely affect the resistance of the niobium alloys to the PCM material and oxidation. The welding process itself can produce chemical changes which reduce the alloy's resistance to oxygen contamination and PCM corrosion. Faults in the heat affected zone of the weld can develop due to the constant exposure of the containment vessels to the PCM material and to large thermal gradients. Over the ten-year design life of the Brayton receiver we postulate that leakage is more likely to develop in a weld area than in any other part of the containment vessel.

High surface tension salts are notoriously difficult to seal and leak-test, while weld sites promote corrosion. To minimize corrosion and potential system failure, Sanders has reduced the length of weld exposed to the PCM material to approximately 0.6% of our competitors' designs (see Table 4.5). Further improvements in DAR reliability over competing designs are provided in three ways. First, the corrugated cone containment vessel used for the Sanders DAR design provides easy access to both sides of the welded joint for inspection. Second, the containment vessel is designed so that the welds on each end of the cone will be coated with a non-wetting substance (pyrolitic boron-carbide or pyrolitic graphite). This will keep the LiF from wetting the weld zone. At the request of Sanders, NASA has performed a compatibility analysis of the non-wetting materials. In a 500 hour test, no chemical changes were observed. Finally, additional reliability can be achieved by adding redundant top and bottom rings on each end of the cone, if later desired. These redundant walls will increase the reliability of the welded joints while only increasing the receiver weight by an estimated 5 kg.

Table 4.5. LiF EXPOSED WELD COMPARISONS FOR BRAYTON RECEIVER DESIGN

RECEIVER DESIGN	LENGTH OF EXPOSED WELD (M)
Baseline	1306 structural +508 fins
Sanders DAR	11

We also believe that the DAR design provides increased reliability in other less quantifiable ways. The effect of thermal ratcheting and DV/V mechanical stresses is difficult to predict over the required ten-year operational life. However, the DAR alleviates most of these concerns observed in other designs with two unique features. These are volumetric solar absorption which more uniformly softens the rigid PCM crystal, and the non-confining configuration of the corrugated wick. By causing melting to occur throughout the PCM volume with a tailored absorption coefficient, the ability of the LiF to impose expansion stresses on the heat exchanger wall is greatly reduced. Additionally, since there is no confining wall, the liquefying PCM is free to expand.

The space environment also presents several hazards for which long-term effects are not known, such as the attack of atomic oxygen and the prolonged vacuum affects on metal alloy constituents. In this regard, we believe that the DAR limits these risks by isolating the high temperature cavity elements with the window. By isolating the refractory metals from these potential degradation factors, we have increased their life. The window is exposed to this environment, but it does not require significant strength. Moreover, most of the window substrata candidates have already demonstrated excellent stability in this environment. For example, oxide thin-film coatings applicable to all window candidates have been proven to be inert in this environment by Lockheed and others. Conversely, Haynes 188 and the columbium alloys display a susceptibility to chromium sublimation and atomic oxygen degradation.

4.2.4 FABRICABILITY AND COST COMPARISON

The preliminary design studies of all LiF/Brayton RSUs, including the Sanders DAR concept, indicates a requirement for refractory metals. For this reason, fabricability must be considered as a potentially key technical issue because of cost and risk associated with machining, forming, welding, weld inspection, heat treating, and special tooling. All of these factors were considered during DAR design with consultation with Teledyne Wah Chang. This study indicates that the DAR design will result in a much less costly development and production program than the Baseline.

The previous reliability discussion pointed out that the Baseline Brayton RSU requires approximately 1.8 kilometers of weld length in contact with LiF. This is compared to only 11 meters for the Sanders DAR. These figures are used for comparison because these welds are considered to be the most critical and involve refractory metals. The non-exposed welds for manifolds and ducting have been excluded because of the lack of details for competing designs. However, our studies show that again the DAR holds a significant cost advantage over the multi-tubular approaches.

It is also important to note that the DAR weld length is composed of two simple welds conducted in two separate operations. The alternate designs can also claim that each weld is a relatively simple problem. However, there are a great number of them. For the Baseline PCM canisters alone there are over 40,000 separate weld steps in the fabrication of the doughnuts alone. These operations, to be considered at all feasible, must be highly automated. This new facility would not only have to perform the welding, but must also handle the LiF to maintain the highest purity standards. ORNL has outlined some rather elaborate procedures for avoiding contaminating the LiF and advocates the addition of a small percentage of alkali metal to the PCM. This surplus alkali metal (Na or Li) serves as an active getter and is needed to ensure long-term high temperature compatibility. This is not being conducted for the IOC space station unit because of the lower operating temperature and hence, lower reaction kinetic, but is strongly recommended for LiF/refractory metal systems.

The ORNL process involves a first step where the alkali metal is purified in the liquid state. Next, this liquid must be injected into the low pressure LiF container through a snorkel valve. To allow this process to occur, the LiF module must be maintained at a temperature at or above the metal's melting point. This demands highly refined processes. To consider mass production on the order for thousands of components implies a major investment in technology and facilities.

The Sanders DAR design, on the other hand, requires only one filling procedure step. The laboratory quality solid LiF material would be loaded from a glove box into the upward facing receiver aperture. The aperture flange would be sealed with metal "o-rings" to a port at the base of the glove box. The glove box and receiver cavity chamber may be either evacuated or back-pressured with argon or reducing (HF) atmosphere. Alternatively, if a distilling procedure is required, the liquid metal charging, although elaborate, must only be performed once.

We also believe the Sanders DAR has other fabricability advantages. Both tubular heat exchanger designs involve large fixtures for welding the tubes and manifolds. The DAR heat exchanger is formed from a single corrugated sheet. Our proposed subcontractor, Teledyne Wah Chang, regards forming the refractory metal skirt to be a standard and relatively inexpensive process. This is emphasized by Teledyne Wah Chang's price estimate for the entire RSU refractory metal (Cb-1Zr) assembly, consisting of the corrugated heat exchanger, integral conical vessel, and all manifolds and ducting for under $50,000, including nonrecurring tooling (approx. $20,000).

Figure 4.5 shows an exploded view of the DAR and illustrates the straightforward assembly. We believe the low part count and minimal tooling requirement will yield a very cost-effective prototype and final production module.

4.3 DISCUSSION OF CRITICAL BRAYTON TECHNICAL ISSUES

Advancement of any technology demands experimental verification of novel concepts. We have identified three critical subjects requiring experimentation to define the detailed DAR design and reduce programming risk:

ELEMENT	REQUIREMENT
PCM liquid control	Confinement of PCM to heat exchanger corrugations in micro-gravity.
Window	>95% transmissivity for 10 years.
PCM Absorptivity	Dope LiF to optimize direct absorption

A major difference between the Sanders DAR and other RSUs is that the PCM volume is small compared to its container volume. The single, large DAR container utilizes surface tension forces to control the liquid PCM location within the cavity. Although the problem of liquid management is new to solar dynamics, it is not new to other space-based systems such as fuel tanks and water handling systems.

Direct Absorption Brayton Receiver

(Component Breakdown)

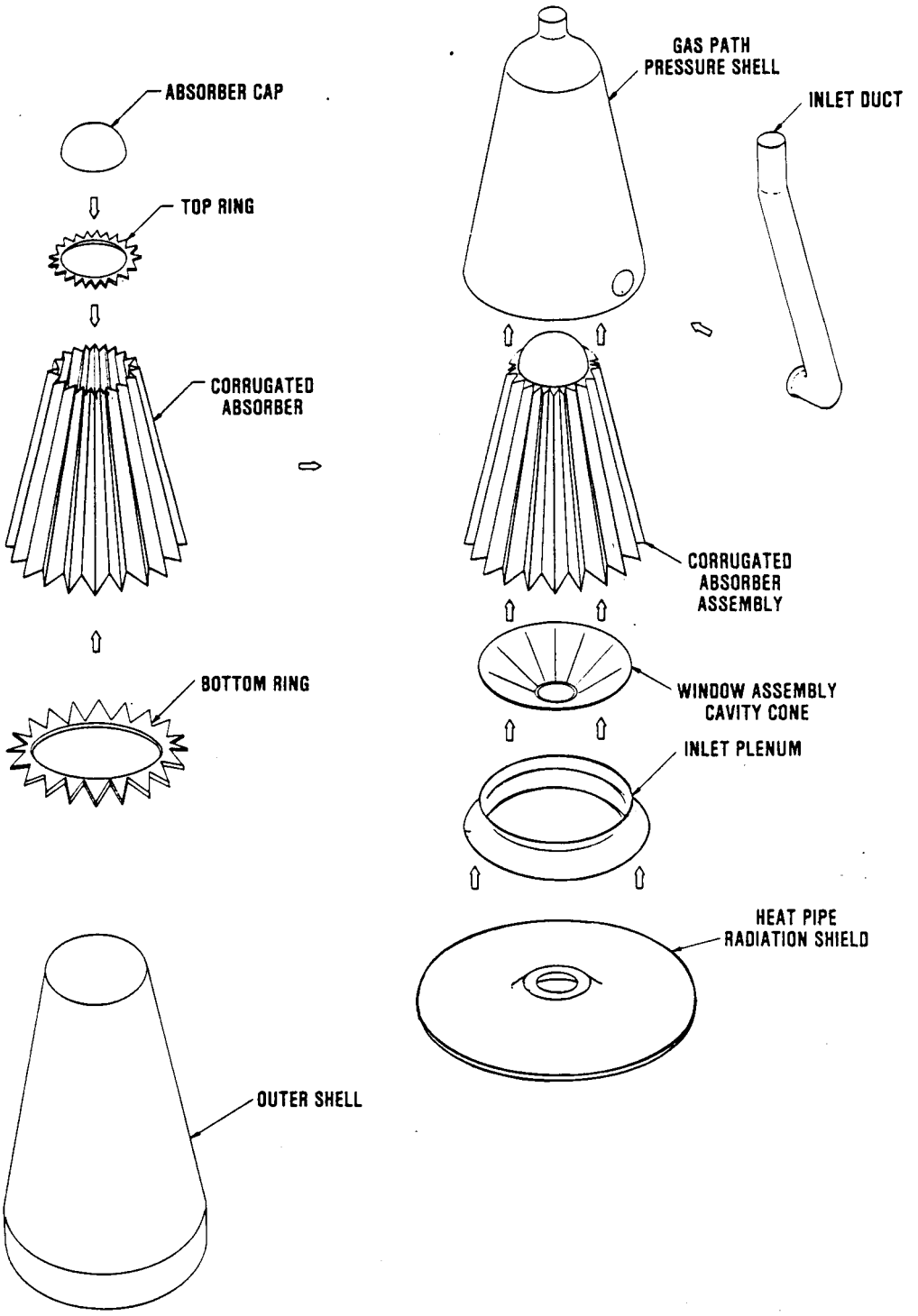

Figure 4.5 Brayton DAR Component Breakdown

The transparent window is required to contain the small but significant vapor pressure of LiF in the solar cavity. Without this window the vapor would escape at a rate of approximately 50 Kg/yr through the 16cm diameter aperture (7kWe). This represents an unacceptably large mass loss. The incorporation of a solar transparent window solves this problem but raises issues of long term corrosion compatibility with LiF. We set as our goal that the solar transmissivity remain above 95% for the 10 year operating period. However, due to efficiency gains in other areas, a transmissivity of only 90% would still result in a net energy efficiency for the DAR equal to that of baseline RSU.

While the IOC Baseline receiver performance is limited by the low thermal conductivity of the PCM and its container walls, the DAR is directly thermally charged, radiatively. The absorption coefficient of LiF in its single crystal of its liquid phase is very low over the solar spectrum as illustrated by Figure 4.6. Doping of the LiF with selected transition metal-fluorides provides a means for tailoring its absorption coefficient to optimize the percentage of incident solar energy absorbed by the LiF. The bulk absorption sought for low earth orbit system is in the range of 40 to 70% of incident power. The concentration of the dopant must remain small so as to not influence the PCM melting point.

The following paragraphs discuss in more detail these three issues and our progress to date. Section 5, Critical Technical Experiment Recommendations, describes our planned experiments and analyses to resolve these fundamental challenges.

4.3.1 LIQUID PCM DISTRIBUTION AND CONTROL

With the residual effects of earth's gravity less than 10^{-6}G, other normally subtle forces emerge to control the distribution of liquid. On the space station, there may be small gravity gradient forces depending on the location with respect to the structure's center of mass. Also, on-board accelerations such as the firing of small rockets and astronaut movement result in "random noise" on the order of 10^{-3}G.

In the DAR, like most space-based liquid management systems, surface tension is the dominating force affecting liquid distributions. In typical terminology, a "wick" effect is used to control the liquid.

The liquid PCM in the DAR has been designed to be quasi-statically confined to the corrugated heat exchanger wall. Some minor movement of the liquid due to thermal gradients and the tapered channel geometry is not likely to be significant. As illustrated in Figure 4.2, the corrugated absorber geometry of the gas side heat exchanger also serves as a suitable PCM wick. Preliminary analysis indicates that the design requirements for gas to PCM primary heat transfer area inherently provides a geometry with more than enough liquid PCM suspension force. For example, the thermal analysis was conducted with a corrugation spacing of 4cm at the widest point in the cavity tapering to 1cm at the discharge end. This provides a minimum capillary pressure of approximately 6 N/M^2, capable of retaining the PCM against a normal acceleration of more than O.1g; two orders of magnitude above the background forces.

In addition to the requirement for wicking surfaces within the cavity, there must also be non-wetted areas. Several low surface energy materials have been identified for this application. Graphite is a common material for handling molten fluorides in commercial crystal manufacturing facilities such as those at Sanders. The photograph in Figure 4.7 of solidified LiF in our test crucible illustrates the high contact angle indicative of the non-wetting condition.

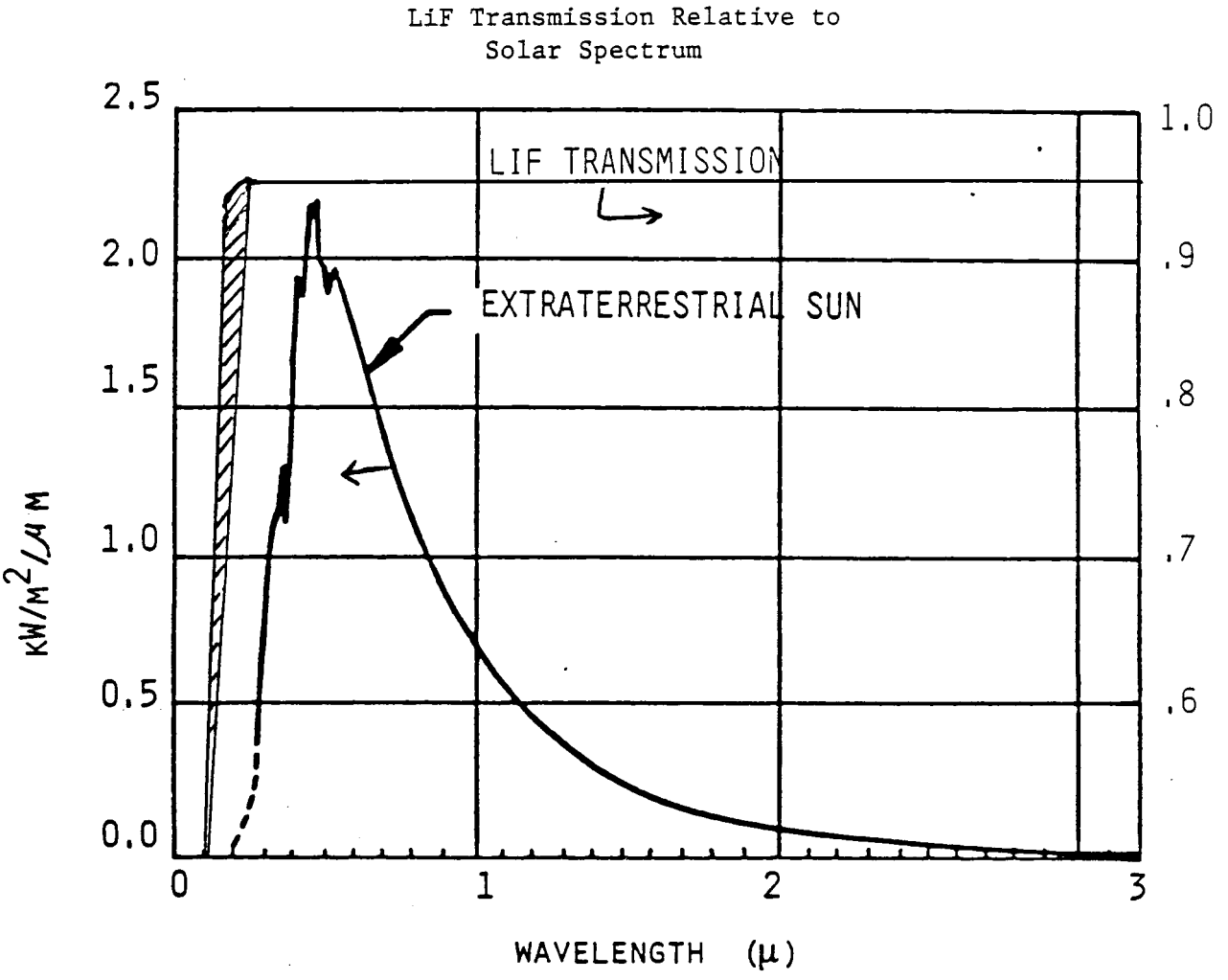

Figure 4.6

The only nontransmitted component of the solar spectrum is the result of Fresnel reflections (2.6%/surface) (Ref.1). Absorption is essentially zero out to about 6 microns for a 1 cm thick sample.

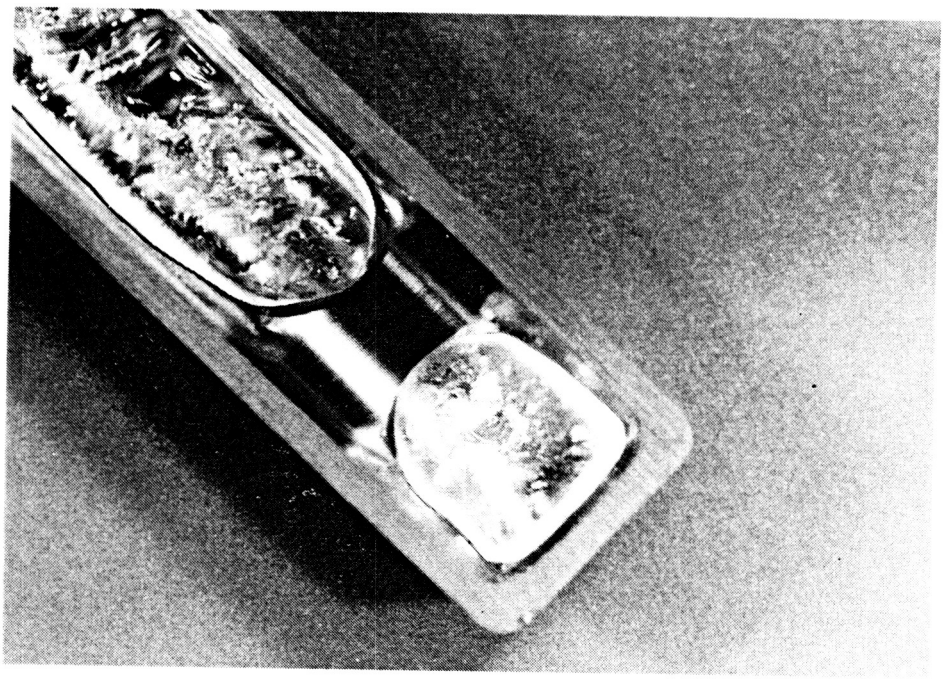

Figure 4.7 LiF Solidified in a Non-Wetting Crucible

Other low energy materials such as boron nitride and boron carbide have been tested successfully at NASA Lewis for compatibility with molten LiF. One design approach is to pyrolitically apply either the boron carbide or the graphite to a metal alloy similar to that selected for the absorber. Sanders routinely manufactures systems with these coatings within our Infrared Countermeasure Group. Also we often use refractory metal substrates with these coatings.

Two other operating requirements also affect the DAR cavity design: (1) maintaining the PCM within the corrugations during launch, and (2) surviving a high-G impact while operating. During launch, the PCM is frozen within the heat exchanger corrugations (wick) as illustrated in Figure 4.8C. The tenacity of the LiF-niobium alloy bond needs to be evaluated prior to finalizing the launch configuration. Simulated launch forces could be imposed on a simple niobium alloy crucible to access the feasibility of various launch design configurations. If the frozen bed is sufficient, the PCM could simply be frozen in place prior to launch.

A more positive alternative solution would be to hold the solid LiF in the corrugations with a thin wire screen fabricated from one of the metals presently identified for the LiF doping (Figure 4.8C). Once the system was operational, the wire would dissolve in the melt, and thus serve a dual purpose. Copper and nickel wires are currently being evaluated for this application.

A screen mass of less than 0.01% that of the PCM would be sufficient to fulfill the doping requirements. With the PCM secured in the corrugations prior to entering the micro-gravity environment, solarized system start-up would be facilitated. The screen would serve as a neutral density filter, stopping a percentage of the solar flux at the PCM interface. Much of the solar flux would penetrate directly to the gas heat exchanger surface to produce an immediate heating of the working fluid. Even with the high thermal inertia of the cool PCM mass, it will be possible to bring the engine to a self-sustaining idle. Conversely, with the Baseline serially heated configuration, a great deal more alternator power and time would be required to reach the self-sustaining point.

Two alternative launch configurations are also described in Figure 4.8. The simplest scenario is to launch the RSU with the PCM precast in the bottom of the cavity (see Figure 4.8b). As before, the receiver aperture is oriented upward so that the non-wetting discharge plenum dome contains the PCM. In starting the system, the solar flux will be absorbed on the gas heat exchanger without the PCM. The engine would be rapidly brought to a power producing state. The control system would be required to regulate the load to maintain acceptable discharge temperatures. Meanwhile, the PCM would be melting and capillary forces would cause the corrugated wick to fill. To test this start-up approach, we propose two experiments for future programs.

First, a 20-second Lear Jet micro-gravity test should be conducted to demonstrate the ability of the molten PCM to migrate from the non-wetting plenum into the wick. Secondly, we would perform full scale solar tests on the DoE Test Bed Concentrator without PCM in the system. These tests are described in Section 5.1.

Another launch/startup concept is shown in Figure 4.8a. Here the PCM is premelted electrically prior to solar operation. Therefore, the PCM will be able to achieve its equilibrium position within the wick prior to introducing the solar flux. Again, the Lear Jet experiment described in Section 5.1 will demonstrate the feasibility of this approach.

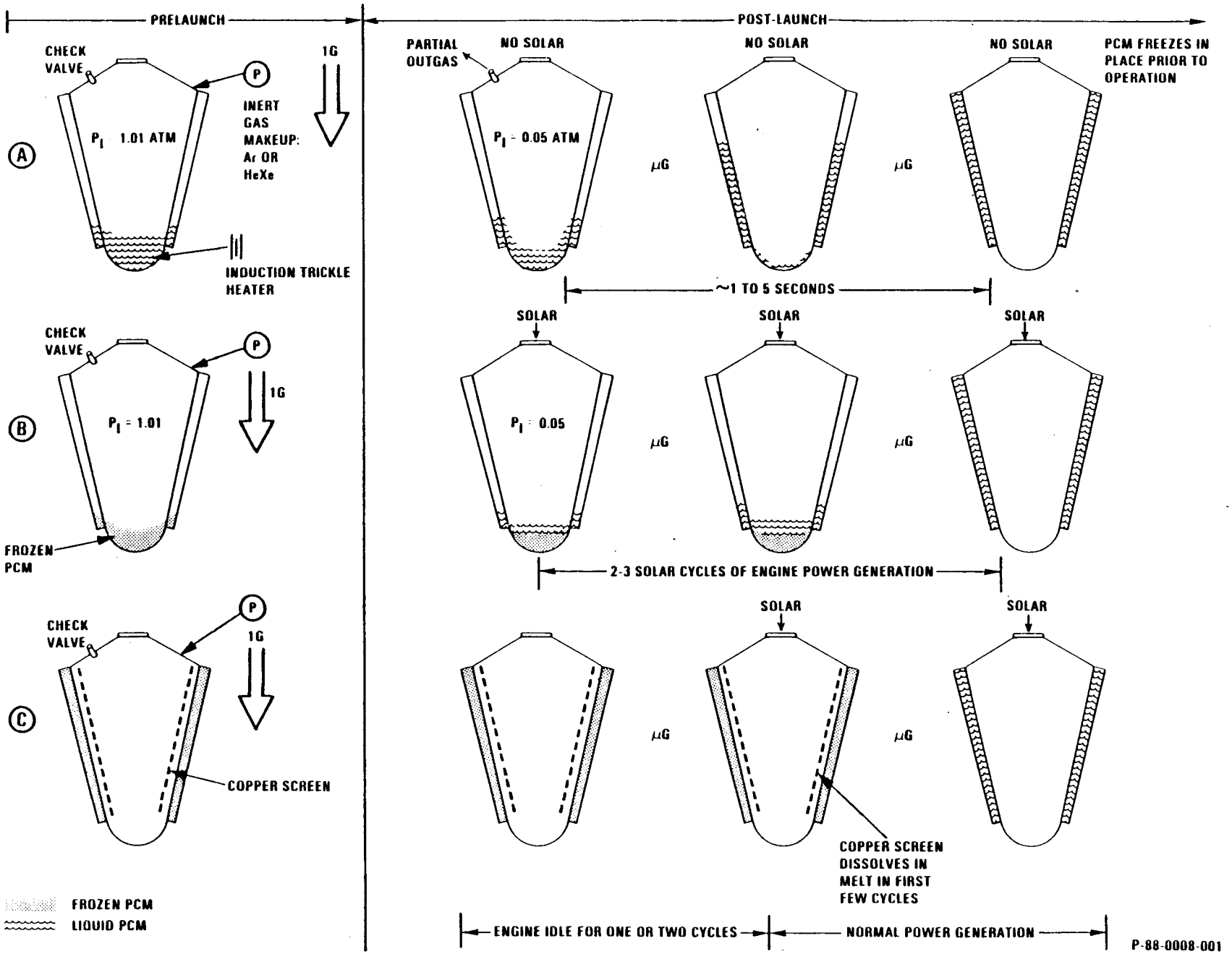

Figure 4.8 Three Launch/Start-up Scenarios

There is the potential for an external acceleration force to overcome the capillary suspension force holding the LiF in the corrugation. Although this has not yet been presented as a design requirement of this program, we believe that some planning for this possibility is required. The worst case would result in some of the liquid LiF detaching from the absorber and contacting the window. Under these conditions, the minimum design requirement would be to at least contain the mishap. This adds the requirement for safety factors in two areas of the design. First, the absorber must survive sustained solar irradiation without the contacting PCM as a heat sink. Secondly, the window must not break and release the PCM to the environment. Our preliminary stress analysis of the absorber and the window indicates this can be readily accomplished. Moreover, the volatility of the irradiated PCM should return the system to its normal operating condition as the PCM vapor condenses on the gas-cooled absorber corrugations. However, this would place more stringent requirements on the window design.

4.3.2 WINDOW ANALYSIS AND EXPERIMENTAL RESULTS

A transparent window located in the vicinity of the cavity aperture is required to retain the small LiF vapor pressure. The vapor pressure of the liquid just above it's melting point is .0089mmHg (10^{-5} ATM). At the highest predicted cavity temperature of 1160 degrees K, this value has increased to only .020mm Hg. Because the window is exposed to the LiF vapor, corrosion and condensation on the window are concerns. It is possible to control the condensation rate by controlling the window temperature and by the addition of non-condensable gases.

Aside from the actual window material, the window temperature is the next most important parameter to consider. Our analysis has determined that the window temperature can be controlled over a wide range by its geometry and the application of thin film coatings. For example, a concave window will be hotter due to radiative interchange between itself and the cavity while a convex design will be cooler.

Equally important in controlling window temperature are the window radiative absorption characteristics. The power in the solar spectrum diminishes significantly at around 2.5 to 3 microns, while the cavity radiates approximately 70% of its energy above this threshold. Therefore, the IR absorption characteristics of the window contribute to the so-called "green house" effect, which may be enhanced with selective thin-film coatings applied to the outside window surface. Anti-reflective (AR) coatings, which are designed to reduce the Fresnel reflections in the solar spectrum will also generally increase the reflection of the cavity IR reradiation at the window.

The introduction of a non-condensable gas into the RSU cavity will have a great influence on the condensing phenomenon. The non-condensable gas, probably a noble gas, will move with the vapor towards the cooler condensing surface. However, since these gases do not condense, they accumulate in the vicinity of the liquid-vapor interface impeding the LiF condensation rate.

Thermal and mass transport design theories indicate that there are three possible design scenarios for the window as illustrated in Figure 4.9.

In Figure 4.9a, the window absorbs negligible amounts of solar energy compared to the PCM condensate. The PCM layer deposited nightly is evaporated during daily solar exposure. This scenario represents the most severe window corrosion condition.

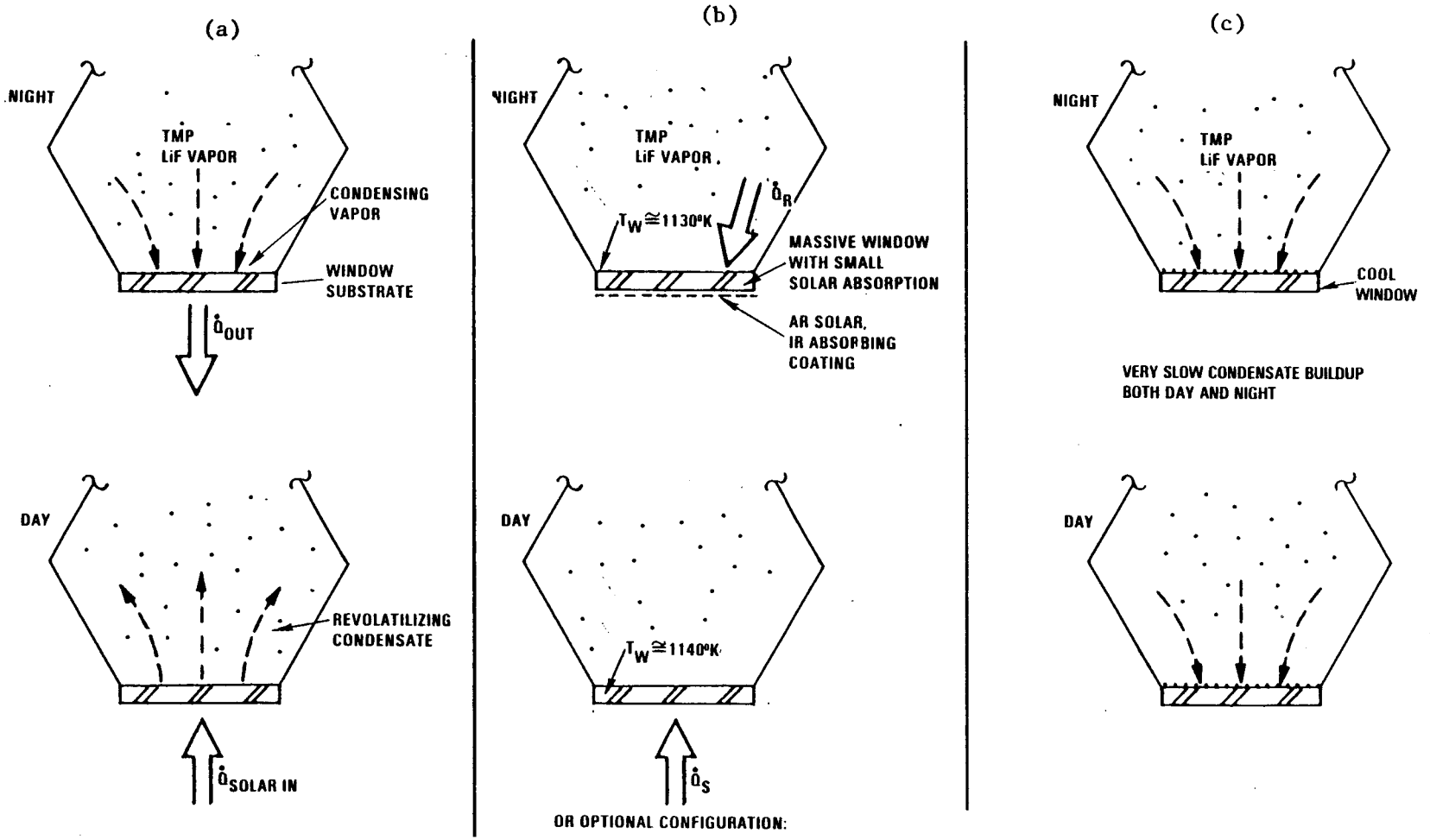

Figure 4.9abc Three Window Design Options

Figure a Condensate on window absorbs appreciable amount of solar energy.

Figure b Window absorbs appreciable amount of solar energy (1 to 2%) and interior surface maintains temperature over PCM melting point.

Figure c Low solar absorbing window always remains below PCM melting point.

In Figure 4.9b, the window or coating absorbs approximately 2% of the solar power, raising the interior (cavity side) window surface temperature slightly above the LiF melt temperature. Aided by multilayer IR reflective or absorbing coatings, the fairly massive window maintains an interior surface temperature above the PCM temperature through the night, so no condensation occurs.

In Figure 4.9c, the low solar absorption window always maintains its temperature below the PCM melting point, and condensation accumulates with every cycle. A slight pressurization of the cavity with a non-condensable gas will minimize the PCM deposition rate. Experimental results presented in this paper indicate that deposited layers of LiF will remain transparent on many window substrate materials.

Experiments were conducted on ten window candidates listed in Table 4.6. Two 200-hour tests simulated the window environment representative of the three operating scenarios. In these two tests, window samples were maintained at temperatures above and below the melting point of LiF. An argon partial pressure of slightly more than one atmosphere served to minimize the potential for external contamination within the furnace and duplicated the desired effect of a non-condensable gas. The three heating zone furnace allowed the establishment of a range of thermal gradients along the 1 meter by 10cm diameter furnace interior. A graphite crucible containing molten LiF at 875°C (18°C above the melting point) was located nominally 22cm from the grouping of window samples. In the two tests the window samples were maintained at 860°C and 650°C respectively. This apparatus is shown in Figure 4.10. Window transmissivity and mass measurements were made before and after the 200 hour exposure to the condensing vapor. Three of the promising samples, diamond, YAG, and MgF_2 also underwent X-ray photoelectron spectroscopy (XPS) and infrared spectroscopy (IRS) analysis.

Table 4.6 WINDOW SAMPLES EVALUATED IN STUDY

Oxide Samples
- Single Crystal Mg Al_2O_4 (Spinel)
- Single Crystal MgO
- Single Crystal Al_2O_3 (Sapphire)
- Single Crystal ZrO_2 (Yttrium Oxide Stabilized Cubic Zirconia)
- Single Crystal $Y_3Al_5O_{12}$ (Yttrium Aluminum Garnet, YAG)
- Single Crystal $Gd_3Ga_3O_{12}$ (Gadolinium Gallium Garnet, GGG)
- Fused SiO_2 (Synthetic Quartz)

Fluoride Samples
- Single Crystal LiF
- Single Crystal MgF_2

Other
- Natural Diamond

In essence, Configurations 4.9a and 4.9b represent similar window designs where the goal is to minimize if not eliminate the deposition of LiF on the window by achieving the highest practical window temperature over the orbital cycle. However, for either configuration it is desirable to select a window material which is resistant to LiF etching. When simulating Configuration 4.9b in our experiment all oxide samples showed varying degrees of surface fogging. However, fused silica which was demonstrated to be highly reactive with molten LiF maintained its high solar transmittance for the 200-hour test duration despite the

(a) Experimental Configuration for Condensation/Corrosion Investigation

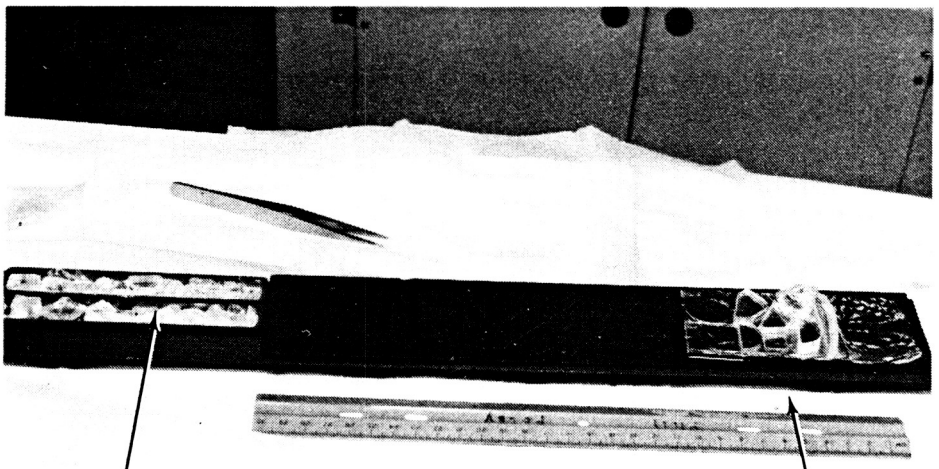

CRUCIBLE CONTAINING
LiF MAINTAINED AT
875° C

10 WINDOW SAMPLES
AT COOL END OF FURNACE
SUB-MELTING POINT

(b) Thermal Gradient Controlled Furnace

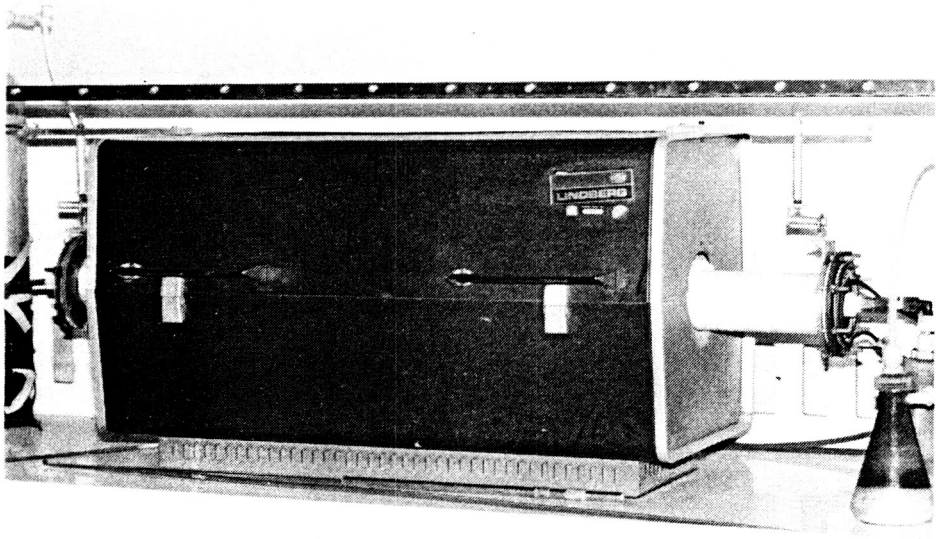

Figure 4.10 Window Corrosion Experimental Apparatus

Oxide Window Canidate Transmission Measurements

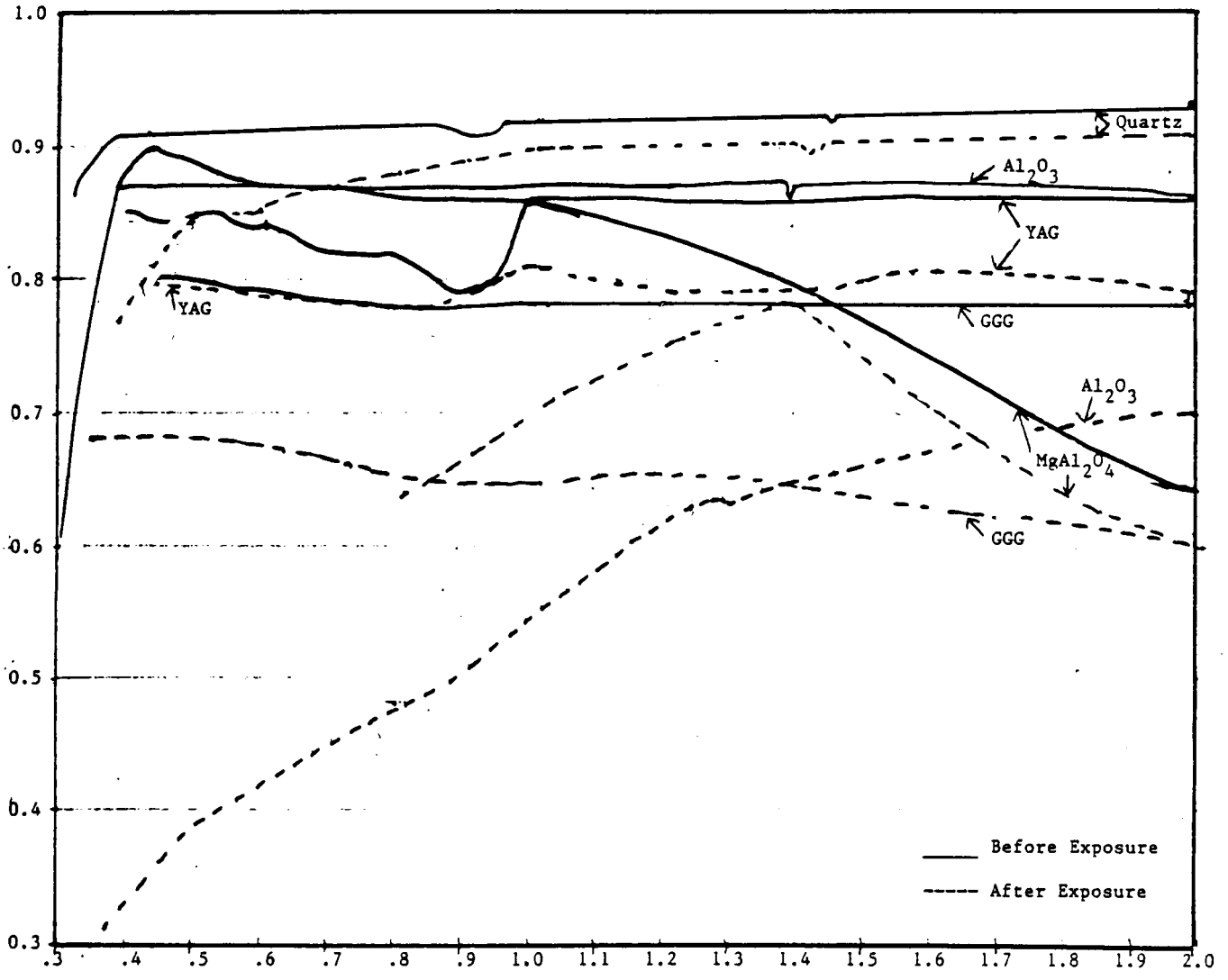

Figure 4.11

Measurements obtained with Cary 14 Spectrophotometer. Lithium fluoride melt maintained at 875°C while window samples at 860°C for 200 hours.

slightly observable haze on the surface. The before and after exposure data in Figure 4.11 indicates that most materials exhibited a significant drop in transmissivity. In addition to these flat samples, a 1/4 carat natural diamond and a large 10-gram nugget of cubic zirconia were exposed to the vapor but their geometry would not allow transmissivity analysis.

Although transmissivity is the ultimate criteria, the measurements are somewhat misleading. Since the spectrophotometer only measures the transmitted component of the energy, it is not capable of distinguishing absorption from reflection. When comparing the transmissivity data before exposure (Figure 4.11) to the theoretical values it is evident that essentially all of the measured loss is attributable to the Fresnel reflections from the two surfaces. A high index of refraction is a significant disadvantage of oxide windows in general. Thin film antireflective (AR) coatings, applied to the space side surface of the window can reduce losses by as much as 40%. Interior cavity reflection losses can be reduced by incorporating a significantly convex window geometry. An alternative approach would be to apply a compatible oxide as a thin film (wavelength /4) on the interior surface of a window with a lower refractive index. This is obviously the approach which would be taken with diamond-like window materials.

Many of the oxide window samples developed a fogged surface after the 200 hours at 860^{o}C. As expected, their transmissivity dropped significantly. This data, however, is not sufficient to distinguish the difference between the scattering from a non-reacting polycrystalline deposition of LiF and a surface reaction. If there is no reaction, the polycrystalline phase might only accumulate in the night phase and in the day it would either revaporize or liquefy and become transparent again. Also, to be considered an acceptable solution, the total deposition over 10 years would have to remain small.

To evaluate the extent of the surface reaction, the YAG and diamond samples have been inspected with the XPS and the IRS. The LiF exposed YAG sample revealed the presence of lithium and fluoride compounds other than LiF at the surface. Thus, the visibly fogged surface which resulted in about a 10% transmissivity drop was the result of corrosion. Another important finding from this analysis was that the depth of the deposition/affected layer was less than 100 angstroms. This implies that the 10 year accumulation layer would be less than 5 microns. However, etching of the surface, even though the affected layer is small, suggests that YAG and probably our other similarly fogged oxide samples are not suitable for the DAR application.

The diamond surface, when examined with the same instruments exhibited a very different condition. Again the deposition layer was on the order of 100 angstroms but only LiF and diamond compounds were detected. The fluoride binding energy was detected and was consistent with that characteristic of the LiF molecule. Since no binding energy shifts were detectable we are able to conclude that no interaction with the diamond occurred. This is encouraging and suggests that diamond-like coatings on various substrates is a possible window option. Currently diamond film technology is at a point where coatings are routinely applied to 4 to 6 inch diameter silicon semiconductor wafers. This suggests that at least the size of the window for 7kWe receiver will not present a problem. Also researchers at The University of North Carolina Research Triangle viewed quartz as a good diamond coating substrate.

Many alkali metal-fluoride windows have suitable transmissivity for the lower temperature window design as shown in Figures 4.3. These fluorides also have low indexes of refraction and excellent broad-band solar transmissivity. The theory in designing with these materials is to control the LiF deposition rate and

crystalline morphology so as to develop a transparent layer of LiF on the substrate. This process can be controlled by the substrate temperature and the presence of a non-condensable gas.

Single crystal magnesium fluoride and lithium fluoride window samples were included in the lower temperature (650°C) 200-hour simulation experiment previously described. Spectral absorption data in the literature (10) agrees with our transmissivity measurements. In the solar spectrum, the only non-transmitted component of energy is associated with Fresnel reflections. Some of these losses may also be avoidable in the DAR, depending on the window geometry and the application of anti-reflective coatings.

A comparison of the transmissivity traces before and after the 200-hour exposure is presented in Figure 4.12. This data confirms the visual inspection which indicates no loss in clarity. Unlike most of the oxide samples, the fluoride samples did not appear fogged. These results are very encouraging since the deposition layer formed as a clear amorphous layer on the single crystal substrate, devoid of crystallites which increase solar scattering.

Since no reaction of LiF deposited on LiF is possible, only the MgF_2 substrate was analyzed with the XPS and IRS. As with the YAG and diamond samples, only a very small amount ($<<100$ angstroms) of LiF was detectable on the surface. Unlike the YAG sample, the lithium binding energy did not appear. The only binding energies observed were those for MgF_2 and LiF thus implying that no interaction took place. The test conditions with the LiF melt at 875°C and the window at 650°C constitutes a realistic environment for the DAR. Also, with approximately one atmosphere of argon present, the total accumulation over a 10 year period can be extrapolated to be less 5 microns.

Appendix C contains a series of calculations of the window operating temperature. Based on these calculations, window surface temperatures will not exceed 800°C under exposure to the highest possible solar fluxes (16,000 suns). MgF_2, CaF_2, BaF_2 and other fluorides are useful up to that limit.

4.3.3 LiF DOPING EXPERIMENTS

Preliminary crystal growth experiments were conducted to evaluate the doping affinity of LiF with materials exhibiting optical absorption bands within the solar spectrum. In the first phase of this study several rare earth and transition metals were identified which form fluorides with acceptable absorption bands. Some of these candidates are presented in Figure 4.3.

A screening process was conducted on several of these candidates by simply mixing the metal-fluoride powder in varying concentrations with a measured quantity of LiF in a graphite crucible. The mixture was then melted, allowed to equilibrate for 4 to 6 hours, and then cooled back to room temperature. The actual freezing took place over a period of 30 to 60 minutes, comparable to the rate required for the orbiting DAR. The room temperature PCM samples were then sliced into a 3mm thick wafer, polished to remove the scattering marks of the saw, and then optically characterized.

Initial experiments focused on rare earth dysprosium and samarium fluorides because of their broad band absorption. However, both DyF_2 and SmF_2 samples yielded "chalky" two phase solids. Evidently the gross mismatch in the size of the two fluoride molecules precluded the formation of a single crystal.

Fluoride Window Candidate Transmission Measurements

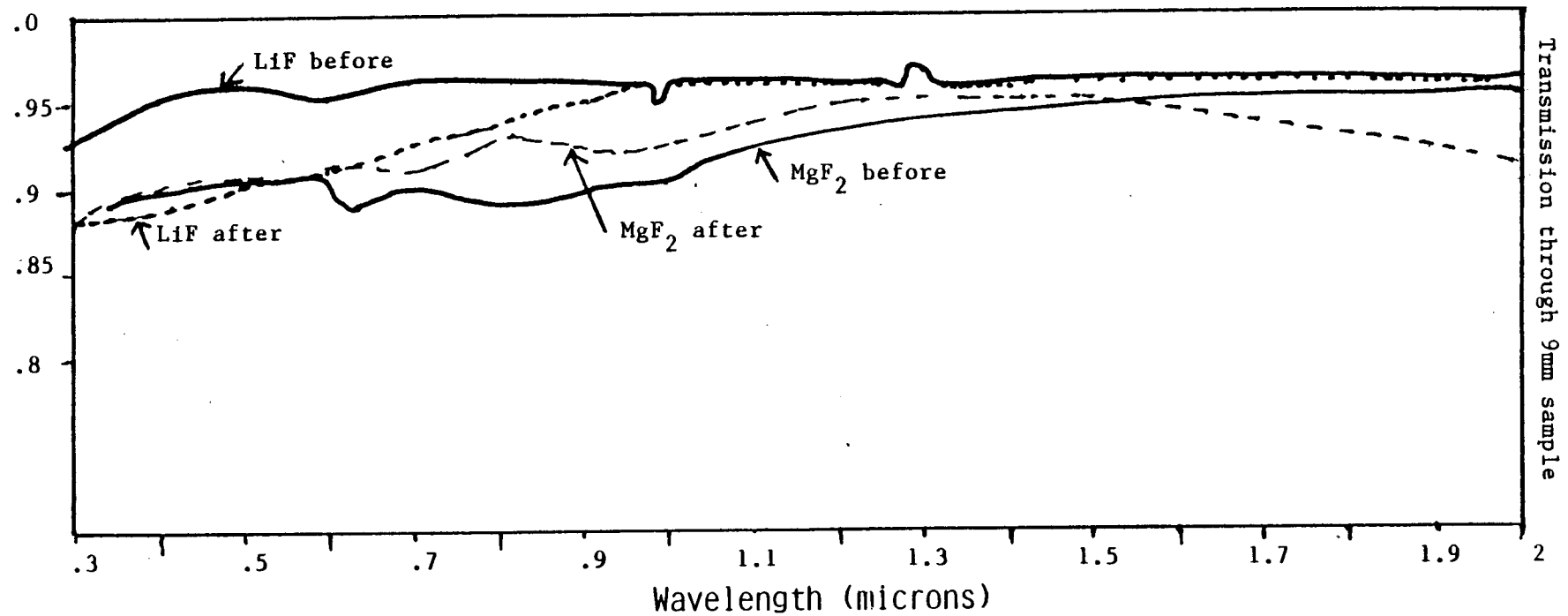

Figure 4.12

Transmissivity measurements before and after exposure to LiF vapor at 875°. Sample maintained at 650°C for 200 hours, measurements made with Cary 14 Spectrophotometer are subject to errors of +_ 3%.

Transmission tests of these two doped samples indicated that virtually all of the energy would be either absorbed or scattered. The high scattering coefficient is indicative of the polycrystalline lattice. High scattering would not necessarily translate into high receiver losses since the many internal reflections within the large cavity would insure that only a very small percentage would escape through the relatively small aperture. A design could be configured where the internal reflections were used advantageously to diffuse the peak flux while sacrificing no more than 1% in actual reflection losses. However, at this stage of the study it appears that our overall goals could be better met with a lower scattering single crystal.

The investigation of transition metals suggested that nickel, chromium, copper and cobalt exhibited strong absorption in the solar spectrum. Due to program constraints, we limited the experimental analysis to cobalt. In the manner previously described, cobalt fluoride powder was mixed with the LiF with the initial ratio of 0.5%M (.005 molar). The resulting pink crystal was obviously saturated and again two phase. However, due to the relatively rapid freezing rate characteristic of the low earth orbit, the crystallization kinetics are such that a near homogeneous solid was produced. Observable segregation of the dopants occurred in the "opaque" sample where a high scattering polycrystalline structure was distinctly present in the last zone to freeze. Surface scattering in the first zone to freeze was similar to the clear undoped control samples.

Lower doping percentages of .03, .014 and .003% produced progressively larger pink single crystal regions in the zones first to freeze. The transmissivity of the light pink single crystal samples were then compared with a similar section from an undoped LiF crystal grown under identical conditions. This data, shown in Figure 4.13 illustrates a distinct correlation of absorptivity with dopant concentration. Additionally, the effect on the absorption appears to be very broad band with the peak occurring in the 1. to 1.8 micron spectrum.

The .03%M sample had much less single crystal-like regions, such that it was difficult to prepare an optical test sample which excluded inclusions. Figure 4.14 presents three data sets obtained from different locations on the polished sample. It is believed that a portion of the different transmissivity values are due to both absorption and scattering.

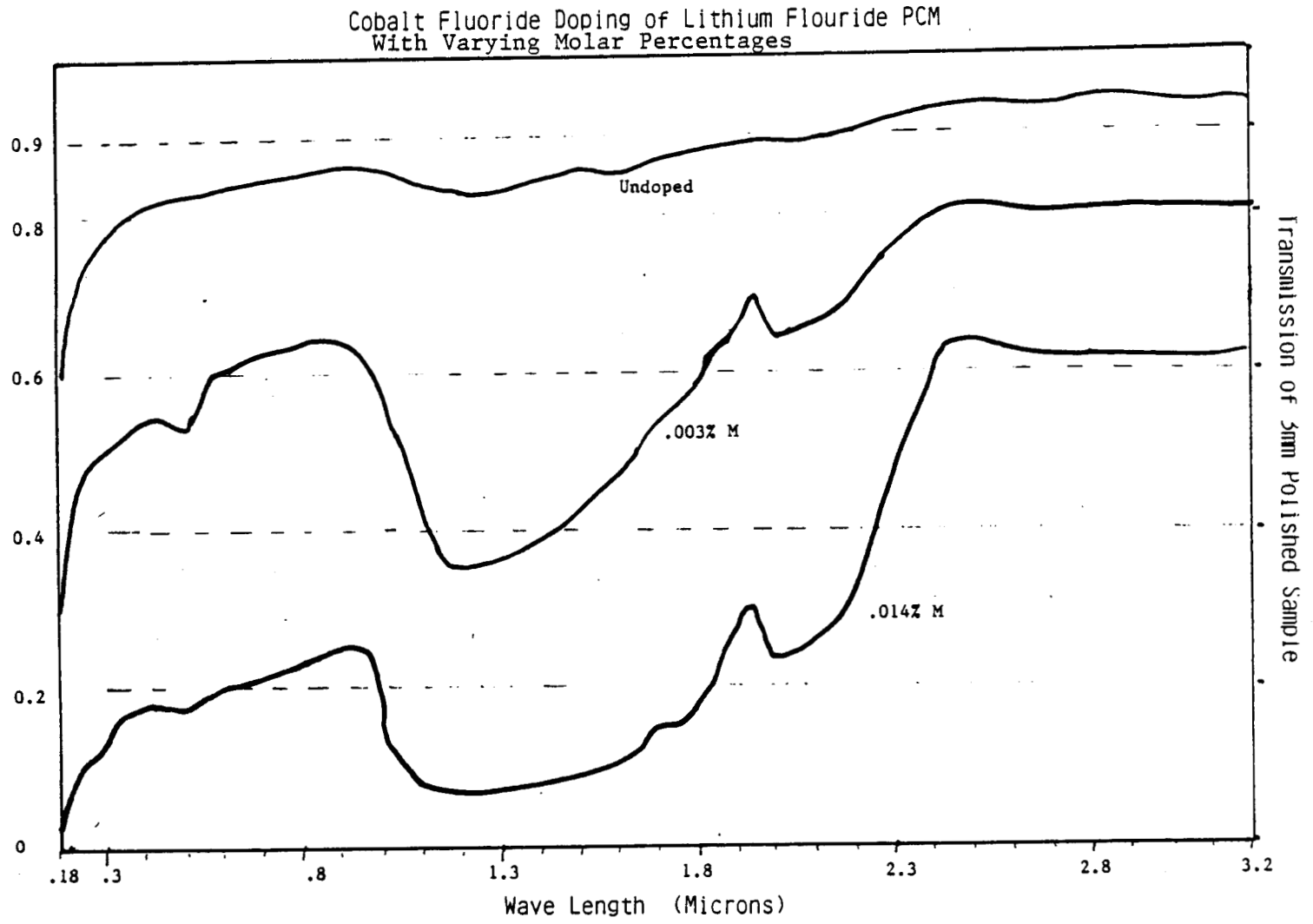

Figure 4.13

Measurements made with a Perkin-Elmer Lambda 9 Spectrophotometer. Values obtained through a 0.125 inch diameter region of the polished sample were affected by various amounts of inclusions.

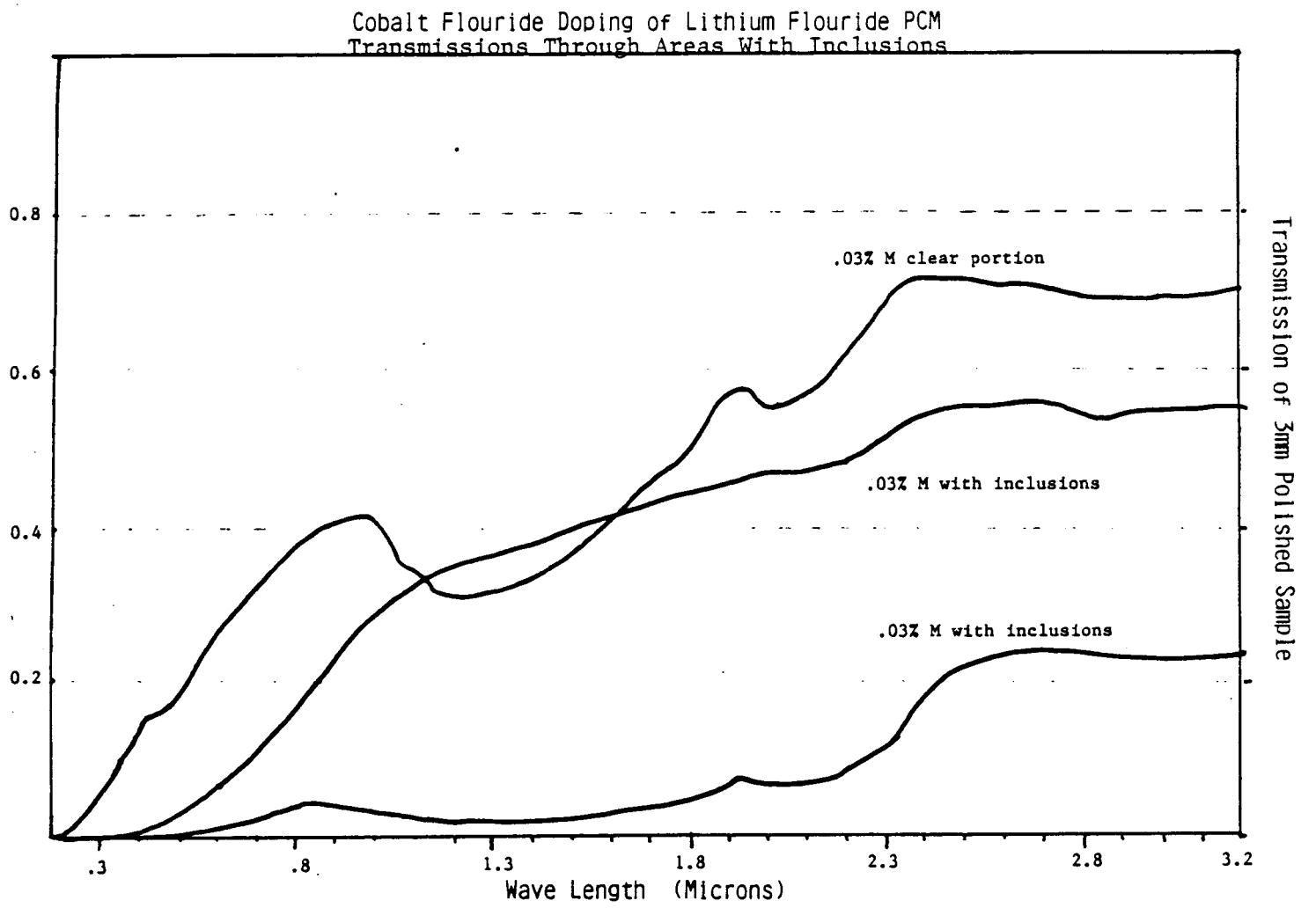

Figure 4.14

Much of the crystal contained areas of inclusions where high scattering occurs. These inclusions congregated in the core of the sample, at the last place to solidify.

5.0 ANALYSIS OF SELECTED STIRLING ADVANCED CONCEPT (TASK III)

5.1 STIRLING CAVITY HEAT PIPE RSU DESIGN

Cavity heat pipe is a term which describes a concept for integrating conventional "heat pipe" technology with a solar receiver cavity. In this approach, the characteristic heat pipe principles are employed. A heat transport fluid (sodium) is evaporated from a wicking system on the heat addition side of the transport loop and condensed back into the wick on the heat rejection zone. This new application of heat pipe technology takes advantage of the very high flux capacity of the evaporative/condensing mechanisms without the constraints of common tubular geometry.

In the Sanders' Cavity Heat Pipe (CHP), a single vapor-filled cavity couples the very different heat exchanger geometry of the receiver absorber and the engine heater head and the PCM module interface. As shown in Figure 5.1, during the solar period sodium evaporates off the back side of a domed solar absorber and condenses simultaneously on the engine heater head and internal PCM container modules. A continuous wick/artery system connects the heater head condenser, the PCM modules, and the absorber/evaporator dome. During the orbital eclipse, the sustained thermal release from the PCM continues to supply vapor to the heater head.

This artery system, referred to as a plenum artery, is a unique feature of this CHP design. As shown in Figure 5.2, liquid returning from the condenser sections flows through a low fluid resistance sealed volume to the evaporating surfaces. It is vented to the vapor cavity only through the various wick pores of the dome, PCM modules and heater head. This feature allows for the several different wick structures to be reliably connected during the assembly process.

Because of the very high power transport capacity of the vapor, the surface areas of the dome, the PCM modules and the heater head are the limiting factors in the heat transfer through the system. The CHP, unlike conventional tubular heat pipes, allows these heat exchangers to be designed independently to best accommodate the specific characteristics of their heat source or sink. With regard to the solar absorber, this means that the cavity absorber geometry can be selected to effectively capture the solar energy while experiencing the minimum stress within the smallest possible volume. For the Stirling engine heater head, this means coupling a necessarily high heating flux to the compact heat exchanger optimize for the engine. For the PCM modules, the design flexibility exists to select a geometry which minimizes the thermal ratcheting potential and maximizes the thermal performance of the low conductivity PCM. The design of each of these independent heat transfer problems is discussed in the following paragraphs.

5.1.1 HEATER HEAD/CONDENSER INTERFACE DESIGN

A key advantage of the Sanders' CHP condenser is its flexibility in accommodating engine heater heads. The interface requirements between the RSU and the heater head are very critical and therefore are given the highest design priority. The heater head is not only the most highly stressed component but it is also very sensitive from a performance standpoint to geometry parameters. The Stirling engine heater head may be any one of the several concepts discussed in Appendix D, including those for the dual opposed piston configurations. Multi-tubular (like the SPDE), tube-shell modules proposed by Sunpower and MTI or pure annular configurations like the smaller 3 kWe MTI and Sunpower engines can all be readily accommodated.

Cavity Heat Pipe Stirling Receiver

WITH FINNED TUBE/SHELL HEATER HEAD

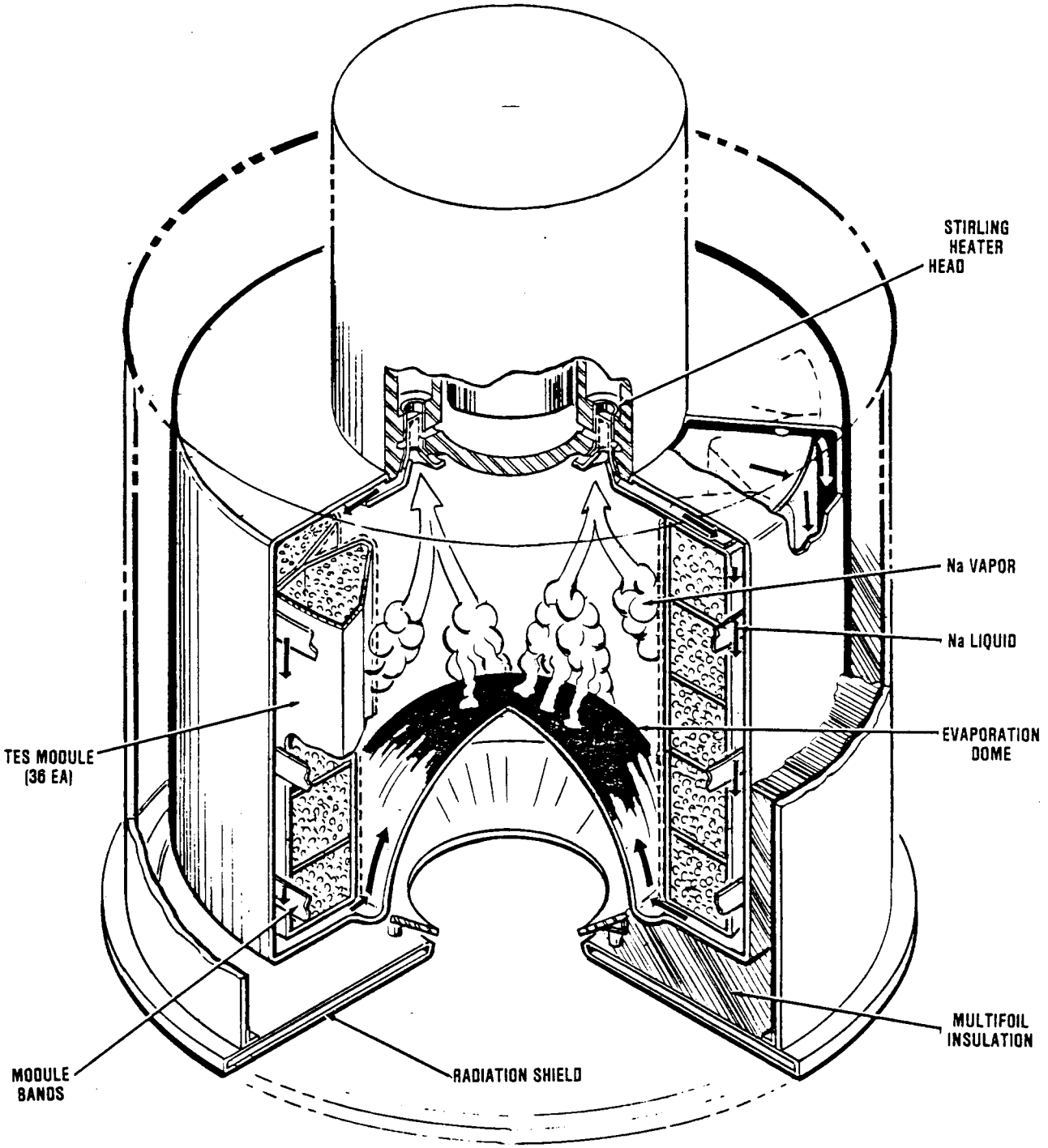

Figure 5.1 Cross-Section Cavity Heat Pipe Stirling Receiver

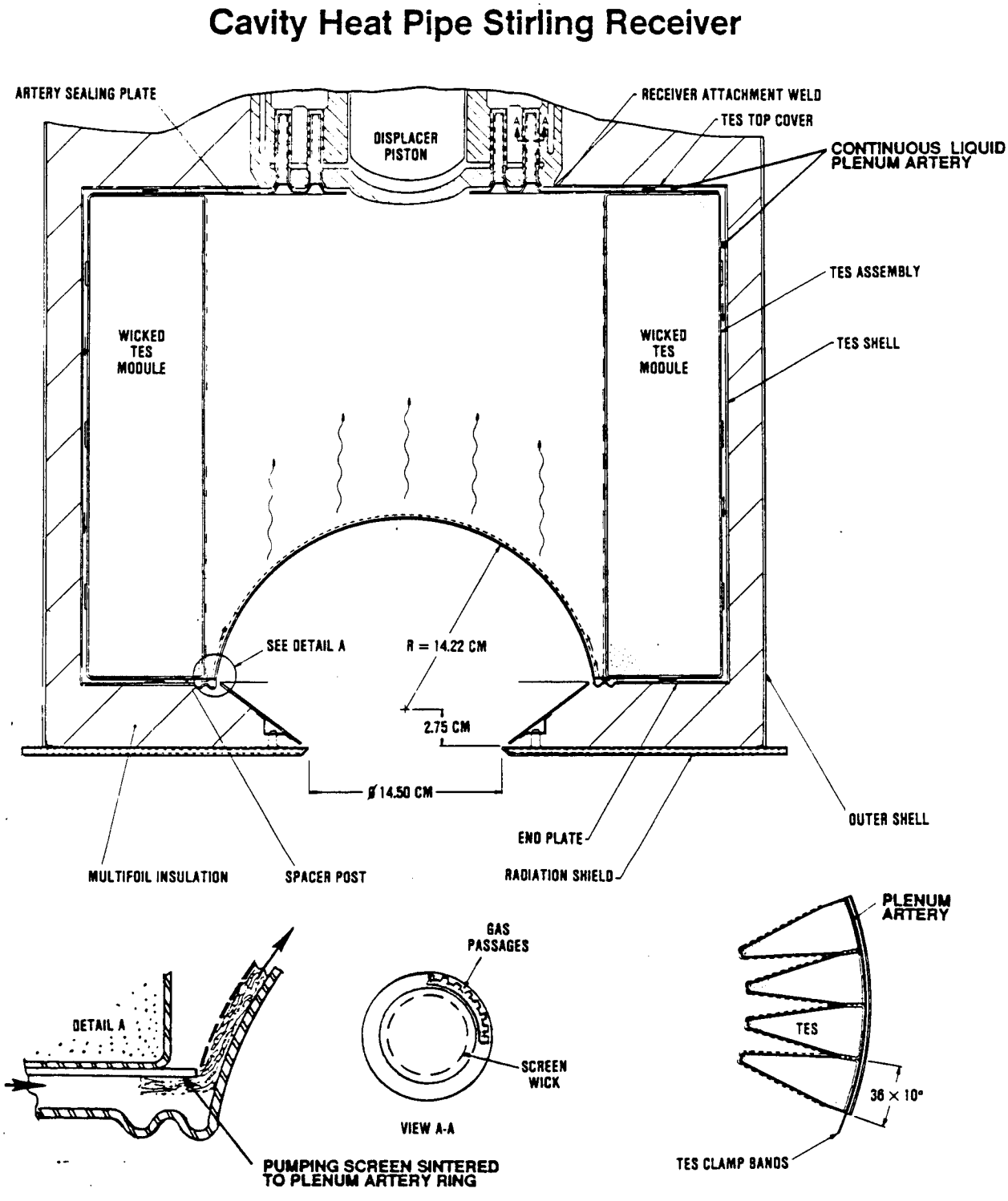

Figure 5.2 Cross-Section Cavity Heat Pipe Stirling Receiver

In addition to these three existing head designs, some new variations of these concepts which might better integrate with the solar receiver will be described in this section.

The results of future NASA-sponsored trade studies involving engine scaling, performance improvements, and head fabrication will certainly impact future receiver development. Moreover, engine development for the foreseeable future is likely to be directed towards other non-solar applications. For these reasons, the versatility of the CHP is a necessary receiver characteristic.

The second major advantage of the CHP evaporator is its ability to maintain nearly isothermal conditions on all gas passage wall surfaces. When the many parallel flow passages of the helium gas are not maintained at a common temperature, entropy mixing losses arise. In the single large CHP, vapor flows freely to the zones demanding the greatest power input. The condensing phenomenon is thus a strong mechanism for isothermalizing the heated zone.

The adaptation of the CHP condenser to the three heater head configurations is shown in Figure D2 of Appendix D, and is discussed in the following sections. Each of the designs can be readily integrated without interfering with the optimization of the solar cavity or the PCM heat exchanger.

5.1.1.1 MULTI-TUBULAR HEATER HEAD INTERFACE

The greatest challenge in integrating a multi-tubular heater head with the CHP is in the large number of closely packed tubes. For instance, one half of the Space Power Demonstration Engine (SPDE, 12kWe) contained 1628 0.088 inch (.035cm) OD tubes. The vast number of tubes precludes connecting arteries to each tube. Without an artery, the condensate layer is likely to become too thick and bridge between tubes, greatly limiting the heat transport to the condenser and resulting in unsatisfactory performance.

The problem with adapting to this configuration is that it was originally designed for a pumped liquid heat transport system. However, with a reconsideration of heater head design parameters, a more suitable multi-tubular configuration can be devised to better integrate with the condensing vapor heat transport concept. This parametric study would yield a head with fewer larger tubes resembling the DoE 25 kWe terrestrial engines. Unfortunately, to maintain the same primary heat transfer area with larger tubes requires an increase in the total tube volume. This compromise results in a small degradation in efficiency due to the additional upswept heater head volume. Since these DoE engine efficiencies are projected to exceed the 29% NASA specification for this program, this approach can be considered as an option. A complete CHP RSU incorporating this concept is shown in Figure 5.3. Either single or opposed cylinder engine configurations are acceptable.

Having obtained a design with a more manageable number of tubes (approx. 100), it is possible to consider various artery schemes. Figure 5.4 illustrates a concept for attaching a small 1/16 inch outside diameter (OD) screen artery on each heater head tube prior to its assembly into the engine. The screen hose has a short sleeve of tubing welded into one end while the other end is closed off. The screen hose-tube assembly would be temporarily held together with wire clips prior to applying a powder metal wick. One procedure utilized by Thermacore would be to paint the assembly with a slurry of powdered metal prior to sintering in a furnace. A second viable approach would be to plasma spray the tube assembly.

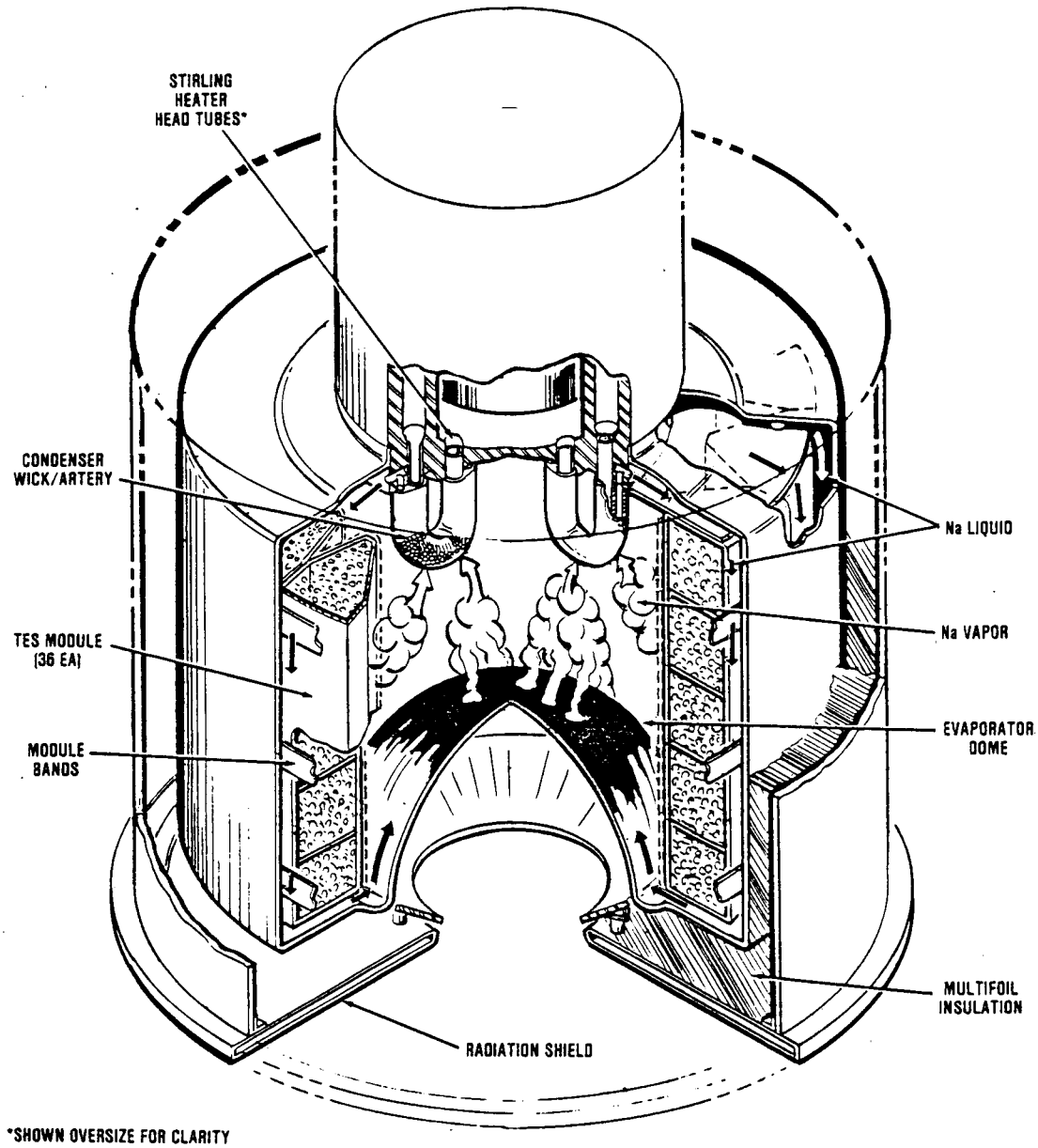

Figure 5.3 Cavity Heat Pipe Stirling Receiver with Multi-Tubular Heater Head

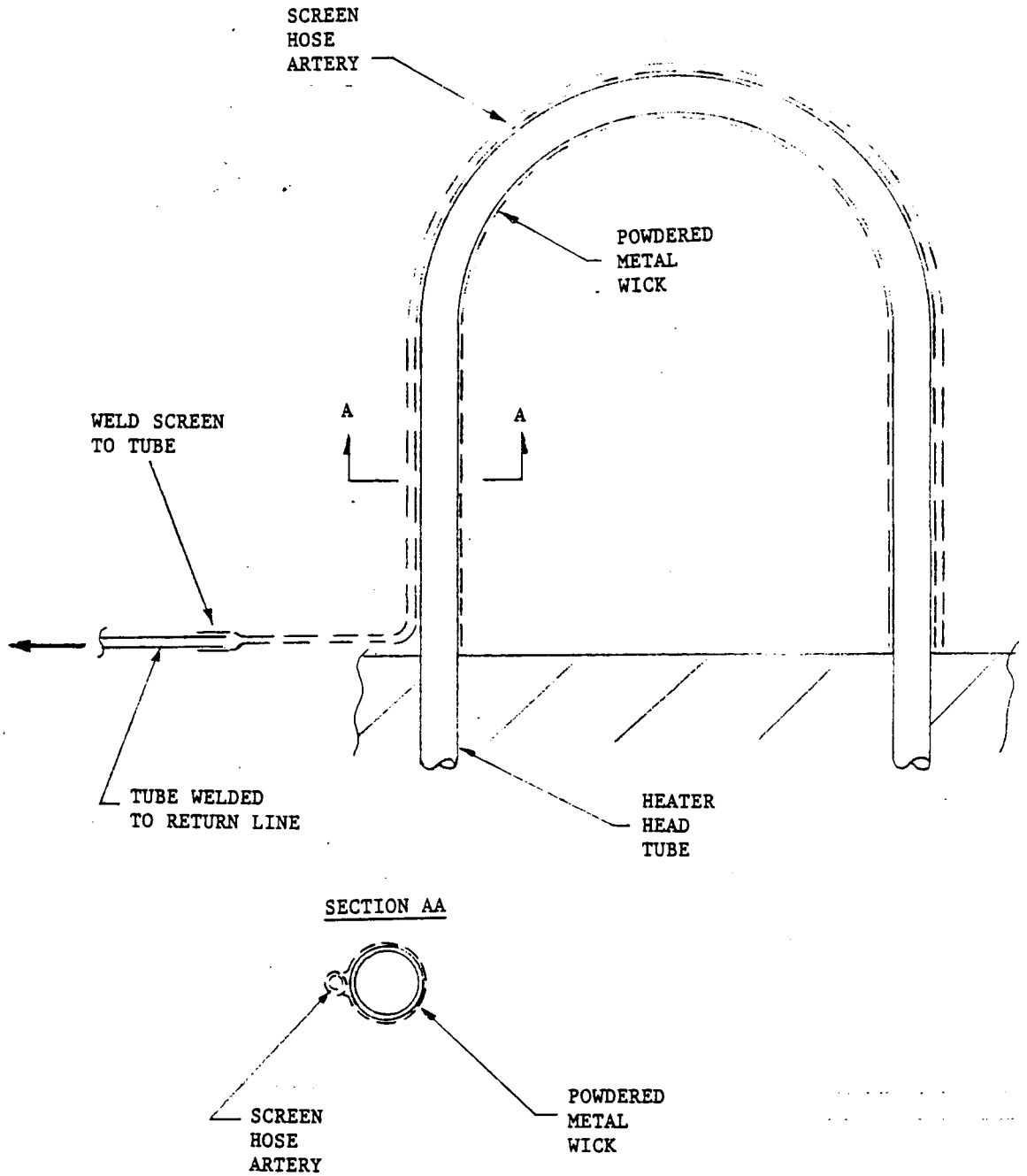

Figure 5.4 Wicked Condenser Design or Multi-Tubular Heater Head

The next step would be to assemble the 100 or so wicked tubes into the head using the engine manufacturer's preferred approach. In assembling the receiver, each of the open artery tube ends would be welded into a disk shaped header to form the common artery plenum. This approach could be equally well implemented for the dual opposed engine configuration.

Although we believe this design is viable, the quantity of parts involved makes the fabrication process complex. However, since the tubular heater head is the most mature of the three general heater head configuration to be discussed, the reduced overall development required will offset some of this complexity.

5.1.1.2 ANNULAR HEATER HEAD INTERFACE

The annular heater heads have the potential to significantly reduce the condenser complexity. With a single large continuous heater head heat transfer surface instead of the numerous tubes, it is possible to use fewer larger arteries. Figure 5.5 shows a Sanders heater head concept which very neatly integrates with the CHP. The engine helium flows through the finned annular path surrounding the cylinder head. By confining the high pressure helium in small slots, the cylinder wall stresses are held to acceptable levels. The finning of the gas path reduces the necessary primary heater surface of the evaporator by as much as a factor of two. More importantly, the continuous cylindrical heat exchanger wall can be serviced with a much less complex artery scheme than required for the individual tubes.

In Figure 5.6a, the screen sleeve is clamped over the tube and welded. The tubes can be welded into the common artery manifold. This reduces the potential for an attachment flaw producing an oversized pore which could limit wick system capillary pumping pressure.

In Figure 5.6b, a composite wick system is connected to the artery plenum. The plenum is sealed with a disk that mechanically clamps the screen. The disk is secured in place by a few spot welds through the screen to the head. The artery for this concept would be served by either 6 to 12 screened tubes (Figure 5.6a) or a composite wick structure (Figure 5.6b). Because of the simple continuous evaporator surface, either a sintered powdered wick, or a wrapped screen wick could be considered. The termination with the plenum artery distribution system is also simplified as shown in Figure 5.6.

5.1.1.3 FINNED TUBE SHELL MODULES

The finned tube shell module has three advantages over the two approaches previously described: (1) it shows significant potential for improving head reliability, (2) it is most readily scaled and (3) it is more easily integrated with laboratory test heat sources. These advantages have led us to choose this as our baseline for 7 kWe and higher power RSU designs.

Figure D4 (Appendix D) illustrates both MTI's and Sunpower's versions of the finned tube modules. Each of the cylindrical cavities were designed to accept a nominal 2.5 kWt per heat pipe. Therefore, ten of these would be appropriate for a 7 kWe system. In scaling down to 7 kWe, we assumed the engine stroke and frequency remained constant and thus the piston areas decrease with power. This new configuration at the 7 kWe level is illustrated in Figure 5.7.

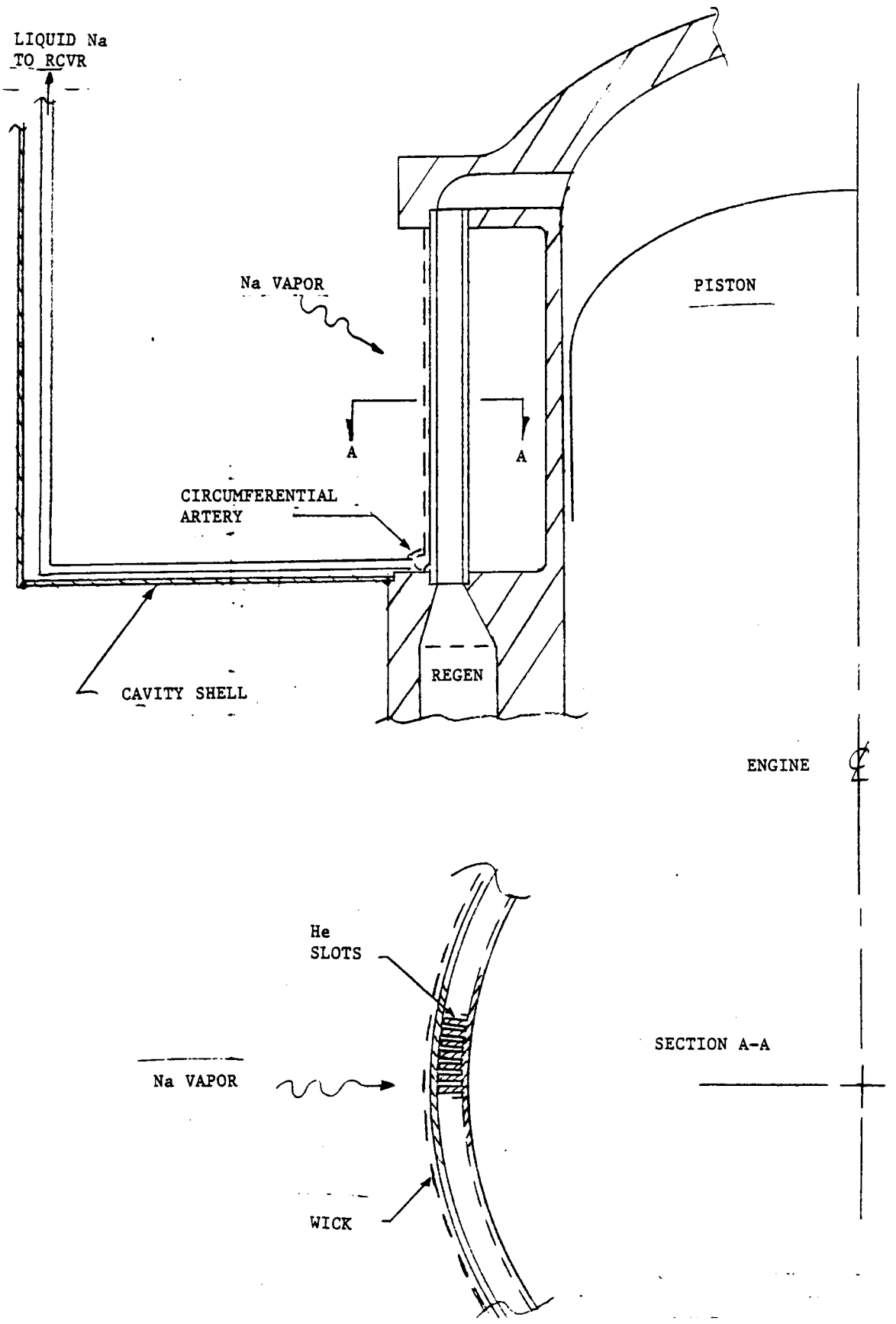

Figure 5.5 Condenser Design for Annular Heater Head Configuration

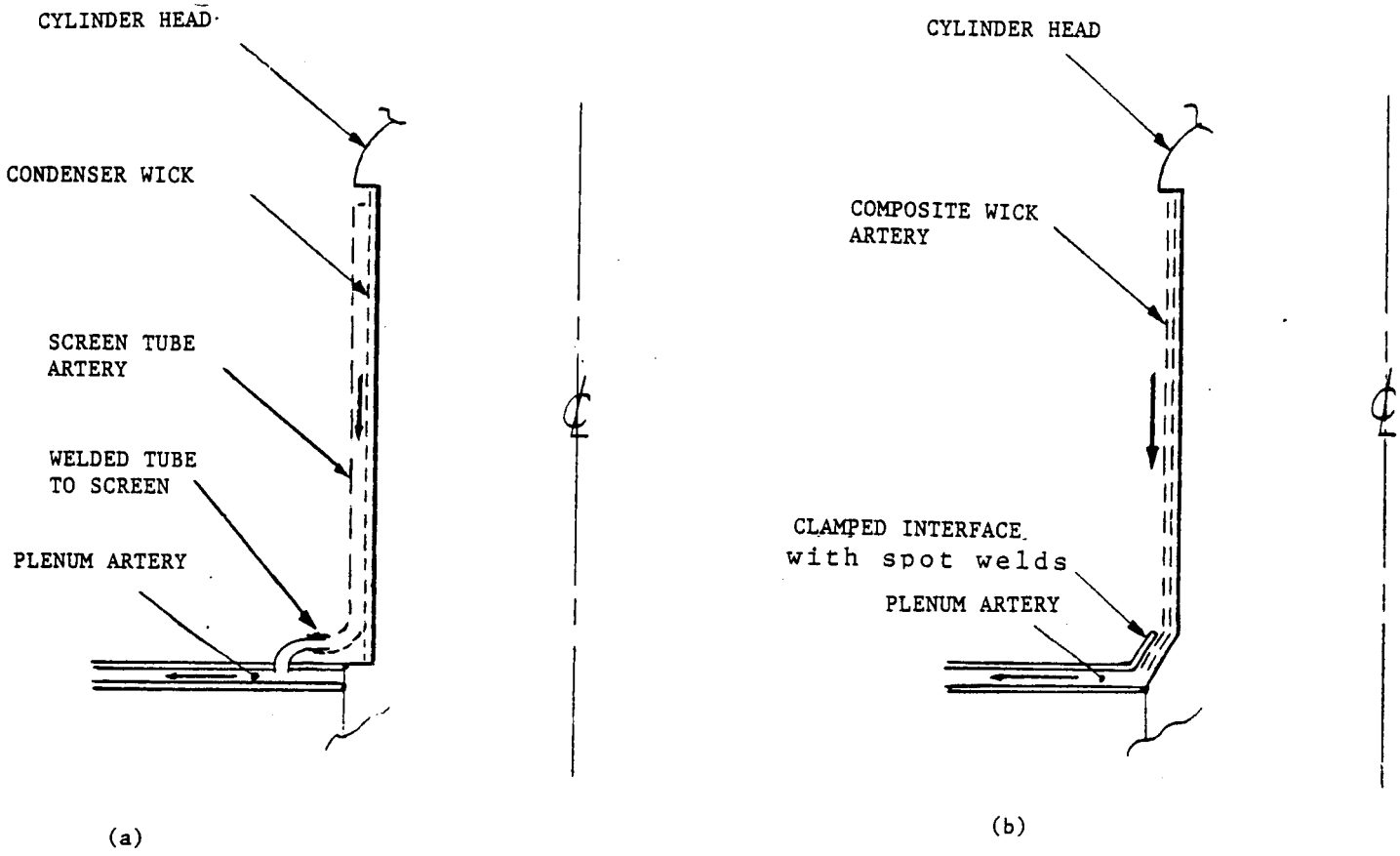

Figure 5.6 Artery Attachment Concepts for Annular Heater Head

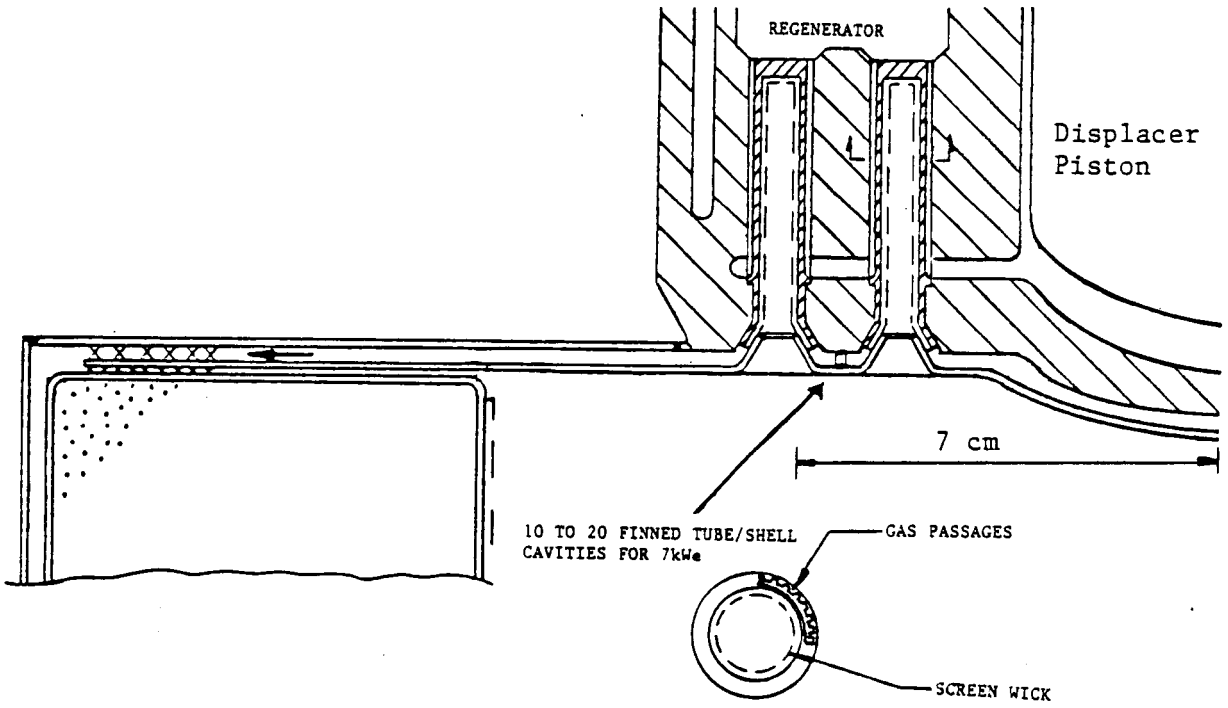

Figure 5.7 . Scaled SPRE Heater Head for 7 kWe CHP

Since heat pipes can simply be inserted into the heater head cavity, the engine can be operated with a range of heat sources. This is an especially valuable feature for the bench test phase of the engine development. It is estimated that a mechanical fit or even a braze interface adds about 20 to 30°C of temperature drop at these high fluxes. Since the source temperature is fixed by the PCM melting point, this will represent a cycle efficiency penalty.

After the engine and heater head have been tested in the lab with an auxiliary heat source, two RSU assembly techniques are feasible. The CHP receiver can either be built as a stand-alone device or integrated with the heater head. If integrated directly with the engine, it is possible to eliminate the temperature drop associated with the inserted heat pipes.

A simple construction scheme is shown in Figure 5.8 which allows the CHP condenser to be directly integrated with the ten engine heater head cavities. This cavity is formed by a finned tube extrusion which is welded or possibly brazed into the head. If the external fins are also brazed to the outer tube which forms the annular gas path, an alloy such as In 600 would have acceptable strength. However, without the support of the outer non-integral sleeve, our calculations suggest that a stronger more creep resistant alloy would be more appropriate. Therefore, to implement this concept in which we directly expose the heater tube to sodium, we will evaluate cladding techniques or the use of an inner thin walled tube. A composite screen tube with one end closed is inserted into the heater head cavity. The composite wick is constructed from two or three layers of a coarse 50 mesh screen with an inner layer of 400 mesh. If the screen tube is formed by cutting a rectangular section of screen on a 45° bias, the rolled cylinder will be very pliable in the axial direction, forming what is called a "chinese finger" which will be tightly sprung into the cylindrical heater head cavity. Perfect contact is not imperative since the annular gap formed by the coarse layers is required only for the liquid return path. This provides a low resistance annular artery along the head tube wall.

The liquid metal leaving the condenser flows through the permeable 50 mesh screen and enters the sealed plenum artery which returns the liquid to the evaporator section. Securing the plenum forming plates to one another to clamp the composite screen can be accomplished by several means. The illustration in Figure 5.8 presents one technique which we feel will meet our life/reliability goals. The open end of the composite screen tube is next attached to the artery plenum in the assembly configuration. The folded lip on the screen is firmly compressed between the plenum back plate and the beveled head cavity. The plenum back plate is then spot-welded to studs to securely clamp the composite wick. Alternative techniques shall be evaluated during the development program. In defining the final recommendations, we will recommend dedicating our attention to the two critical requirements: (1) minimizing crevice corrosion effects and (2) assuring that an oversized gap larger than a 400 mesh pore does not develop.

In summary, this section described how the Sanders' CHP design accommodates specific features of three general heater head approaches under development today. The Sanders' CHP can also accommodate the single counter balanced or dual opposed engine designs discussed in Appendix D. This is a unique advantage of this approach and is not shared by the competing designs which incorporate an array of tubular heat pipes.

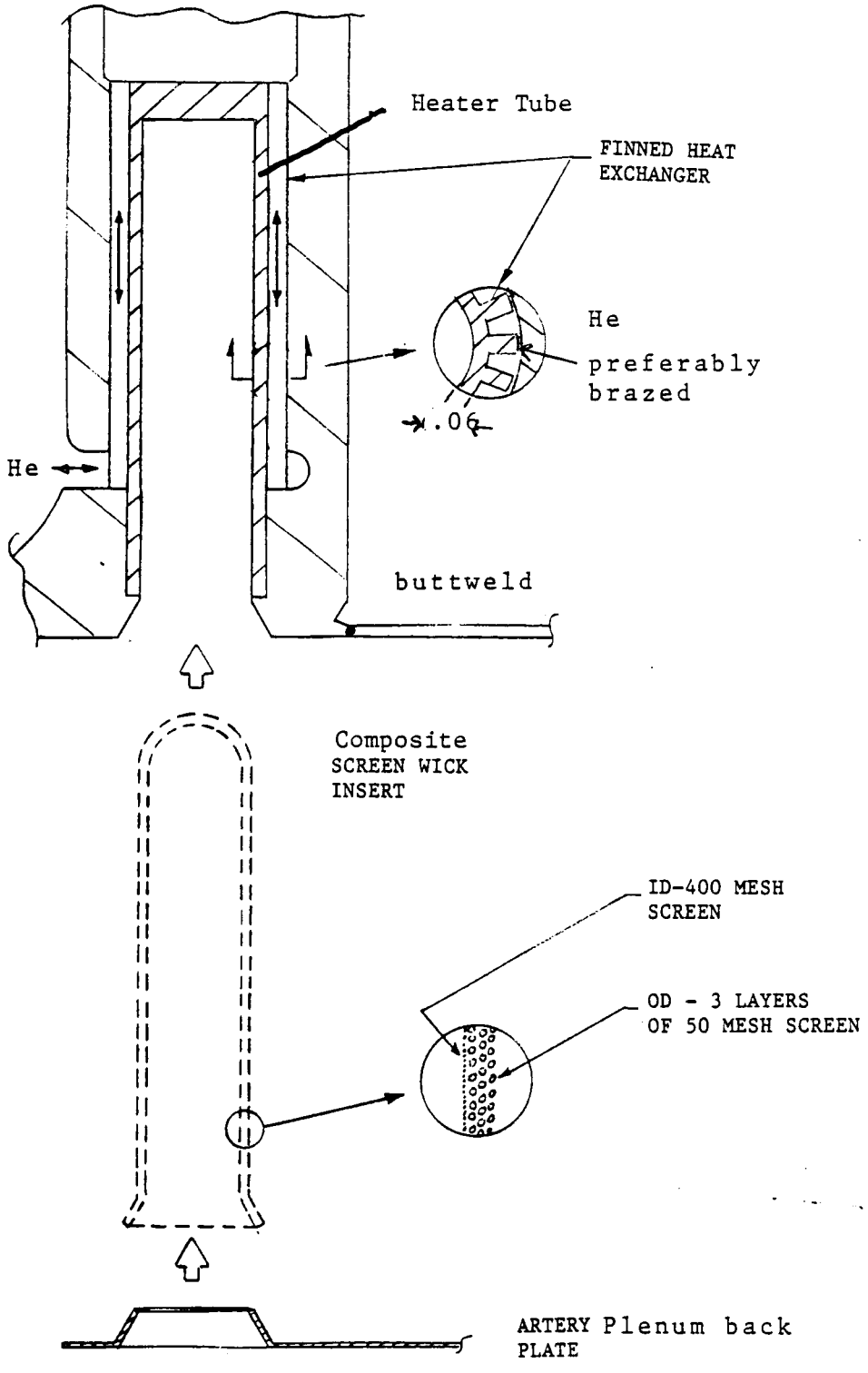

Figure 5.8 Condenser Assembly (with 10 finned tube cavities)

5.1.2 EVAPORATOR/SOLAR ABSORBER DESIGNS

The design of the solar absorber is conducted essentially independently of the heater head condenser and TES heat exchanger designs. Therefore, the shape of the absorber/evaporator can be optimized for mass, efficiency, stress and fabrication simplicity without affecting design elsewhere in the system. This phase of the study focused on the critical aspects of this component. These are a thermo-optical model of the various wick compositions for a range of solar absorber geometries, two-dimensional and three-dimensional Finite Element Stress Analysis considering realistic solar flux anomalies and a manufacturing feasibility study.

Our stress and fatigue analysis was jointly conducted for our NASA/DoE terrestrial Stirling receiver designs. On these programs, we investigated Cb-1Zr, In 600 and Incoly 800 absorber designs. In summary, our findings indicated that the hemispherical shell is a very forgiving vessel because it is very tolerant of thermal expansion and pressure loadings. Also, the edge conditions are out of the flux zone and are easily resolved.

An analysis of the three-dimensional thermal stresses was conducted where we considered a combined set of worst case flux gradients and peak fluxes at the most structurally vulnerable locations (arteries and welds) of the absorber/evaporator. So called "hot spots" were assumed to be twice the nominal peak flux value derived from our Monte Carlo ray tracing model of the concentrator. In addition, we assumed that this extreme peak would drop to 1/3 of its value within one inch away from the hot spot. Sanders has adopted these rigid standards from years of design and test experience with "real world" concentrators. The result of this stress/fatigue analysis are summarized on Figure 5.9. This modified Goodman diagram indicates that a significant safety factor can be obtained with the superalloys. The stress analysis, reviewed in Appendix E, also demonstrated that a thinner dome best withstood stress, and buckling criteria indicated a large safety factor for even the thinnest feasible dome.

The principal material selection criteria is that of compatability with sodium. Based on the extended life testing at Thermacore, we feel that it is safe to proceed with their recommendations of Incoly 800 or IN 600. Also, nickel wick materials have demonstrated excellent stability in Thermacore's three to four years of continuous operations. Both of these choices met our stringent stress life criteria.

During this program, we also conducted heat pipe performance modeling coupled with the stress analysis. In summary, our evaporator performance model illustrated in Figure 5.10 allowed us to simultaneously solve the momentum, continuity, and energy equations at a continuous set of points within the wick. Through this analysis, we were able to design the wick structure and dimensions based on capillary and permeability characteristics of various screen and powdered metal candidates. In designing this wick we assumed the additional influence of gravity for test purposes, and a solar flux safety factor of two in the peak flux zone. Also, in meeting these criteria, we maintained less than $5^{o}C$ of super heat in the sodium, which implies an additional safety factor. Table 5.1 lists the various wick designs which simultaneously meet the super heat and stress/life criteria.

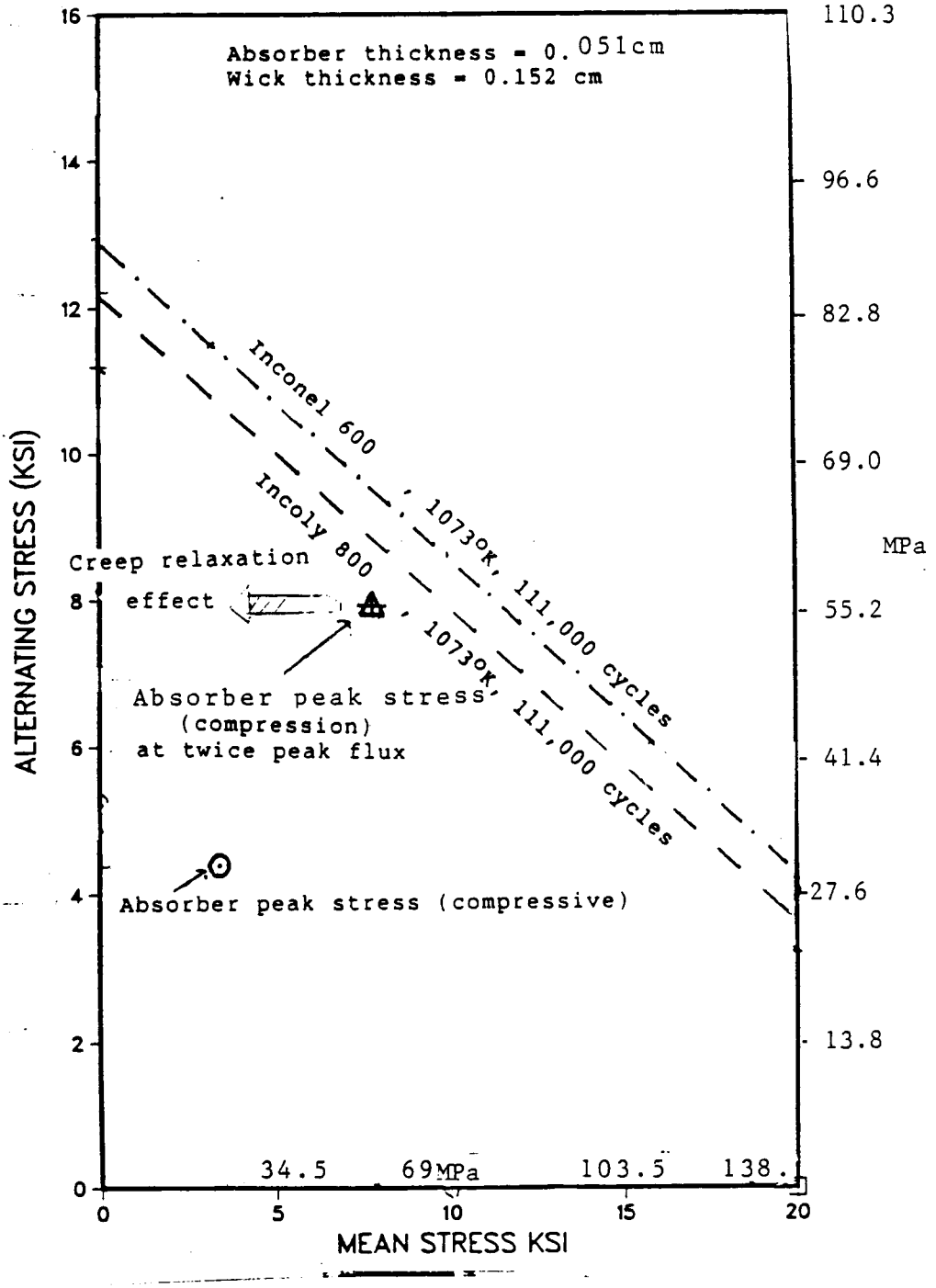

Figure 5.9 Results of Stress/Fatigue Analysis

C-2

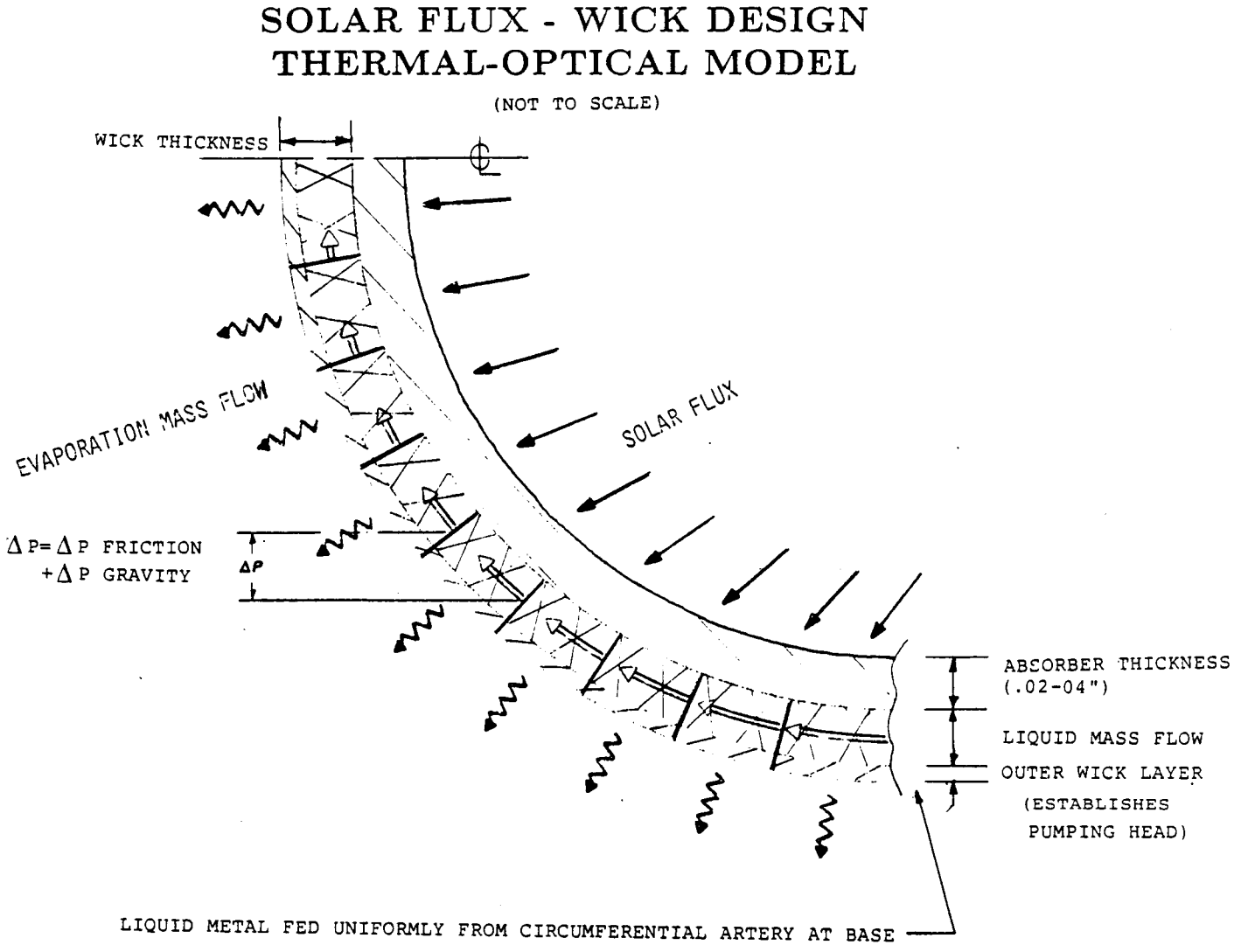

Figure 5.10 Evaporator Performance Model

Table 5.1 EVAPORATOR CHARACTERISTICS

A RANGE OF ACCEPTABLE WICK DESIGNS
ARE ABLE TO SATISFY THE BOILING AND CAPILLARY LIMITS
FOR A 28CM DIAMETER HEMISPHERICAL ABSORBER.

STRUCTURE	FLOW PERMEABILITY Cm^2	CRITICAL PORE RADIUS Cm	WICK THICKNESS Cm (inches)
*400/Annular	--	0.315E-2	0.006 (0.0024)
400/50	0.6635E-5	0.315E-2	0.0066 (0.0026)
400/200	0.771E-6	0.315E-2	0.0559 (0.0220)
Sintered Powder	0.60E-7	0.19E-2	0.152 (0.060)
60/80% Grooved	--	0.215E-1	0.152 (.060)

*Vapor Interface Mesh/Substrate Mesh

Several wick designs have been studied by Sanders on previous NASA and DoE programs. Of these, we see the greatest potential advantages for the composite screen wick. The results of our extensive stress analysis indicated that the screen has the greatest likelihood of achieving NASA's life goals. Powdered metal wicks, such as those that we have researched with Thermacore raise greater life-related concerns. We advise continued evaluations of these and other alternatives from a performance and fabrication standpoint. Such alternatives include etched groove wicks as employed by Lockheed and plasma sprayed powdered metal wicks.

The following discussions present the advantages and disadvantages of the two competing evaporator wick design approaches.

5.1.2.1 SINTERED POWDER METAL WICKS

Because of the relatively small pore size, the effective permeability of powder metal wicks is such that their liquid transport capability is limited by frictional pressure drop. Also, since wick thickness must be kept low enough to avoid nucleate boiling, the practical liquid transport distance is not very long. The solution to this problem is an array of arterial wicks located on top of the thin base wick to reduce the required liquid transport distance. The frictional pressure drop through the relatively large artery (0.15 to 0.25cm typically) is orders of magnitude below that of the powder metal per unit transport distance.

The problem with arterial wicks is that if a vapor bubble enters the artery, it will block the replenishment of the evaporator wick. Owing to the single dimensional characteristics of the heat transfer through the absorber, the actual presence of the relatively thick artery raises the local super heat level, potentially inducing nucleate boiling. Various design techniques have been demonstrated to raise the local flux

tolerance well above that required for our application (40-50 w/cm^2). However, their development appears to be more costly than screen alternatives.

The principal issue surrounding powdered metal wick/artery systems is their longevity under conditions of thermal fatigue. It was shown through the Method of Universal Slopes that the absorber will tolerate the extreme number of thermal cycles. However, little material data exists for the highly porous powder metal, or its interfacial bond to the absorber wall. As a critical technical issue in our terrestrial receiver program (MTI) we recommended conducting an accelerated simulated thermal cycle experiment. This, again, will add cost to the recommended development program.

5.1.2.2 SCREEN WICKS

Screen wicks, often sintered in layers, are the most commonly used form for heat pipes. However, they may distort or wrinkle when formed over a full hemisphere. Secondly, the surface mounted arterial wick concept will require special attachment procedures to ensure intimate contact over the dome surface.

The screen wick approach studied in detail by Sanders on both terrestrial and space Stirling engine programs is the composite wick artery. In concept, low frictional resistance liquid flow path is contained between the small pore pumping screen and the absorber. The performance limitation in this design, as with arterial wicks, is to avoid nucleate boiling and consequently vapor generation in the wick. However, because the artery is, in effect, spread out over the entire surface, it can be kept much thinner than the powder metal tubular arteries.

Our analysis showed that sufficiently low superheat (approximately $5^{o}C$) values, in addition to adequate capillary pressure drop conditions, could be simultaneously met with several screen arrangements. The 60 mesh over the grooved (or coarse mesh) 0.06 inch flow gap, or the 400 mesh over the 0.003 inch gap satisfied boiling, frictional pressure and stress criteria in the zero gravity environment. Therefore, the remaining issue in the development of a screen evaporator dome wick is principally its formability. Since this appears to be less risky than the powder metal wicks, and our geometry is somewhat flexible, we recommend this approach for the follow-on development program. Since our stress/life and performance results indicated that a full hemispherical section was not imperative, subsequent development should evaluate the practical limit of curvature of various screens This subject is addressed in the discussion on critical technology issues in Section 5.3.

5.1.3 CHP THERMAL STORAGE SYSTEM DESIGN

A successful thermal storage system must accomplish three principal objectives:

- Accommodate the 18 percent volumetric change during the phase transition without developing excessive thermal ratcheting stresses
- Minimize the engine temperature droop during heat rejection that is caused by voids acting as thermal barrriers.
- Accomplish these goals with the minimum mass.

With the Sanders CHP concept, it is possible to select a PCM container configuration which will achieve these goals without impacting the absorber or heater head designs.

The PCM modules are to be surrounded with a composite screen wick sintered to its surface. As shown in Figure 5.11, when banded together, the annular array of modules defines the plenum artery at its outer diameter. The liquid sodium exposed to this surface will then be wicked radially inward to the PCM evaporating surface at night. This same surface, serving as the storage module condenser during the solar period, will pump the condensate back to the plenum artery.

The principal concern in the design of the PCM containers is the stress resulting from the liquid expansion. The problem arises when the expanding melt is confined by the unmelted PCM crystal at the heat addition wall. To make matters worse, the LiF-CaF_2 eutectic has unusually high strength at temperatures near its melting point.

Although the baseline approach to this problem has been to confine the PCM in small containers (doughnuts), this has not guaranteed immunity from the ratcheting phenomenon. Since surface tension forces dominate and tend to hold the liquid to metal surfaces in the fully charged state, the freezing process will likely result in void migration to the middle region of the crystal. Therefore, the fundamental conditions necessary for thermal ratcheting are present upon the return of solar flux.

Sanders' approach to this problem takes advantage of two features of the CHP that are not applicable to the Baseline Brayton. The first is the extensive flexibility allowed in selecting the geometry of the PCM container geometry. Conversely, the Baseline and other similar concepts are constrained to an annular PCM configuration about 2cm thick to allow for total energy extraction. Secondly, our selected geometry is located within the isothermal environment of the sodium vapor-filled cavity. Thus, the condensing vapors raise the temperature of the entire wicked surface of the module slowly and uniformly during the solar period. The directly irradiated PCM containers of the Brayton Baseline will develop transient hot spots, resulting in local liquefaction-induced stress. The distinction between these heat exchanger designs is that the surface of the CHP module experiences isothermal heat loads while the Baseline PCM module experiences a constant (in time not spatial) flux heat load.

To eliminate thermal ratcheting, we will exploit these two features, uniformity of surface temperature, and geometric flexibility, as well as employing non-wetting surface coatings on the module interior. With the application of low surface energy coating materials such as graphite, boron nitride, or boron carbide, we can affect the PCM liquid distribution. Used in conjunction with container geometry, this approach will both encourage the formation of the void in the desired location and minimize the strength of the crystal-to-wall bond. This so-called "non-stick" surface of the ceramic coating will minimize wall shear stress and allow the crystal to translate, so that excessive tensile (ratcheting) stress does not develop in liquefying zones.

Figure 5.12 illustrates the wedge-shaped TES containment module and grouping to form the interior wicked surface of the cavity. The flat edges of each module which are banded together will be essentially adiabatic due to symmetry. It is likely that the heat transfer through the back surface of each module will also be very small compared to that occurring on the wicked surface. The wicked surface forms a tapered wedge analogous to draft in a casting mold, allowing the melting PCM to free itself from the surface, while imposing the minimal amount of stress on that wall.

TES Module Wick Configuration
SODIUM FED FROM BACKSIDE OF TES MODULES WITHOUT ARTERIES

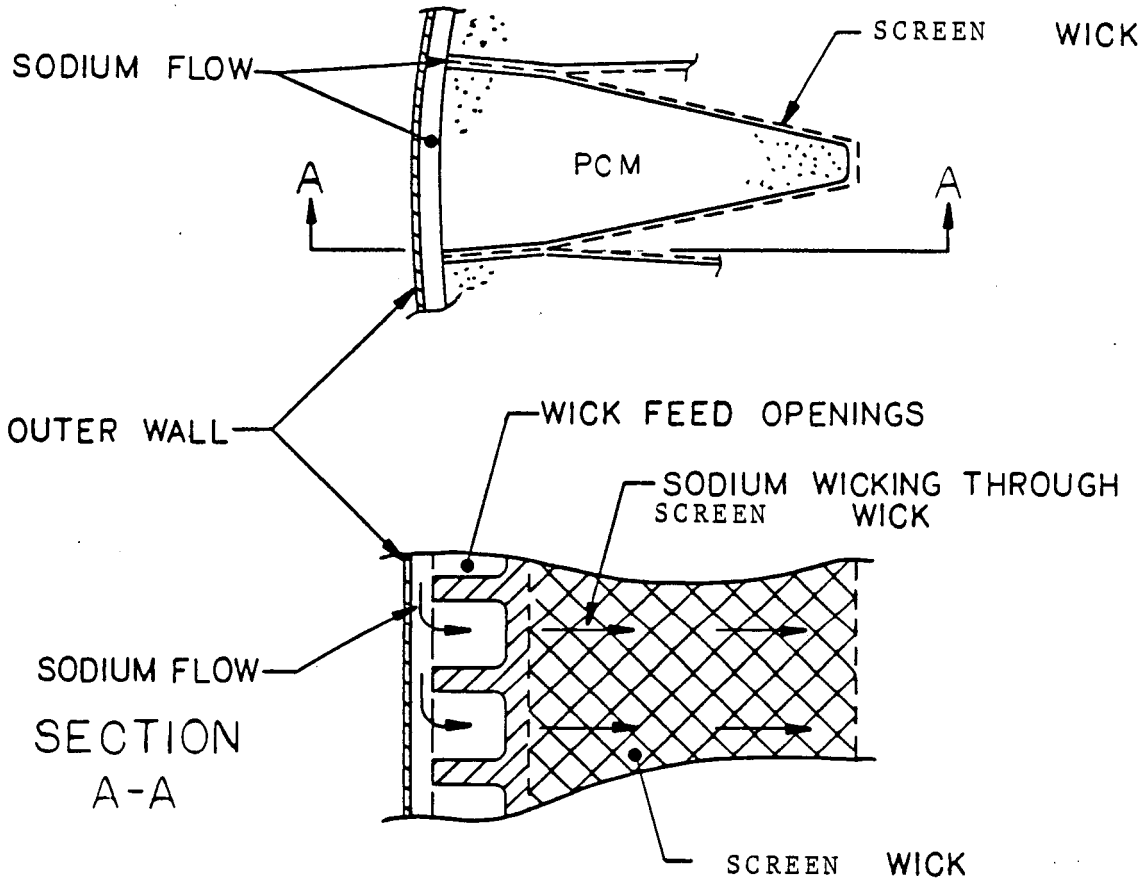

Figure 5.11 TES Module Wick Configuration

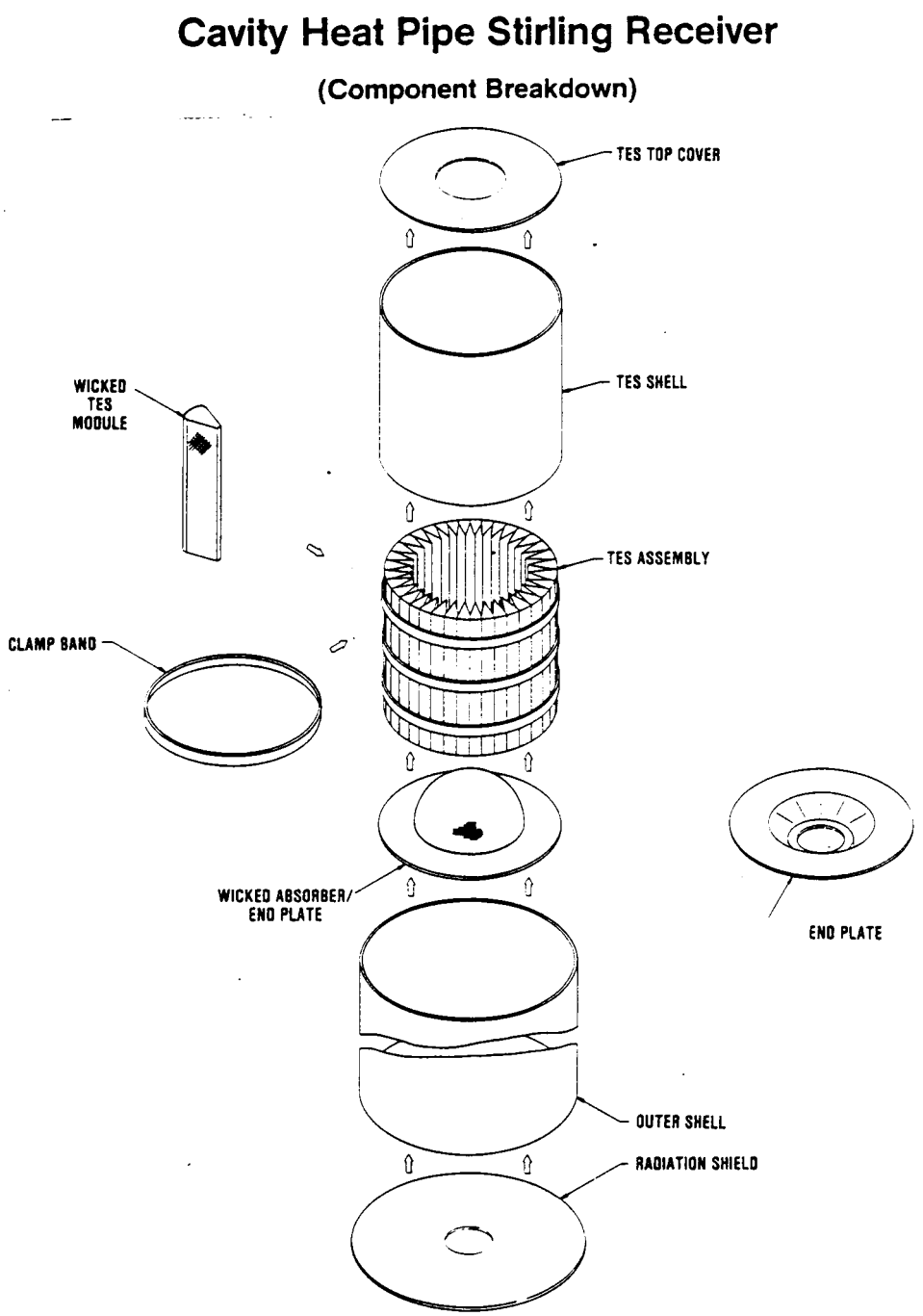

Figure 5.12Cavity Heat Pipe Stirling Receiver Component Breakdown

Figure 5.13 illustrates three candidate geometries. In each of these cases, we have oversized the container by 10 percent based on the liquid volume. Therefore, we expect voids accounting for nominally 28 percent of the solid volume. Since it is possible to influence the void location during the liquid state through non-wetting coatings, we provide this small excess volume. Also it appears that the desirable tendency for the liquid to congregate to a single void may be enhanced by the addition of a small partial pressure of an inert gas. Since the sodium cavity pressure is nominal, 0.4 atm, some pressure approaching this level will be acceptable.

Through the discriminate use of wetting and non-wetting coatings it is our design strategy to influence the 10 percent liquid void to occur in a location which will be readily accessible to the surface liquefaction region at the beginning of this solar period. For example, in Figure 5.13a where no non-wetting coatings are applied to the surface, the void is shown to migrate to one of the ends of the module. Alternatively, with all wetting surfaces the void might congregate in the back region illustrated in Figure 5.13c. However, the minimum free energy theory model employed by Sanders indicates that this is less likely for this geometry. Therefore, assuming the PCM is liquefied in position in Figure 5.13a, as it solidifies an additional extension of this void will occur. Without precisely knowing the new void geometry, we can still state that there exists a void of about 10% of the volume at the end of the container which is accessible to the liquefying zone along the isothermal wicked surface. As melting initially occurs from the wicked surfaces, the expanding liquid will progress along the inner module surface into the end void, thus minimizing the wall stress.

To more actively promote this freeze-thaw scenario, Figure 5.13b illustrates the use of non-wetting coatings on the end of the module. Coating the last 28 percent of the length would encourage the liquefying and contraction voids to congregate at the desired end.

Figure 5.13c illustrates an alternative where the adiabatic rear section of the module is coated with the non-wetting material. The triangular end pieces would also be coated, leaving only the sodium wicked wall with the wetting metal interiors. The geometry of the wedge can also influence the liquid formation. The tapered configuration, common in other space-based liquid management systems, serves to "attract" the liquid to create the minimum surface energy condition. As liquefying of the totally solidified PCM occurs at sunrise, the liquid would again have an accessible volume in which to expand. Additionally, with the tapered "mold release" shape there would be little resistance for the remaining crystal to move backward into the void. The movement of the PCM would be resisted only by the adhesive force of the unmelted PCM to the wall. Shearing this bond (especially if it is coated with the non-stick ceramic) should be relatively unstressful as the crystal is pushed away.

Because this configuration provides better utilization of the available heat transfer area, a shorter, less impeded liquid relief path, and the mold release feature, it is our recommended approach.

An additional feature of this CHP PCM module design is its effectiveness as a heat exchanger. By exposing a large amount of primary heat transfer surface area to the condensing vapor, the total container mass is most efficiently utilized. Conversely, secondary heat transfer surfaces, such as internal mesh, fins or container wall material, not directly exposed to the heat pipe surface provide less effective heat transfer surface per unit mass. The actual wedge geometry and the extent of the non-wetting coverage which relates to the heat exchanger's number of heat transfer units (NTUs) can be selected independently from

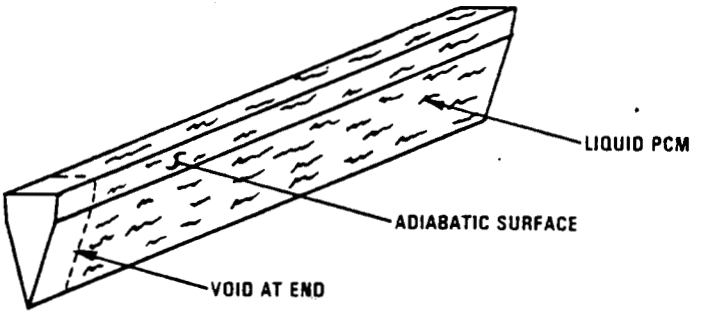

(a) Likely void location while in fully liquid state where no non-wetting coatings are applied

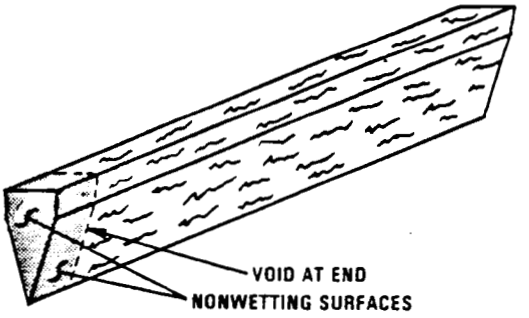

(b) Voids congregating in the end while in liquid state aided by the application of non-wetting coatings

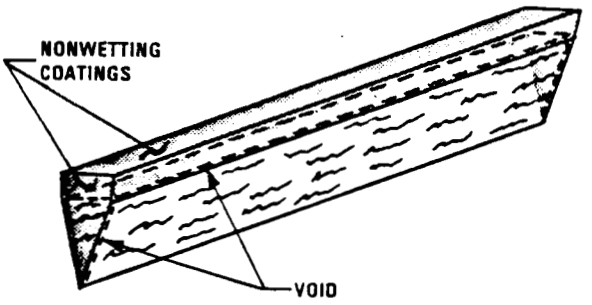

(c) Non-Wetting Coatings in Rear

Figure 5.13 Potential void formations in Thermal Storage Module

the absorber and heater head design requirements. We feel that this flexibility can be used to maximize the NTUs per unit mass as well as providing the necessary immunity to the thermal ratcheting.

Sanders has investigated the feasibility of application of non-wetting coatings of ceramics to surfaces on this program as they relate to our our advanced Direct Absorption Receiver for the Brayton module. In this work, Sanders and NASA Lewis have conducted compatibility tests on various candidates. Graphite, a common crucible material, used in fluoride crystal growth facilities such as those at Sanders, has demonstrated excellent stability. Moreover, it is a very low energy (<100 dynes/cm) surface exhibiting a large (>>90^{o}) contact angle with molten LiF. Likewise, 500 hour exposure tests of boron carbide have shown no reaction with LiF. Those surfaces are also highly non-wetting. Another advantage of these materials is that they can be pyrolitically applied to metal surfaces. Sanders employs these techniques extensively in several of our infrared countermeasures products.

Finally, ongoing development programs at NASA could yield results which would offer other PCM module design alternatives. The development of low density ceramic fibers for thermal conductivity enhancement would influence our PCM module studies. For example, a higher bulk conductivity storage medium would allow us to select fewer, but larger, wedge modules and eliminate the 10% oversize of the modules specified in the previous approach. In this case, we would save container weight to offset that of the fiber. This would also further reduce the tendency for thermal ratcheting by promoting a distribution of small voids. In addition, the fiber could significantly reduce the solidified PCM strength, thereby limiting the expansion stresses imposed on the container. Thus, there would exist some potential for additional weight savings by reducing the module wall thickness.

Mesh filled systems can only be assured of providing thermal conductivity enhancement to the liquid phase. The solid phase filled with a dispersed distribution of pore-sized voids may yield a lower bulk thermal conductivity than the pure crystal. For this reason, we have not been encouraged by their potential in the Baseline series heating approach for conducting the solar power through the PCM module to heat the engine working fluid. In that approach, the engine sustination power (consuming 63% of the total absorbed solar energy) must always conduct through the high impedance void filled solid phase. The use of mesh conductivity enhancement becomes more viable in designs such as ours where only the portion of energy to be stored enters the module. Since this energy (37%) is conducted into, as opposed to through, the modules, only the enhanced conductivity liquid layer stands between the heat source and the heat sink. Also, the unattractive weight penalty of the mesh would be less severe, since lesser quantities of the mesh would be required for the lower heating rates. Moreover, when analyzing the mass of this design, it is evident that the CHP can achieve the NASA Lewis 50% goal even with a substantial quantity of mesh. The component mass breakdown is presented in Section 5.2.1 along with the comparison with the Baseline.

5.1.4 CHP ASSEMBLY

The simple design and minimal number of parts in the CHP receiver makes assembly an easy task. Another important feature of this design is that it minimizes the presence of crevices that could promote crevice corrosion. This design also permits nondestructive disassembly of the receiver for inspection or modification - an important feature during preliminary development.

The assembly sequence is illustrated in Figure 5.14 by steps 1 through 5, and is described in detail below:

Stirling CHP Receiver Assembly Sequence

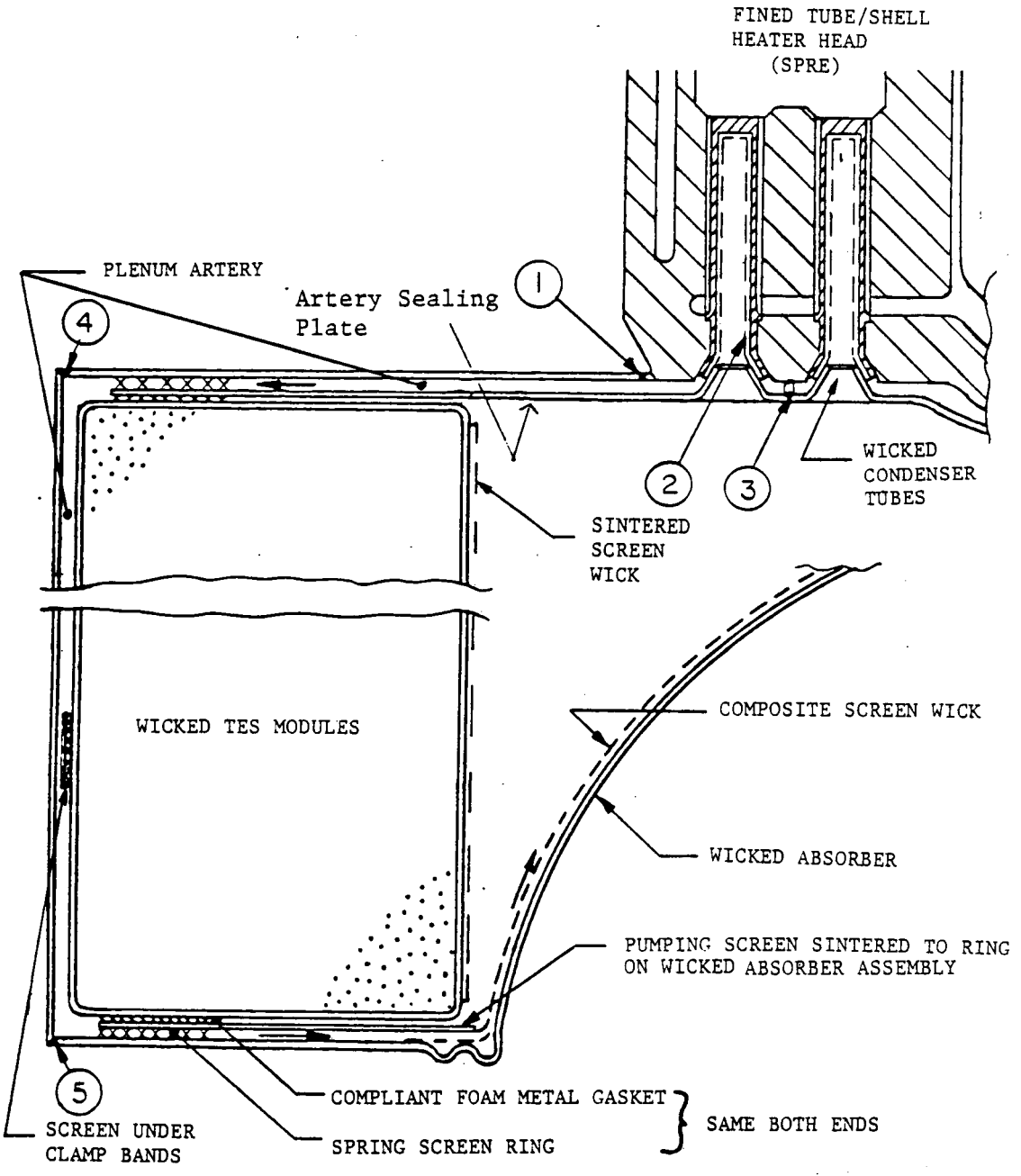

Figure 5.14

A five step sequence is reqired to hemetically assemble the CHP. This allows for inspection of both sides of all welds except for the final butt weld.

1. The receiver top cover plate is butt-welded to a mating flange on the heater head and inspected on both sides.

2. The preformed tubular screen wicks are slid into the condenser tubes in the heater head.

3. The artery sealing plate has a spring screen ring spot-welded to its perimeter to secure it while the sealing plate is laid in place. The sealing plate is then pressed firmly until it contacts the spacer studs to which it is then spot-welded. The spot weld covers the entire face of the stud and thus creates no crevices. Pressing the sealing plate down serves to force the conical holes in the plate firmly against the flared out screen wick in the condenser tubes to effect a tight seal. The spot welds then hold the plate in place. Two or three small spot welds through the plate and multiple screen layers to the head may then be used to assure permanent intimate contact without impeding the liquid flow.

4. The outer shell of the receiver is now welded to the top cover and the weld inspected on both sides. Then the subassembly of TES modules, banded together to form a cylinder, is lowered in to rest against the artery sealing plate.

   The TES module subassembly is produced by setting up the individual TES modules in a ring and then banding them tightly together with three sheet metal bands. The bands are lined with screen wick material to avoid crevices between the bands and the modules. Next, a compliant foamed metal gasket ring is tack-welded to each end of the TES cylinder and the entire assembly placed between two disks in a press. The press is then used to squeeze the gaskets with the relatively low force required to conform it to the irregularities on the ends of the TES cylinder. This achieves a good seal and a smooth, flat surface against which the artery sealing plate and the ring on the absorber flange will readily seal.

5. The final step is to install the absorber dome. Its composite screen wick will have been sintered or welded to the sealing ring which in turn has a spring screen ring spot-welded to its perimeter. At this point the receiver assembly is still in an inverted position, supported on the top cover. The flange of the absorber dome assembly is then pressed down to preload the upper and lower spring screen rings and is welded to the outer shell.

The receiver is then ready for vacuum baking and charging with sodium through an appropriate snorkle.

Disassembly can be accomplished simply by cutting away weld (5) and removing the absorber dome and TES modules.

5.2 COMPARISON OF STIRLING CHP WITH BASELINE RSU

The following section addresses the key design goals emphasized in NASA's original problem statement. The Sanders Advanced CHP design is compared with the Baseline Brayton design information obtained from Reference 8. The following subsections address,

- Mass and size
- Efficiency
- Reliability / Life Factors
- Fabrication, complexity and cost

5.2.1 MASS AND SIZE COMPARISON OF STIRLING CHP WITH BASELINE RSU

Table 5.2 compares the component masses of the Stirling CHP RSU with the 7kWe version of the Baseline Space Station Brayton (Ref 8). To provide a fair comparison, we scaled component masses of the Stirling from the Brayton for such items as insulation, the outer shell and the aperture shield by area. Unfortunately we did not have a Baseline component breakdown with the detail that we would like. Due to the dissimilar design concepts, the greatest difference between the two concepts is shown in the second row of Table 5.2.

Table 5.2 7 kW STIRLING RECEIVER MASS COMPARISONS

COMPONENTS/ RECEIVER	BASELINE BRAYTON (KG) (scaled)	SANDERS CHP (KG)
PCM	70	73
Absorber/ PCM Containment/ Heatpipes	150	72
Aperture Reflectors/Shields		7
Multifoil Insulation		6
Outer Shell		9
Baffles/Supports		14
Misc.	241	4
TOTAL	461	186

The Sanders' CHP design minimizes weight by incorporating a single dome shell (.030 inches) as the heat pipe evaporator. The most massive elements in the unit are the 36 wedge-shaped PCM containers. The insulated exterior shell and aperture shield were scaled from the information provided in Reference 8. Therefore, the more compact CHP is able to achieve some mass advantage by requiring a smaller insulated enclosure. In conclusion, the CHP design exceeds NASA's goal with a Baseline weight reduction of approximately 60%.

The relative size of the competing 7 kWe RSUs are compared in Table 5.3. The CHP diameter is much smaller because the absorber geometry is not dictated by the PCM and heater head integration

requirements. The dome diameter of 28 cm was selected after a detailed stress life and evaporator design analysis.

Table 5.3 STIRLING RECEIVER VOLUME COMPARISONS

DIMENSION/ RECEIVER	BASELINE BRAYTON	SANDERS CHP
DIAMETER (m)	1.146	0.546
Length (m)	2.08	0.457
Surface Area (m^2)	9.55	1.252
Volume (m^3)	2.15	0.1070

Overall, the Sanders CHP receiver storage unit volume is only 5% of the Brayton Baseline. In fact, it appears that the entire Stirling CHP and engine would fit easily into the cavity of the competing RSUs. This enormous advantage is illustrated in the outline drawings of Figure 5.15.

5.2.2 EFFICIENCY COMPARISON OF ADVANCED STIRLING CHP AND BASELINE

The first group of loss mechanisms shown in Table 5.4 involve thermal losses. In forming these comparisons, we assumed a common receiver aperture diameter (16 cm) and insulation thicknesses as described in Section 2.1.3. The cavity losses were shown to be essentially equal after aperture diameter corrections because both designs assumed an average cavity temperature slightly above the PCM melting point in the day period and slightly below at night.

Table 5.4 COMPARISON OF STIRLING RSU EFFICIENCY (THERMAL POWER LOSSES)

PARAMETER	SANDERS CAVITY HEATPIPE	BASELINE BRAYTON
Insulation Losses (kW)	0.25	2.57
Day Cavity Loss (kW)	1.13	1.89
Mean Cavity Temp (^oK)	1049	1142
Night Cavity Losses (kW)	1.09	1.86
Mean Cavity Temp (^oK)	1039	1118
Reflective Losses (kW)	0.90	1.1
RSU Shading Losses (kW)	0.41	1.41
Total RSU Thermal Losses (MJ per orbit)	12.37	34.0

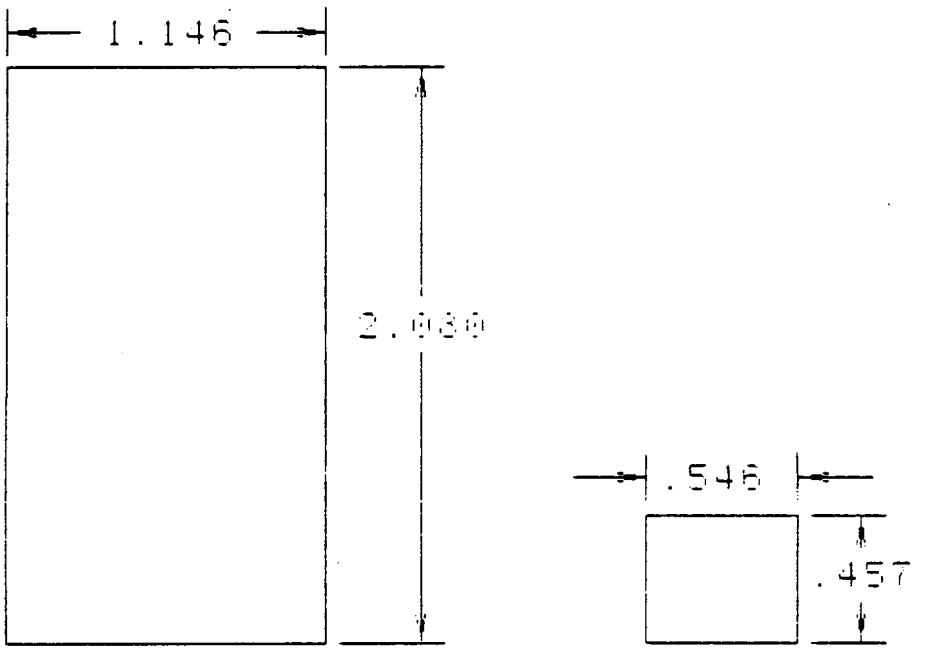

Figure 5.15 Stirling Receiver
Volume Outlines (units in m)

Total Solar Thermal Input (MJ per orbit)	148.5	180.0
RSU Thermal Efficiency (%)	91.7	81.1

Thermal losses through the outer shell of the RSU are shown on Table 5.4. For consistency, we have adopted insulation characteristics identical to those implied in the Reference 8 for the Baseline design. Conforming in this manner allows us to ratio the surface areas of competing designs to estimate the relative magnitude of these heat losses. The highly compact CHP design therefore achieves heat loss on the order of 13% of the Baseline Brayton (LiF).

Reflection losses were calculated for the CHP absorber design. Appendix E contains a conservative estimate based on diffuse reflections from a 0.9 emissivity naturally oxidized Inconel hemispherical cavity.

Shading, similar to reflection losses, is relatively small in magnitude and is only present for the sunlight period of the orbit. The values derived for Table 5.4 are based simply on the projected area of the receiver onto the concentrator. If an offset concentrator arrangement is used, like that proposed for the space station, this loss would be eliminated. In summary, the smaller overall envelope of the CHP is the primary factor in its advantage in thermal efficiency.

This 64% reduction relative to the Baseline in thermal losses for the CHP will further reduce the system volume and mass by reducing the concentrator size. Based on an assumed advanced concentrator specific mass of $2Kg/m^2$ (Ref 10), the improved thermal efficiency of our CHP RSU will save an additional 9.6 Kgs. or 4.8 square meters of concentrator area.

The second category of efficiency degradation factors described in Section 2.3 are referred to as engine integration losses. These arise when the RSU configuration dictates non-optimum alterations in the heater head gas path volume, or flow resistance. The CHP is not expected to introduce any additional losses in these categories since we propose no alterations to the heater head.

The third integration inefficiency common in the historical attempts to solarized Stirling engines is the inability to homogenize the typically non-uniform solar flux distribution within the cavity. This may become even more of an issue for the offset concentrator configuration planned for the space station. In the Avanco/USS Stirling module, which is the only quantified solar experience that we are aware of, variations on the order of $\pm 20^{\circ}C$ resulted in an engine efficiency drop of 6% (Ref. 8). This loss should be attributed to the RSU, not to the engine, however in practice it is often difficult to discriminate between the two. This again translates into a requirement for a larger concentrator. Based on the advanced concentrator specific mass, (24Kg/kWe) one should expect the effect to equate to an increase of about 12 Kgs and an increase in concentrator area of 2.7 m^2.

5.2.3 RELIABILITY COMPARISON OF STIRLING RSU's

The vast number of day/night thermal cycles during a system's operational lifetime is the principal reliability design challenge. This entails about 56,000 Earth orbits in the ten year system life. Moreover,

if creep relaxation occurs, each orbit imposes two thermal stress cycles on the solar absorber, one when the solar flux is applied and one when it is removed. To quantify the working life of the absorber, during this program we performed a detailed finite element stress analysis and employed the Method of Universal Slopes for fatigue correlation. In summary our findings indicate that the hemispherical absorber/evaporator dome can exceed the 10 year life goal with either IN 600 of Incoly 800.

Our stress and fatigue analysis was jointly conducted for the AHRCDS and our NASA/DoE terrestrial Stirling receiver designs. On these programs, we investigated Cb-1Zr, In 600 and Incoly 800 absorber designs. In summary, our findings indicated that the hemispherical shell is a very forgiving vessel because it is tolerant to thermal expansion and pressure loadings. Also, the edge conditions, out of the flux zone, are easily resolved.

Based on the stoichastic optical analysis, the hemispherical cavity is also near optimum for achieving flux uniformity. By comparison, a cylindrical cavity produces a characteristically sharper flux gradient in the axial direction. In the Baseline cavity concept, sharp flux gradients will exist along the circumferencial axis of each tube. This will introduce thermal stresses not encountered in our CHP dome absorber.

As addressed in the initial background discussion in Section 2.1, the space environment also presents several hazards for which the long term effects are not known, such as the attack of atomic oxygen and the prolonged vacuum affects on metal alloy constituents. In this regard, we believe that the CHP has also limited these risks by minimizing the exposed surface area and temperature of cavity materials.

Studies at Lockheed and elsewhere have indicated that fully oxidized materials provide the best resistance to atomic oxygen. Ni CO Cr Al Y or the application of flame sprayed ceramic coatings on the absorber hemisphere will achieve the desired stable surface. Another advantage of such oxide coatings is an increase in solar absorbance.

Corrosion from both the PCM and the heat pipe alkali metal is a less quantifiable life limitation. Corrosion within the heat pipe can lead to a clogging of the wick, as well as a reduction in structural integrity. Corrosion within the PCM modules is primarily a containment issue. To provide the greatest level of confidence in these areas, we have selected materials which have previously demonstrated excellent stability. Incoly 800 sodium heat pipes have been on test for more than 25,000 hours at Thermacore. Incoly 800 also meets our stringent stress/life criteria with a sufficient safety factor, and has therefore been selected as our absorber material.

In choosing the sodium-exposed materials, it is preferable to use similar alloys. Often, with powder metal wicks, it is not possible to use the structural container material. Nickel/In 600 or Nickel/Incoly 800 have been demonstrated to be stable combinations. Much less is known about refractory metal wick/wall longevity. FS-85 appears to be a particularly difficult alloy to work with, because of the large number of constituents. With a niobium wick, diffusion effects between the two alloys are likely over time. Such combinations have not yet demonstrated the stability and life that this application demands. We believe that the screen wick approach that we have adopted provides the best long term stability. With this approach we could readily make the screen wick from the same alloy used in the absorber and condenser.

The screen wick is the simplest to fabricate and has the fewest potential reliability problems. Wick/wall compatibility is less of an issue since the pumping wick need not be bonded to the absorber as with the sintered powder metal. Additionally, the key reliability issue associated with the latter, maintaining adherence to the wall over 56,000 thermal cycles, is virtually eliminated. Sanders' detailed stress analysis of the shear stresses at the wick/wall interface showed that long term attachment of the powdered metal to the wall was questionable. In our terrestrial Stirling receiver program, in which we proposed a dome using the Thermacore powder metal approach, we recommended an extensive experimental evaluation of fatigue effects. However, in our space-based CHP we can avoid significant development efforts by using the screen wick system.

To minimize sodium corrosion problems within our superalloy CHP, we will investigate metal cladding of the heater head. Since the heater head is not likely to be either of the wrought superalloy candidates considered for our dome, some developmental risk would be eliminated if a protective coating of a proven material were applied. This issue has been addressed on our DoE programs with MTI and STC. Both materials compatibility tests for the head material (In 713) and the application of an Incoly 800 barrier should be evaluated in future programs.

At this time we recommend Hastalloy B and Haynes alloys for the TES modules. Like the evaporators, cladding procedures are possible to minimize the materials exposed to the sodium. Pyrolitic coatings of non-wetting ceramic, such as boron nitride and graphite will be considered on the interior. Also nickel cladding of Inconel series alloys could reduce the severity of PCM corrosion. Such procedures are feasible with our CHP because of the relatively few parts involved.

Relating to both corrosion and stress/life issues are the potential life limitations of welds. Welds introduce flaw sites for enhanced corrosion, coupled with the possibility for alterations of material characteristics in the heat affected zone. The Sanders' CHP will involve welding only superalloys.

The Sanders' CHP advantage over the Baseline and other concepts in length of welds and number of sealed containers is shown in Table 5.5. We also feel that our CHP has an additional advantage in allowing access to the sodium side of the weld during assembly. In the unique assembly process for the large CHP, most welds can be inspected from both sides to detect flaws which could enhance corrosion.

In summary, we believe that the CHP concept is inherently more reliable than the Baseline RSU concepts for the following reasons:

The CHP has:

- Proven, non-refractory metal wick/wall combination with greater than 30,000 hours demonstrated
- A minimum length of heat pipe welds, most of which can be inspected and corrected, if necessary, from both sides due to its unique accessibility
- Far less total weld length, including the PCM modules

- o Minimum cavity temperatures and stresses
  - lower flux gradients on hemispheric surface
  - no solar irradiated insulation and structure in cavity
  - absorber surface coatings to minimize atomic oxygen attack
- o Lowest parts count.

After a detailed stress and life analysis, we have concluded that the CHP can meet the NASA performance and reliability goals with superalloy hot section parts. Moreover, the CHP concept is inherently less costly to fabricate for the reasons presented above.

Table 5.5 COMPARISON OF STIRLING RSU RELIABILITY FACTORS

RECEIVER WELDS	SANDERS CHP	BASELINE BRAYTON
Weld Length Exposed to PCM: (m)	33.8	1814.
Weld Length Exposed to Sodium: (m)		
Total	5.53	0
Noninspectable	1.53	
Number of Sealed Containers:		
PCM	36	5016
Sodium	1	0

5.2.4 STIRLING RSU COMPARISON SUMMARY

The CHP RSU has shown the potential for substantial improvements over the IOC Space Station Brayton design in all areas specified on this program. In addition to a mass reduction of 60%, volume reduction of 95% and a more than 50% reduction in thermal losses, its inherent simplicity will allow us to achieve the 10-year operational lifetime goal without the use of refractory metal components.

Finally, the Sanders' CHP concept is extremely versatile in accommodating any number of Stirling heater head configurations. Therefore, the ability of the CHP RSU to proceed with the development of the evaporator and TES elements of the design, without constraining the engine heater head technology, is a valuable advantage that other RSU concepts do not share.

5.3 DISCUSSION OF KEY TECHNICAL ISSUES

The key issues pertaining to verification of the CHP principles are generic in that they exist in all heat pipe and LiF-CaF2 PCM systems. These key issues include:

Heat Pipes

- o The longevity of sintered powder metal wicks (fatigue chemical diffusion)
- o Performance (boiling limits) of arterial wicks
- o Corrosion: clogging in sintered powder metal wicks, wire breakage in screen wicks.

LiF-CaF_2 Thermal Storage

- o DV/V induced stress in container
- o Corrosion

5.3.1 HEAT PIPE KEY TECHNICAL ISSUES

During this program we identified simple screen wick designs for all three sections of our CHP. On the heater head condensers, the wick geometry calls for a simple composite layer tube capped on one end. For the thermal storage design each module is wrapped in a similar sheet of composite wick material. The evaporator design, however, is less straightforward due to the added dimension of curvature required for the dome wick. In addition to the formed screen wick, we see a potential for powder metal wicks. To incorporate the screen requires deforming the mesh around a nearly hemispherical dome. In Section 5.3, various fabrication options are discussed along with a program plan designed to reach a final recommendation.

The issues of long term compatibility of sodium with the metals remains controversial, even after many tests have been conducted. Understanding corrosion in heat pipes requires more than a study of the thermodynamic rates with coupon tests because of the mechanisms at work within the heat pipes. Configuration issues are important, such as the characteristics of welds, stress corrosion, the electrolytic effects in crevices, sodium flow rates, the generation of noncondensible gases, alloy constituent migration to the evaporator surface, the presence of contaminants, and the effectiveness of gettering materials. Some of the powder metal versus screen wick trade issues are important to the overall corrosion study. Adverse grain boundary effects are much more prevalent in the powder metal wick, as is the potential for clogging and cracking or flaking. High porosity composite screen designs, on the other hand, are less prone to clogging, and due to their wrought characteristics would be expected to exhibit less grain boundary effects.

Because of the difficulty and inconclusiveness of simulations, we believe it is most definitive to conduct full scale life tests of the complete heat pipe assembly, implying a requirement for 1-g operation. In Section 5.1.2, we considered a range of wicks and configurations and found that designing for no gravity head allowed the use of relatively coarse, easily formed screen wicks. However, by employing lower pore size screens, two more important benefits arise. First, full scale 1-g life tests can be conducted on each. Secondly, this choice implies that a large performance capacity safety factor will exist when operated in space.

5.3.2 THERMAL STORAGE KEY TECHNICAL ISSUES

Like the heat pipe, corrosion in the PCM modules, especially in the vicinity of welds, is an issue which requires cyclic life testing. This of course applies to all RSU designs and concerns the specific container geometry and fabrication techniques, as well as the material selection. However, the second important issue concerns coping with the DV/V induced stresses. In designing for this condition, Sanders proposes to utilize favorable geometry combined with non-stick ceramic wall coatings. The CHP concept provides a unique flexibility in the geometry selection of the PCM container. Moreover, Sanders and others have shown graphite and other covalently bonded ceramics to be relatively inert, as well as non-wetting in the presence of LiF. The lower temperature Stirling eutectic should be even safer.

As an augmentation to the above, we recommend consideration of immersed ceramic fiber mesh systems. The mesh concept has the potential to increase the effective thermal conductivity of the liquid phase while encouraging the formation of a dispersion of pore-size voids. In any other PCM container it is nearly impossible to predict or simulate the void distribution. The mesh, however, has the potential of minimizing the effect of gravity by introducing dominating capillary forces which immobilize the bulk movement of the liquid. With finely distributed voids, the potential for thermal ratcheting is greatly reduced.

Mesh-related research and development is presently underway for space station RSUs. When applied to this Baseline technology, it may possibly reduce the transient hot spots caused by void formation on the solar absorber surface, as well as the ratcheting stresses. However, when applied to the Baseline receiver concept, we do not see it as allowing for a significant specific mass reduction. Since most of the solar power must pass from the absorber side through the envelope to the gas-cooled wall, the relatively low conductivity porous solid always limits the charging rate and thus the cavity volume. Ceramic mesh, rather than metal, could conceivably cut in half the mesh mass in the Boeing RSU for example, but that is not nearly enough to meet NASA's 50% total specific mass reduction goal.

Alternatively, we feel the mesh systems are much more applicable to our CHP system. In this case, the PCM and the engine working fluid are heated in parallel rather than serially as in the Baseline scheme. In our design, only the night storage power passes into the module, as opposed to through the module, resulting in a significantly lower charging rate. Moreover, the liquid layer, is the predominant charging limitation and its conductivity would be significantly enhanced by the mesh. For this reason, we also feel that a lower volume fraction of the mesh would be required in our CHP modules than in those which transmit the full solar flux.

Several ceramic mesh materials are being studied at NASA Lewis. Initially there was a focus on graphite fibers because of their high thermal conductivity/density ratio. However, the non-wettability of the graphite-PCM system would tend to discourage the wick suspension phenomenon which we most desire. Alternatives are under consideration which could increase the wettability.

The mesh/PCM systems provide the only means for overcoming the effects of Earth's gravity. Although maintaining the long term stability of the mesh charactersitics has been found to be a difficult problem, in principle, the capillary forces within the fiber matrix can immobilize the PCM. For this reason the concept is unique since it yields a system which can be adequately verified on Earth. All other PCM designs cannot be simulated in Earth testing. Our recommended development approach would be to first determine the worst case DV/V scenario of the non mesh filled PCM containers. Then an experiment would be set up to demonstrate a sufficient safety factor at that worst case set of conditions. As a fall back position we will consider implementing mesh systems. Because the CHP has such a weight advantage, even with

state-of-the-art Nickel mesh systems, our calculations indicate that we can meet NASA's 50% Baseline mass reduction goal.

6.0 CRITICAL TECHNOLOGY EXPERIMENT DESCRIPTIONS

The following section provides a description of a predominantly experiment based program which addresses the key technical issues associated with the novel DAR Brayton and CHP Stirling RSUs. "Critical" in this context refers to those issues which NASA perceives to possibly contain a fundamentally unsolvable technical obstacle. Some of the experiments outlined at the end of this section are not classified as critical and have been termed follow-on testing. Most of the work described in this chapter was conducted in Task III of the AHRCDS.

Several solar dynamic critical issues are associated with controlling liquid PCM movement inmicrogravity and the resulting thermal and ratcheting stresses. These technical issues inevitably are traceable to the lack of experience with the space environment that is common to all solar dynamic systems. No substitute for micro-gravity space testing has been found where sufficient thermal cycling can be accomplished. For this reason we have attempted to identify RSU concepts which are less prone to the long term DV/V unknowns. Short term liquid management questions are those which can be adequately addressed within the 20 to 30 second low gravity test time of the microgravity research aircraft. A combined use of the research aircraft and earth-based testing is the approach considered in this study. Extraterrestrial flight testing is clearly beyond the near term scope of this program. However, the programs to be described in this section are believed to be sufficient to resolve the critical issues and thus significantly limit the risks associated with the ultimate deployment of these receivers in space.

Table 6.1 reflects the two general problem areas which confront solar dynamic systems. The specific Brayton and Stirling RSU topics addressed in this section are listed below these headings. Fortunately, the material fabrication issues can be directly addressed through earth-based testing. Rigorous stress/life testing coupled with a thorough evaluation of materials and fabrication techniques is proposed in the following pages. Two-phase, (or three-phase as present in PCM systems) behavior in the micro-gravity environment is studied in a series of research aircraft low-g maneuvers.

6.1 BRAYTON DAR CRITICAL TECHNOLOGY PROGRAM PLAN

Three experiments are planned to investigate the issues of liquid PCM control and window design and selection. These tests are as follows:

1. Window corrosion/condensation analysis in furnace (continuation of AHRCDS testing)
2. Small scale solar simulator windowed cavity test.
3. Lear Jet (NASA Lewis) or B-707 (NASA Marshall) low gravity wicking test of full scale RSU cavity.

Table 6.1 CRITICAL TECHNOLOGY ISSUES FOR SOLAR DYNAMICS

	Micro Gravity Fluid Management	Materials/Fabricability
General		
Solar	DV/V Performance effects	Cost/complexity PCM corrosion (welds)

Dynamic	DV/V Stress (ratcheting)	Material selection
DAR Brayton	Liquid suspension in Heat Exchanger DV/V fatigue	Refractory metal embrittlement Window performance PCM corrosion
CHP Stirling	DV/V performance DV/V stress (ratcheting)	Alkali metal corrosion PCM corrosion Wick forming methods

6.1.1 WINDOW COMPATABILITY AND DESIGN

This task addresses the first two experiments listed above, and will complete the experimental effort described in Section 4.3. As discussed, these experiments have identified several candidate materials which have passed our initial screening tests by demonstrating a negligible reduction in clarity over a 200 hour LiF vapor exposure test. Short tests of this nature are sufficient to determine the extent of the chemical reaction as well as to predict the deposition rate through common surface chemical analysis techniques. In addition to the fluoride window materials, we also considered thin-film amorphous coatings and diamond-like coatings. The most probable substrate for these coatings is fused silicon dioxide (synthetic quartz).

Additional testing in the manner described in Section 4.3.2 should be conducted on the encouraging window candidates identified in our prior tests. These include calcium fluoride, barium fluoride, strontium fluoride and diamond-like coatings. A 1000 hour test duration would yield a thicker layer of deposition which could provide better insight into the condensation rates.

An analytical model of the condensation phenomenon within the furnace cavity will be constructed. This model will be correlated with the new data as well as points already acquired in the existing experimental set-up used during this program. This will allow us to consider the effect of different thermal gradients and the presence of non-condensable gases. A thorough investigation of the interaction of the window materials with LiF and its effects on physical, chemical and optical properties of the materials will be carried out. Scanning electron microscopy (SEM) will again be used to detect morphological changes if they occur on the window due to condensation and/or reaction. Surface analysis techniques, Auger Electron Spectroscopy (AES) and X-ray Photoelectron Spectroscopy (XPS), will be utilized in evaluating the reaction products, if any. These techniques are highly surface sensitive and are uniquely suited for this purpose because of their high sensitivity for light elements, such as oxygen, nitrogen, carbon and lithium.

Having investigated chemical surface effects, measured the deposition rates on the various window materials and correlated a condensation model of the cavity, it is appropriate to conduct a more complete simulation of the cavity. Figure 6.1 illustrates a scaled solar experiment of the window and cavity environment. The solar flux on the window is necessary to determine its effect on the condensing phenomenon. For example, the various window operating characteristics for the design scenarios depicted in Figure 4.9 a, b, and c, are highly dependent upon the window and condensate spectral absorption.

The proposed test apparatus will be either an existing solar furnace (such as those at Georgia Tech, Sandia Albuquerque or White Sands) or a solar simulator. Since a small scale experiment can simulate all of the

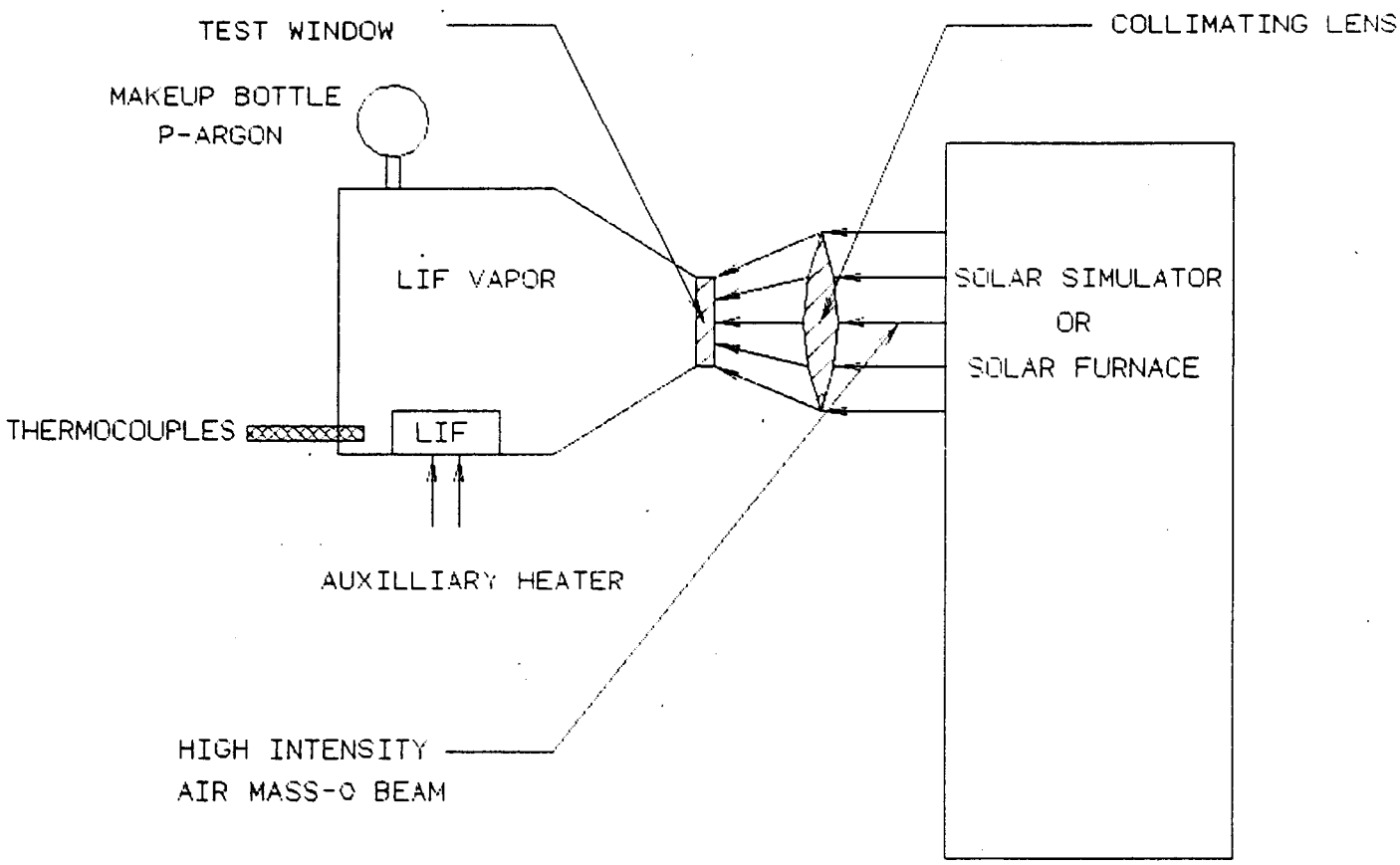

Figure 6.1 Scaled Solar Experiment of Window and Cavity

significant operating conditions, the test will be very informative and inexpensive. The solar simulator is preferred because test conditions can be more precisely controlled. Moreover, the terrestrial spectral content of the sun lacks the extra-terrestrial UV contribution, and several window candidates exhibit finite UV absorption. The solar simulator would have the added advantage that it could be used to conduct a significant number of thermal cycles and duration testing. The Spectrolab X-25 solar simulator can develop a flux in excess of 30 w/cm^2 over a 2 to 3cm diameter target.

After a prolonged exposure of 1,000 hours, with 30 minute on/off cycles, the post test evaluation will involve the same surface chemistry analytical techniques employed in the initial screening experiments described in Section 4.3. The two key evaluation parameters are, however, transmissivity and the deposition thickness. With cyclic testing as described, we believe that it will be feasible to extrapolate the data to the 10 year operating life.

6.1.2 LIQUID PCM CONTROL WITHIN THE CAVITY

The purpose of this experiment is to verify the zero-g wicking ability of the DAR corrugated heat exchanger geometry. The most conclusive approach is therefore to conduct a full scale test on a research aircraft, preferably the NASA Lewis Lear Jet.

The approach will be to take time lapse photographs of doped liquid LiF moving from the non-wetting reservoir into the corrugations during the 20 to 30 second aircraft maneuver. Figure 6.2 illustrates the simple test configuration. LiF is maintained in the molten state at the domed end of the reservoir by a heater during the aircraft's pre-test maneuvers. The domed end of the receiver will be coated with non-wetting pyrolytic boron carbide (or graphite). As the gravity decreases to near zero over a two to three second period, the liquid will begin to wick up the corrugation channels. With only viscosity to impede it, the capillary driving pressure would accelerate the liquid up the length of the channel in approximately 1.5 seconds. Upon reaching the non-wetting aperture cone, the capillary driving force will cease and the PCM will stop. Based on a test period of 20 to 30 seconds, it appears that ample time exists to totally fill the corrugations and demonstrate static liquid suspension.

The doping of the LiF may have some effect on the liquid mixture's surface tension properties and therefore these additives should be included in this test. With our present knowledge of the optical effects of various dopants, we will be able to select a material and concentration appropriate for the test. Detailed doping experiments necessary to optimize the thermal performance of the system will be conducted in follow-on testing.

6.2 FOLLOW-ON BRAYTON DAR ANALYSIS AND TESTING

The effort described in this section does not address what we consider to be critical technical issues. Rather, having demonstrated solutions to the liquid management and window survivability issues, common engineering principles should be applied to the structural design of the cavity heat exchanger. The proposed experiment is designed to simulate worst case stress, fatigue, and corrosion under operating conditions. The specific subjects pertain to the measurement of the peak temperatures and stresses as well as evaluation of weld integrity and possible corrosion effects.

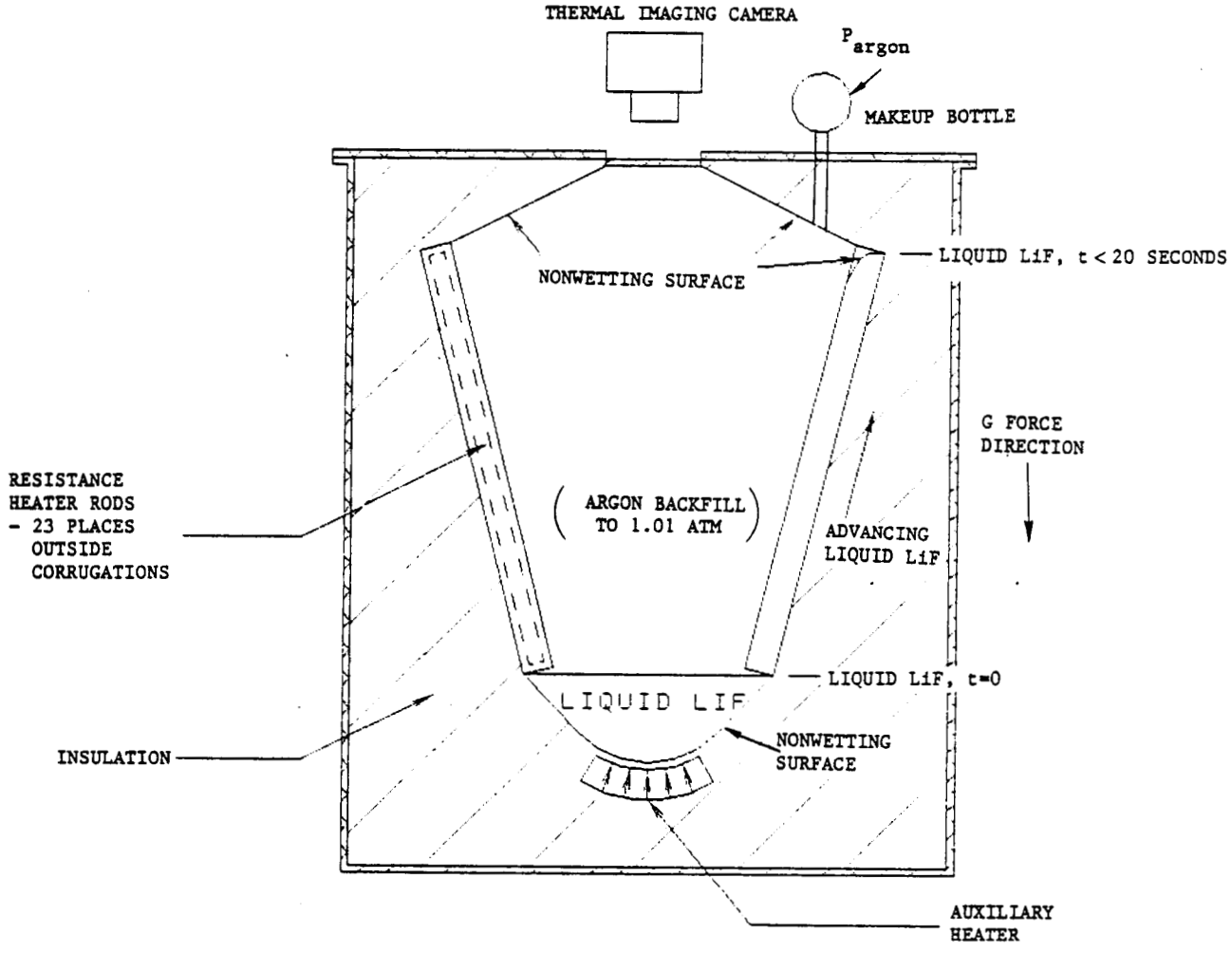

Figure 6.2 Liquid PCM Management Test Configuration for Lear Jet

In this task, we recommend first expanding the stress analysis already conducted and correlating the results with a scaled experiment. The finite element method (FEM) analysis should focus on the peak stress zones defined in this program. This analysis should consider pressure, and thermal stresses in the absorber heat exchanger and in the attached manifolds.

The stress predictions and experimental correlations will provide the basis for fatigue and creep life extrapolations. In the evaluation of fatigue (predominantly thermal), we recommend the construction of a modified Goodman diagram utilizing the Method of Universal Slopes. Creep life can be estimated with commercial product test data or Larsen-Miller correlations.

Using previous solar test experience as a basis, we believe that it is important to apply safety factors to the solar flux profile as well as the material characteristics. In the completed Stirling absorber FEM analysis, we incorporated a 2:1 local peak flux safety factor and an adverse flux gradient of 3:1 per linear inch at the peak flux zone. These factors are required because of the inaccuracies in predicting the real life local flux anomalies in the cavity. These standards that we have adopted, although realistic, are more rigorous than those used by other receiver designers in the literature.

To validate the stress and thermal models, we propose a laboratory scale test. This experiment, illustrated in Figure 6.3 will evaluate the performance of an unrolled section of the DAR cavity. This apparatus will lie horizontally to contain the PCM within the channels in a manner similar to what is expected in actual low-g operation. Figure 6.4 illustrates that indeed it is not possible to precisely simulate a capillary-dominated distribution of liquid at the required scale in the presence of Earth's gravity. However, this figure also suggests that the 1-G test would present a worst case condition with respect to the critical corrugation tip temperature.

In this test, the helium xenon mixture or a simulated working fluid will be circulated in a closed loop. Either closely coupled xenon arc lamps or electrical resistance tungsten wire heaters will be used to simulate the required flux distribution over the 10 to 16 cm wide test section. It is not imperative that the exact solar air mass-0 (outer space) spectral distribution be simulated for this test. The resistance heater will operate at about 2,000^{o}C in a vacuum and irradiate the test section with about 10kW. This temperature, although below that of the sun, is acceptable to evaluate the performance of the doped PCM. The doping concentrations will be re-adjusted to evaluate and optimize the absorption characteristics of the PCM. Appendix I contains a preliminary design of a heater for this application. The next step in the development of the DAR should involve the testing of a full scale receiver storage unit.

The complete system test program should include solar, vibration, and other environmental issues. Terrestrial solar testing can be conducted on the SNLA Test Bed Concentrator (TBC). As illustrated in Figure 6.5, this system has more than enough power and optical quality to meet our needs. However, it has a problem in meeting one of our test requirements. It is designed with a nominal focal length to diameter ratio (f/d) of 0.6. This value can effectively be increased when we stop-down the receiver aperture from its typical value of about 8 inches to our 6 inch (16 cm) diameter. Since we anticipated a f/d = 0.5 for the typical space concentrator, the cavity flux distribution will be substantially different. Roughly, the total included acceptance angle of 0.5 f/d is about 120^{o} while we might expect most of the power within 50^{o} to 60^{o} from the TBC. Alignment modifications of the 220 individual TBC mirrors can be undertaken to achieve a more representative flux profile within the cavity. Alterations of our RSU

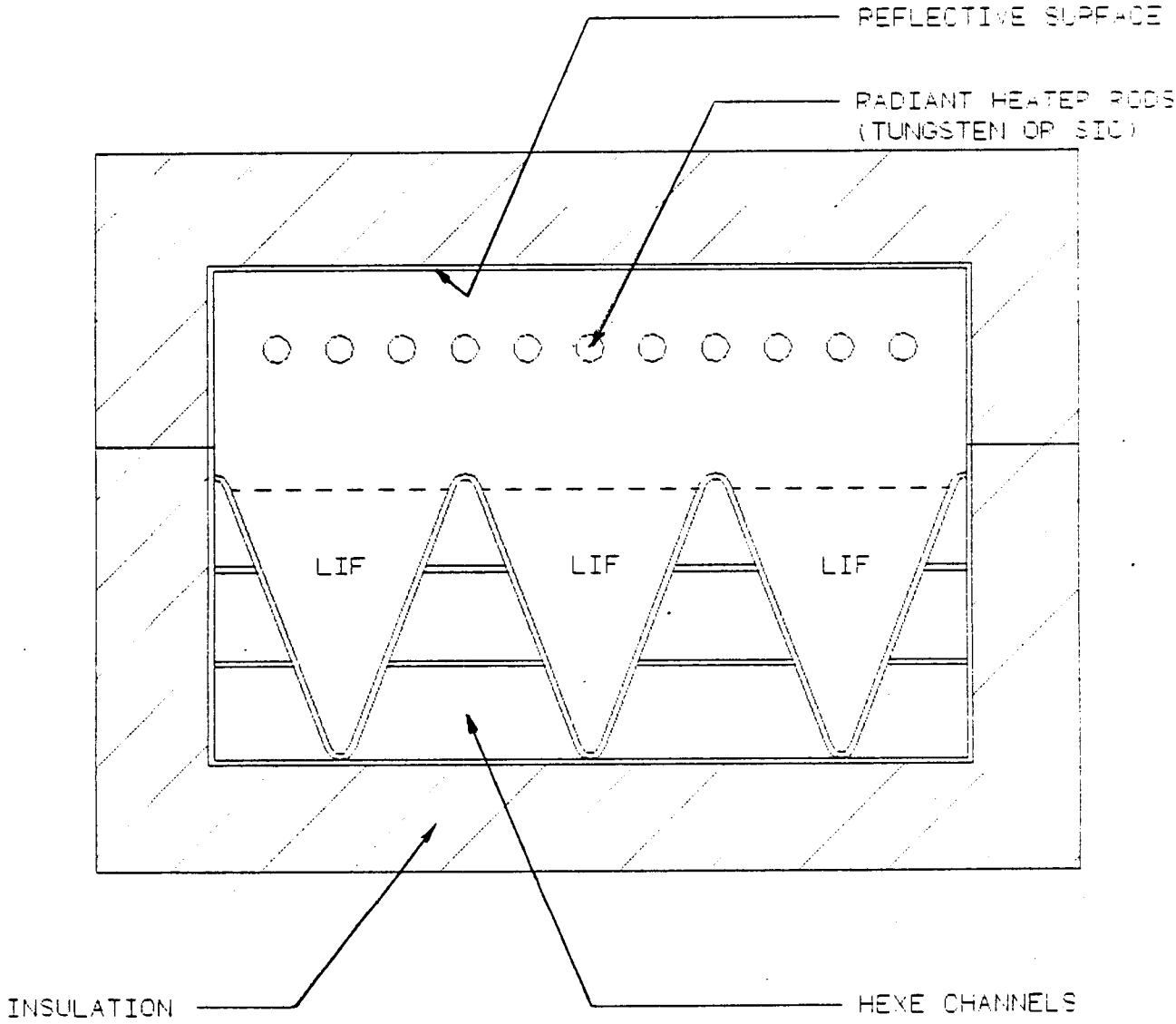

Figure 5.3 Full Scale Brayton Cavity Section With TES Module

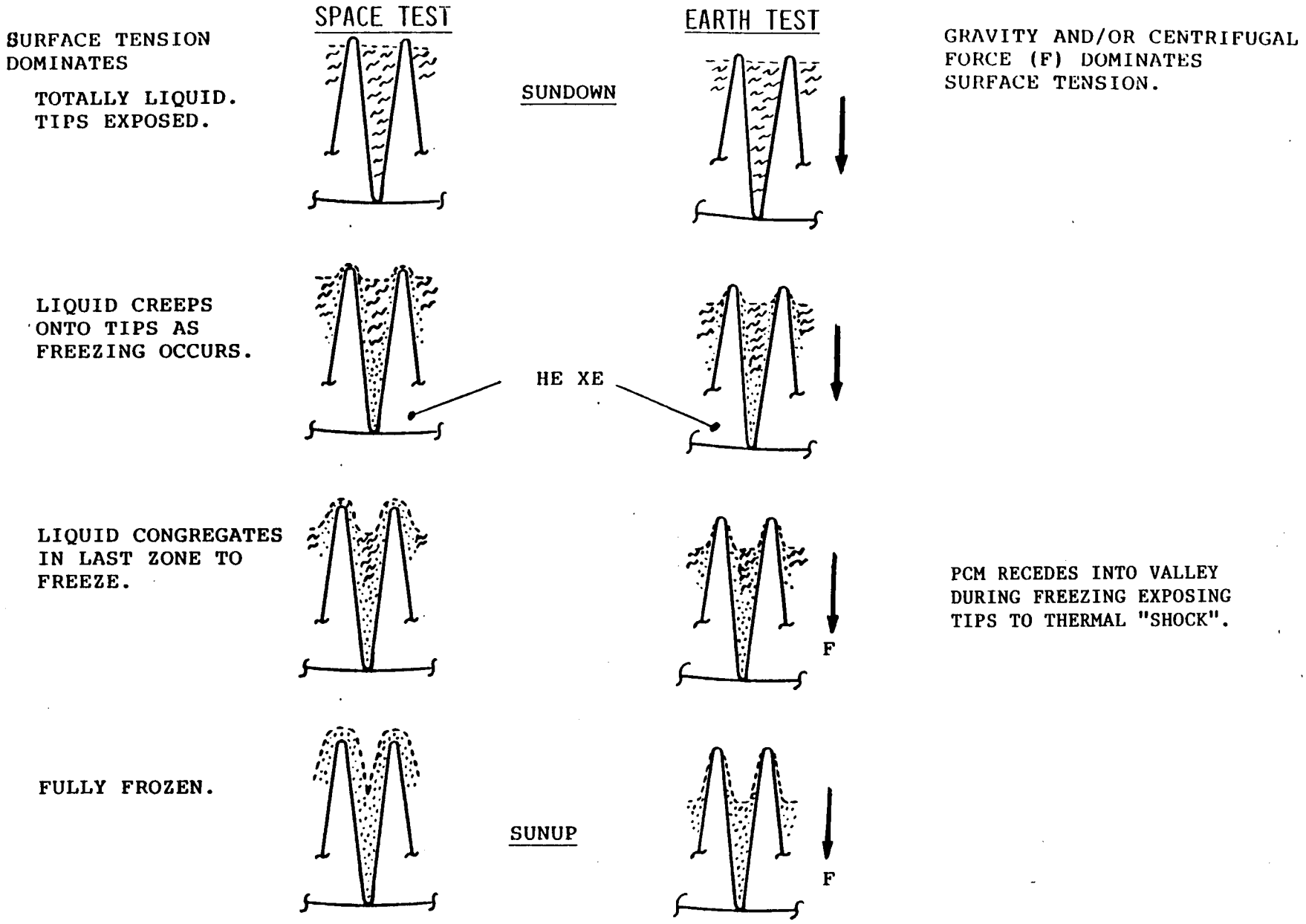

Figure 6.4

Comparison of Freezing Patterns of PCM in Brayton TES.

This figure illustrates that the transient tip temperature would be higher in an Earth test than in the actual environment.

FULL SCALE RSU FIELD TEST

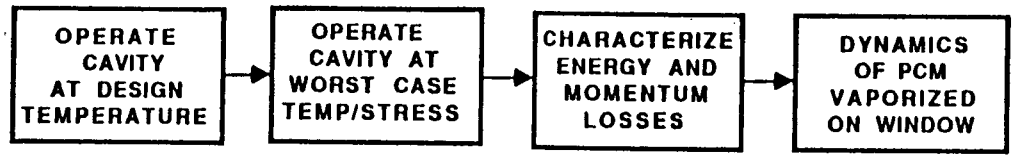

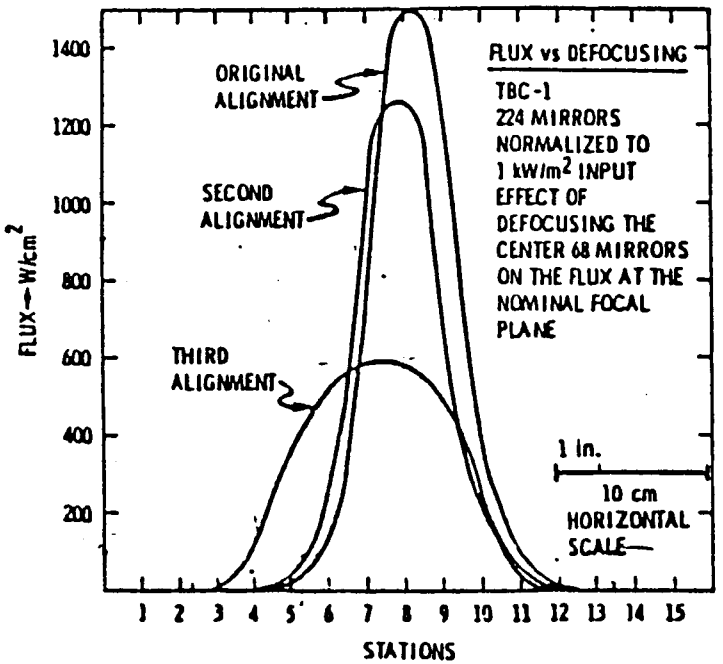

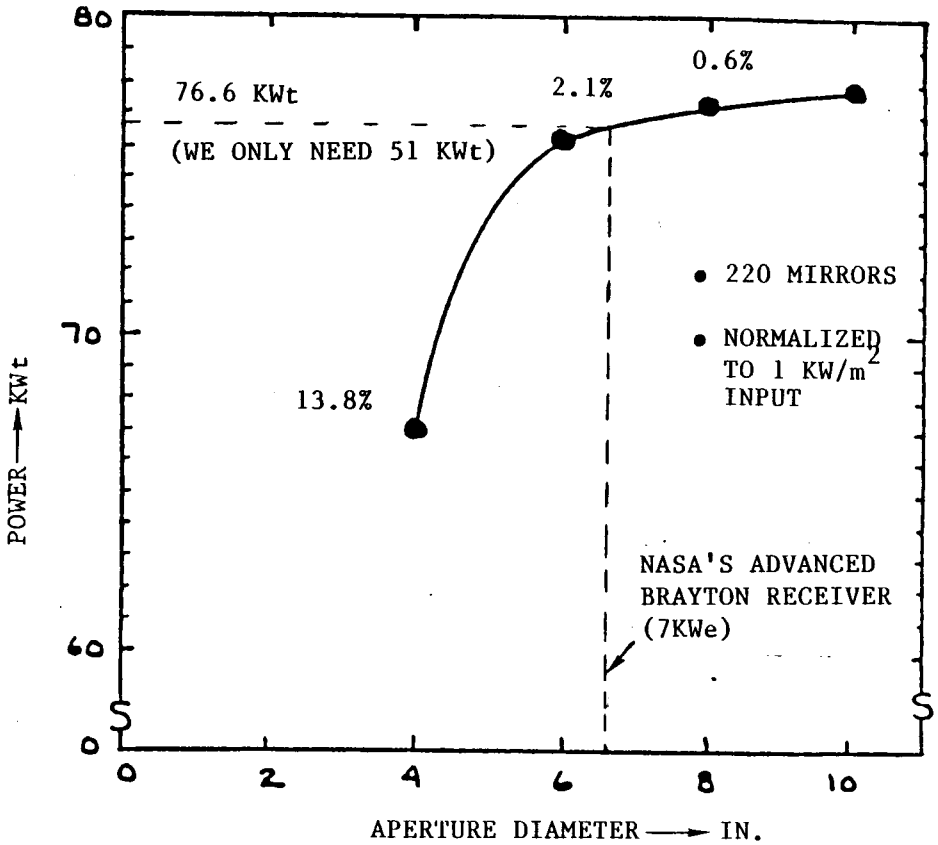

Figure 6.5 Solar Flux Measurements on Test Bed Concentrators.

cavity are a less desirable option. Some optical modeling of the TBC/DAR system should be undertaken in preparing the final test plan.

Although these tests will have to be conducted without the PCM, the absorber heat exchanger will be designed so that it can withstand the full solar input without the PCM, thereby demonstrating its substantial safety margin. To conduct this test we would increase the simulated engine mass flow by 40% to maintain the nominal design exhaust temperature. This would be analogous to increasing the engine speed to operate at a higher power level.

When testing the receiver on Earth, it is imperative to maintain an oxygen free environment around the refractory metal alloys while operating at high temperatures. To achieve this, and to accurately simulate the window pressure stresses, we will maintain a slight positive cavity pressure with argon gas. This will also be the practice for space deployed systems while in the pre-launch state. With an LiF-filled system, we would similarly maintain a small positive gas pressure within the cavity which would bleed out through a check valve during launch. As described in Section 4.3.2 we would maintain a partial pressure of a few torr during operation to control condensation on the window.

6.3 STIRLING RSU CRITICAL TECHNOLOGY EXPERIMENTS

In Section 5.3, the discussion of key technical issues centered around the evaporator and PCM module design. Considered in this design are the fundamental challenges of fabricating the wicked dome and averting thermal ratcheting in the PCM containers. To address these issues and generate the design data required to meet NASA's performance and life goals, we propose a rigorous Phase I test program for the evaporator and the PCM modules. The elements of this program are outlined in Table 6.1, and discussed in the following sections.

6.3.1 EVAPORATOR DOME PERFORMANCE TEST

To evaluate evaporator performance, we recommend the fabrication of three or four sample composite wicks using the wick structure defined in Section 5.1.2.

To evaluate the various evaporator designs, a test has been devised to measure the maximum flux capacity of the wick system. This measured data will be correlated with our thermo-optical wick model as described in Section 5.1.2. If we discover that capillary or nucleate boiling limits are encountered at fluxes lower than originally anticipated, further design iterations should be conducted to lower the operating flux by either enlarging the dome, slightly adjusting its shape or adjusting the wick parameters. Exploring various wick compositions, pore sizes and permeabilities will also introduce valuable test data that can be applied to formulating the final design configuration.

The first step in designing the hemispherical screen wick will be to evaluate several fabrication techniques. Any fabrication procedure will result in distortion of the screen grid pattern and its porosity as it conforms to the dome shape. However, there are several which we believe will yield acceptable wick characteristics.

The composite screen wicks described in Section 5.1.2 have a relatively fine top layer (the vapor surface) which covers a more porous underlayer in which the liquid flows. In the top layer, called the pumping layer, the maximum pore diameter across the surface is critical and therefore requires the greatest care during the forming process. Although the underlayer pore size is not critical, its thickness, which affects the boiling characteristics, is very critical.

To meet the required evaporator design characteristics we recommend evaluating four pumping wick forming methods: drawn screen, hydroformed screen, spun screen, and etched and drawn sheet metal. The following paragraphs briefly describe these approaches.

Newark Wire Cloth Company has fabricated experimental samples of 60, 200 and 400 mesh stainless steel screen drawn with an existing 11 inch diameter mandrel to a nominal three inch depth (the limit of their tooling). In this process, the hemispherical punch draws a disk of annealed wire mesh into a stationary ring surrounding the punch. This distorts the square wire mesh pattern to conform it to the hemispherical mandrel. At some point in this drawing process, determined by the porosity of the screen, the maximum distortion of the screen is reached and wrinkles start to form as the excess screen material overlaps itself. Our initial attempts with this approach yielded a satisfactory curved section for only about 80^{o} of curvature.

Hydroforming is similar to drawing except that the hemispherical mandrel presses the flat screen disk into a block of soft rubber, rather than drawing it through a ring. We expect this technique to allow a somewhat deeper draw before wrinkling occurs, as there is a greater tendency to stretch the screen toward the outside diameter of the dome.

The spinning process is another feasible method of forming a hemispherical screen wick assembly. The first step of the process is to clamp the disk shaped blank against the male hemispherical form which is mounted on a spinning lathe. The spinning blank is then forced to conform to the shape of the hemispherical form by the application of radial force from a stationary forming tool pressed against the surface of the blank. The effect of this process is to stretch the blank material to conform to the desired shape. Work hardenable materials such as Incoly 800 used for the evaporator dome assembly require intermediate anealing steps to retain the necessary ductivity.

To successfully form the hemispherical screen wick it would be necessary to sandwhich the screen material between two disks of sheet metal to protect it against severe abrasion during the spinning process. A promising technique would entail using soft aluminum disks to sandwhich the screen so that the pressure of the spinning operation would tend to emboss the screen into the mating surfaces of the disks and thus cause it to stretch in the same manner that the disks are stretched during the spinning process. This would tend to prevent wrinkling of the screen around its perimeter. After the spinning operation was complete the disks would be discarded and the screen placed over the evaporator dome. Some experimenting will be required to determine whether one or more layers of screen can be successfully fabricated at a time.

The fourth approach involves etching a hole pattern in a flat disk of thin sheet metal and then hydroforming it into a dome. This offers great design flexibility, but does require some special tooling. The principle is that the amount of stretching and distortion of a sheet metal disk as it is hydroformed to

the desired hemispherical section can be accurately determined and an etching mask prepared which compensates for this distortion by varying the etched pore diameter as a function of its radial position. Thus, when the pores have been etched in the disk and the disk hydroformed into a hemispherical segment, the resulting pore size will be nominally uniform over the entire surface. Another advantage of this technique is that it permits heavier wall sections between pores which will extend the corrosion life of the pumping wick. This technique could also permit the etching of radial grooves on the surface of the hemisphere that could serve as the fluid transport path and eliminate an inner screen wick.

Prior to conducting the performance testing, the fabricated evaporator domes will be inspected for oversized pores in the pumping wick layer. Two tests are planned. First, using the bubble method and then an optical comparator, the maximum pore size will be identified and measured. Figure 6.6 shows the simple bubble test apparatus to be employed. The total dome and wick junction at the base circumferencial artery feed plenum, temporarily sealed, will be slowly pressurized with air. With a 400 mesh screen, for example, a gas pressure head equivalent to about 30 inches of water can be achieved prior to overcoming the capillary pressure. As the gas pressure slowly approaches this limit, a pore with greater than the standard pore size will release a stream of bubbles. By measuring the gas pressure at the onset of this bubbling it is possible to derive the approximate pore diameter at that location. The optical comparator would then be employed to make a quantitative measurement. Presuming it meets our minimum specifications, we would then prepare it for the performance tests with sodium.

To demonstrate this evaporator design, we recommend conducting performance tests next. The test apparatus shown in Figure 6.7 allows the evaporator to be operated independently of the remaining CHP components. The thermal performance of the wick system can be evaluated by determining the maximum power throughput.

The system can be powered with either an RF induction coil or an electrical radiative source. Both appear to be feasible means of achieving the required power density. Each approach does however have limitations. The RF induction approach can achieve the higher power density, exceeding our nominal 50kW demand. However, a relatively costly, high frequency power supply ($70,000 to $100,000) appears to be necessary to satisfy this requirement. The high frequency (400-500KHZ) is required to achieve the required shallow penetration depth of the RF flux. Custom fabrication of the heating coil would not be as challenging as a radiation source since it could be constructed from copper tubing.

The radiation source is more limited in its power density capability but can still meet the 50kW load. Two resistant source design options are described in Appendix F. The first utilizes commercial silicon carbide heater rods and the alternative uses tungsten wire. Since SiC can not be readily purchased in shapes other than rods or tubes, it is not feasible to consider building a hemispherical source as would be desired for the lowest watt-loading and temperature. For this reason we limited our present effort to a parallel array of rods forming a radiating disk. Alternatively, utilizing refractory metal wire (tantalum, molybdenum, tungsten) it is possible to consider a spiral shaped heating element.

The energy can be removed from the system with a simple condenser coil. Controling the fluid flow rate and inlet temperature can provide the necessary flexibility to conduct the test. Additionally, a gas gap calorimeter should be incorporated by designing the condenser with either concentric tubes or shells. A variable concentration of helium and argon flowing in the gap between the shells provides control over the thermal conductivity of the gas gap. This allows better control of the heat removal fluid temperature

Bubble Test Apparatus

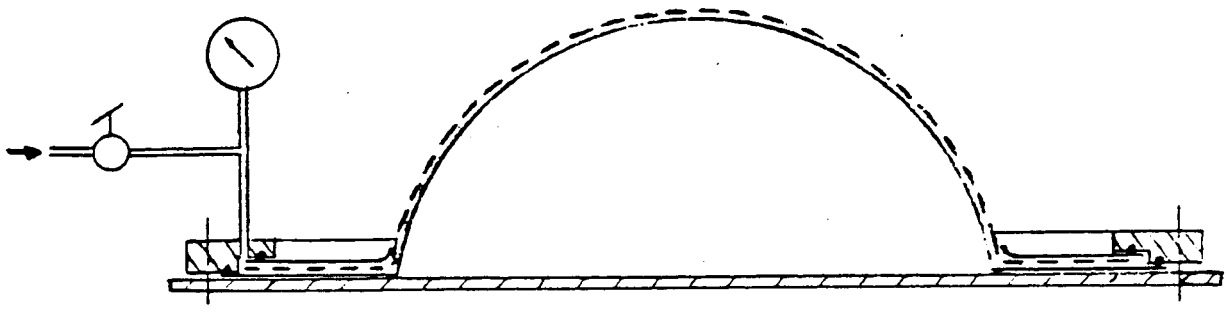

Figure 6.6

A water solution bubble test will be performed to assure that all pores and thebond to the absorber flange meet standards.

ACCELERATED LIFE TEST OF EVAPORATOR DOME

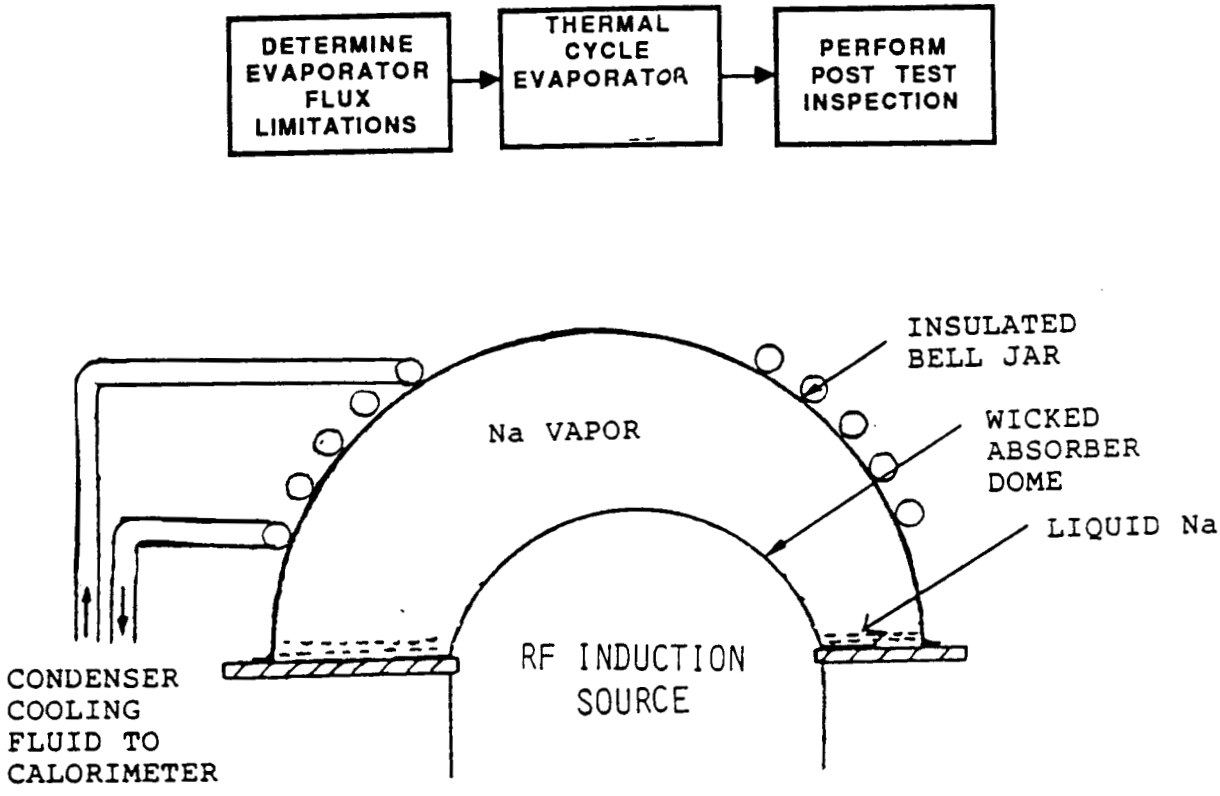

Figure 6.7 Test Rig for Testing Evaporator Performance Independently of Entire CHP

flowing in the calorimeter. The condensed sodium will drip into a circumferencial liquid reservoir, which then feeds the composite wick.

This system can be monitored with thermocouples tack-welded to the concave side of the dome or a thermal imaging camera. Strain gauges should withstand the environment for a period long enough to make meaningful measurements. A calorimeter, composed of a flow meter and thermocouple, will continuously measure the system power output. Assembly of the evaporator dome into this apparatus, would employ the wick fastening and welding techniques selected for the final CHP design.

The test will determine the flux limit at a nominal vapor temperature of 1039^{o}K. This can be a relatively short duration test using the best of the wicked domes fabricated. By simultaneously raising the power input and the calorimeter power extraction to maintain 1039^{o}K, the total flux through the wick will be increased. Two occurrences should signal that the "burn-out" or wick dry-out condition has been reached. Normally the thermocoupler on the absorber surface will indicate a temperature higher than the internal vapor temperature by an amount proportional to the local flux. The point at which the absorber temperature readings radically depart from the vapor temperature indicates the onset of either a vapor blockage in the wick due to nucleate boiling, or the capillary limiting dry-out. The location where the phenomenon is initiated will indicate whether the capillary or boiling limits were exceeded.

Real-time monitoring of these temperatures and a slow escalation of input power will provide enough time to react and shut down the system before a failure occurs. When the burn-out point is detected, the electrical input power will be immediately stopped. Because the thermal mass in the heat source is relatively low, the wall temperature will drop rapidly. In the unlikely event of an absorber failure, the air will rush in to the subatmospheric system, precluding sodium release.

In Section 6.3.2 we propose non-critical follow-on testing of the evaporator dome performance, including thermal cycling using the same test rig. A complete post-test corrosion evaluation is also described in that effort.

6.3.2 THERMAL STORAGE MODULE LIFE TEST

The objective of these tests is to determine whether geometry control and the application of non-wetting coatings is sufficient to eliminate DV/V thermal ratcheting. The approach will be to combine research aircraft low-g tests with a rigorous worst case earth-based thermal stress endurance test. In orbit, some flexing of the module is acceptable provided fatigue limits are not reached. Any plastic deformation would be indicative of thermal ratcheting and would likely escalate to the point of rupture. Therefore, it must be assumed that any measurable plastic deformation resulting from DV/V stresses in our tests is unacceptable. Should results of these tests indicate that it is not possible to achieve this immunity, we will consider fiber mesh enhancement of the PCM. However, our work to date indicates that these mesh systems will not be required, and would therefore be implemented in the final design only if they could provide a means for reducing the overall weight. This decision cannot be made at this time due to the developmental state of NASA's work on ceramic fibers. Although implementing nickel mesh would increase our total specific mass, our design would still meet NASA's goal of a 50 percent reduction of the Baseline RSU mass.

We recommend first conducting a micro-gravity test on the Lewis Lear Jet or Marshall B-707 to observe the behavior of a liquid in various thermal storage module geometries. As described in Section 5.1.1, we will make each module with a volume 10 percent greater than that occupied by the PCM in the liquid state. By selectively applying non-wetting coatings, we will attempt to influence the position of this void in the liquid state. As solidification occurs in the actual micro-gravity environment, theory indicates that the void will grow in its existing location.

We will conduct these tests with a liquid simulating the PCM but not requiring heat input onboard the aircraft. Also, by avoiding use of the highly corrosive PCM, we can construct the container module from an inexpensive transparent material such as glass. These modifications of the actual system will enormously simplify the test, while allowing a definitive visual monitoring of the liquid. As long as the relative wetting and non-wetting liquid wall characteristics are duplicated, the final result will be similar to that for the actual PCM module. A precise matching of all of the various interfacial surface energies would only affect the rates in which the migration occurs. The final equilibrium void distribution will be essentially the same for both the simulated and the actual PCM modules.

Various liquid and wall combinations will be evaluated in this task. One simple, but very feasible simulated module design would consist of a glass vessel with various surfaces of the interior coated with Teflon. Water, with a small concentration of a coloring dye, would serve as the liquid. A VCR camera will record the 20 second micro-gravity event. Several module vessel shapes and surface coating arrangements could be simultaneously tested.

We believe that a test of this nature will provide valuable insight into the liquid PCM behavior, and the results can be correlated with our liquid management models. Since the tapered PCM module geometry is rather simple and in fact resembles a common configuration used in micro-g liquid management systems, we expect good correlation.

The predictions of the liquid void position will allow us to conduct a worst case thermal ratcheting test of the final module shape. Using gravity to force the location of the void to the region expected in micro-gravity, the modules can be subjected to a series of freeze-thaw cycles. Figure 6.8 illustrates the test apparatus that uses a condensing environment to heat and cool the PCM modules uniformly as in actual CHP operation. A simple pool boiler arrangement will be used to heat the modules. Liquid refluxing will occur, since the wick on the module surface is essentially inactive. When the temperature of the pool is reduced below the PCM melting point, the wicked modules act as an evaporator and draw liquid replenishment from the pool. In this arrangement, the wick design is not critical in that the evaporative heat fluxes, when properly simulated, are relatively low ($<1 W/cm^2$). Therefore, capillary and boiling limits are very easy to avoid.

Three or four module designs will be evaluated simultaneously in the same test apparatus. We will vary the geometry, wall thicknesses and the application of non-wetting graphite coatings. Oak Ridge National Labs (ORNL) will fill and seal the modules for us. The materials selection, although not yet completed, will consider LiF resistant alloys such as Hastelloy B and Haynes 188, as well as sodium resistant alloys like Inconel 600 and Incoly 800. At this time, the only candidate which has been tested successfully in both LiF and Na is nickel 201. Since the coefficient of expansion of Ni 201 is an excellent match with both Inconel materials, we will consider modules clad on the interior with the nickel.

STIRLING THERMAL ENERGY STORAGE (TES) MODULE

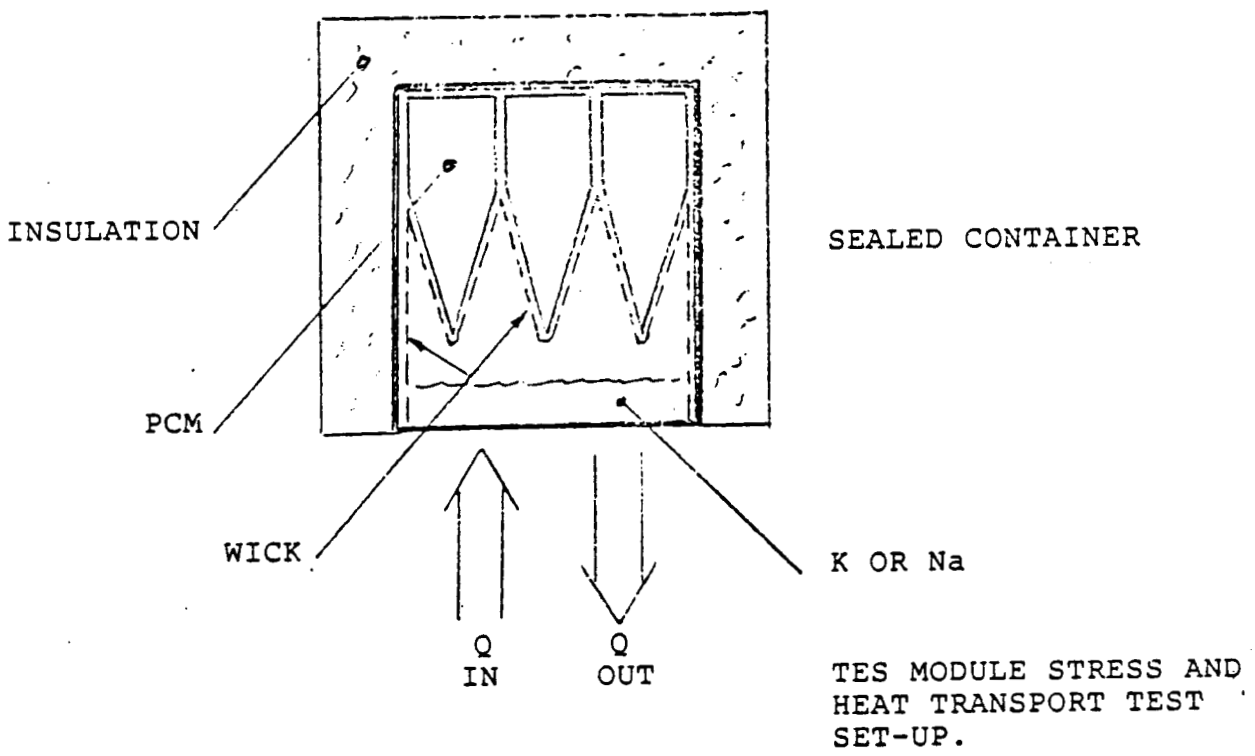

Figure 6.8 Freeze-Thaw Cycle Test Rig

In this simulation we will charge and discharge energy from the module at the rates dictated by the low Earth orbit. To evaluate the cyclic freeze-thaw effects, we propose to measure the flatness of the modules before and after, the tests. After 10, 100 and 500 cycles, the boiler plate will be removed and the module surface inspected. Either a dial indicator or an optical device will be employed to inspect for deformation.

Some minor deformation is expected in the first few cycles. However, if between 10 and 500 cycles a measurable amount of plastic deformation occurs, this would be evidence of a serious ratcheting condition. Since 56,000 cycles are required for 10 years in low Earth orbit, virtually any measurable bulging of the module would be unacceptable. In this event we would then consider immersed fiber mesh, or a thicker, more rugged module design.

Once it has been demonstrated that the design is resistant to thermal ratcheting, we recommend that a more detailed post-test evaluation be conducted to assess the extent of corrosion during the noncritical follow-on test phase.

6.4 FOLLOW-ON STIRLING CHP ANALYSIS AND TEST RECOMMENDATIONS

This section describes the recommended heat pipe life testing which is of fundamental importance for heat pipe designs using sodium. To evaluate the corrosion effects as they specifically relate to the final evaporator configuration it is recommended that the test rig used for the critical technology experiments be operated for an additional 1000 hours. This component life test is divided into two categories; 1) accelerated thermal cycling, and 2) post test corrosion analysis. These tasks are described in the following subsections.

6.4.1 EVAPORATOR THERMAL CYCLING TEST

In conducting this fatigue test, we will select an operating point which exceeds the expected peak solar flux. With a uniform flux distribution on the hemispherical surface, matching the peak flux would imply operating at a power level 50 to 60 percent above the design value. This will constitute a somewhat more adverse set of operating conditions than the design demands, but less than what we have applied to the analytical model. In our stress analysis model, we have assumed peak fluxes of twice the theoretical. We also analyzed the effects of very sharp circumferencial and azimuth solar flux gradients. However, it is unlikely that we could experimentally operate the system with a peak flux (equaling the average) at twice the theoretical value considered in the design. This would imply approximately a 300% increase in power throughput. Final testing on the Test Bed Concentrator (TBC) would more accurately simulate the true environment.

The thermal cycling should be microprocessor controlled. With a steady heat rejection flow rate through the calorimeter, it is possible to simply toggle the electrical input to the heat source to reverse the flux and thermal stresses. When the source cavity temperature reaches 1030^{o}K, the power will be turned back on, allowing up to 56 cycles per hour and thus 56,000 full cycles representing the 10 year design life in the 1000 hour test program. This implies ramping the temperature in less than 28 seconds, which we predict is achievable with this design. Our estimations of the thermal mass of the test apparatus indicate that with the calorimeter loop flowing continuously, the wall temperature will drop about 100^{o}C/minute. Therefore, the control requirements for the rapid cycling test are relatively simple.

6.4.2 EVAPORATOR POST-TEST EVALUATION

Following the 1000 hour test, the evaporator dome will be removed from the apparatus and inspected. Scanning electron microscopy (SEM) will be used to detect morphological changes present on the wick and wall materials. Surface analytical techniques, Auger Electron Spectroscopy (AES) and X-ray Photoelectron Spectroscopy (XPS or ESCA), will be utilized in evaluating the reaction products. These techniques are highly surface sensitive. It may be useful to prepare a polished cross-section of the dome wall, or a test coupon for examination of possible grain boundary degredation.

SEM studies of the selected base materials and joints will be conducted on the corroded surfaces and sections. Section evaluations, using SEM and X-ray analysis will determine the extent (or depth) of corrosion damage and, together with surface evaluations, will provide an accurate description of corrosion damage. Surface analysis using AES and XPS will identify reaction products and their distribution on the surface. The high surface sensitivity of these methods permits evaluation of interactions between the metal and the sodium after only short exposure times. Such accelerated tests minimize the time required for these preliminary corrosion experiments and accelerates the material selection process. In addition to these methods, the technique of Secondary Ion Mass Spectroscopy (SIMS) is available for evaluations requiring high elemental sensitivity. This technique is also capable of analyzing for all elements including hydrogen and provides selected chemical state information derived from molecular fragmentation patterns in the SIMS spectra.

Both AES and XPS are highly suited for this application because of their key attributes listed below:

- o High surface sensitivity, providing analysis of the top 5-20 angstroms region.
- o Sensitivity for light elements, including Li. Only H and He are undetected.
- o Chemical state information which is useful in identifying the reaction products.

Information obtained from these analytical tests will allow us to predict the reaction rates and extrapolate to the desired life. We will pay the closest attention to the corrosion in the wick, welds and any crevices which may exist. To gauge the severity of various crevice geometries, in a non-critical area of the dome retention flange, we will construct various flows and crevice joints to simulate worst case conditions. The corrosion rate in the wick is critical because of the relatively thin wire to be used.

To determine the fatigue effects, we will first measure the dome surface contour both before and after performance and life tests to detect any permanent distortions. Secondly, we will examine the microstructure of the absorber surface and the inner evaporator wall surface. The presence of serious microfractures would imply that in the actual application there would be a combined corrosion enhanced fatigue interaction. However, a fatigue life prediction using the method of Universal Slopes (Section 2.3) does not predict that cracks would occur since we have incorporated such large safety factors in the design.

7.0 DISCUSSION OF RESULTS

This report describes the four-task Advanced Heat Receiver Conceptual Design Study. Under guidance from our NASA program manager, eight advanced receiver concepts were proposed and studied. From these eight concepts a Stirling and a Brayton receiver storage unit (RSU) concept were recommended. These selected designs were then analyzed in more detail. The results of this study are in the form of conceptual drawings, preliminary performance analysis, experimental data and final experimental recommendations. The following paragraphs summarize the objective and results of each of the four program tasks.

7.1 TASK I: DEFINITION OF THE BASELINE

The specifics of a Baseline RSU design were defined to provide a basis for a quantitative comparison of past and future receiver storage unit (RSU) designs. the specifics of a Baseline RSU design were defined. The Baseline design was originally envisioned to be a scaled version of the 11kWe NASA/GE RSU (2). Later our managing office at Lewis pointed out the fundamental similarities between the GE first generation and the current I.O.C. Rocketdyne/AiResearch designs (8). Consequently the selected Baseline concept was physically modeled after the I.O.C. design. Performance projections were however derived from data obtained in the earlier GE/NASA tests since the I.O.C. design had not been built or tested.

7.2 TASK II: CONCEPTUALIZE 4 ADVANCED BRAYTON AND 4 ADVANCED STIRLING RSUs

Eight innovative RSU concepts were prepared for a Task II review at NASA. All of these designs met the primary program goal of a 50% specific mass reduction. In studying a vast range of potential concepts and theories it became evident that the Baseline concept of a central gas tube surrounded by an annular ring of PCM could not simply be reconfigured to achieve the ambitious NASA specific mass goals. Each of the eight design concepts embodied principles which had not previously been applied to space dynamic RSUs. Some of these concepts did however reflect principles employed in some terrestrial receivers. The new RSU designs which Sanders introduced to this space application use such principles as direct solar absorption in doped PCMs, windows, honeycomb matrix absorbers, micro-encapsulation of PCMs, pumped sensible heat storage, and large single heat pipe absorber cavities. Many of these theories are expected to play an important role in future RSU development.

7.3 TASK III: ANALYSIS OF SELECTED BRAYTON AND STIRLING CONCEPTS

Following the recommendations obtained in the Task II presentation, a single Advanced Brayton and Stirling were selected. These concepts, later referred to as the Direct Absorption Receiver (DAR) for the Brayton and the Cavity Heat Pipe (CHP) for the Stirling, were analyzed in more detail in this task.

The Brayton DAR analysis consisted of a transient thermal finite difference analysis of the critical heat exchanger elements. The thermal analysis led to a geometry which is predicted to produce turbine inlet temperatures within $+10^{0}$K to -20^{0}K of the PCM melting point. In addition to a reduction in thermal losses, the DAR analysis showed that important systems efficiency gains would occur over the Baseline. The combination of a higher mean turbine inlet temperature (both systems using LiF) and lower heat addition pressure drops resulted in a net system efficiency gain of 8%.

The stress analysis coupled with the thermal analysis of the DAR provided the basis for RSU mass calculations. The mass and dimensions of the subsequent design are shown in Table 7.1 to beat the NASA advanced goals.

Significant progress was also made towards the Advanced goal of higher reliability. Recognizing the inter-relationship between reliability and complexity we adopted the parts count, total weld length contacting the highly corrosive PCM, and the number of individual weld segments as comparative parameters. In all cases (Table 7.1) the DAR exhibited significant advantages.

The Stirling CHP analysis focused primarily on the design of the domed absorber. A comprehensive model of the heat pipe performance was coupled with a Monte Carlo optical analysis of the solar cavity. This lead to the definition of a range of acceptable wick and dome designs. Two and three dimensional finite element analyses were conducted to explore the creep and fatigue limitations of the evaporator/absorber when exposed to extreme flux levels and flux gradients. The results concluded that high nominal peak fluxes on the order of $60w/cm^2$ with a sodium fluid and superalloy materials could exceed the 10 year operating life goal.

Regarding NASA's specific goals for a 50% Baseline mass reduction, lower volume, and higher efficiency, significant advancements are predicted in all categories. Table 7.1 illustrates the attributes of the CHP design. The high flux capacity, single heat pipe design yields a highly compact, low mass unit. The volume which is less than 1/20th of the Baseline results in a reduction in exterior shell thermal losses.

Table 7.1 Advanced RSUs display significant advantages over the Baseline

NASA's Key Parameters	Stirling CHP	Brayton DAR	Baseline RSU
Mass (kg)	186	212	461
Volume (m^3)	0.107	.354	2.15
Efficiency			
o Thermal (%)	91.7	86.0	81.1
Reliability/Life Cycle Cost			
o Predicted Operational Lifetime Years	10	10	7
o Meters of Weld Exposed to PCM	39	11	1814

* Reference 8

7.4 TASK IV: CRITICAL TECHNOLOGY EXPERIMENT IDENTIFICATION

The definition of critical technical issues led to a series of recommended preliminary and follow-on experiments. The critical issues identified for the Brayton DAR were 1) longterm window optical performance, 2) PCM doping, and 3) Liquid PCM management in micro-gravity. For the Stirling CHP, the experimental recommendations are intended to address the critical issues of 1) evaporator dome fabrication and performance, and 2) PCM module thermal ratcheting.

Much progress was made in resolving two of the critical technology issues required to make the Direct Absorption Brayton Receiver (DAR) a viable design. Fluoride windows, specifically lithium and magnesium fluoride, accept the deposition of LiF in a manner which does not degrade the solar transmittance. Also, a natural diamond sample, too small for transmissivity analysis, exhibited no corrosive effects in the condensing LiF environment. Since the window is very lightly loaded by the internal cavity pressure, the only remaining concern is the deposition rate. Analytical predictions as well as surface chemical analyses and mass measurements after the 200 hour test agree that the total deposited condensation after ten years of operation will be insignificant. This deposition rate is controlled to a large extent by the addition of noncondensible gas and thin film coatings which affect the window substrate temperature. Our success with the two fluoride samples suggests that a simple window configuration is feasible. Several other fluoride window candidates exist which can meet our goal of 95% total transmission. Diamond-like coatings are an alternative, but more expensive option that may be considered.

Preliminary doping experiments have narrowed the field of candidates to a few transition metals. Rare earths such as dysprosium and samarium demonstrated their broad band absorption characteristics but have insufficient solubility in LiF to produce a single domain doped crystal. The polycrystalline solid exhibited high surface scattering due to crystallite formations. Large single crystal zones within the PCM are desired to reduce the optical scattering characteristics of the polycrystalline mixtures. This has been demonstrated to be achievable with small concentrations of CoF_2 of less than .014%M. These samples exhibited sufficient solar absorption to meet our direct our direct absorption receiver design goals with low scattering. Our success with small doping percentages of cobalt leads us to believe that other transition metal-fluorides will also produce acceptable results.

Building from these experimental findings it was then possible to formulate two experiments to address the remaining key unknowns. First a small scale windowed cavity simulation is proposed to realistically analyze the window environment. Using a Xenon arc lamp solar simulator it would be practical to both operate at the actual temperature and thermally cycle the device. This experiment will provide an accurate prediction of the window temperatures and condensation rate. A post test chemical analysis and transmission test are proposed to address long term performance issues.

The second experimental recommendation involves the performance of a full scale micro-gravity liquid management demonstration. By flying the RSU through parabolic maneuvers approximately 20 seconds of microgravity can be simulated. This time is more than sufficient to wick the liquid LiF from a reservoir at the base of the cavity into the corrugations. This accomplishment will demonstrate the dynamic stability of the cavity thermal storage systems.

Also during Task IV the details of an experimental investigation of the Stirling CHP was formulated. This involved a study of acceptable heat pipe fabrication techniques and the identification of various wick forming procedures. The final recommendation regarding a preference for screen or powdered metal wick system could not be made in this study. Thus an experimental program and text rig was designed to obtain the

data necessary to make a final decision. It is recommended that testing first explore the limits of the more conventional screen wick technology. Powdered metal wick systems were found to have two limitations. Firstly, the cost of developing the powdered metal dome was found (through inquiries of vendors) to be much greater than that of screens. Secondly, there is a lack of material property data which is necessary to access the long term integrity of the powdered metal and its bond to the absorber wall.

The final test was devised to observe thermal ratcheting within the PCM containment module. Through the preliminary experiments conducted in Task IV it was determined that the solid PCM to crucible bonding strength varied somewhat between wetting and nonwetting combinations. The recommended experiments were designed to evaluate the potential affects of container geometry, freezing geometry, and the application of nonwetting coatings on thermal ratcheting.

8.0 CONCLUSIONS

To meet the demands of future NASA space missions, advances in solar dynamic technology are necessary. The receiver storage unit is a key element in both Brayton and Stirling systems because it represents the most massive subassembly in the system, is the hottest section, and contains gravity sensitive fluids. The clearly stated goals of this program relate to achieving improvements in mass, efficiency and reliability over the so-called Baseline space station designs. The most challenging goals are to achieve a 50% mass reduction with a 10 year operating life.

The program was structured in four tasks; 1) Baseline definition, 2) conceptual studies, 4) detailed analysis (and experimentation) and 4) critical technology experiment recommendations. This led to the design of innovative Brayton and Stirling RSUs which are predicted to meet the ambitious NASA goals.

The Direct Absorption Receiver (DAR), conceived and analyzed in this program shows a drastic improvement in simplicity and mass minimization over a LiF-based low earth orbit solar dynamic receiver. It's major mass element is a refractory metal corrugated plate-fin type heat exchanger. The simplicity of the receiver is illustrated by the comparison of more than 1800 meters of welds exposed to the corrosive PCM in the Baseline versus only 11 meters in the DAR. Additionally, a price quote for the prototype fabrication by Teledyne Wah Chang - one of the most experienced refractory metal fabricators - indicates a cost for the fully operable heat exchanger, manifolds, and ducting subassembly of only $57,000.

Due to the dual function of the refractory metal skirt as both the PCM container and gas heat exchanger, there is essentially no additional mass associated with PCM containment - a conventionally massive element of the Baseline concepts. As the PCM is melted through volumetric solar absorption it softens in a manner that minimizes the potential for liquification stresses. In addition, the mechanisms that cause thermal ratcheting are not present. That is, the cyclic accumulation of plastic deformation in the heat exchanger is not possible for the following reasons;

1) The expanding PCM is not confined by a container wall.

2) The internally pressurized corrugations resist permanent deformation. (fatigue is negligible).

3) The melt does not nucleate at container surfaces which are bound by the frozen PCM.

Thermal ratcheting combined with the presence of excessive temperatures caused by the impedance of voids is the most significant issue which confronts solar dynamics. It represents a long term failure mode which is driven by highly gravity sensitive effects. Since the system must endure 56,000 liquification cycles (10 years in LEO), even a "gas can" experiment of about 100 cycles barely represents a significant test. Thermal ratcheting effects had just started to become apparent in the first NASA/GE receiver (3) after 2000 cycles of earth based testing. This argument illustrates the serious economic and scheduling obstacle which Solar Dynamics must overcome to prove itself. It also implies the strong motivation for obtaining a design with the greatest immunity to the ratcheting effects.

The DAR represents an innovative solution to NASA's performance goals which utilizes the natural advantages of the micro-gravity environment. In this sense, it foreshadows the use of this environment for certain commercial applications on the Space Station. Both would exploit the benefits of low gravity to perform a function better than would be possible on earth.

The Stirling Cavity Heat Pipe (CHP) has been shown to be exceptionally well suited for the Stirling cycle. The intermediate working fluid (sodium) links the extremely varied requirements of the three RSU heat exchangers. The geometries of these heat exchangers - the helium-filled heater head, the PCM containers and the solar absorber - may each be independently optimized. The intuitive concept that combining two or more of these heat exchanger geometries could lead to a lower weight, more compact design was rigorously tested in our conceptual design Task II where two such versions were analyzed. Flowing the helium through a windowed cavity with a directly irradiated honeycomb matrix containing the PCM served as one example of a complete integration of the three heat exchangers. However, severe engine cycle performance penalties resulted in several areas. Consequently, the heat pipe mechanism was adopted to reduce the design constraints on the heat exchangers.

Multiple heat pipe arrays were also ruled out following the evaluation of the work performed by GE and the Jet Propulsion Lab (JPL) for terrestrial Stirling RSUs. In addition to being relatively heavy and complex, the multi-heat pipe concept also imposes unacceptable compromises on the heater head and solar absorber configurations. The most attractive concept from the standpoint of mass, volume, system efficiency and fabricability was found to be a single cavity-sized heat pipe.

A thermal, optical, and stress analyses of the solar absorber lead to the selection of a hemispherical dome cavity. With nominal peak fluxes of approximately $60W/cm^2$, the cavity diameter is only 27% of the Baseline. The thin hemispherical shell was found to be especially tolerant of solar flux anomalies and thermal induced strain.

The principle issue regarding the CHP thermal storage system design, like the Baseline, involves DV/V effects. Thermal ratcheting and thermal impedances arising from the volumetric changes of the PCM are gravity sensitive and therefore are difficult to verify on earth. The proposed CHP design does, however, have several advantages over the Baseline which are expected to relieve these concerns. Because they are located within the uniformly condensing vapor filled cavity, the shape of the storage containers is not constrained. Secondly, the condensing atmosphere produces isothermal conditions at the heat addition surfaces. These two features are predicted to alleviate the ratcheting and impedance effects of the voids. Moreover, with control over the geometry and heating characteristics it is feasible to implement a combined experimental/analytical approach to test the design theories proposed in this report.

The Stirling heater head is the most highly stressed, life limiting component in the system and is currently the subject of much analysis. Also, the cycle efficiency is highly sensitive to its internal flow geometry. For these reasons there is not yet a consensus among engine designers regarding the best heater head configuration. It is unlikely that a single configuration will satisfy the total scaling range of 1.5kWe to 35kWe outlined for this program. Therefore, our highest priority in this area was to develop an RSU design which could accommodate a range of head geometries and not impose any additional constraints on the difficult task of the engine designers. The CHP meets this objective. It also has several advantages over the other receiver interface concepts. Again the single vapor source produces an isothermal heating of

the helium heat exchanger despite the highly irregular flux characteristics of the solar absorber. This effect has been proven to yield engine efficiency advantages as well as minimize the head stresses.

The CHP design exhibits significant advances in each of the areas emphasized by NASA. The specific mass is predicted to be only 40% of the Baseline's while its volume is reduced to merely 5%. Because of this compactness the thermal losses will be only about half as large as the Baseline's. This yields additional mass saving by a reduced concentrator area, which also lowers the atmospheric drag on the solar dynamic system.

APPENDIX A

MONTE CARLO METHOD

APPENDIX A
MONTE CARLO METHOD

In the evaluation of various concentrator systems for the purpose of receiver design, the principal technique employed at Sanders incorporates the Monte Carlo method. This technique has been applied to four concentrators: at the Georgia Institute of Technology (GIT), the DOE Solar Thermal Test Facility (STTF) in Albuquerque, the JPL Test Bed Concentrator (TBC), and the LaJet LEC 460. The results of this modeling have provided valuable design data used for sizing the receiver aperture and for the investigation of internal cavity flux distribution. Also, in the case of the GIT and LEC 460 test programs, valuable diagnostic information for the two concentrators was also obtained. These two concentrator systems performed below the original design expectations while the Sanders modeling efforts located critical design defects.

One advantage of the Monte Carlo method over other optical analysis approaches lies in its ability to break out and quantify critical parametric effects which define the trajectory of the reflected ray. This flexibility was especially important in the analysis of the GIT and LEC concentrators when problems were traced to distortions in the individual facet shapes. These experiences demonstrated the gross magnitude of misconception that could result from relying only on individual facet slope error measurements. Surface quality measurements of the LEC 460 facets conducted by JPL and 3M (the manufacturer of the film) initially lead to high expectations. Without incorporating the real effects of the actual membrane shape and position, the image "size" was underestimated by roughly a factor of four.

The 80 kWt TBC has demonstrated extremely good performance. The Monte Carlo model developed by Sanders during the design and test of our high temperature solar thermal receiver (HTSTR) on their concentrator checked closely with JPL's pretest characterization. The results of this model were used to determine the flux distribution and consequently the stress and performance predictions for a series of

rather complex cavity shapes. The flux distribution predicted at the focal plane provided inputs for a three-dimensional finite element (ANSYS) stress model of the quartz window and its retaining mechanisms.

The Sanders model of the STTF was the only one of the four Monte Carlo models which was generated after the complete characterization of the mirror field. Upon adjusting model parameters to correlate with test data, the analysis was used to solve the complex radiation effects in the cavity of a rotating kiln. This kiln was designed under contract for the Institute of Gas Technology for the calcination of limestone.

The two concentrator models for the STTF and the TBC were developed to the point of useful engineering design tools in less than two man-weeks each. Through the appropriate application of extensively developed Monte Carlo techniques and expertise at Sanders, concentrator analysis for the purpose of the receiver design can be accomplished efficiently and cost-effectively for any point focus concentrator system.

An additional benefit of the generic Monte Carlo codes is that they can be directly coupled to the cavity reradiation modeling and other custom FORTRAN software. This approach would be most practical for complex cavity geometries involving four or more distinct surfaces or asymmetries. Also certain bodies which cannot be assumed as gray or diffuse are often best handled with Monte Carlo statistical formulations. This involves a relatively simple mathematical extension of the model to incorporate an additional dimension for wavelength dependence or for the specularity of the emission angle.

Finally, Sanders experience with many concentrator modeling approaches and our diversity of solar thermal test experience has proven the Monte Carlo techniques to be a powerful, yet cost-effective tool for these applications. Not only has reliable correlation of predictions with test data been achieved, but a physical grasp of the design parameters has proved indispensable.

APPENDIX B

CYCLE POWER LOSSES

APPENDIX B

CYCLE POWER LOSSES

The engine power loss due to the specified 2% RSU pressure drop has been assessed with the following methodology:

Turbine work loss due to pressure losses

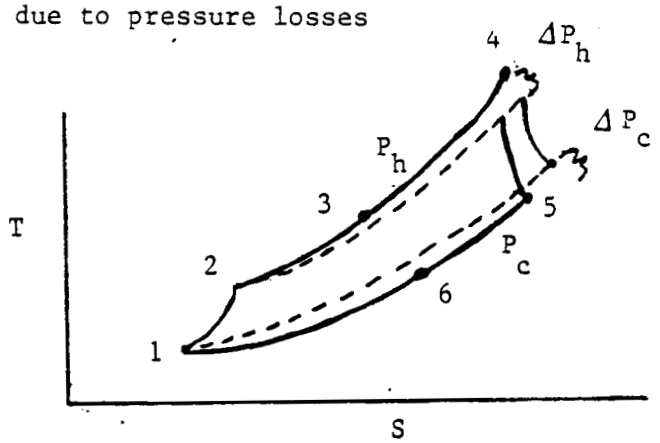

$$\dot{W}\ \text{Ideal} = \dot{M}CP\ (T_h - T_c)$$

$$= M\,\eta_t\ CP\ T_h\left(1 - \frac{Pc}{Ph}^{\frac{\gamma - 1}{\gamma}}\right)$$

$$\dot{W}\ \text{Actual} = \dot{M}\,\eta\,CP\ T_h\left[1 - \left(\frac{Pc + \Delta Pc}{Ph - \Delta Ph}\right)^{\frac{\gamma - 1}{\gamma}}\right],\quad K = \frac{\gamma - 1}{\gamma}$$

$$= 1 - \left(\frac{Pc + \Delta Pc}{Ph - \Delta Ph}^{K}\right) = 1 - \frac{Pc}{Ph}^{K}\left[\frac{1 + \frac{\Delta Pc}{Pc}}{1 - \frac{\Delta Ph}{Ph}}\right]^{K}$$

Using a binomial expansion and dropping higher order terms:

$$= 1 - \frac{Pc}{Ph}^{K}\left[1 + K\,\frac{\Delta Ph}{Ph} + K\,\frac{\Delta Pc}{Pc} + \frac{K(K-1)}{2!}\left[\frac{\Delta Ph}{Ph} + \frac{\Delta Pc}{Pc}\right]^2 \cdots\right]$$

$$\Delta \dot{W}_{Loss} = \dot{W}\ \text{ideal} - \dot{W}\ \text{actual}$$

$$\frac{\Delta \dot{W}_{Loss}}{\dot{M}\eta_T\ C_p T_h} \cong -\frac{\gamma - 1}{\gamma}\,\frac{Pc}{Ph}^{\frac{\gamma - 1}{\gamma}}\left[\frac{\Delta Ph}{Ph} + \frac{\Delta Pc}{Pc}\right]$$

With $\gamma = 1.65$, $\dot{M} = 1.03$, Pc/Ph = 0.578
calculate adiabatic turbine efficiency (Ref. 3)

$$= \frac{T03-T04}{T03}\left[1-(1Prt)^{\gamma-1/\gamma}\right]^{-1}$$

$$= 0.898 \text{ (seems too high)}$$

$$\Delta W \text{ Loss} = \frac{0.65}{65}\left[.578^{.65/1.65}\right](.02)\quad(1.03)\quad(.898)\quad(.059)\quad(1960)$$

= 0.679 Btu/s (0.72 kW-shaft)

Assuming alternator efficiency = .92, calculate equivalent thermal input loss.

Q = (0.72 * .92) /.27 = 2.44 kWt

APPENDIX C

BRAYTON WINDOW

TEMPERATURE CALCULATIONS

APPENDIX C
BRAYTON WINDOW
TEMPERATURE CALCULATIONS

Questions on Brayton:

1. What is the anticipated peak solar flux level on the aperture window?

High quality terrestial concentrators in this size range have demonstrated peak flux levels as high as 1400 W/cm2 at the parabolic focal plane. In this case, with the TBC, the JPL test site personnel were able to perform a slight refocusing of facets to obtain essentialy the same bulk capture in the design aperture. In doing this they were able to defuse the intense hot spot (about 1 cm in diameter) to about 1/3 of this value without significantly impacting the receiver capture (see figure 3-6 of proposal). Typically concentrator designers strive for the best possible focus condition but rarely achieve peak value over 500 w /cm2 and average values of 200 W/cm2 on earth. In the extraterrestrial environment these levels would inflate by roughly 30% due to the greater intensity of the sun.

Although we have successfully operated quartz windows with the high peak fluxes of the TBC, we prefer more moderate peak to average ratios. Also since we are considering fluoride substrates for the Brayton DAR, the design operating temperatures must be in the 600 to 800 C range. MgF2 softens at 800 C, while CaF2 is useful up to 900 C (ref 1).

The absorption coefficient for these materials is extremely low in the region where the solar intensity is the greatest. This is implied by the transmissivity plots of figure 1 in that there is essentially no measurable difference in transmissivity between the thin and thick samples. The nominally 5% non-transmitted component is the result of Fresnel surface reflections. In the near IR where the most precise calorimeter-type measurements begin to become feasible some data is available. Table 1 presents MgF2 absorption data and the percent absorption implied for a 3mm (0.12 inches) thick sample. Since more than 97% of the solar spectrum falls below 2.7um, we are operating well away from the spectral cut-off point and therefore expect this to be a conservative estimate. Likewise absorption in the UV region is not significant above 0.25um while less than 1% of the extraterrestial energy falls below this wave length. Additionally, much of the solar energy outside the wide transmissivity range of MgF2 is not reflected by the concentrator. Surface coatings protecting the metal reflector as well as the actual metal spectral reflectivity characteristics limit much of the extreme wavelength energy from reaching the receiver aperture.

For the purpose of a rough estimation of the survivable window flux limit we present the following conservative assumptions:

$\beta = 8.6X10^4/cm$,	absorption coefficient at 2.7um probably high
Tw = 800 C,	maximum window temp. desired for MgF2 (ref 1)
$\alpha = 0.22$	Black body absorption beyond 6um from 1140 degrees K cavity
$\epsilon w = 0.20$	Window emissions based on black body emission beyond 6um, while at 800 degrees C

The energy balance for a unit centimeter zone in the peak of the incident solar flux distribution is therefore:

Qs + Qcav = Qw + Qcond

Where:

Qs = the solar flux absorbed on a 1cm area
Qcav = the predominantly IR cavity radiation absorbed
Qw = the window radiation from both sides of the unit area control volume
Qcond = the radial conduction which we neglect

Therefore:

$$Io(1-e^{-\beta x}) + 0.22\sigma(1140^4) = 2(0.2\sigma 1073^4)$$

Where:
I o = the tolerable solar flux limit
x = the window thickness (cm)
σ = the Stefan-Boltsmann constant

The results of this simplified calculation is presented in Table 2. This indicates that a 3mm thick window will survive a peak solar flux of over 11, 000 solar constants. Thinner windows would survive much higher fluxes. From this conservative analysis we believe that the window can be designed to tolerate fluxes in excess of expected levels.

TABLE I

WAVE LENGTH (μM)	ABSORPTION Coefficient (cm^{-1})	ABSORPTION/3MM %
2.7	8.6×10^{-4}	.059
3.8	4.7×10^{-4}	.067
5.25	1.4×10^{-2}	.962

TABLE 2

THICKNESS (X)	TOLLERABLE SOLAR INTENSITY (I_o)	
MM	SUNS	W/CM2
1	33,160	4,543
2	16,582	2,272
3	11,055	1,515

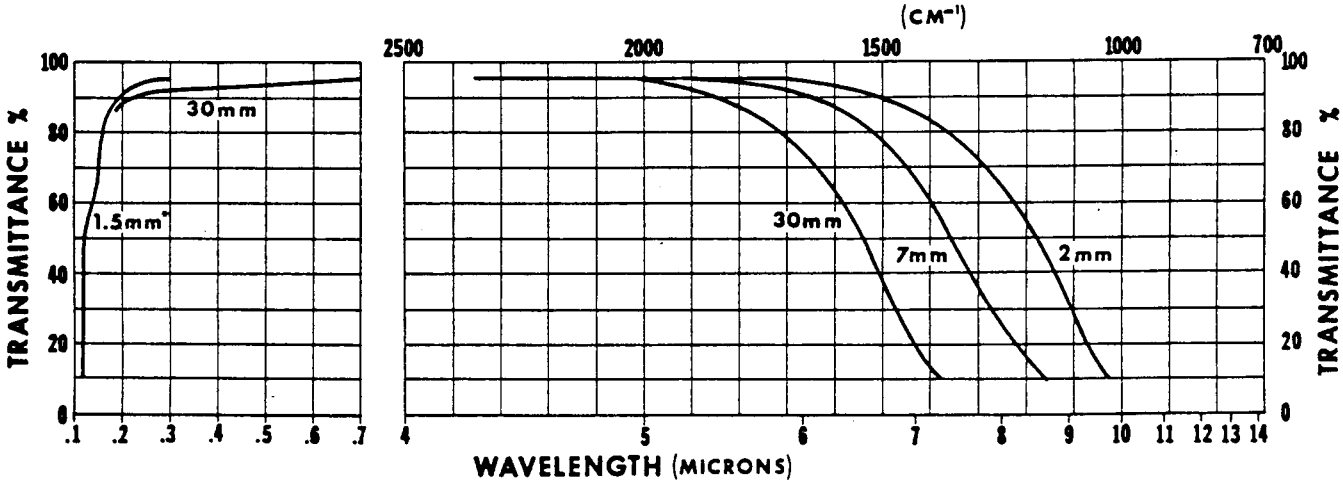

FIGURE 1

APPENDIX D

FREE PISTON HEATER HEAD DESIGNS

RSU/ENGINE INTERFACE. The interface between the Stirling RSU and the engine is not as clearly defined as with the Brayton. The heater head must be integrated with the heat pipe condenser. Heat pipes serve this purpose well because of the variety of shapes that can be manufactured, and their high flux capacity isothermal performance. The heater head, on the other hand, is designed to a stringent set of tightly controlled parameters. For this reason, the best receiver interface requirements do not complicate an engine design. The following paragraphs will review the state-of-the-art in free piston Stirling engine (FPSE) heater head design.

There has been a recent explosion of FPSE designs from around the world. Three U.S. companies are presently receiving NASA funding and have produced notable designs. Table 2-3 lists 11 designs by these manufacturers alone. Numerous other designs have been generated by European, Japanese and other U.S. companies. One notable observation from reviewing these programs is that there is not a consensus among engineers for a standard heater head approach, especially over the wide scaleable power range (1.5 to 35 kW) of interest to NASA. The purpose for discussing some of these designs is to show the importance of an RSU concept that can accommodate the progressive engine designer's present and future plans. In Section 2.3, we will describe our RSU approach which can be effectively integrated with any of the past and present heater heads and will accommodate future advancements in this area. That section will also describe alternate concepts which we do not feel meet NASA's fundamental requirements.

The engine that will ultimately be used for prototype solar dynamic modules is likely to evolve from an ongoing space nuclear application design. It would make the most economic sense to exploit as much development from that program as possible. The Sanders' CHP design is compatible with all concepts presently under development for those applications. To demonstrate our understanding of these relevant issues, a brief review of the ongoing engine trades is described in the following paragraphs.

Table 2-3. Eleven Free Piston Stirling Engine Heater Head Designs by Three US Companies

MTI	SPDE - Multi-tubular
	SPRE - Finned Tube Shell Modules
	3 kW GRI Heat Pump - Annular Head Design
	SSE - Radial Head Modules
	SSE - Thermal Power Modules
	DoE/SNLA 25 kWe Terrestrial
Sunpower	Re-1000
	Spike II
	25 kWe Cooler-Regenerator - Heater Modules
STC	DoE/SNLA 25 kWe Terrestrial
	Pressure Stabilized Annular (SBIR)

Prior to discussing the heat pipe interface with the heater head, there is a very important engine design issue to be addressed which affects the RSU interface. This is the engine orientation with respect to the receiver axis of symmetry. Dual opposed cylinder engines such as MTI's Space Power Demonstration Engine (SPDE) (figure 2-1a) must have the engine piston axes perpendicular to that of the receiver. The single cylinder engine configuration, like MTI's 25 kWe DoE design for example, (figure 2-1b) can be oriented on the same axis as the RSU. The dual vs. single engine concept is presently the subject of performance, reliability, and specific mass trade studies.

The advantages of the opposed cylinder concept are primarily a higher efficiency potential and a complete elimination of vibration. The opposed configuration allows for the elimination of gas spring losses required to damp the vibration of single piston engines. For the higher frequency AC (>100Hz), typically specified for space, gas spring dampers are required. This device consumes five to ten percent of the pressure-volume

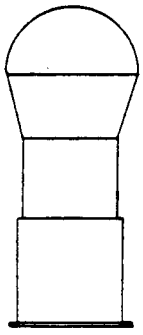

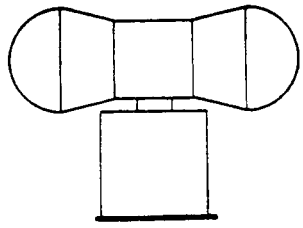

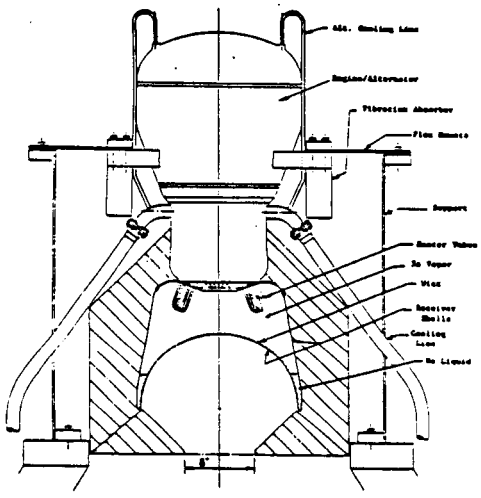

DoE/NASA Terrestrial 25 kWe Power Module
MTI/Sanders/Thermacore

(a)

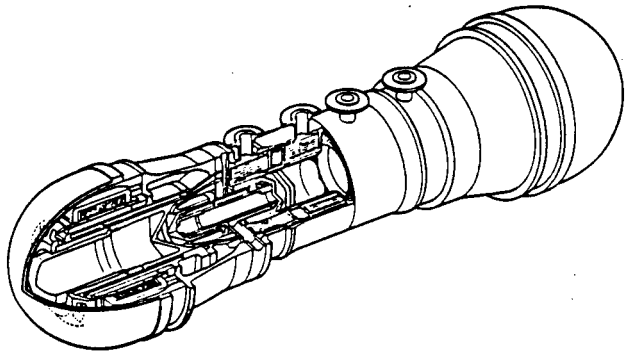

Space Power Demonstrator Engine
MTI

(b)

Table D1 Dual Opposed Cylinder Vs. Single Engine Configuration
Engine/Receiver Orientation

(PV) power to achieve a typical 2-G vibration at 100Hz. The advantage of the single cylinder over the dual opposed engine is primarily associated with the additional parts count and possibly cost. The specific mass comparison of the two concepts is also not fully quantified as yet. The dual engine approach suffers in terms of the normal economy of scale, but makes up for this by eliminating the mass-spring system and the two pressure vessel piston heads.

The next major heater head/RSU integration issue to consider is the helium heat exchanger configuration and dimensions. For the purpose of this discussion, the many various designs will be grouped into three general categories as illustrated in figure D2. These are (1) the conventional multi-tubular, (2) pure annular finned passages surrounding the cylinder passage, and (3) finned tube modules.

The most common heater head configuration utilizes a large number of small tubes. This is not only the general approach to all terrestrial and automotive Stirling engines but also MTI's Space Power Demonstrator Engine (SPDE). The SPDE served as an excellent research tool and revealed valuable performance data which provides a basis for other heater head design. In that design, there were 1628 0.05 inch ID tubes for each 12.5 kWe engine. This reduces to roughly 5 in ^{2}/kWt per inch of tube length of primary heat transfer area. Finning of the working fluid path incorporated into other head concepts can allow for the reduction of primary heat transfer surface (exposed to the sodium) by as much as a factor of 2. These design guidelines have been adopted for our scaling studies. Also, we have considered alternative heater head/condenser concepts which will be described later in this proposal.

The annular finned head is used most extensively on the lower end of the power range of interest. Three such designs are illustrated in figure D3a, b, c. The MTI 3 kWe

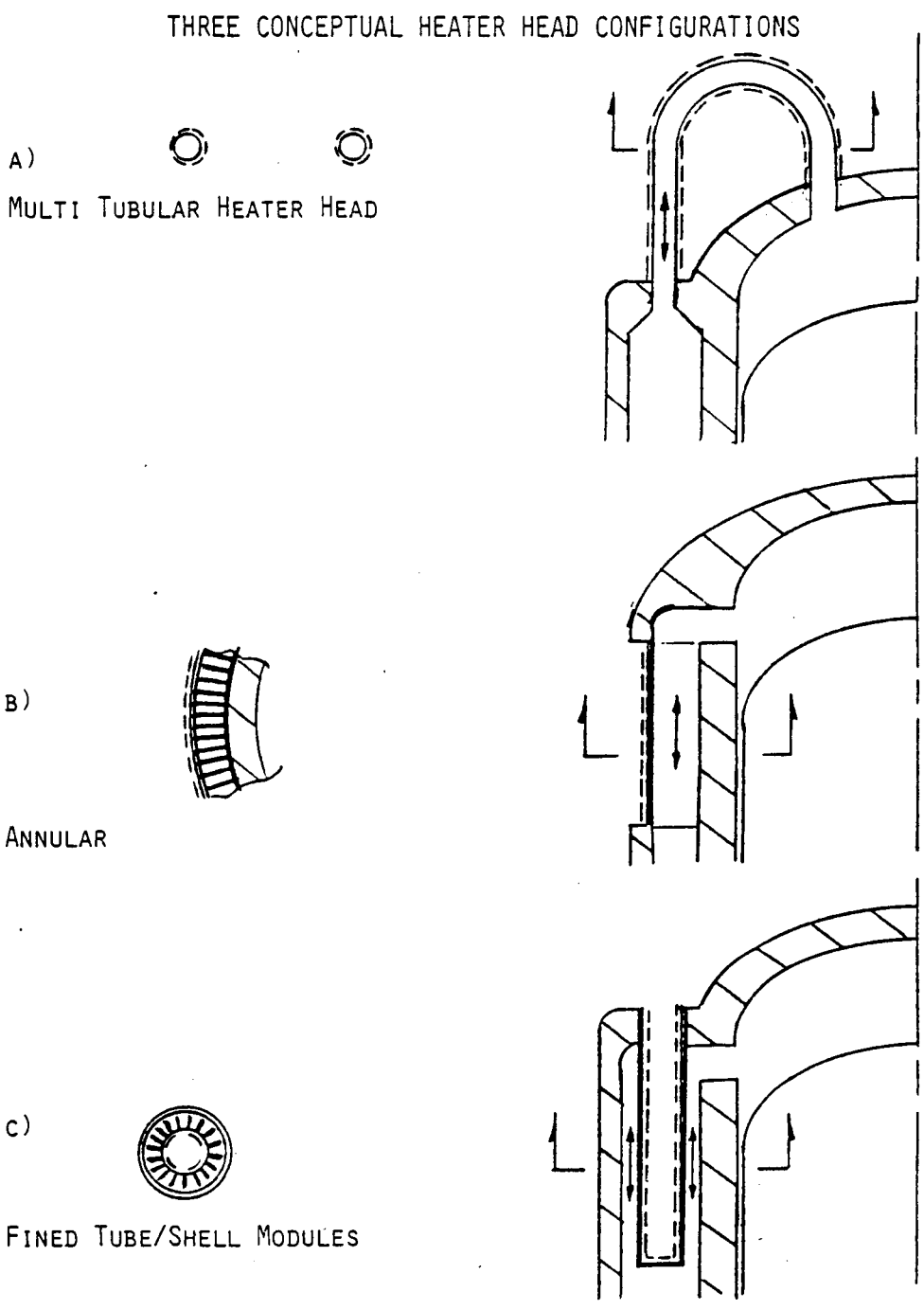

Figure D 2. Three Conceptual Heater Head Configurations

heat pump engine and the Sunpower Spike II 2 to 3kWe engine are good examples. This size, of course, would be suitable for generating the 7 kWe required for this program if a dual opposed engine configuration were adopted. STC is presently working on a NASA Small Business Innovative Research (SBIR) Grant designing their "pressure stabilized" annular configuration for power levels up to 25 kWe. We feel that the annular approach can be effectively integrated with our heat pipe receiver. The annular diameter of a 7 kWe engine would be between 10 and 15 cm, slightly smaller than the receiver aperture. In Section 4412 we present our own conceptual annular heater head/condenser options including one which assumes a dual opposed piston configuration.

The heater head concepts, referred to as finned tube-shell modules, are illustrated in figure D3. Sunpower and NASA pioneered this concept for eventual space engine designs. Variations on this design are the leading candidates for the Space Stirling Engine (SSE) Program which is directed primarily towards nuclear reactor power sources. In this application, the concept has three advantages over the more conventional tubular bundle designs: (1) Safety considerations for isolating the engine from the reactor, (2) a reduction in weld and braze operations, and (3) increased modular testability.

One strong motivation for this configuration is its ability to isolate the high pressure working gas from the reactor transport liquid. After inserting a tubular heat pipe into each of the externally finned head sleeves, the evaporator end of the heat pipe, about 4 inches long, would then be immersed in a liquid metal transport loop. The energy transport loop circulates the fluid thorough the central reactor to as many as six Stirling engines. Therefore, the individual heat pipes serve to isolate a possible engine gas leak from the transport loop and avoid a catastrophe. In this case, the necessarily high safety standards of the nuclear industry are preserved by eliminating the potential of a single point heater head failure causing reactor damage.

Reliably brazing or welding of heater heads is an art not yet perfected. Those engines which have accumulated a significant number of operating hours (>5000) such as the

(a)

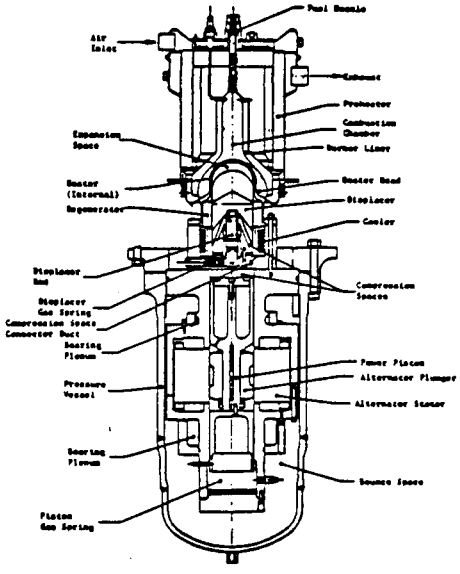

MTI'S GRI Heat Pump

(b)

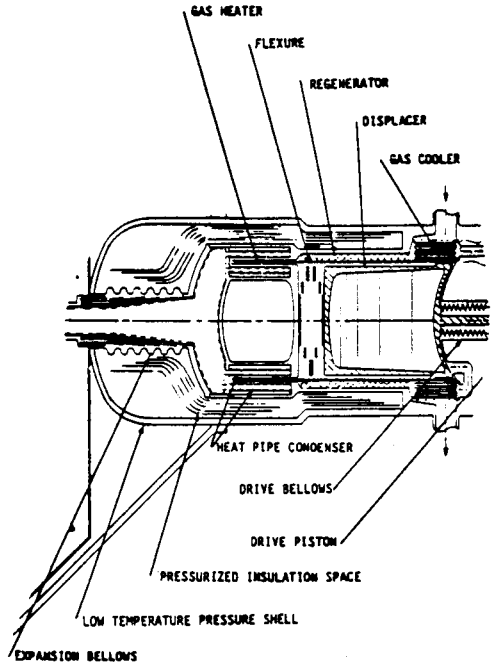

STC's SBIR Concept

(c)

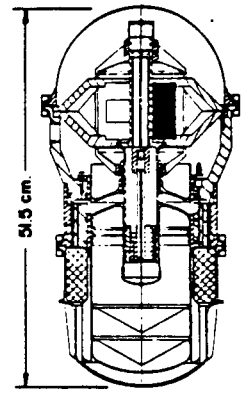

P-88-0008-106

Sunpower's
Spike II

Figure D-3. Three Annular Heater Head Designs

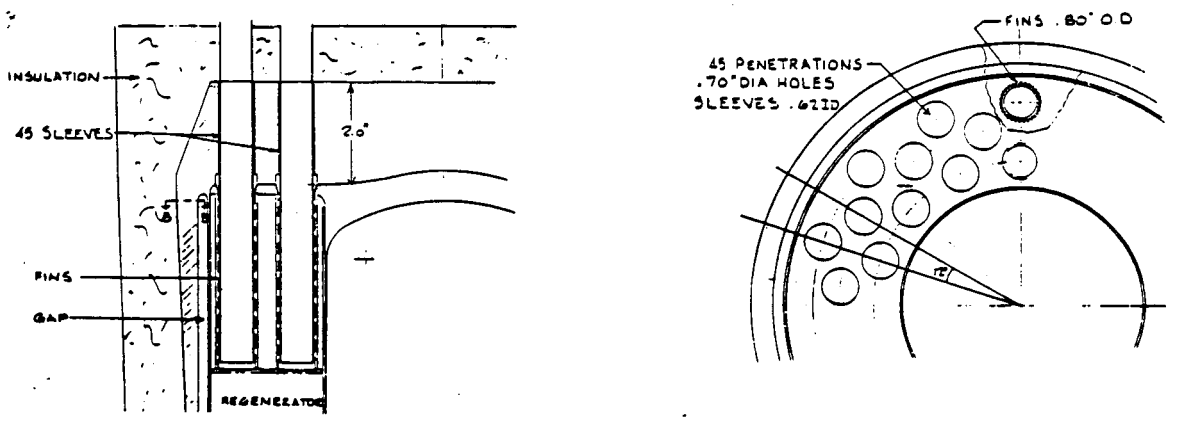

(a) SPRE Heater Head

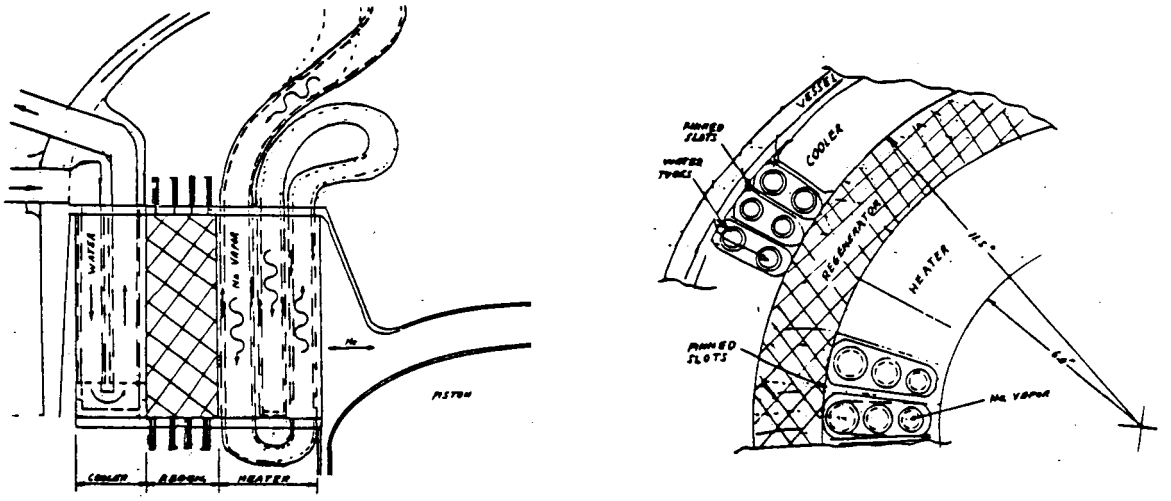

(b) SSE Radial Engine Design

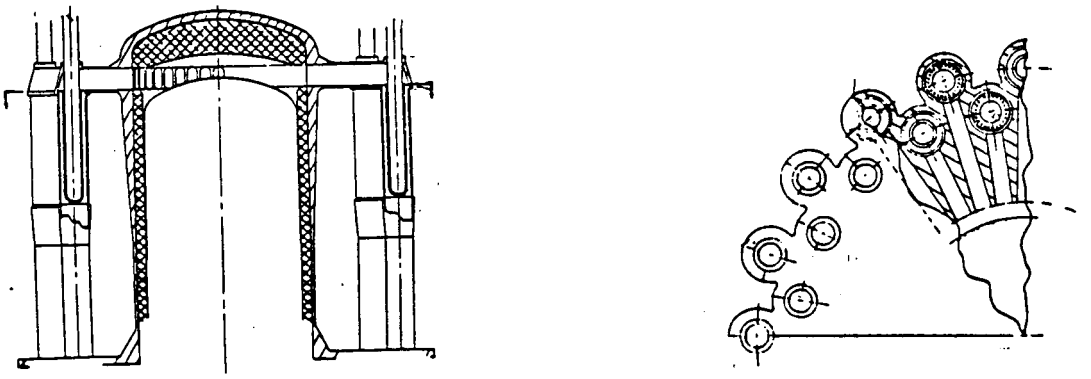

(c) Sunpower Heater-Regenerator-Cooler Design

Figure D4. Three Finned Tube/Shell Heater Head Module Designs

United Stirling of Sweden (USS) P-40 derivatives (4-95) experience numerous and unexpected joint failures. This certainly was the case in the DoE solar testing conducted by Avanco. By comparison, the braze area or weld lengths required for the finned tube shell modules is significantly less than that of a multi-tubular bundle. For example, MTI has incorporated essentially the same heat transfer area into 20 finned tube-shell modules as existed in the 1628 SPDE tubes.

These issues of heater head reliability and fabrication cost are a critical technology driver in Stirling designs. Along with reducing the braze and/or welding requirements is the need for preassembly proof testing. These heater modules, in some designs also integrated with a similar configuration regenerator and cooler, can be pressure-leak tested prior to installation. This should improve engine quality control and ultimately facilitate fabrication.

In Table D1 the nominal head dimensions are presented for power levels of 7 and 12.5 kWe. Assuming a single on-axis receiver/engine configuration, it initially appears convenient to simply extend the axial heat pipes from within the head into a solar cavity. However, for reference, these head diameters are no greater than the receiver aperture. In fact, the very compact MTI radial design is likely to have a diameter significantly less than a required receiver aperture. It is not feasible to assume that straight tubes could match with the solar absorber design requirements. Moreover, if the heat pipes were allowed to fan out into the cavity, large gaps between the pipes would exist. This brief argument serves to point out the obstacles which arise in integrating the very different heat exchange requirements of the solar absorber, the heater head and the PCM. The specifics of these design issues will be expanded in Section 4.4.

Because of the previously described advantages, and the present direction of the SSE program, we have adopted the finned tube-shell module configuration for our 7 kWe detailed CHP design. The preceding discussions of the many unresolved engine configuration issues has been presented to emphasize that a versatile RSU concept is

Table D1 Finned Tube/Shell Module Heater Head Dimensions

Nominal Condenser Diameter

MTI SSE DESIGNS	AS DESIGNED CM (inches)	SCALED TO 7 kWe cm (inches)
SPRE (12.5 kW)	17.2 (6.9)	13.1 (5.2)
"Radial" (25 kWe)	15.2 (6)	8.0 (3.2)
Thermal Power Module (25 kWe)	40.6 (16)	21.5 (8.5)

required at this stage of development. The Sanders CHP approach, described in Section 5 provides this flexibility while exceeding NASA's long range performance goals.

APPENDIX E

CHP ABSORBER/EVAPORATOR STRESS ANALYSIS

APPENDIX E

CHP ABSORBER/EVAPORATOR STRESS ANALYSIS

BACKGROUND:

The Stirling receiver design consists of a truncated hemisphere attached to a cylindrical can as shown in Figure E1. The hemispherical section is a solar absorber. It receives a heat flux load resulting in a varying temperature distribution along its surface.

The hemisphere is a composite of two materials. The absorber side is to be made from IN600. NI201 will be sintered to the other side of the absorber. Figure E1 shows a cross section through the thickness of the absorber. Liquid sodium will flow through the porous sintered nickel and act as a coolant. Several arteries of sintered nickel will be added on to the structure to help distribute the sodium. The receiver is expected to maintain an internal pressure of 6.9 p.s.i.

PURPOSE:

The purpose of this analysis is to determine the maximum stresses resulting from the thermal and pressure loads applied to solar receiver design.

CONCLUSION:

The following are the maximum stresses in the IN600:

Maximum principal stress:	8.0 ksi
Maximum principle shear stress:	4.0 ksi

The following are the maximum stresses in the sintered NI:

Maximum principal stress:	3.5 ksi
Maximum principle shear stress:	1.5 ksi

The maximum shear stress between the two layers of material is:

.75 ksi

ANALYSIS:

Three PAFEC, finite element models were reviewed to determine the stresses in the structure. Because the temperature gradients through the thickness of the absorber are much greater than the circumferencial variations, the circumferencial gradients are not considered and an axisymmetric model is used. However, the sensitivity of the model to thermal gradients in the circumferencial direction shall be checked out in

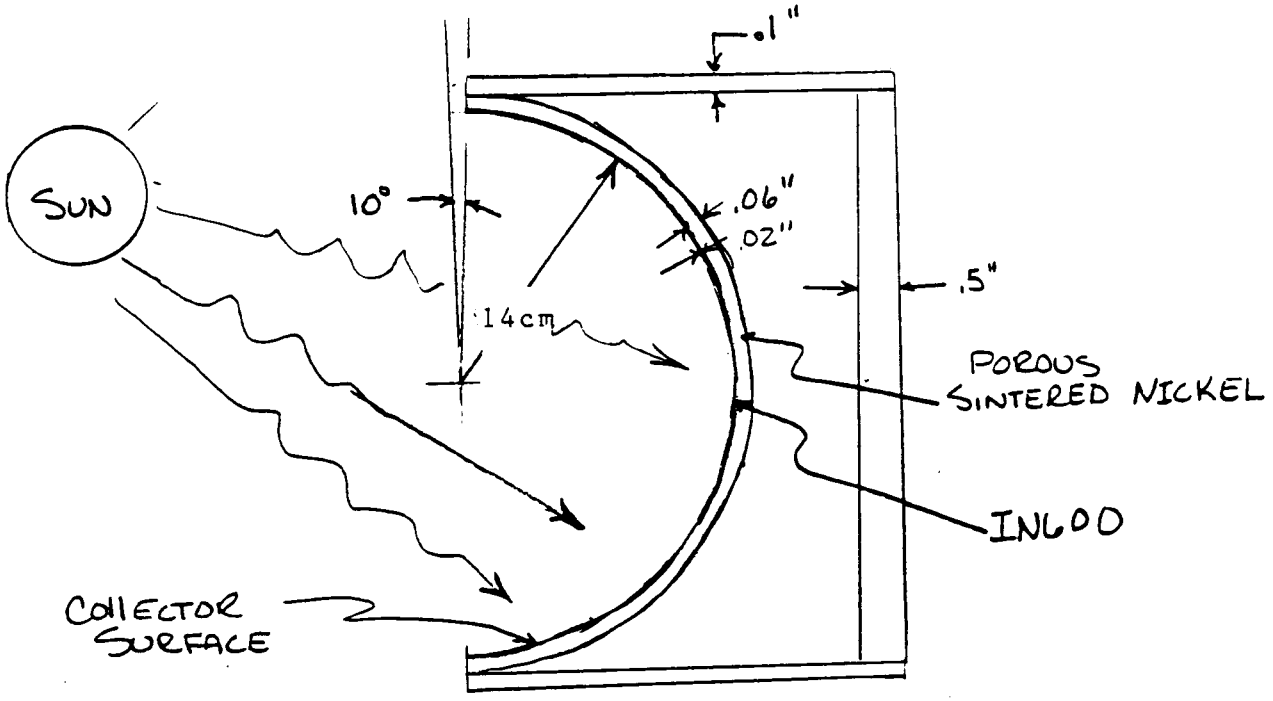

Figure E1

Solar Absorber

the AXSOLRIBTP6 model by applying an extreme temperature distribution along the absorber surface and noting the differences in the local stress results. The following three models were reviewed:

AXSOLARTP5 -	Axisymmetric model of absorber using the temperature distribution indicated in Figure 2.
AXSOLRIBTPF5 -	Axisymmetric model of absorber with artery added between 0 - 38 and 30^{o}. Temperature distribution of Figure E2.
AXSOLRIBTPF6 -	Axisymmetric model of absorber with the rib added and the temperature modified to provide an extreme gradient on the absorber side near the rib (see Figure E3.)

For all of the models, element number 39210 was selected for the thermal analysis and element number 36210 for the structural analysis. These are the eight noded elements used for axisymmetric models.

Elements were defined every 10^{o} on the hemisphere. Except in the area of the rib which required a more refined mesh to achieve convergence in the stress results. Figures E4 and E5 show the geometries of the nonribbed (AXSOLARTP5) and the ribbed models (AXSOLRIBTPF5 and AXSOLRIBTPF6), respectively.

The following material properties are assumed for IN600 (reference MIL-HDBK-5):

o - Coefficient of thermal expansion (see Figure E6)

E - Elastic modules, 22.8E6 psi, ($@1400^{o}F$)

K - Thermal conductivity, 1.25 BTU/hr-in-^{o}F ($@1400^{o}F$)

v - Poissons ratio, .29

The following material properties were assumed for the sinter Nickel (NI201, reference MIL-HDBK-5):

o	See Figure E6
E	The sintered nickel is expected to have a porosity of about 50%, the elastic modulus property will be modified by a factor of .5 to account for this reduction in the area. The elastic modulus used in the model is: 22.8 psi/2 = 11.4 psi
K	The thermal conductivity is calculated by taking the average of the thermal conductivities of NI201 and liquid sodium

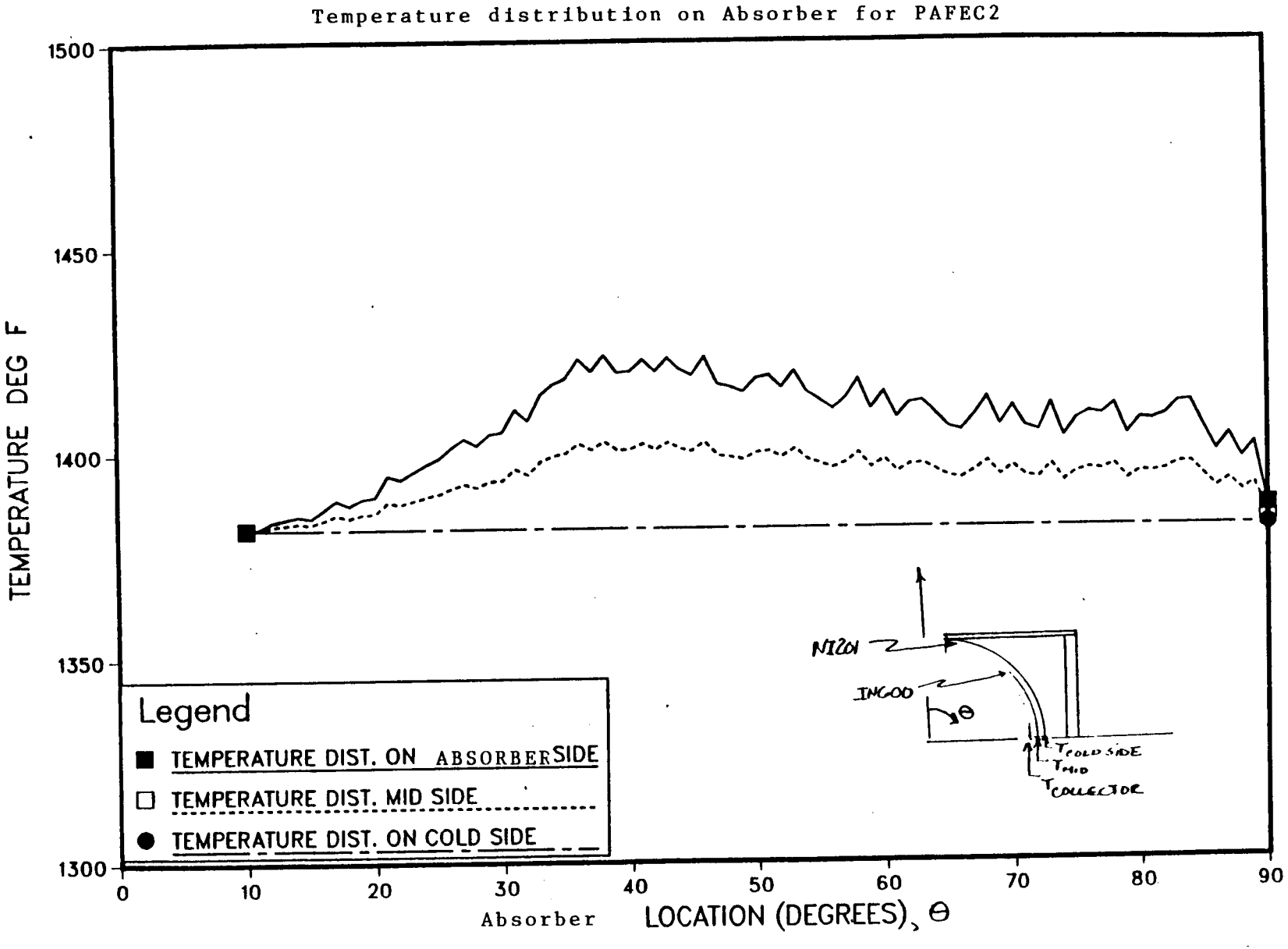

Temperature Distribution used for AXSOLARTP5 and AXSLR IBTP5

Figure E2

Reference for liquid sodium properties: Heat Pipes, by P.D.Dunn & D.A.Ray

RESULTS:

Table E1 reviews the maximum stresses found in the three models.

TABLE E1

MAXIMUM STRESS SUMMARY

Model	Location	o max (ksi)	t max (ksi)	t' max (ksi)
AXSOLARTP5	Collector IN600	7.7	3.7	
				.33
	Sintered NI201	2.5	1.3	
AXSOLRIBTFP5	Collector IN600	7.6	3.8	
				.527
	Sintered NI201	3.3	1.4	
AXSOLRIBTPF6	Collector IN600	7.9	4.0	
				.72
	Sintered NI201	3.2	1.3	

Where: omax is the maximum principle stress

tmax is the maximum principle shear stress

t'max is the maximum shear stress between the IN600 layer and the sintered nickel layer.

Note: All of the stresses reported above were reported at around $O = 38^{o}$.

The results from models AXSOLARTP5 and AXSOLRIBTP5 indicate that the addition of a rib to the model produces a moderate increase in stresses found in the IN600 section of the model. In fact, the maximum principle stress went down in the IN600 which is contrary to what was expected. This decrease is probably due to the refinement of the mesh in the model that was required when the rib was added.

The steep thermal gradient imposed on the model AXSOLRIBTP6 produced a small increase in stress with respect to those calculated in the AXSOLRIBTP5 model. This indicates that the primary stress driver is due to the temperature drop through the thickness, not the smaller thermal gradients along the collector surface.

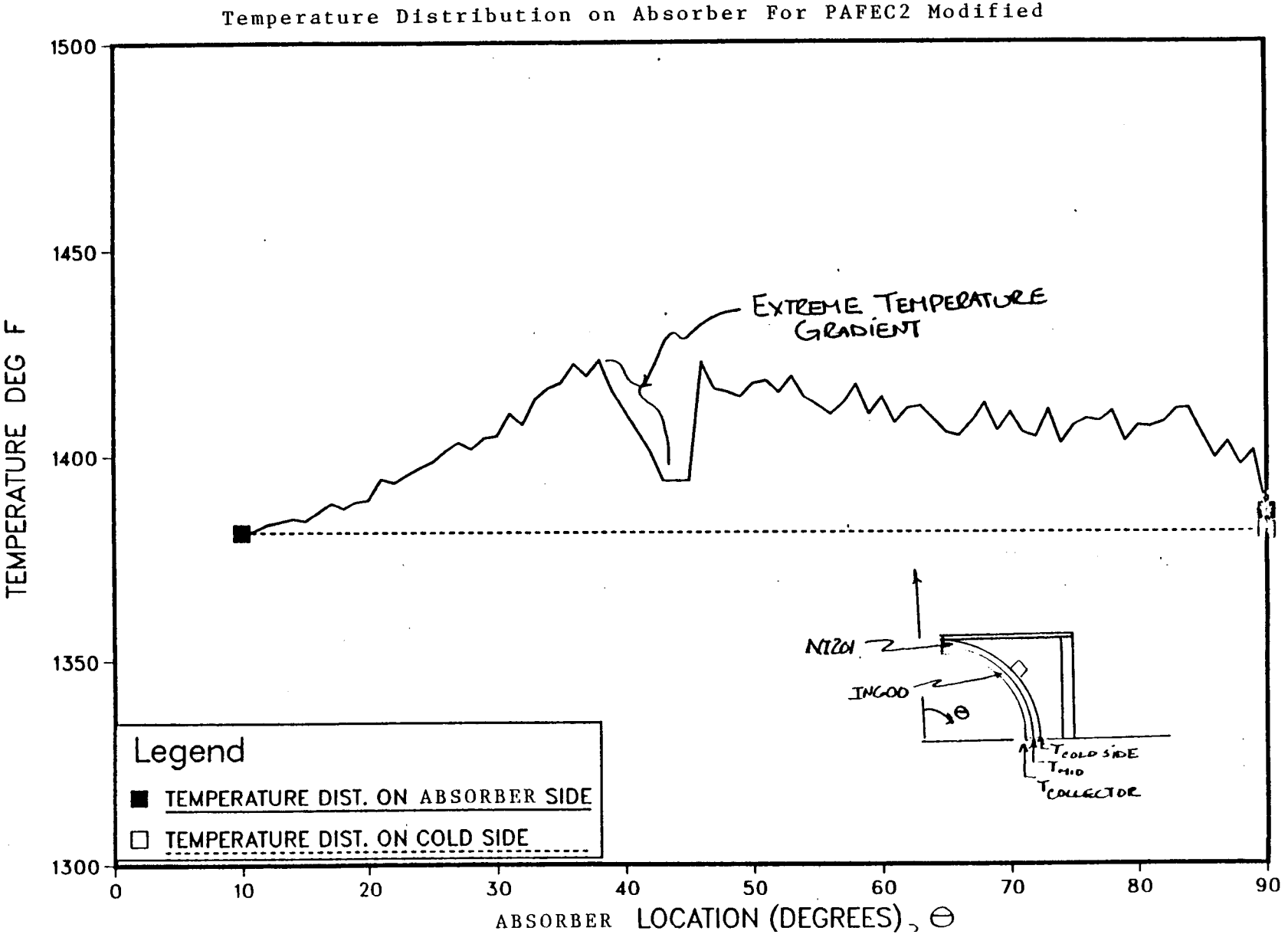

Temperature Distribution used for AXSOLRIBTP6

Figure E3

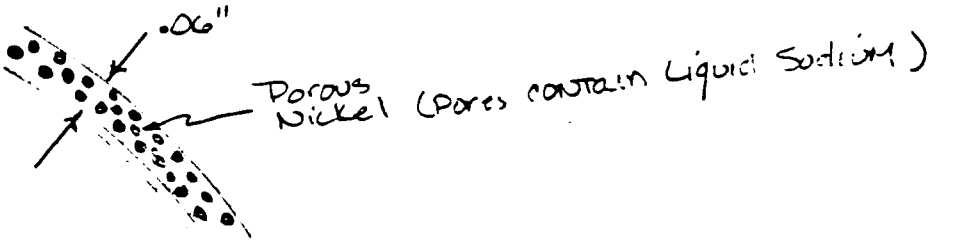

Calculate Thermal conductivity of SINTERED Nickel

Assume 50% NI201
50% Liquid Sodium

$K_{NI} = 3.09 \frac{BTU}{hr\,in\,°F}$ (at 1400° F)

$K_{NA} = 2.8 \frac{BTU}{hr\,ft\,°F}$ (at 1381.4° F)

$$K_{AVE} = \frac{K_{NI} + K_{NA}}{2} = \frac{3.09 + 2.8}{2} = 2.94 \frac{BTU}{hr\,°F\,in}$$

Figure E4

FINITE ELEMENT STRESS ANALYSIS OF ABSORBER/EVAPORATOR

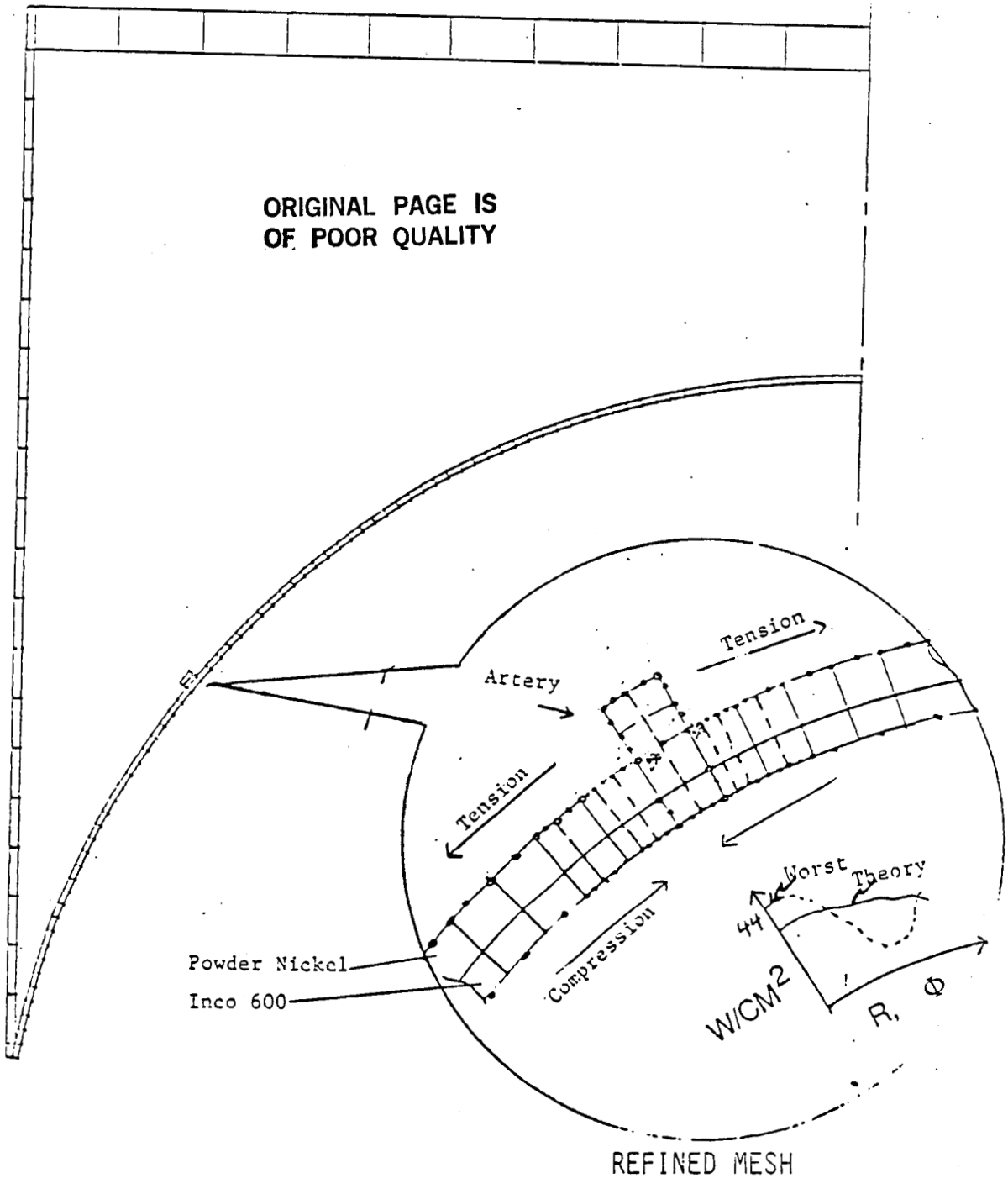

Figure E5

AXSLOARTP6 Model

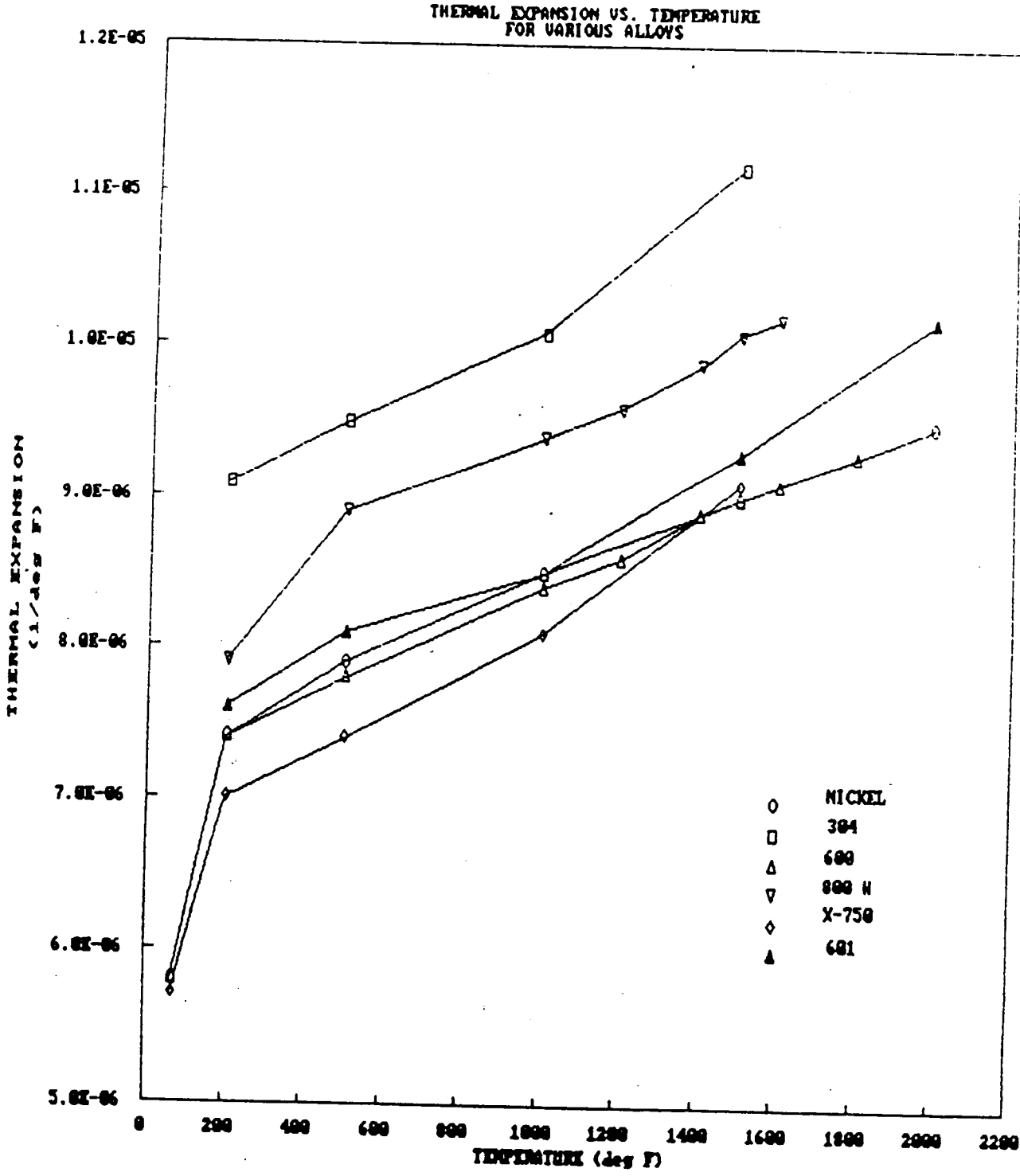

Figure E6

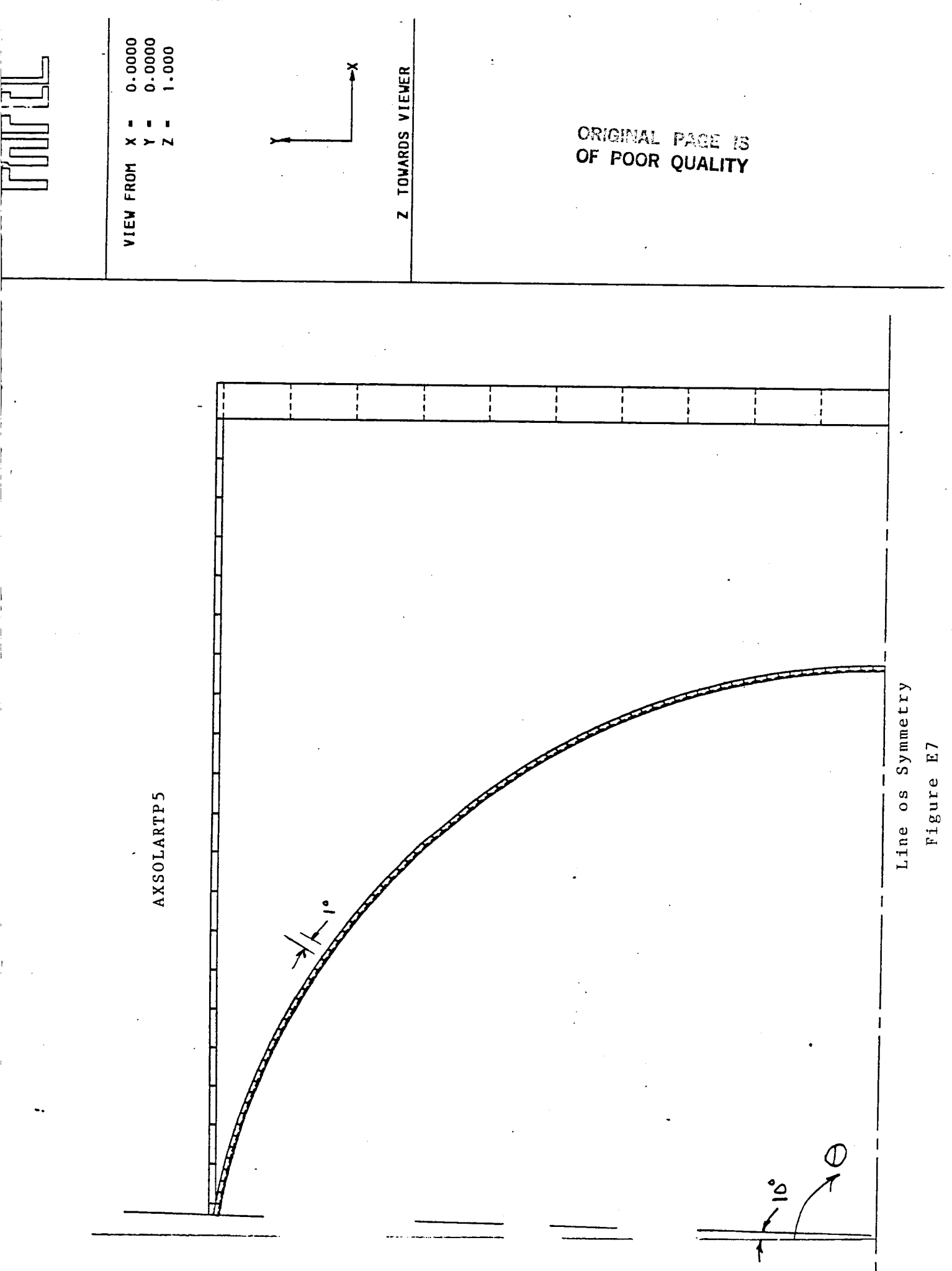
VIEW FROM X = 0.0000
Y = 0.0000
Z = 1.000
Z TOWARDS VIEWER
ORIGINAL PAGE IS
OF POOR QUALITY
AXSOLARTP5
1°
10°
Line os Symmetry

Figure E7

POWDER METAL EVAPORATOR DOME DESIGNED BY THERMACORE

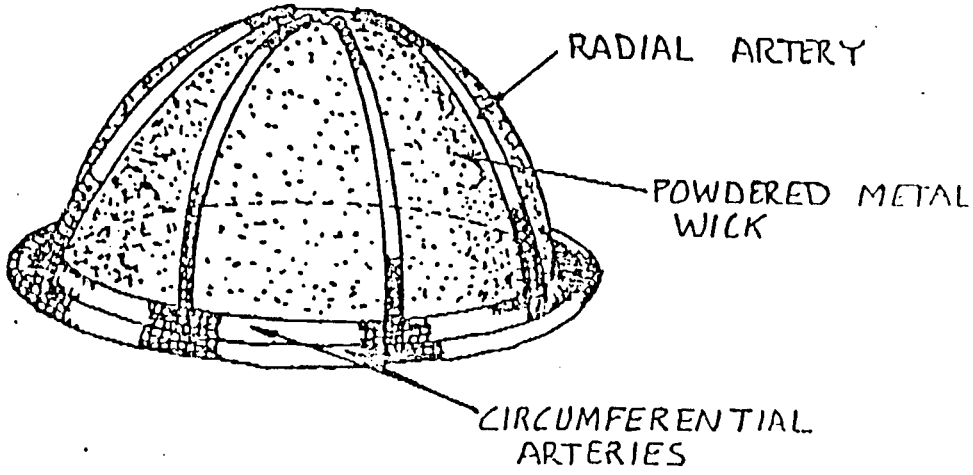

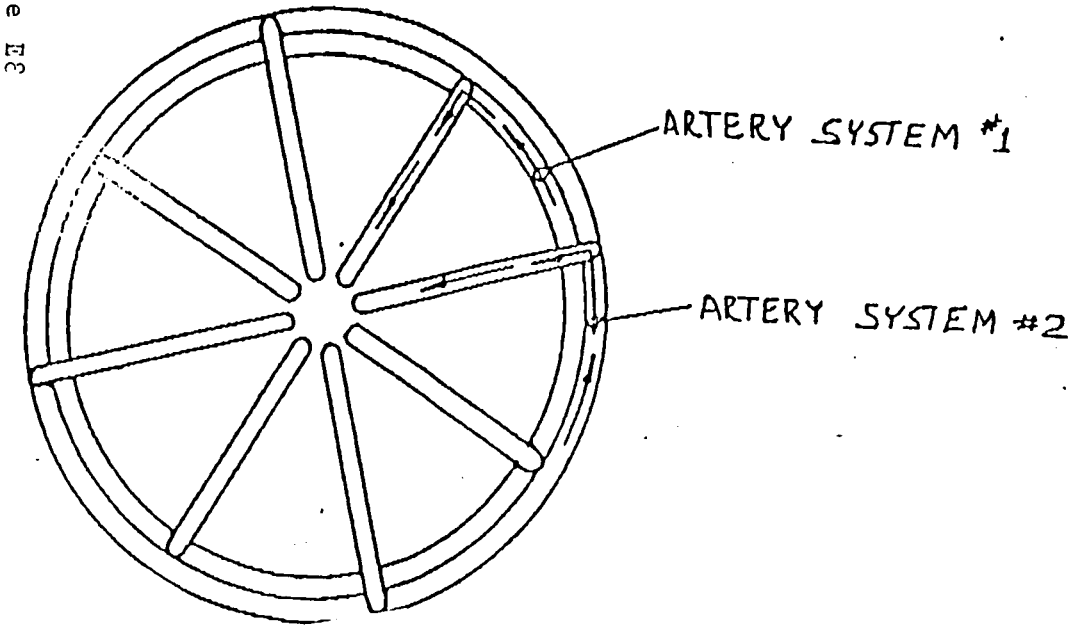

Figure E6

Configuration analyzed in MAdels with Arterys

3-D MODEL

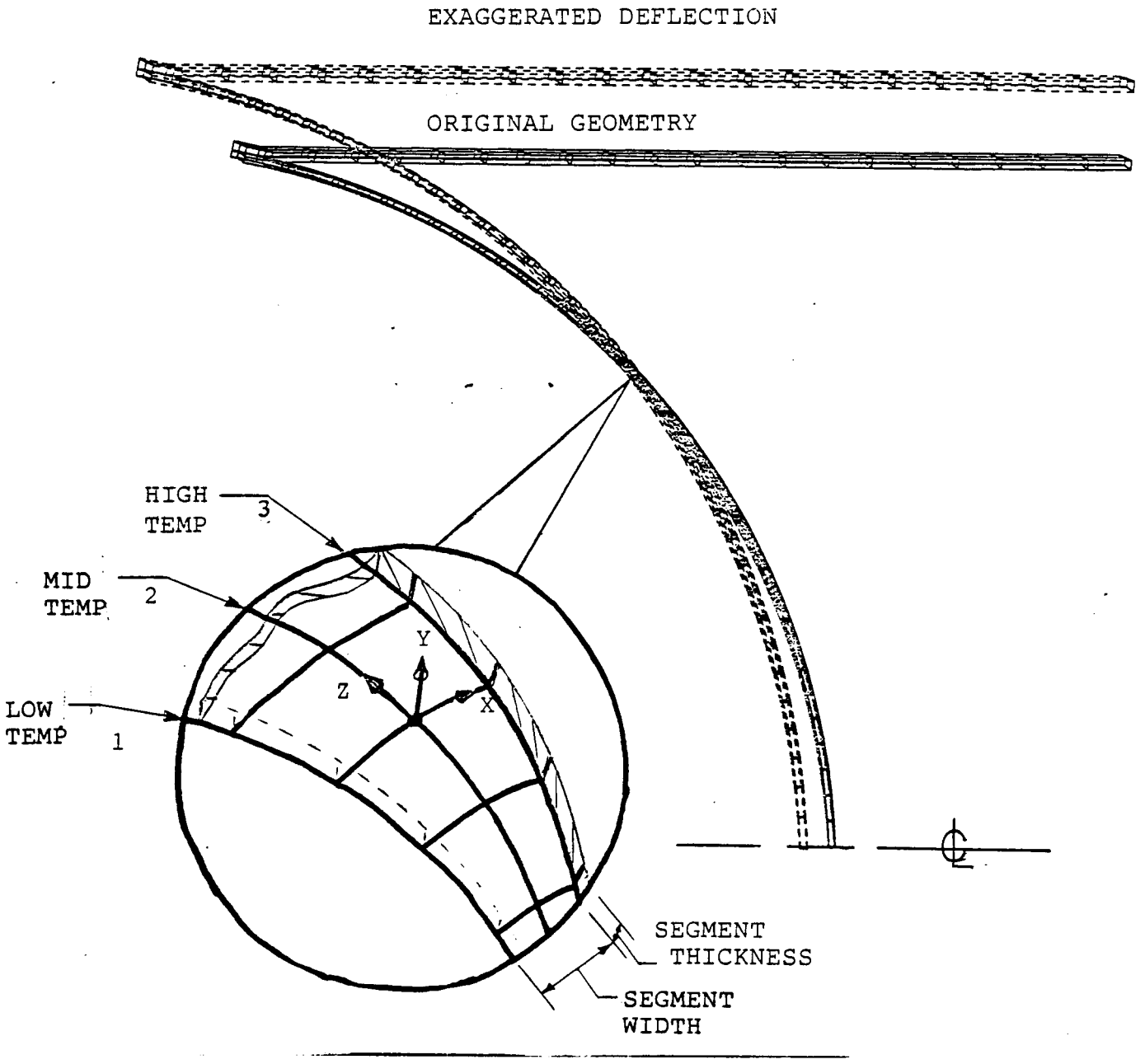

Temperature Distribution on 3-D 14 cm Radius Hemisphere

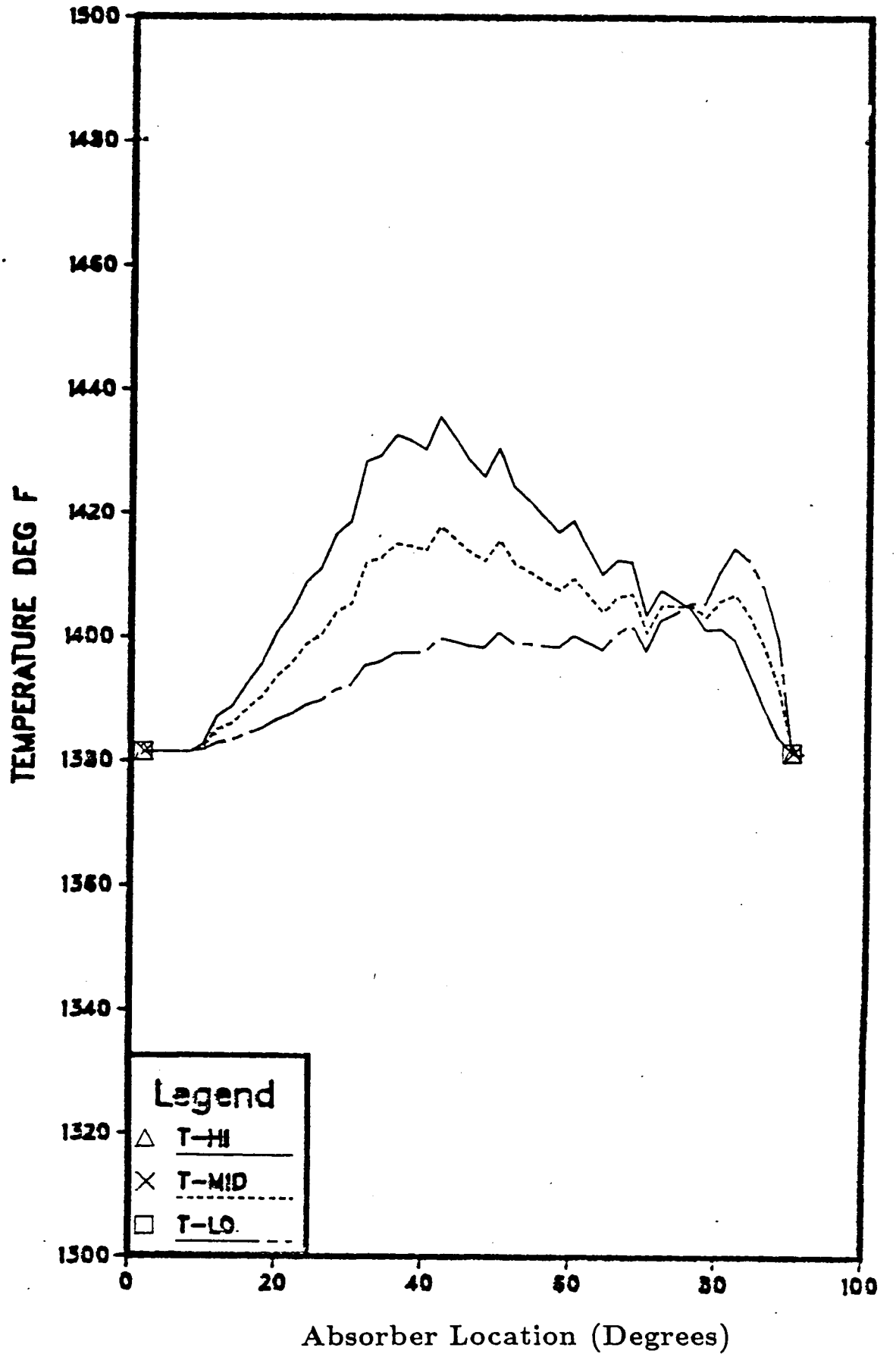

Temperature Distribution on Absorber for 2-D FEM

14 cm Radius Hemisphere

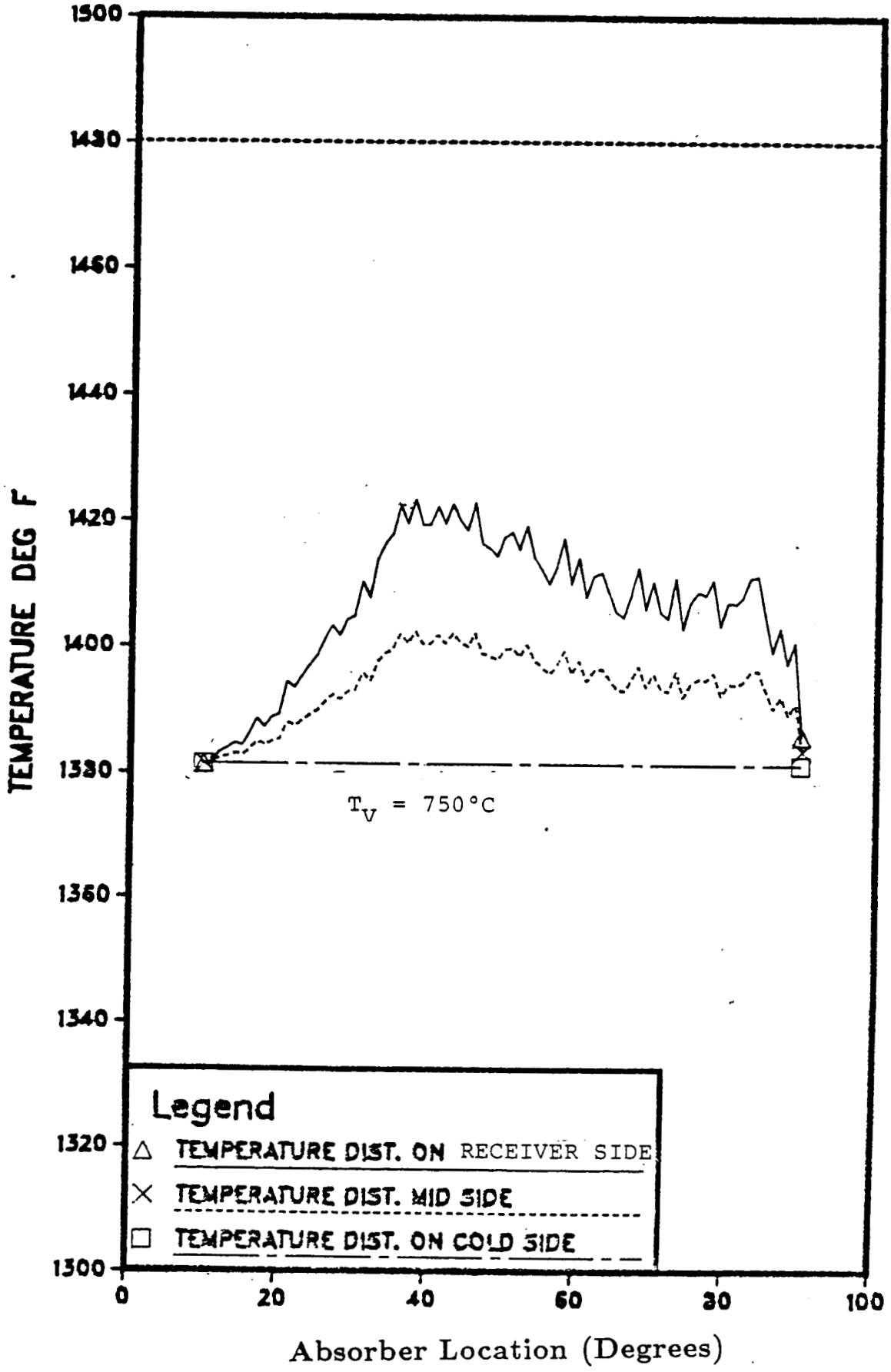

HIGH NODE RESOLUTION VERSION OF 2.D AXISYMMETRIC FINITE ELEMENT THERMAL STRESS ANALYSIS

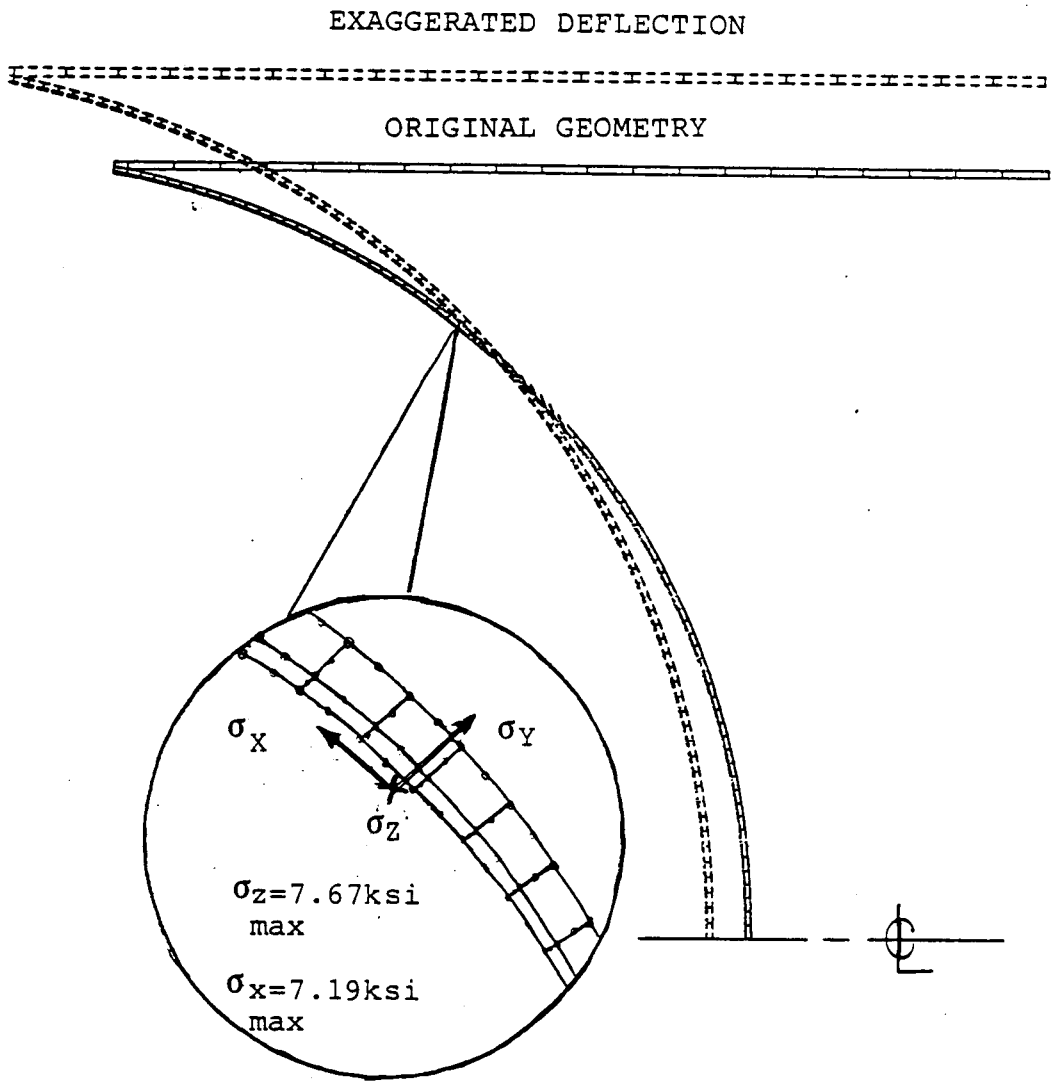

We have much more confidence in these results than those obtained thus far with the low resoltuion 3-D models

ONE DIMENSIONAL STRESS CALCULATION FOR COMPOSITE WICK/ABSORBER

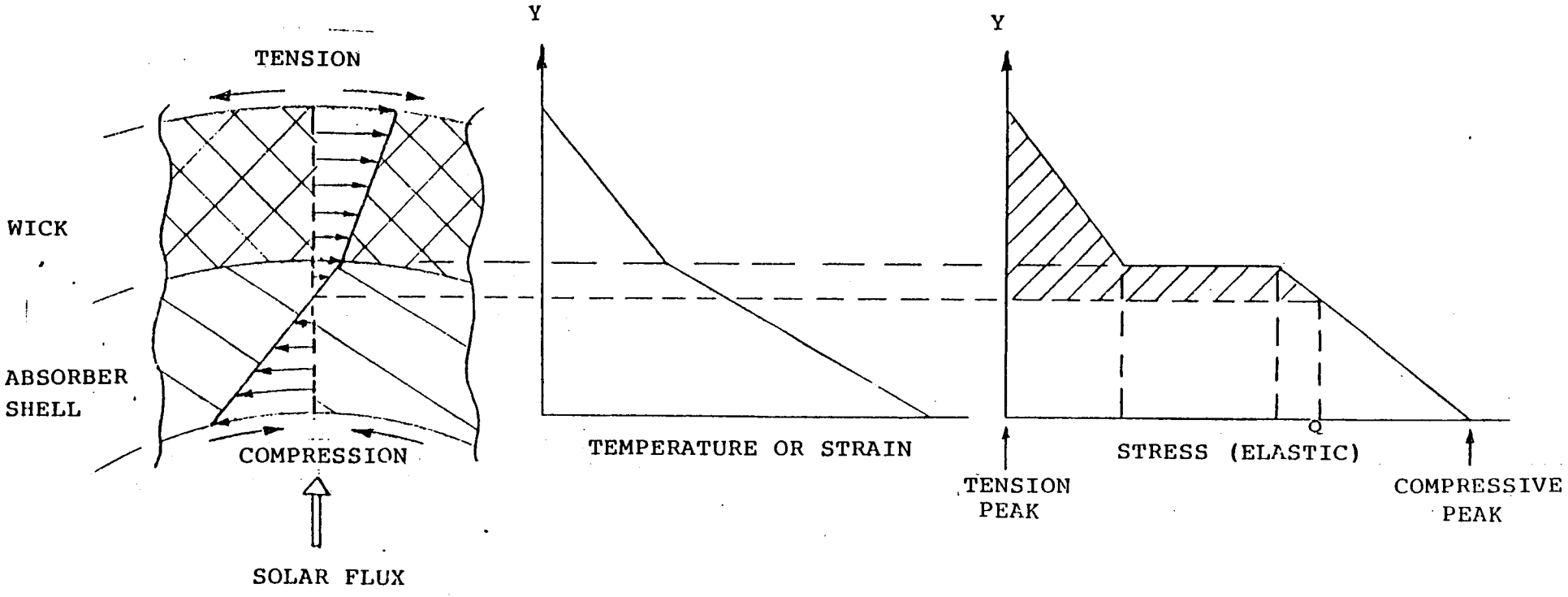

MODEL INCLUDES CONTINUOUS VARIABLE PROPERTIES IN THICKNESS DIMENSION (COEF. OF EXPANSION, THERMAL CONDUCTIVITY, MODULUS OF ELASTICITY)

TRUNCATED CONE CAVITY WITH 400/80% GROOVED

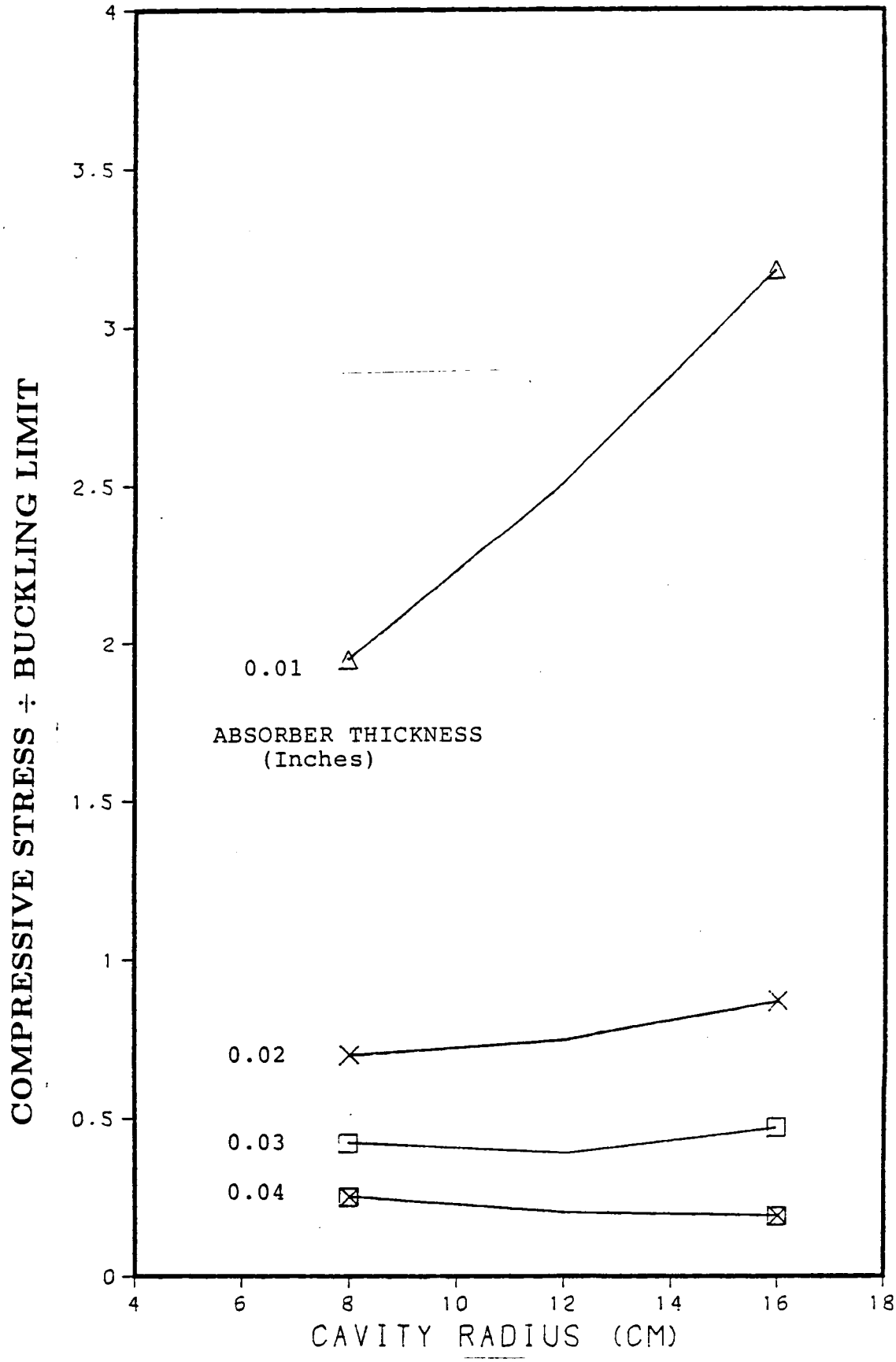

HEMISPHERICAL ABSORBER BUCKLING RATIO FOR 400/GROOVED WICK STRUCTURE

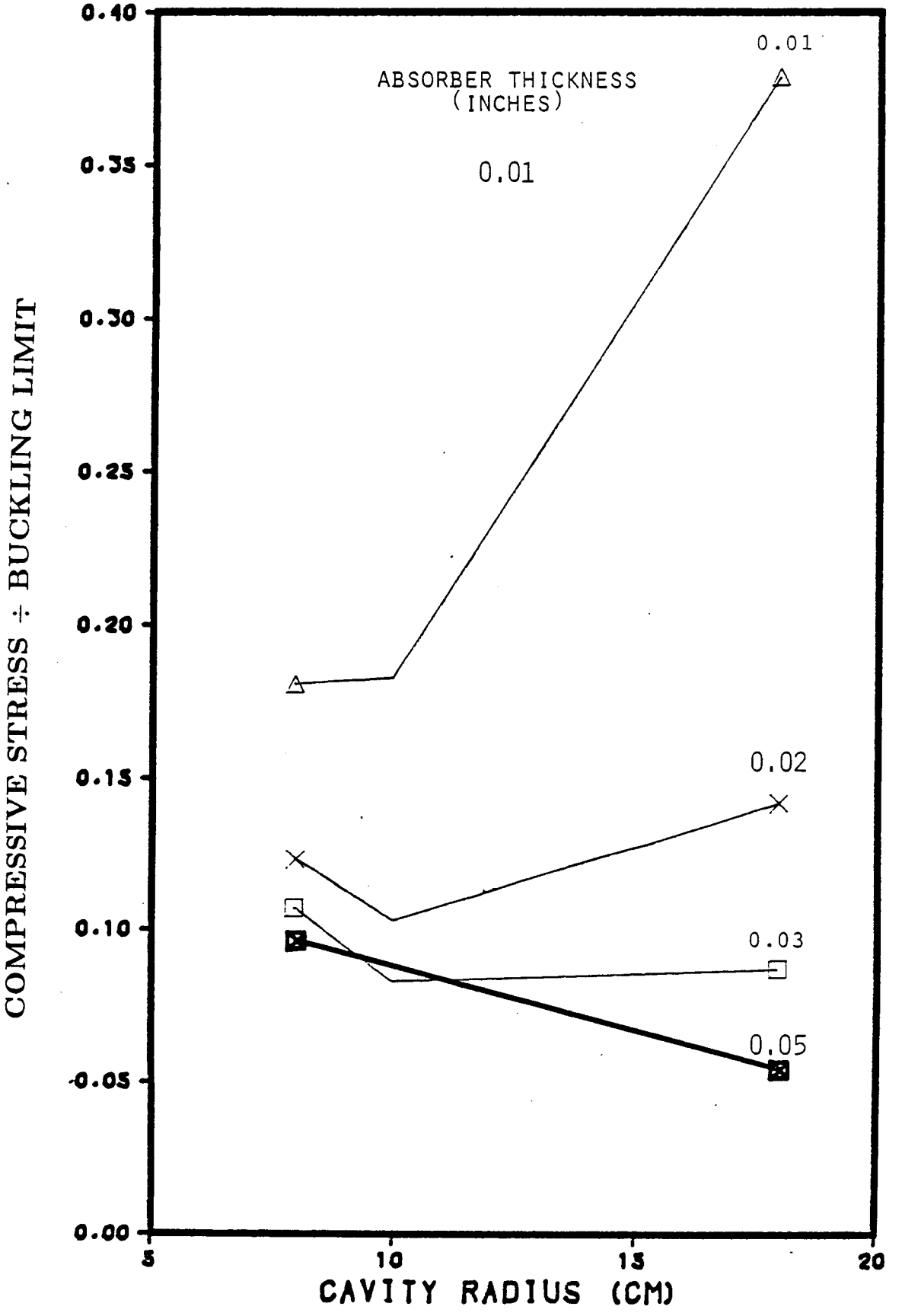

HEMISPHERIC
ABSORBER BUCKLING RATIO FOR 400/50 SCREEN

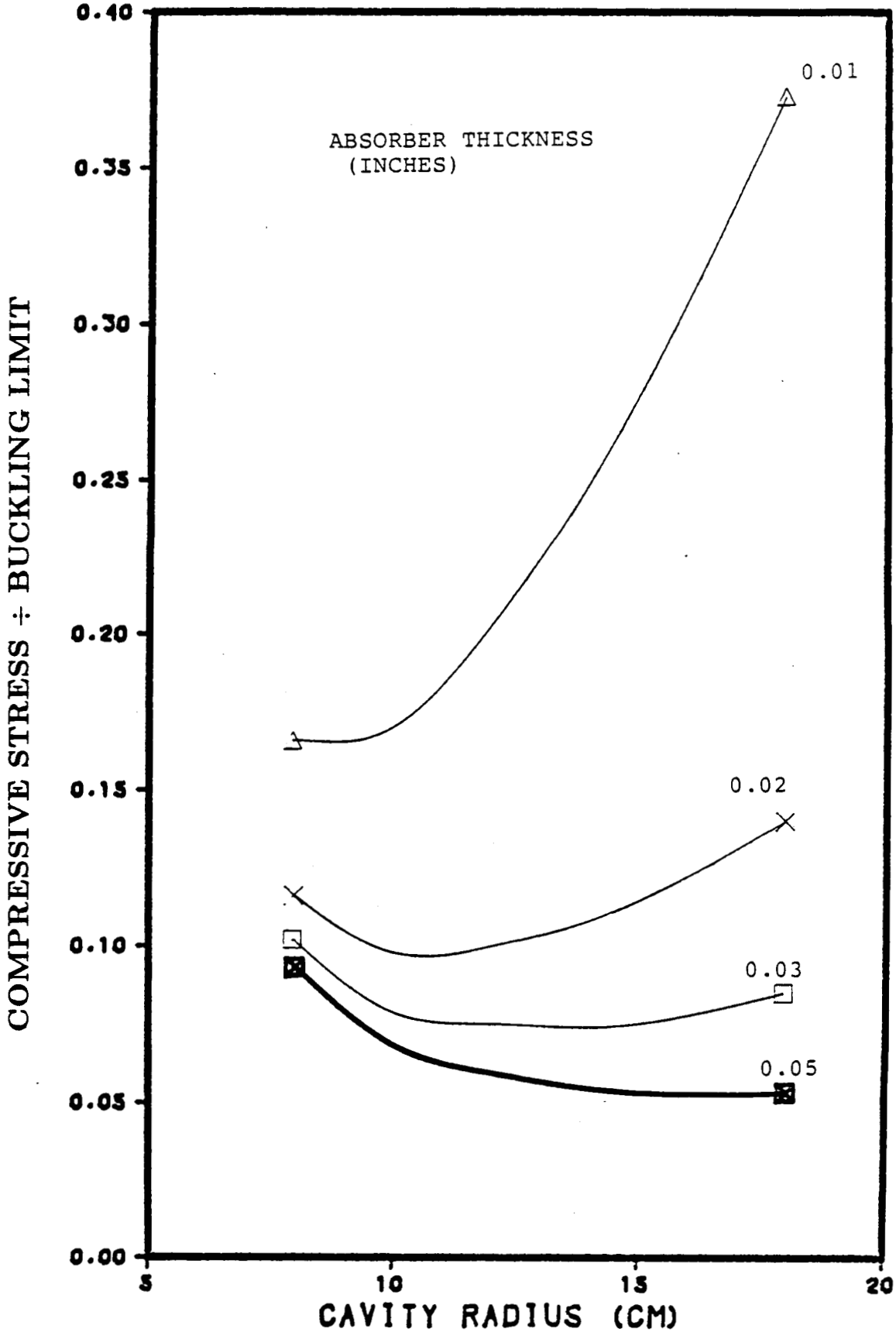

TRUNCATED CONE CAVITY WITH 400/80% GROOVED

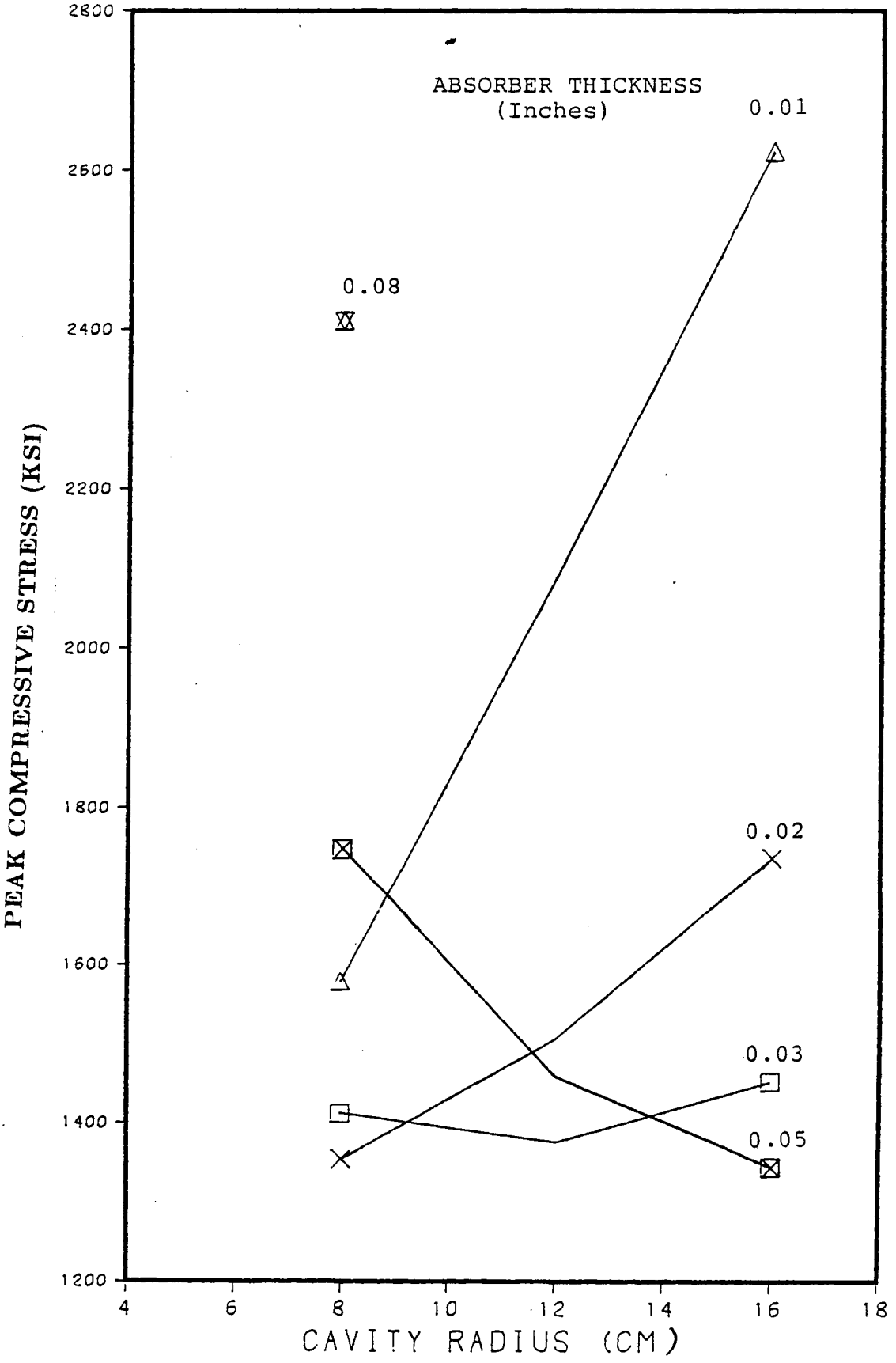

HEMISPHERICAL

ABSORBER STRESSES FOR 400/80 GROOVEI

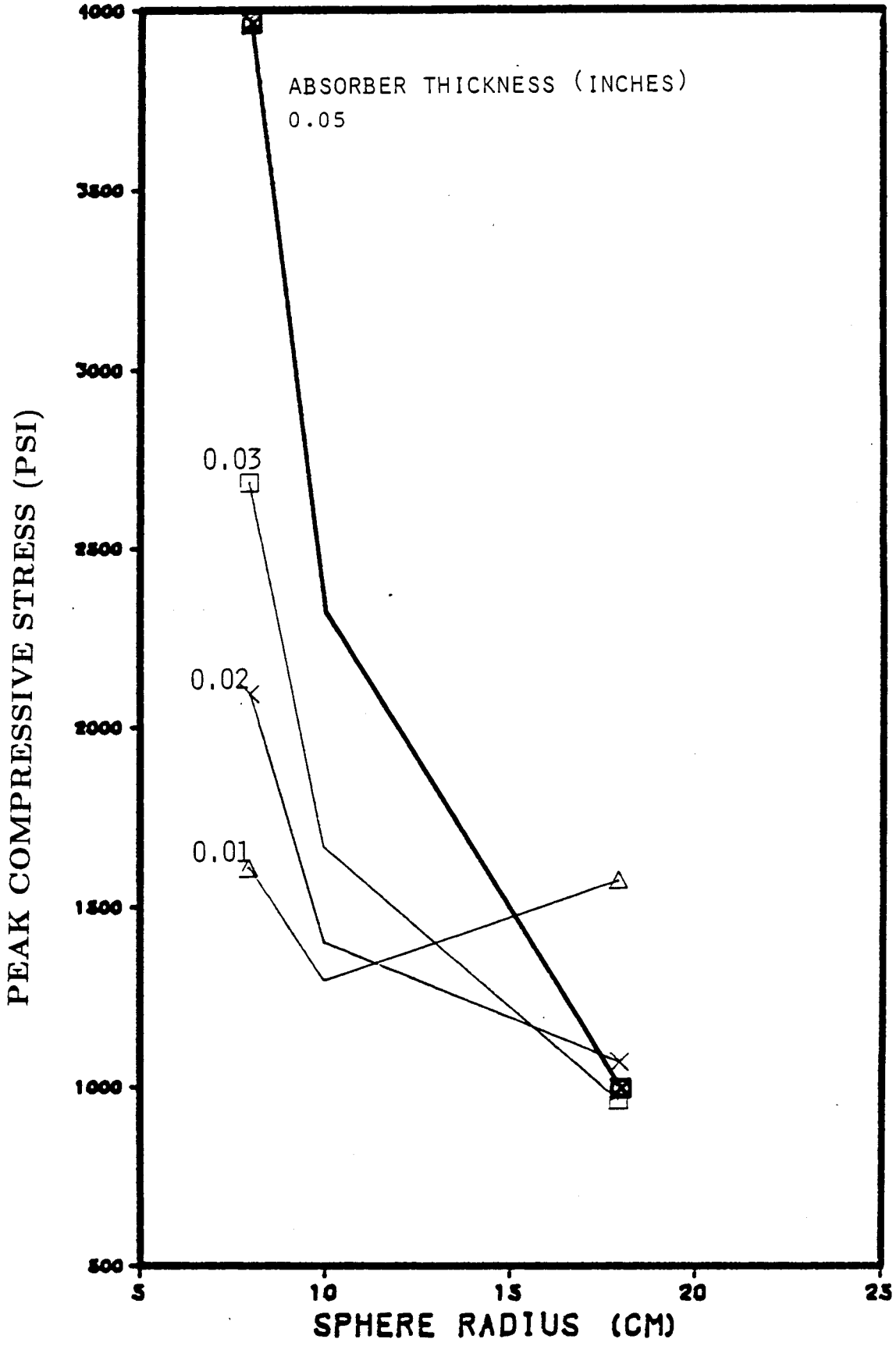

PEAK ABSORBER STRESS FOR 60/Grooved COMPOSITE WICK

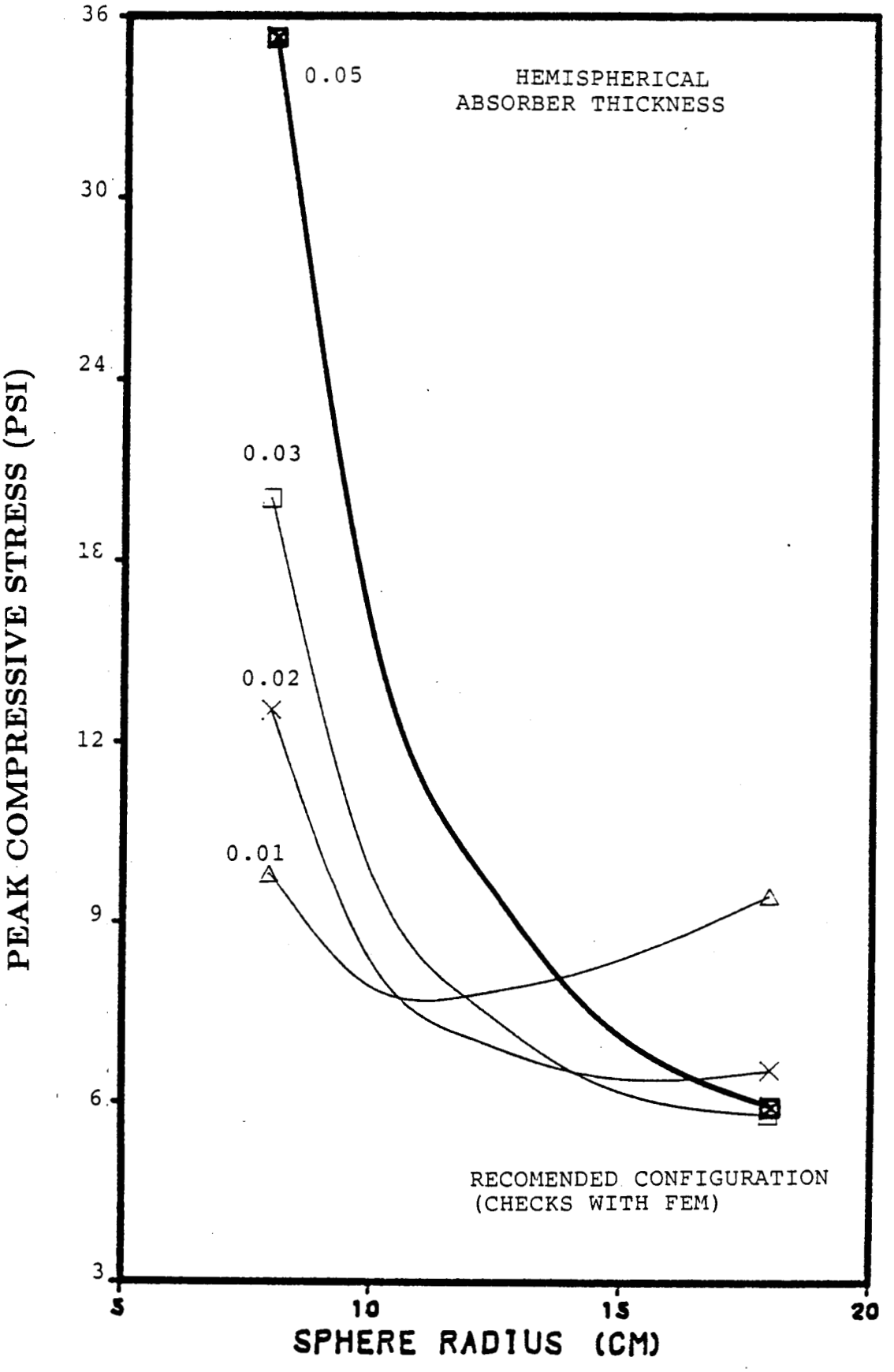

Peak Solar Flux vs. Cavity Radius for Truncated Cones and Hemispheres

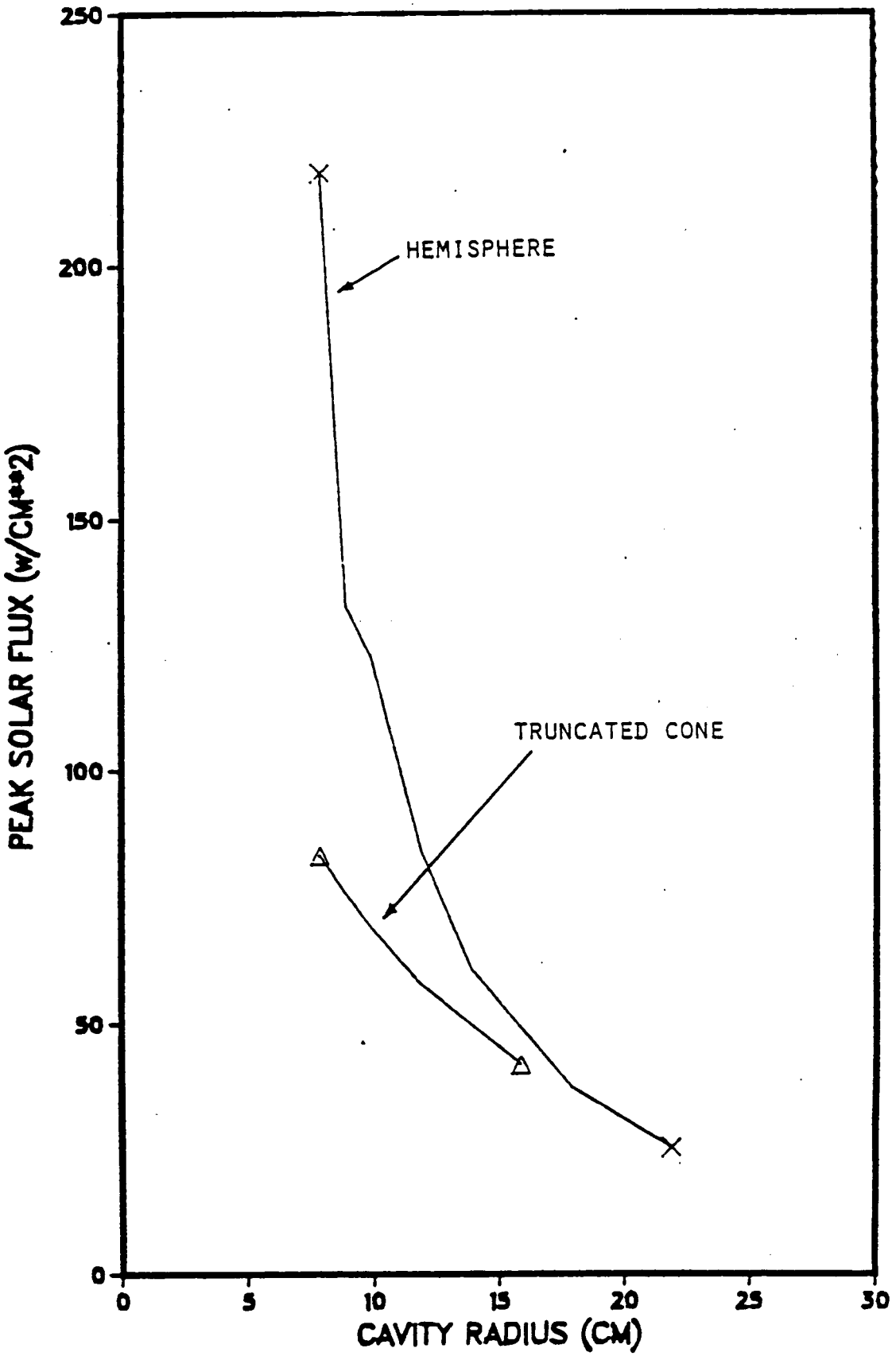

Absorber/Evaporator Stress Analysis Conclusions

- FEM verifies that dominant thermal stresses result from flux through absorber/evaporator composite thickness
- Two dimensional FEM generates high confidence results which are within 20% of one dimensional model
- FEM analysis is only cost effective to use for final evaluation
- Peak stresses in 5 to 7 Ksi range are attained for recommended configuration
- Absorber is critical fatigue element ranging from the peak compressive stress during the day to nominally zero stress at night

Sanders
A Lockheed Company

Conclusion of Buckling Studies

- All realistic cases have plenty of built in safety factors
- Pressure dominates thin wick (prime candidates) with thin absorber shells
- The highest compressive stress usually occurs under peak operating conditions. Earth pressure loads not critical within recommended range

Sanders
A Lockheed Company

Consideration of Buckling in the Selection of Absorber Wall Thickness

Buckling Ratio = Peak absorber compressive stress /critical buckling stress

- Compressive stress is composed of both thermal and pressure stresses
- Buckling determined for composite modulus absorber/wick structure
- Unit value does not necessarily guarantee instability, but as a figure of merit, we recommend a value <0.5
- Each of 4 cone and 4 hemisphere size cases incorporates wick thickness derived from wick/flux model

Sanders
A Lockheed Company

Investigation of Combined Thermal and Pressure Stresses to Select Absorber Thickness

- Same range of absorber geometries considered
  - Hemispheres from 8 to 22 cm radius
  - Truncated cones from 8 to 16 cm
- Each absorber geometry incorporates the predetermined wick thickness and flux levels
- One dimensional composite property model used in trade studies
- Two dimensionsal finite element model used to verify results of one dimensional model
- Three dimensional finite element model used to inspect worst case
  - Real life solar flux maldistribution
  - 3:1/inch flux variations around nominal Monte Carlo prediction

Sanders
A Lockheed Company

C-3

APPENDIX F

75Kw HEATER FOR EVAPORATOR TEST

APPENDIX F

75Kw HEATER HEAD FOR EVAPORATOR TEST

To operate the receiver/heat transport system with a calorimeter as well as the integrated conversion system, a 75 kW power source must be fabricated. Either a radiation or an RF induction heater can perform this function. The RF induction approach can achieve the higher power density, exceeding our nominal 75kW demand. However, a relatively, costly, high frequency power supply $70,000 to $100,000) appears to be necessary to satisfy our requirements. The high frequency (400-500KhZ) is required to achieve a small penetration depth of RF Flux. Custom fabrication of the heating coil would not be as challenging as a radiation source since it could be constructed from copper tubing.

The radiation source is more limited in its power density capacity but can still meet the 75kW load. Two resistive source design options are described. The first utilizes commercial silicon carbide heater rods and the alternative uses tantalum wire. Since SiC can not be readily purchased in shapes other than tubes, it is not feasible to consider building a hemispherical source as would be desired for the lowest watt-loading and temperature. For this reason we limited our present effort to a parallel array of rods forming a radiating disk. Alternatively, utilizing refractory metal wire (tantalum, molybdenum, tungsten) it is possible to consider a wound "bee-hive" shaped heating element.

Silicon Carbide Heat Source

Specifications

- SiC max operating temp.(in air) = 1720oK(I^2RElement Co.)
- rod (or tube) diameter range = .375" to 2.125" (standard availability)
- Emissivity = 0.92 (SiC @ 1500oC)
- Heater diameter = 20 inches
- Output power = 75kW
- Resistivity of SiC(ρ) = 0.1 ohm-cm

Based on the projected (disk) area of the heater, solve for the source temperature for Equation 1.

$$q/A = \epsilon\sigma(T_s^4 - T_{cav}^4)$$

WHERE:
q = 75kW
A = $\Pi(10 * 2.54)^2$
$\sigma = 5.669 * 10^{-12}$
$T_{cav} = 980 \circ K$
ϵ = .98(effective value increased due to area ratio)
Therefore T_s = 1659oK at 37 w/cm^2

This represents the average radiating temperature from the circular area projected by the array of rods.

To operate at a convenient voltage, it is necessary to manipulate the length and diameter of the heater rods as given by equation 2 and 3. If all of the rods are electricaly connected in series to maximize the length, voltage will also be maximized.

Eq 2

$$R = \rho L / A_{cross}$$

Eq 3

$$P = V^2 / R$$

Preliminary calculations indicate that at a voltage of 110VAC standard 5/8 inch rods satisfy our requirements. Figure C1 illustrates the series arrangements of approximately 21 closely spaced (but not connecting) silicon carbide rods. The standard rods supplied by IsquaredR Element Co. utilize a technique of impregnating the end of each rod with aluminum to lower it's resistivity for the cool junction. The ends of these rods would then be inserted into an aluminum terminal block to accomplish the series connections.

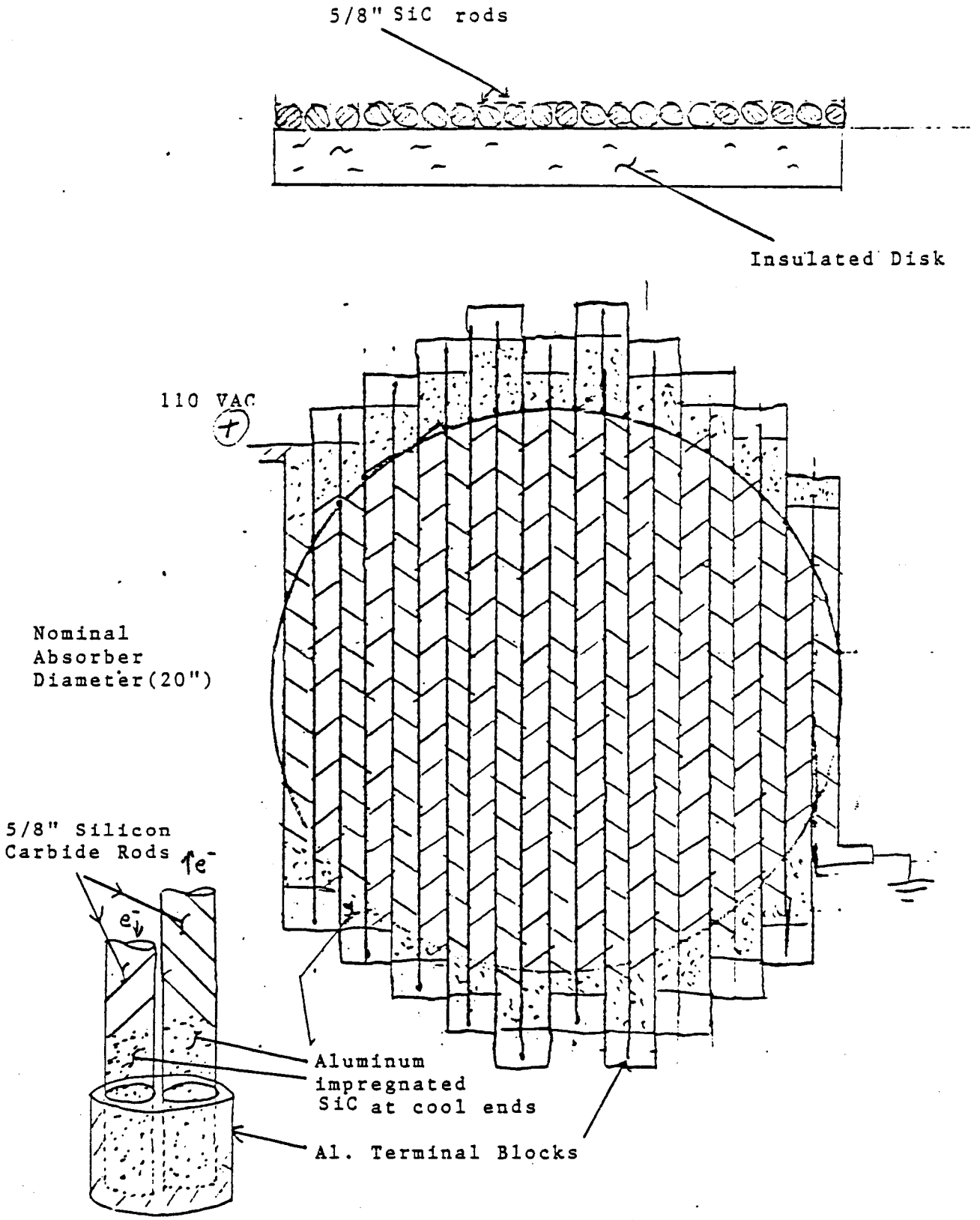

Figure F1
Series configuration of Silicon carbide rod heater operating at 1600°K, delivers 75Kw from 110VAC.

Tungsten Source Test Heater Design

Design Assumptions:

Want highest possible temperature source to shift spectrum toward visible.

Source heater(Tungsten) operates at 2000 $\circ C$ in vacuum.

Want total flux of 75kW.

Use either 110 VAC, 220 VAC or 440 VAC.

$$P = \epsilon\sigma(T^4_{heater,\circ K} - T^4_{test,\circ K})A_{surface}$$

$$R = \rho_{Theater} L/A_{cross}$$

$$\rho_{Theater} = \rho_{20\circ C} + RTC(T_{heater,\circ C} - 20 \circ C)$$

$$P = V^2/R$$

$$A_{surface} = D_{wire} L$$

$$A_{cross} = \pi(D_{wire})^2/4$$

Where:

P = Power, W

ϵ = Emissivity of Tungsten

σ = Stefan-Boltzman Constant, $W/cm^2 \circ K^4$

$T_{heater,\circ K}$ = Temperature of source, $\circ K$

$T_{test,\circ K}$ = Temperature of test section, $\circ K$

$A_{surface}$ = Projected area of source, cm^2

R = Resistance, ohm

$\rho_{Theater}$ = Resistivity of Tungsten at T_{heater}, $\mu ohm - cm$
L = Length of wire source, cm

A_{cross} = Cross-sectional area of source, cm^2

ρ_{20oC} = Resistivity of Tungsten at 20 o C, $\mu ohm - cm$

RTC = Resistivity Temperature Constant of Tungsten, nohm-cm/oC

$T_{heater,oK}$ = Temperature of source, oK

V = Voltage, V

D_{wire} = Diameter of wire source, cm

Figure F2

$\rho_{Theater}$ = Resistivity of Tungsten at T_{heater}, $\mu ohm - cm$
L = Length of wire source, cm

A_{cross} = Cross-sectional area of source, cm^2

ρ_{20oC} = Resistivity of Tungsten at 20 o C, $\mu ohm - cm$

RTC = Resistivity Temperature Constant of Tungsten, nohm-cm/oC

$T_{heater,oK}$ = Temperature of source, oK

V = Voltage, V

D_{wire} = Diameter of wire source, cm

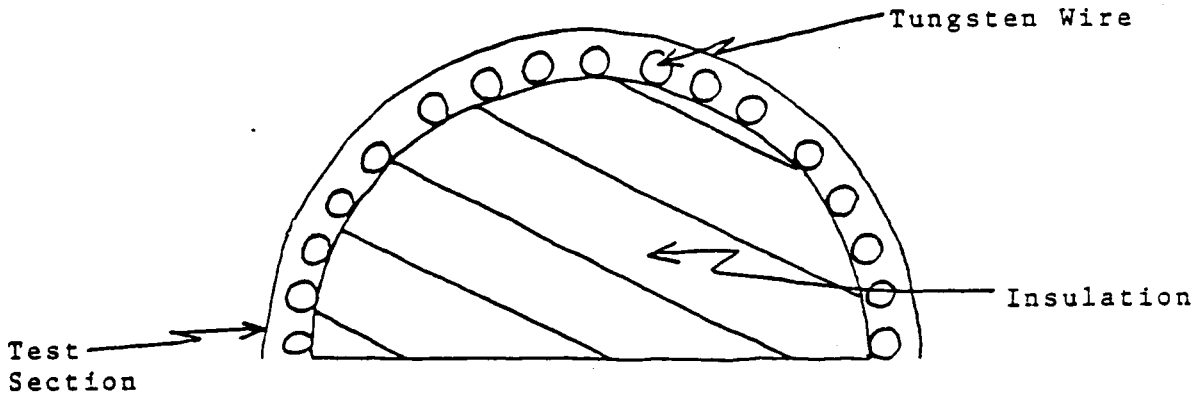

Figure1
(not to scale)

Table F1.

Source Test Heater Design

$P = 75{,}000W$
$T = 2273°K$
$T_{heater} = 973°K$
$\epsilon^{test} = .25$

CASE	$A_{surface}$	R	$\rho_{T_{heater}}$	L	A_{cross}	$\rho_{20°C}$	RTC	V	D_{wire}
1	2051	.161	13.65	3393	.287	5.43	4.15	110	.605
2	2051	.645	13.65	5387	.114	5.43	4.15	220	.381
3	2051	2.58	13.65	8551	.045	5.43	4.15	440	.240
4	2051	.161	14.36	3336	.297	4.84	4.81	110	.615
5	2051	.645	14.36	5295	.118	4.84	4.81	220	.387
6	2051	2.58	14.36	8406	.047	4.84	4.81	440	.244

APPENDIX G
STIRLING CHP CONFIGURATION TRADE STUDIES

Key Issues for Heat Pipe Stirling Receiver

- Solar flux induced stresses on absorber/evaporator
- Evaporator wick configuration and thickness
- Liquid transport from condenser to evaporator

This order reflects the relative amount of attention devoted to each problem in this study

STIRLING HEAT PIPE EVAPORATOR/ABSORBER ANALYSIS

- Investigate solar flux profiles on a range of cavity geometries.
- Determine wick characteristics and cavity geometries for various wick configurations.
- Analyze stresses.
- Investigate buckling characteristics.

Sanders
A Lockheed Company

INITIAL GEOMETRY STUDIES TO COMPARE CANDIDATE CONICAL AND SPHERICAL SECTION ABSORBERS

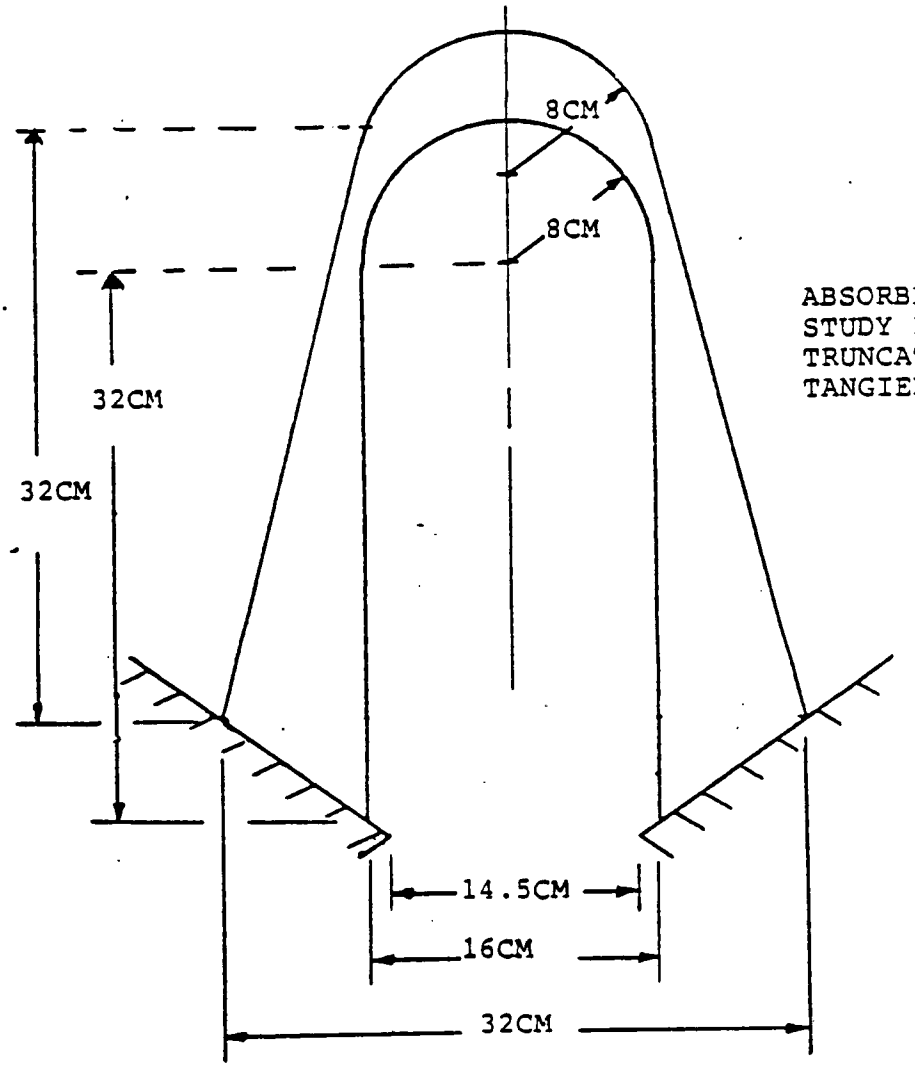

ABSORBER/EVAPORA
STUDY RANGE FOR
TRUNCATED CONE W
TANGIENT SPHERIC

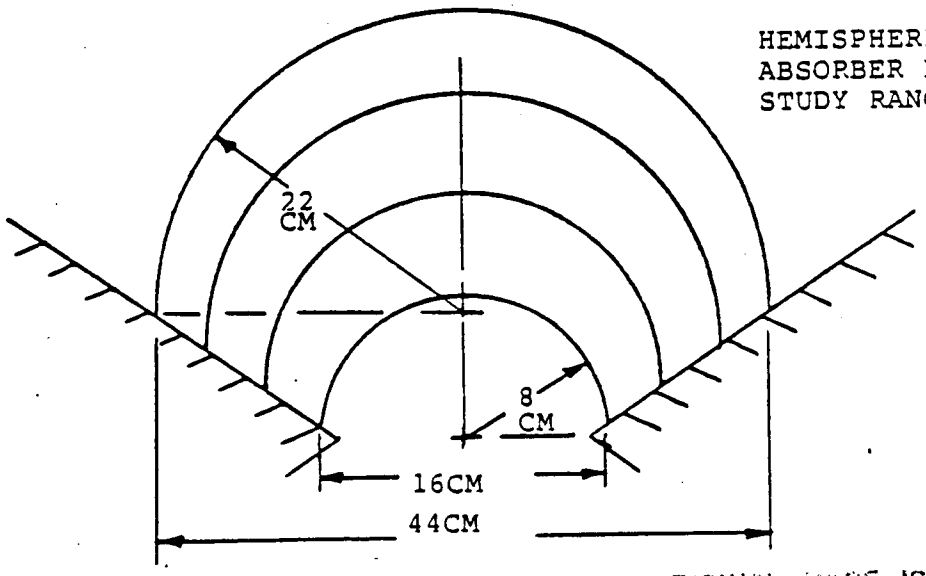

HEMISPHERICAL
ABSORBER EVAPOR
STUDY RANGE

FLUX DISTRIBUTION ON TRUNCATED CONE CAVITIES

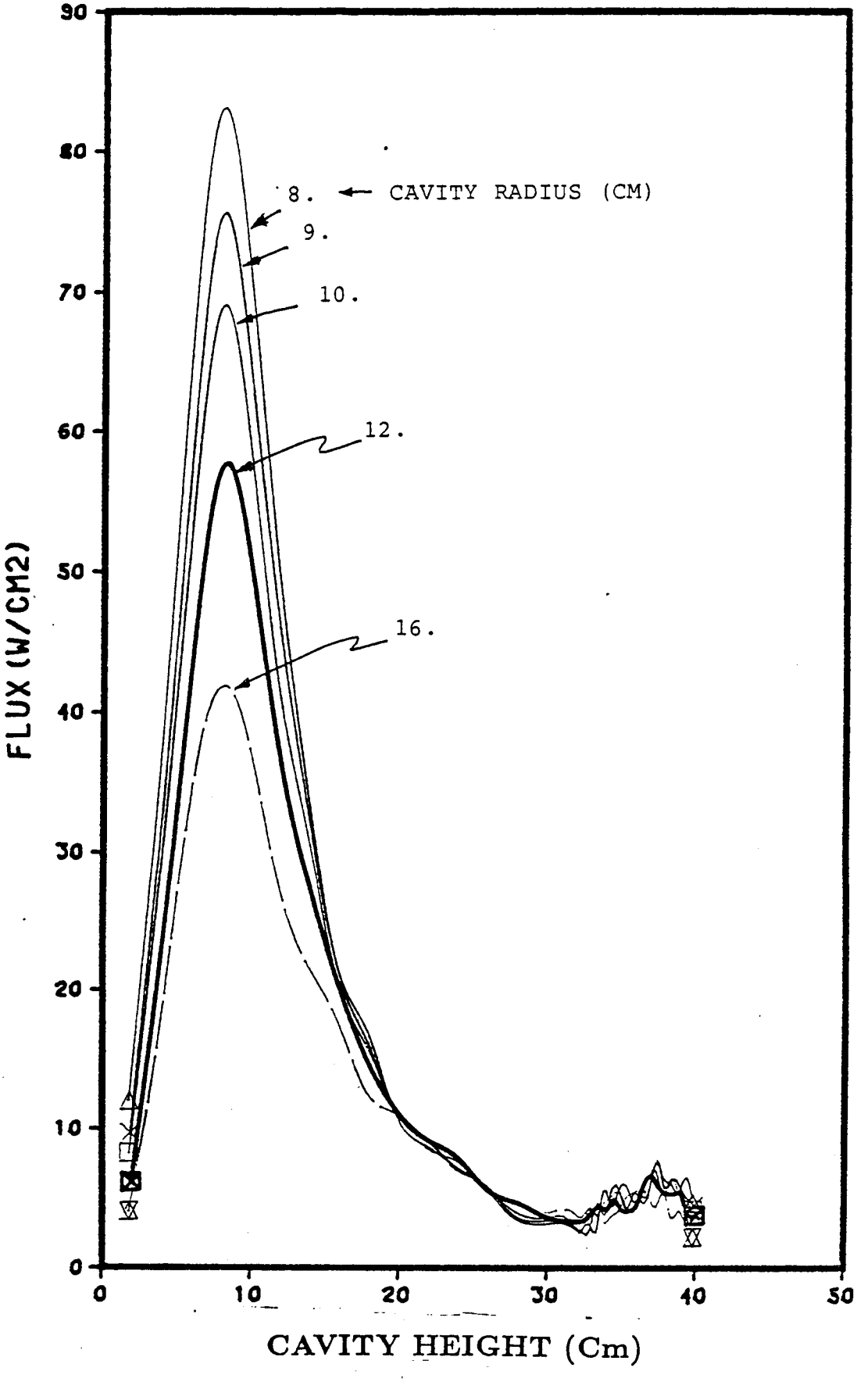

FLUX DISTRIBUTION ON HEMISPHERICAL RECEIVER CAVITIES

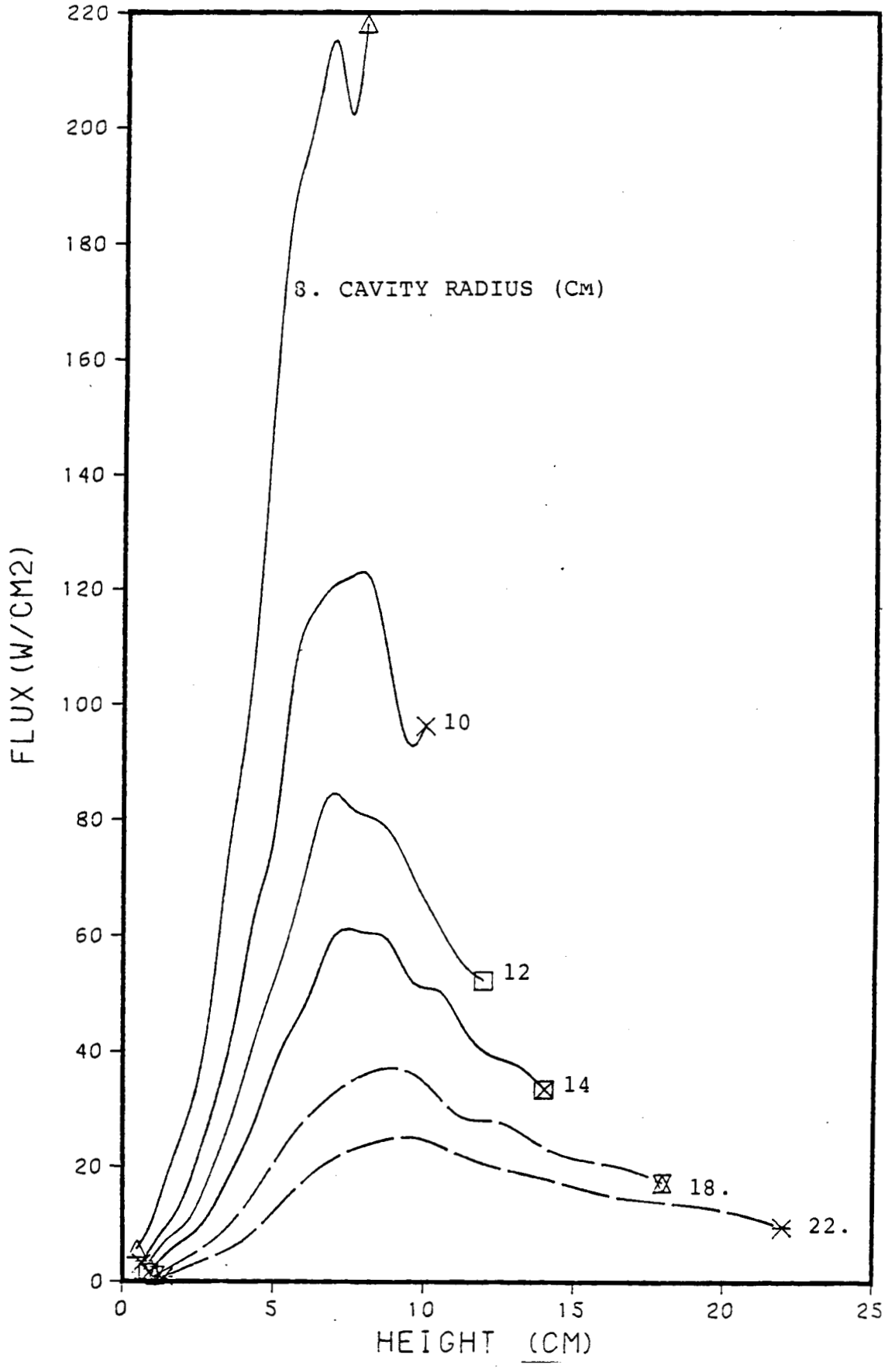

RECEIVER EVAPORATOR WICK OPTIONS CONSIDERED STUDY

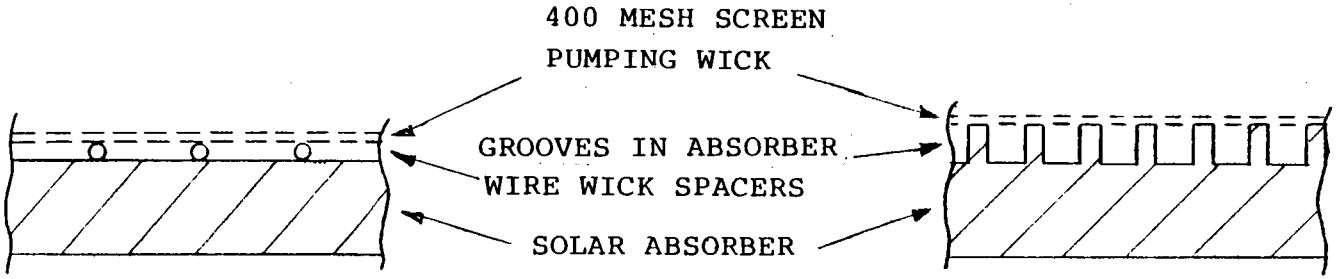

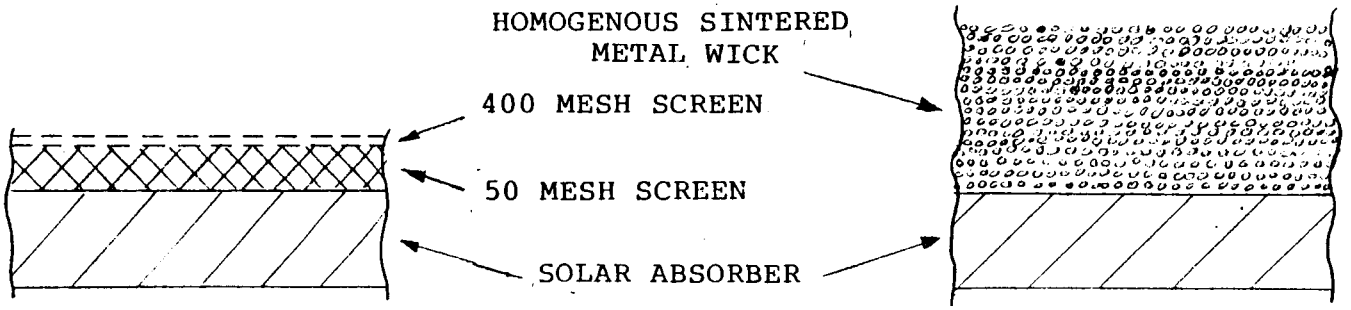

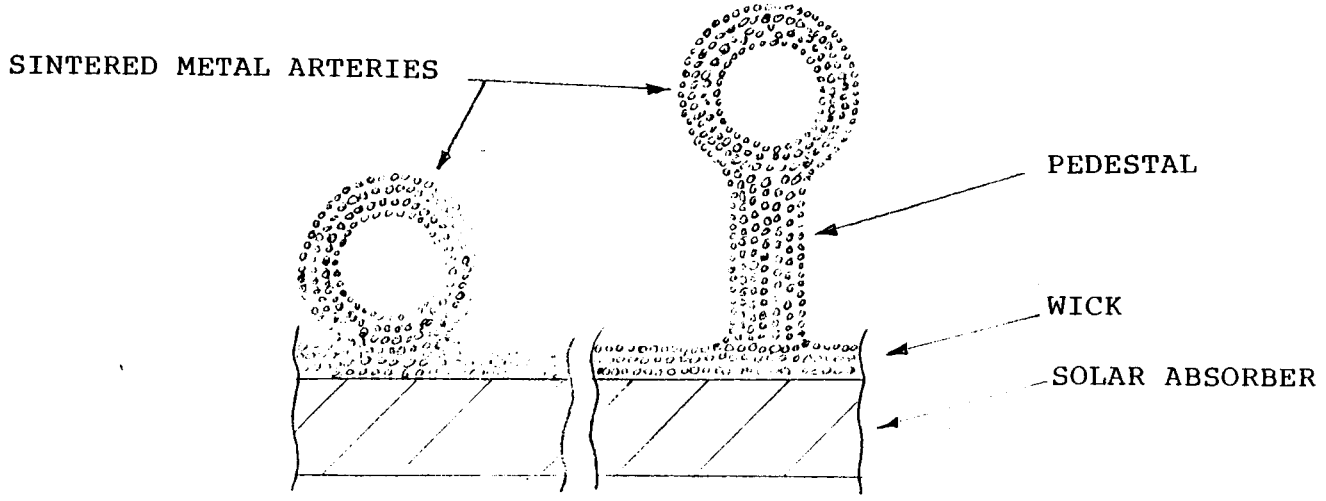

FORMED WIRE MESH

WIRE MESH CAN BE FORMED INTO CYLINDERS, CONES AND DOMES

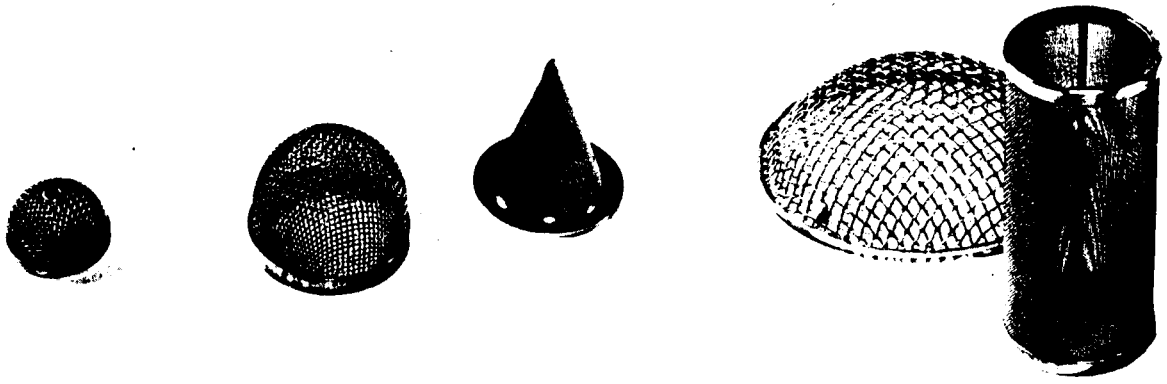

Energy Systems Department
FSG Engineering
SANDERS

Thermo-optical Wick Design Sample Study

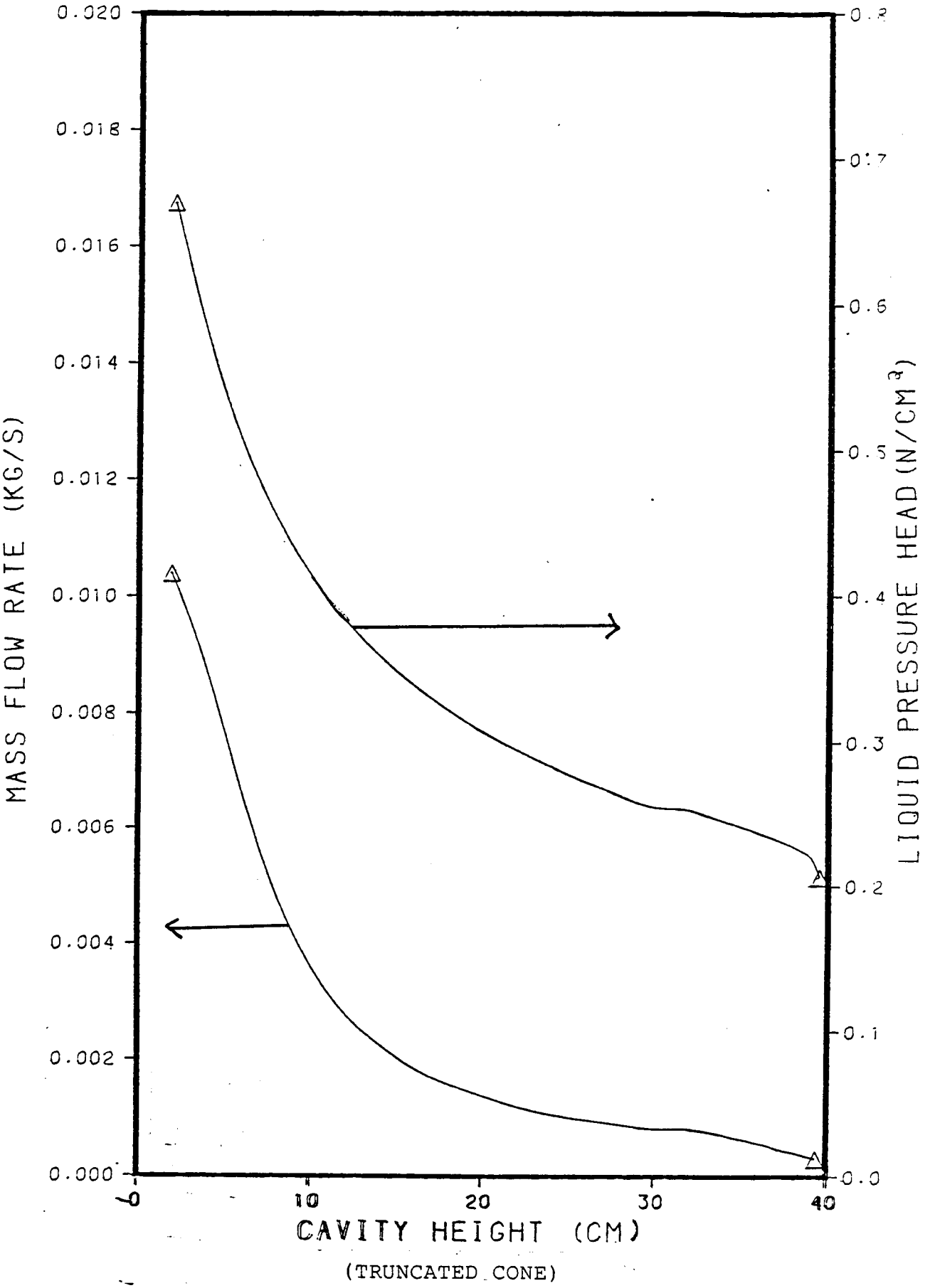

Investigation of Evaporator Superheat Characteristics

- For each of 4 cone and 6 hemisphere cases, the superheat in the liquid sodium has been calculated with the integrated wick/flux model
- Two contributions to superheat value
  - Thermal conduction through wick thickness
  - Pressure depression across miniscus interface
- Liquid feed arteries terminating at cavity base and evaporator apex were considered

Sanders
A Lockheed Company

CONCEPT FOR EVAPORATOR LIQUID FEED SYSTEM– SIMULTANEOUSLY FROM BASE AND APEX

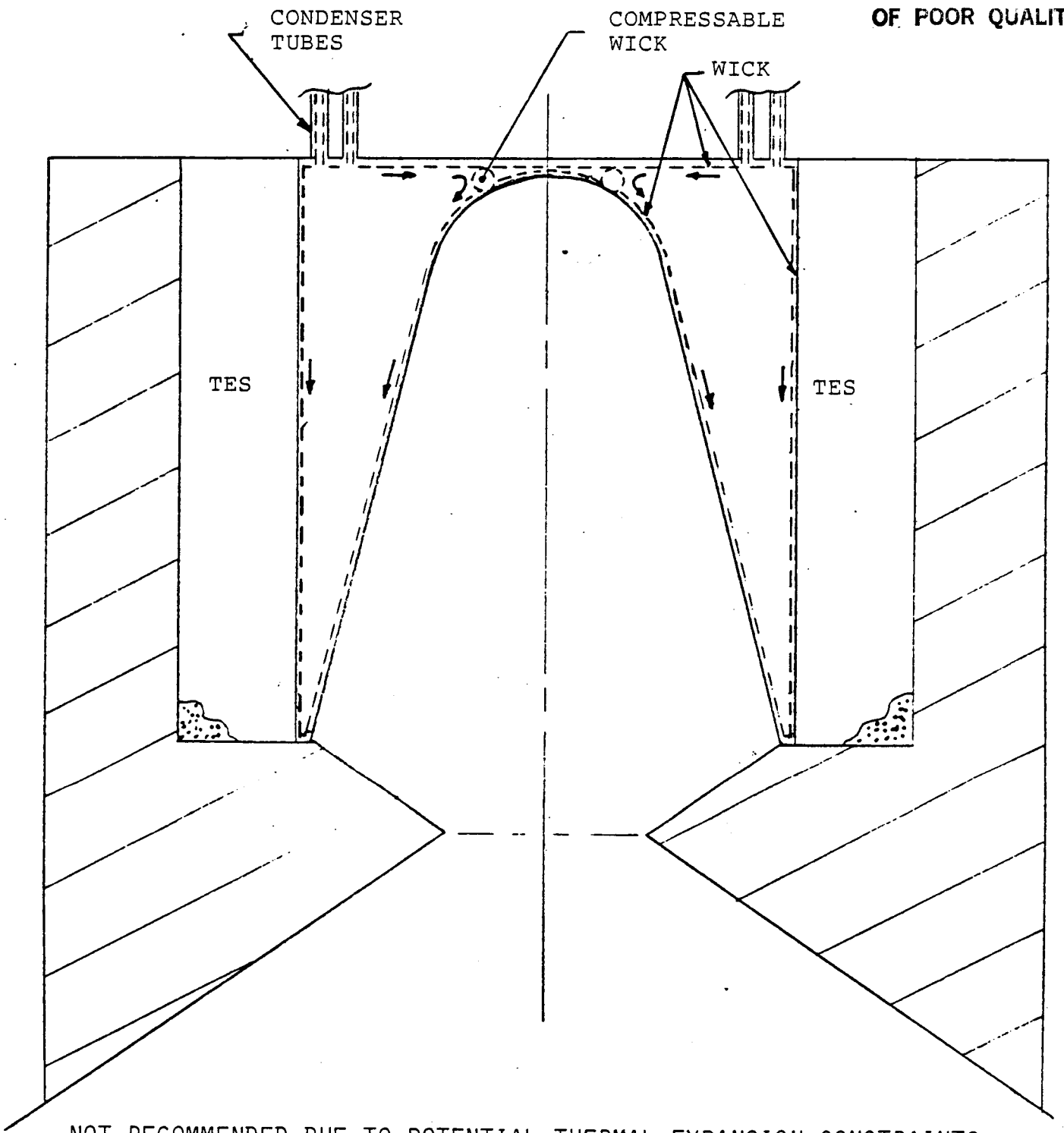

NOT RECOMMENDED DUE TO POTENTIAL THERMAL EXPANSION CONSTRAINTS, POOR LIQUID "COMMUNICATION" FROM HEAD, MORE COMPLEX EVAPORATOR WICK.

SUSPENDED ARTERIAL WICK SYSTEM TO ENHANCE LIQUID REPLENISHMENT OF EVAPORATOR/ABSORBER

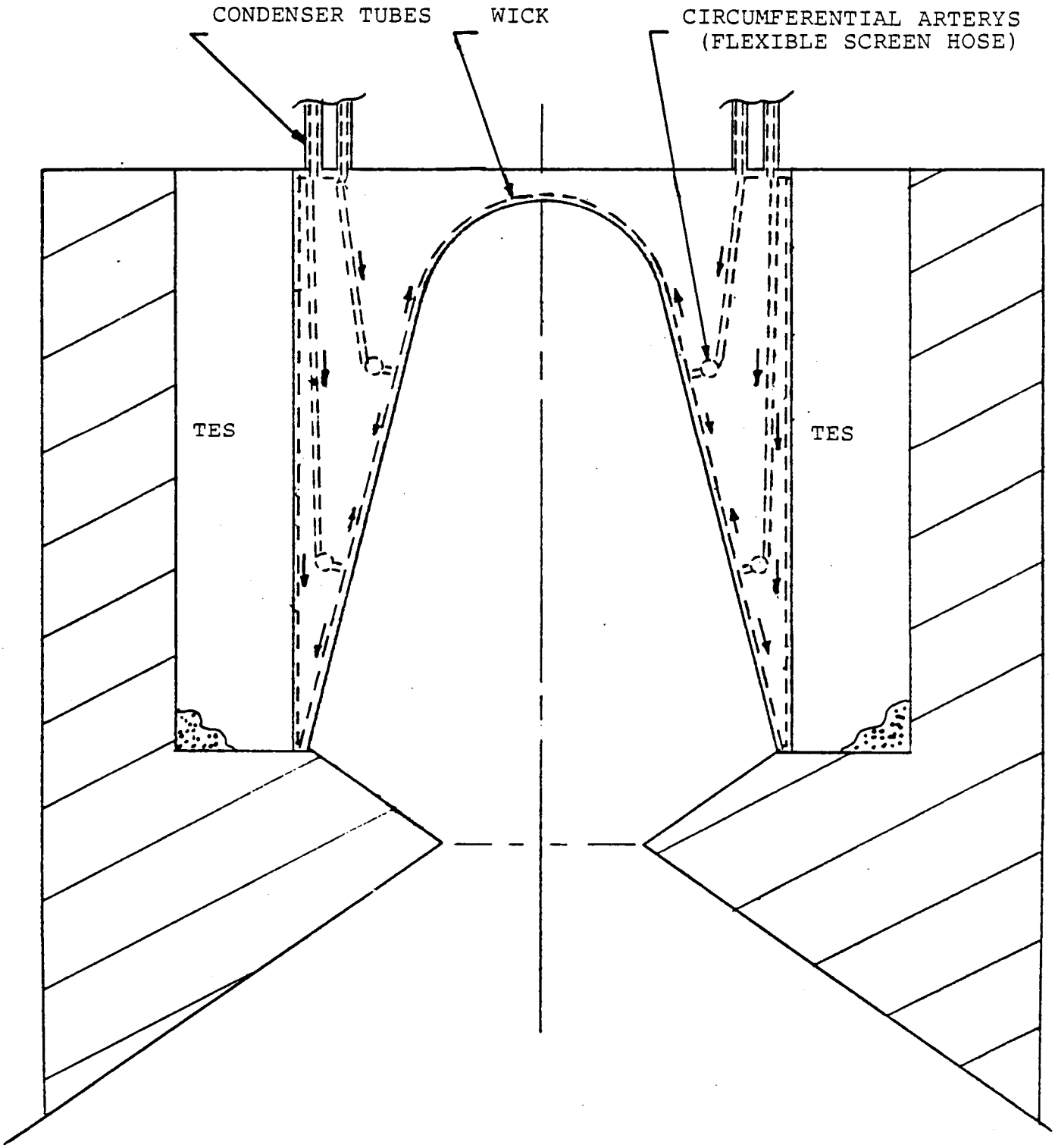

NOT RECOMMENDED DUE TO COMPLEXITY OF FABRICATION

LONGITUDINAL ARTERIAL WICK LIQUID FEED SYSTEM FOR EVAPORATOR/ABSORBER

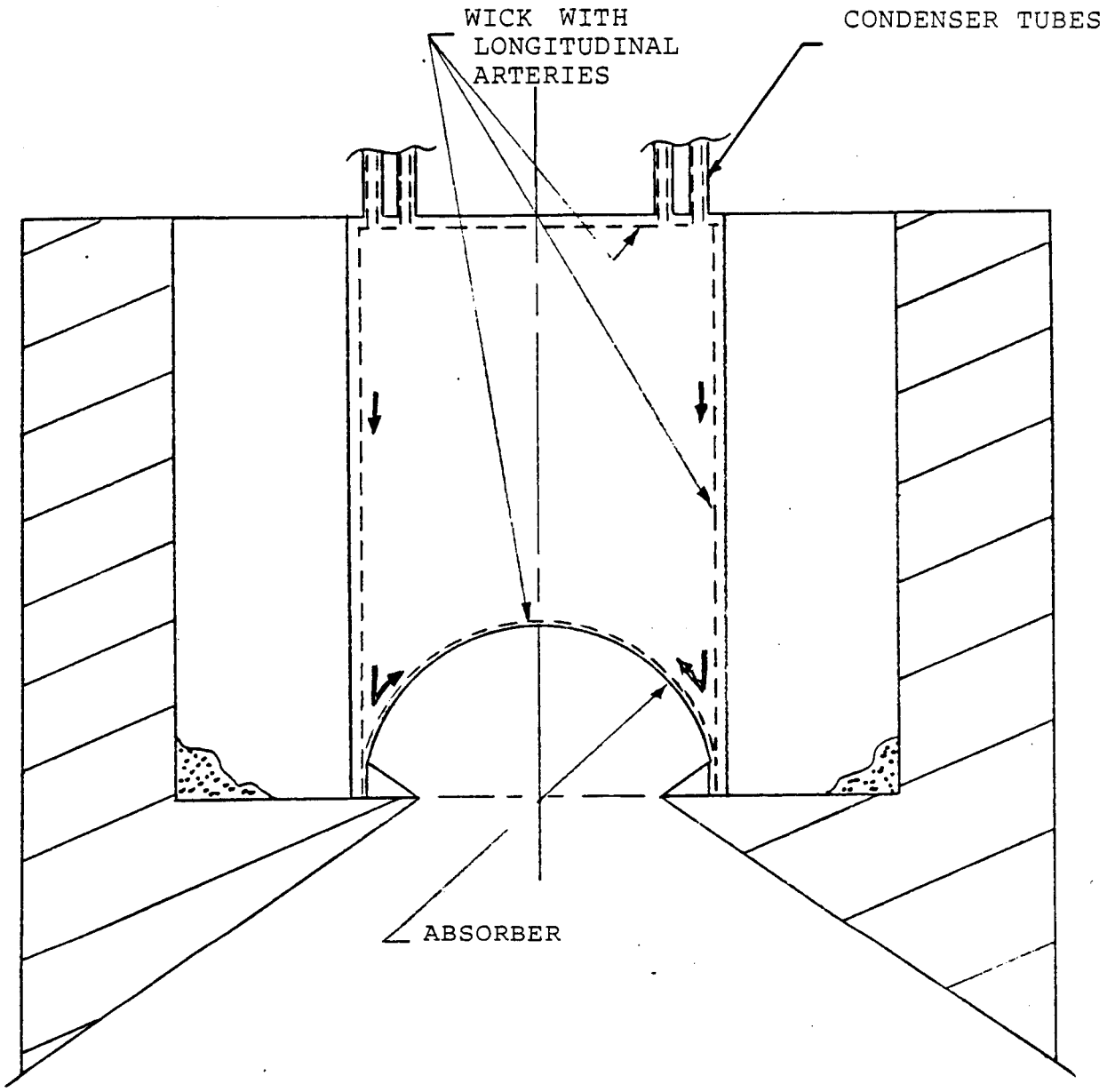

RECOMMENDED: SIMPLICITY WITH ACCEPTABLE LIQUID IMPEDANCE BETWEEN CONDENSER AND ABSORBER

SUPERHEAT AT PEAK FLUX ZONE OF TRUNCATED CONE CAVITY FOR VARIOUS WICK STRUCTURES

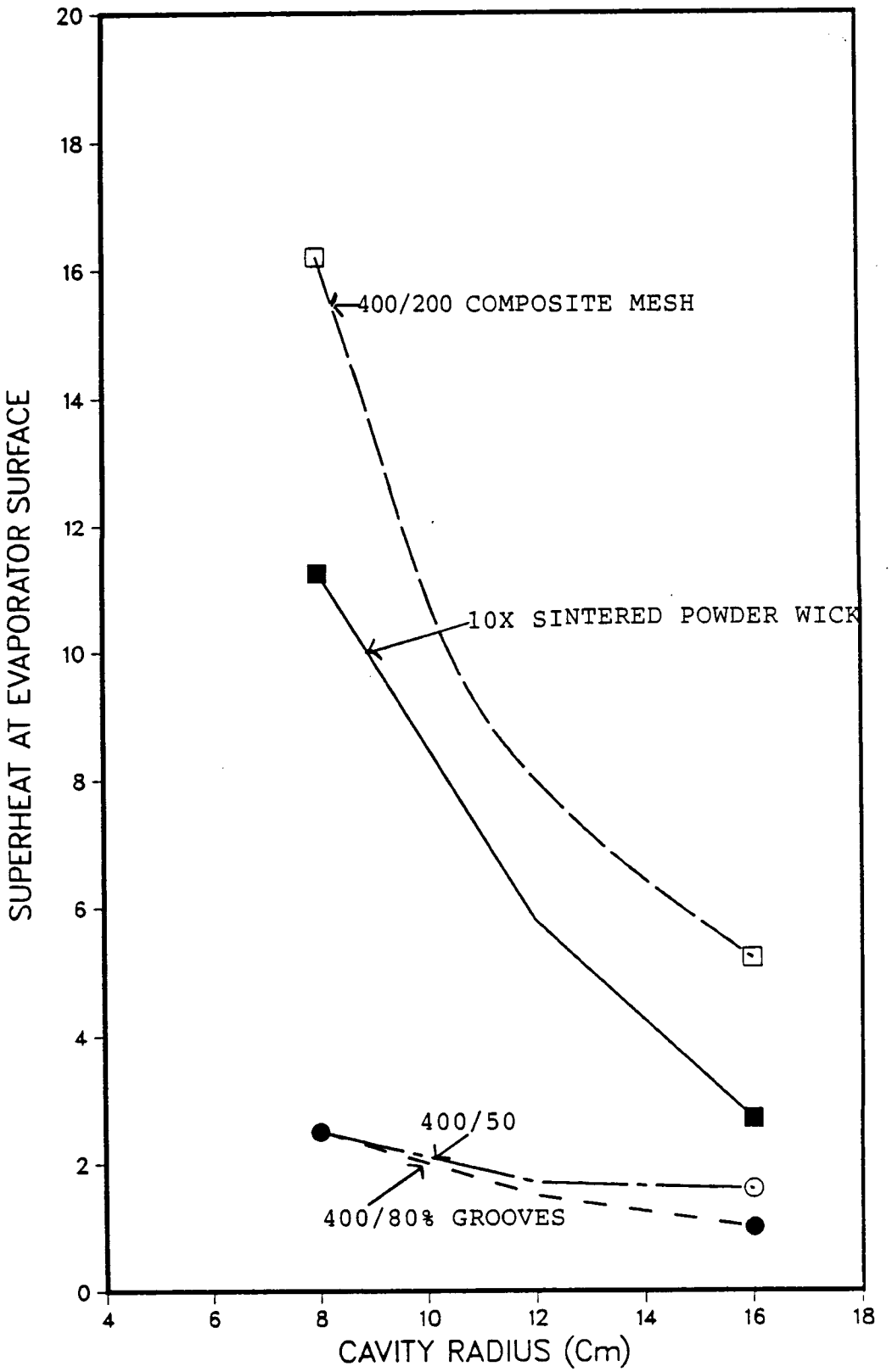

SUPERHEAT AT PEAK FLUX ZONE OF HEMISPHERIC CAVITY FOR VARIOUS WICK STRUCTURES

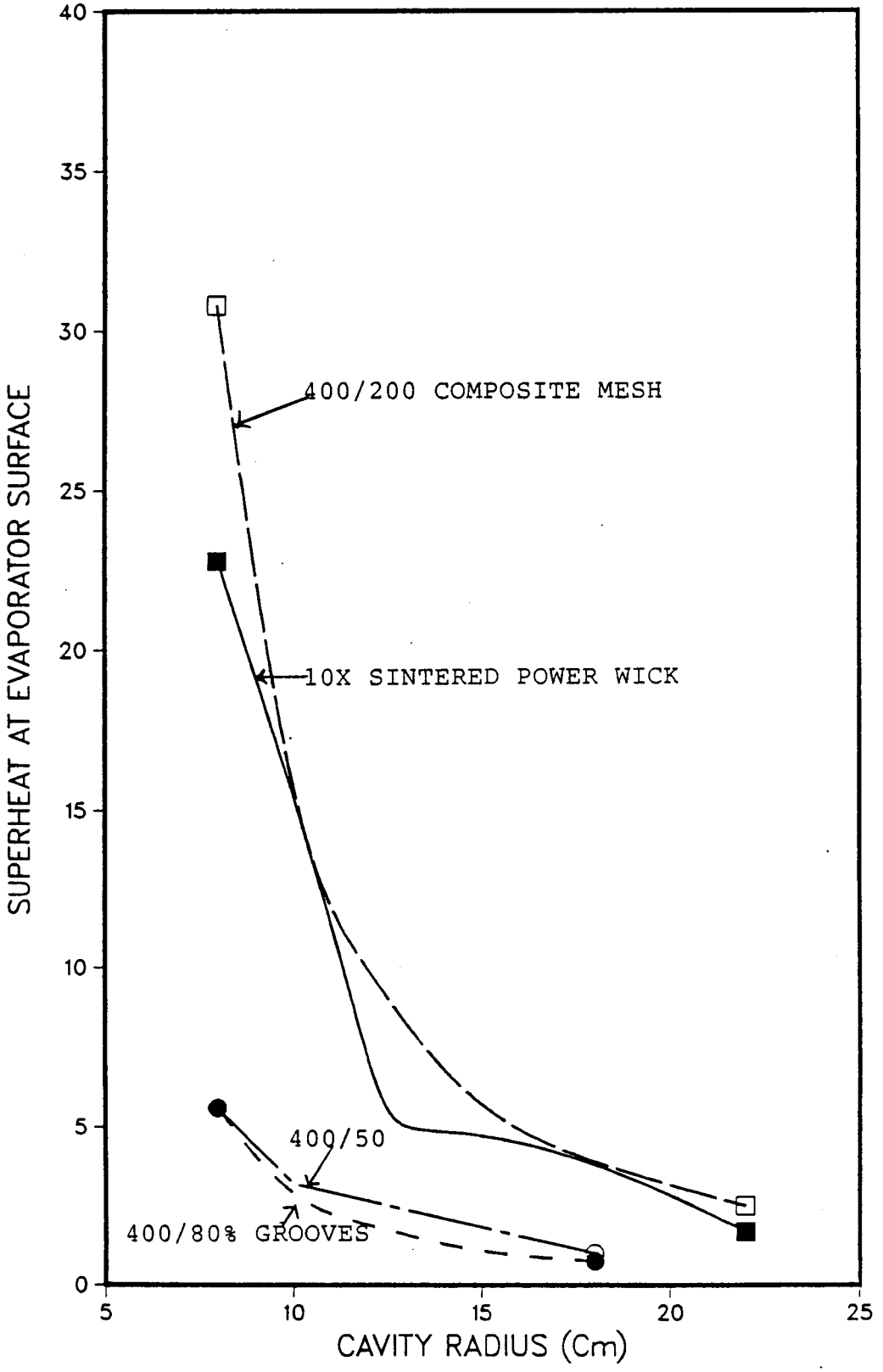

Superheat Investigation Conclusions

- Typical sintered powder metal wicks are not permeable enough to support full liquid mass flow (i.e., wick is much too thick)–need order of magnitude higher permeability
- Evaporator surface arteries are required to transport liquid on sintered powder evaporator
- The packing density of these evaporator arteries is somewhat arbitrary. The closer they are to one another, the thinner the distribution wick
- Pedestal arteries are recommended to minimize the potential bubble generation in artery
- A stress analysis of the pedestal arteries is in progress

Sanders
A Lockheed Company

ALTERNATE ABSORBER WICKING CONFIGURATIONS

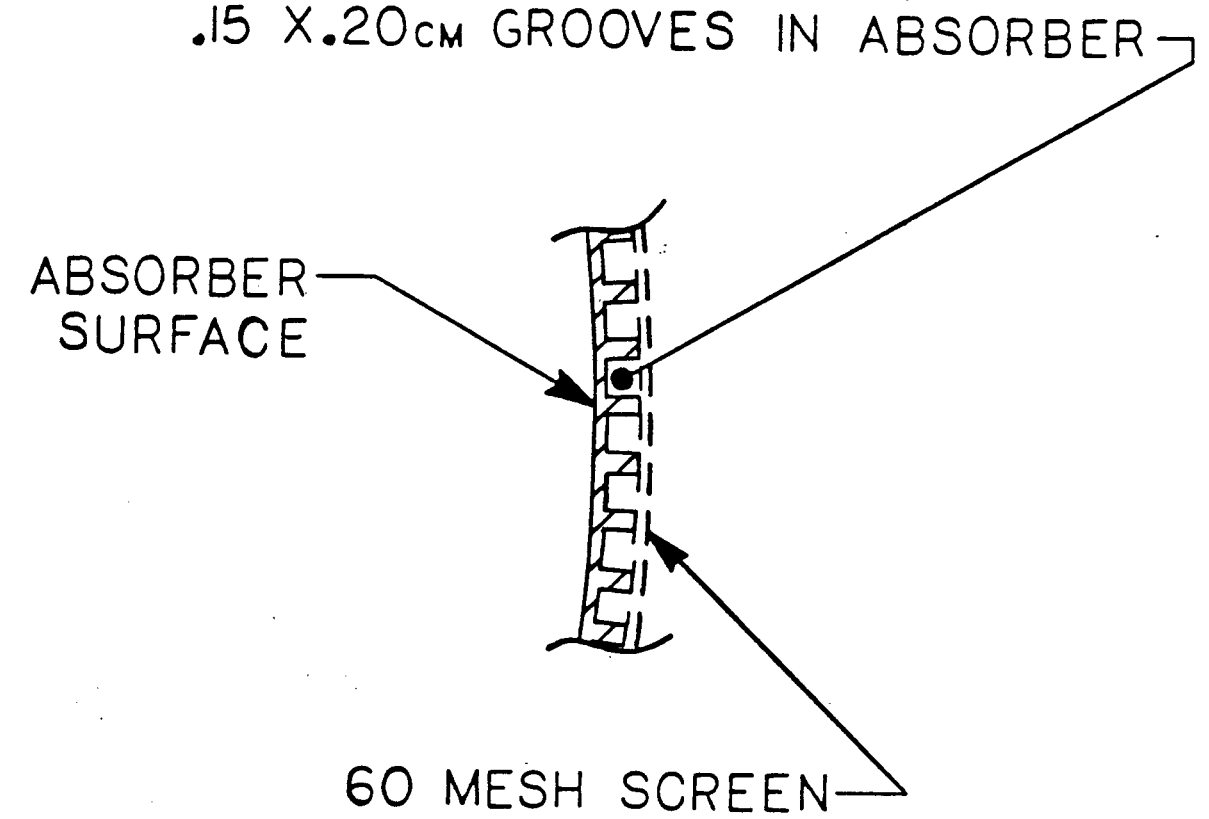

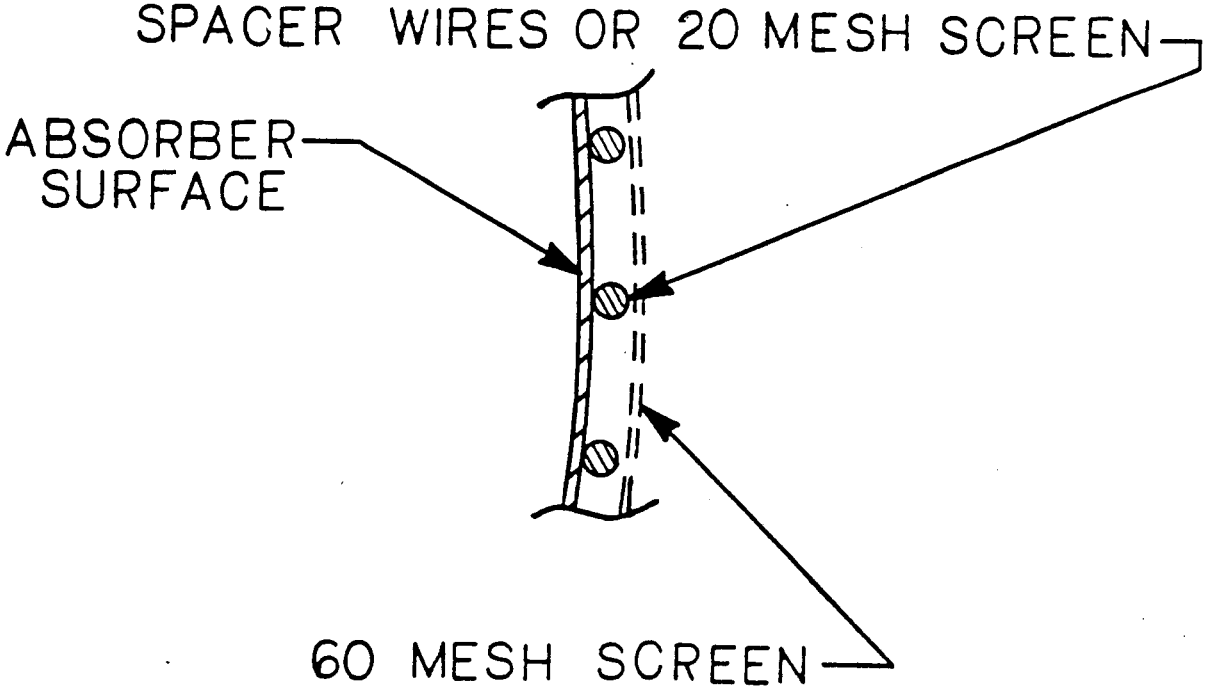

APPENDIX H

BRAYTON DAR THERMAL, STRESS AND MASS ANALYSIS

APPENDIX H

BRAYTON DAR THERMAL, STRESS AND MASS ANALYSIS

The RSU configuration analysis phase was performed in four steps. First, a hand calculation was performed to determine what absorber fin height would be necessary to contain a PCM volume of 30,000 cm^3. This volume of PCM is based on the required energy storage for the night cycle operation. This analysis was performed for receiver cavity sizes of 26cm, 34cm and 40cm. It was determined from first principles (analysis performed in Task III of this program) that these receiver sizes bracket the range of acceptable receiver configurations.

The computer analysis used the program SINDA. SINDA (Systems Improved Numerical Differencing Analyzer) is a general network heat transfer program capable of solving three dimensional steady state or transient thermal problems. A heat transfer model is constructed by dividing the heat exchanger surface into lumped areas or volumes called nodes (assumed to be isothermal). These nodes are then interconnected by thermal conductors using the appropriate conduction, convection, radiation or fluid flow equations. This data (called the model) is read by SINDA which then solves the simultaneous heat transfer network equations.

Second, a hand stress calculation was performed on the absorber fins to determine the required fin thickness. The fins were analyzed using flat plate solutions with pressure loads from Formulas for Stress and Strain by Roarke and Young. The solution for the required fin thickness was bounded by using a clamped plate solution for the lower bound and a simply supported plate solution for the upper bound.

Third, a hand calculation was performed to determine the weight of the corrugated finstock absorber. The absorber and PCM weights are a good percentage of the total receiver weight and therefore give a good indication of the relative weights of the different receiver configurations. The second and third steps were done iteratively in conjunction with fin design changes until it was felt that the design criteria listed in Table H1 were met. The resulting fin configuration was triangular in shape with a tension plate attached halfway up the fin. See Figure H3 for an example of this fin.

Fourth, a computer analysis was performed to determine the approximate temperature of the absorber with particular attention payed to the nonsubmerged tip. The tip, illustrated in Figure H3, is expected to experience the most adverse temperature and stress conditions. This assumption is based on the fact that it is directly irradiated with the peak solar flux while potentially emerging from the heat sinking reservoir of PCM. The design approach incorporated one dimensional, steady state analysis of the peak flux zone of the solar receiver (the peak flux zone used for this analysis matches well with the area of maximum absorber temperature obtained in Task III of this program, see Figure H4). Heat could be convected to the working fluid, radiated from the tip or conducted through the PCM to a boundary (the PCM in its solid state). This analysis was performed for different cavity sizes, fin thicknesses, bend radii and PCM conditions (solid - 70% of fin cavity volume or liquid - 100% of fin cavity volume, see Figure H5). A nodal layout of the fin model is shown in Figure H6. A sample input file for the SINDA program is shown in Appendix A. The results for Phase I are shown in Tables H3 thru H6.

TABLE H1

DESIGN REQUIREMENTS

- Receiver output power of 7kWe
- Creep repair limit for FS85 at 1150 ok and 88000 hrs (10 years)
- Safety factor of 1.5 for stress analysis
- Maximum temperature limit of 1090^{o}C
- Working fluid pressure of 35 psi
- Design for ease of fabrication
- Design for wicking of lithium fluoride
- Design for expansion and contraction of lithium fluoride
- Design for daytime/nighttime operation

TABLE 2

ASSUMPTIONS

- The volume of the PCM (lithium fluoride) required is 30,000cm^{3}
- The equations given in Formulas for Stress and Strain by Roake and Young for a v=.3 are applicable with a small amount of error FS85 which has a v=.38
- Clamped plate solution is for a plate clamped along both long edges and simply supported along the short edges
- Simply supported solution is for a plate simply supported on all sides
- The thermal conductivity of the lithium fluoride (liquid phase) is .01728 W/cm/^{o}K
- The thermal conductivity of the absorber (finstock made of FS85) is .649 W/cm/^{o}K
- Radiation from exposed tip only (Nodes 234-238)
- Receiver mass calculations include the following mass estimates: absorber, pressure shell, sapphire disk, inlet pipe, exit pipe, outer shell and cap. All other items were excluded.

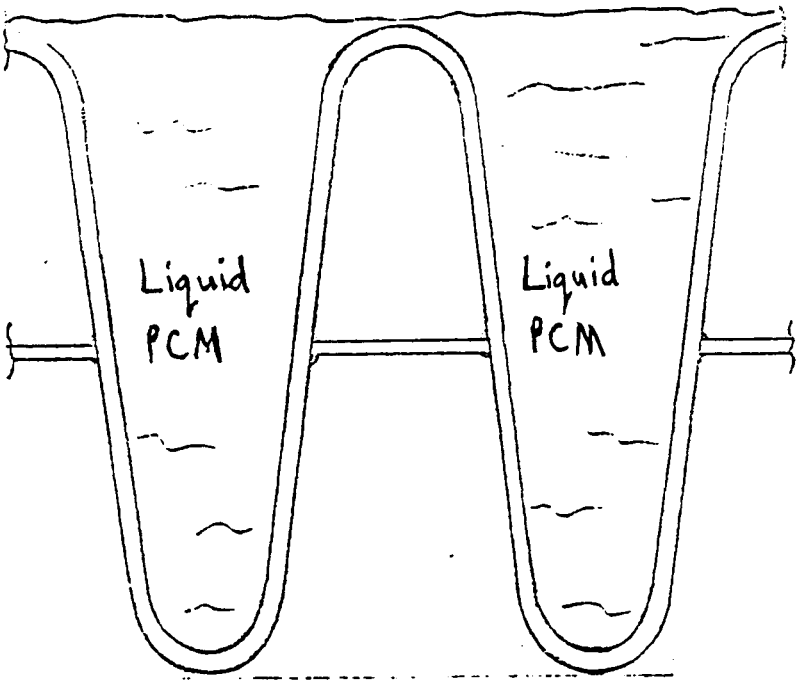

End of Day Period

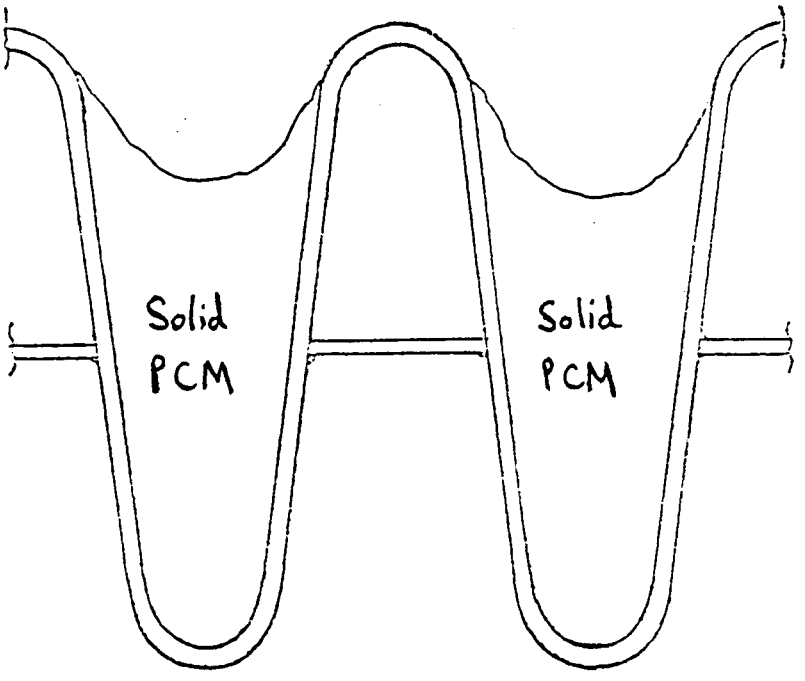

End of Night Period

BRAYTON CONCEPT II:

ABSORBER TEMPERATURE VS. LENGTH (DAY CYCLE)

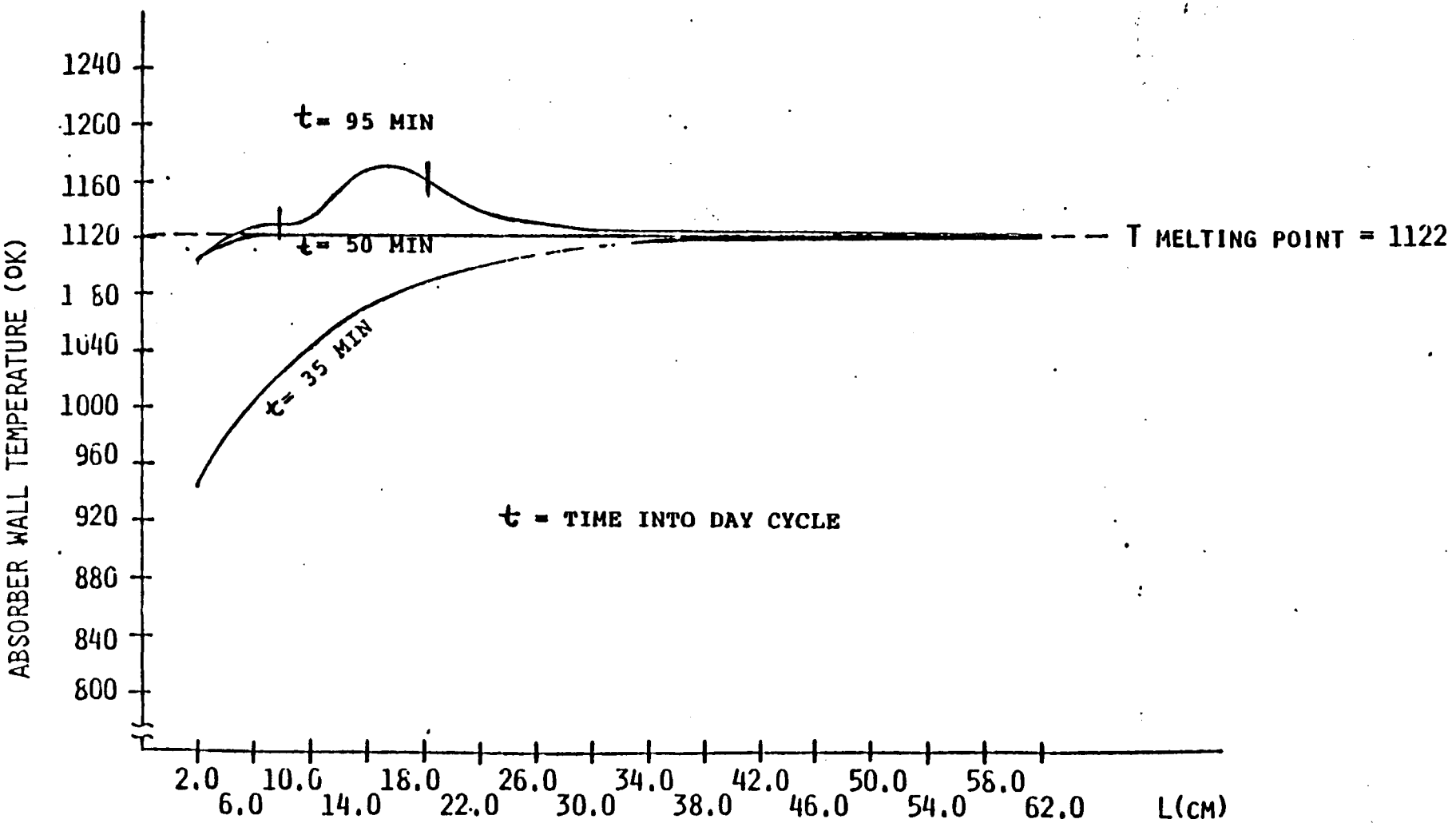

LENGTH ALONG GAS PASSAGES

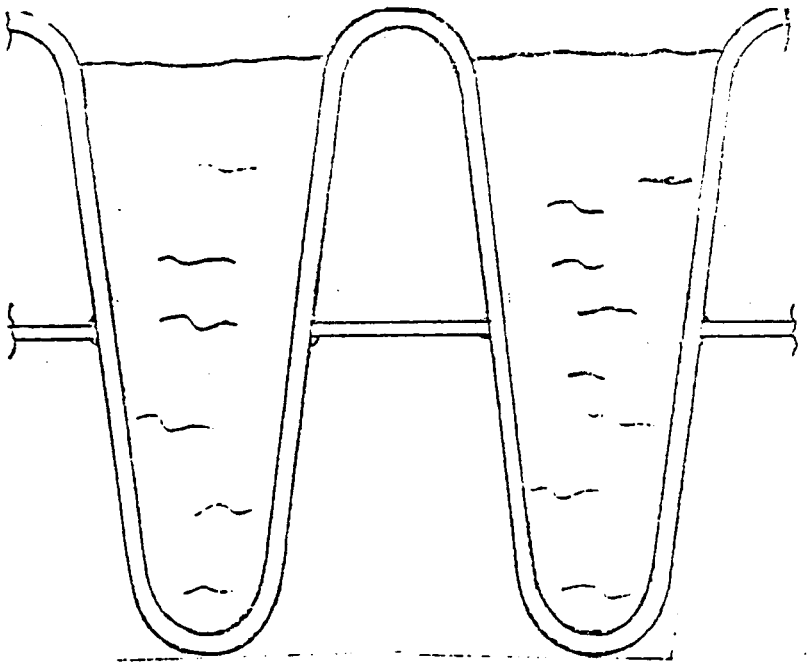

100% Fin Volume

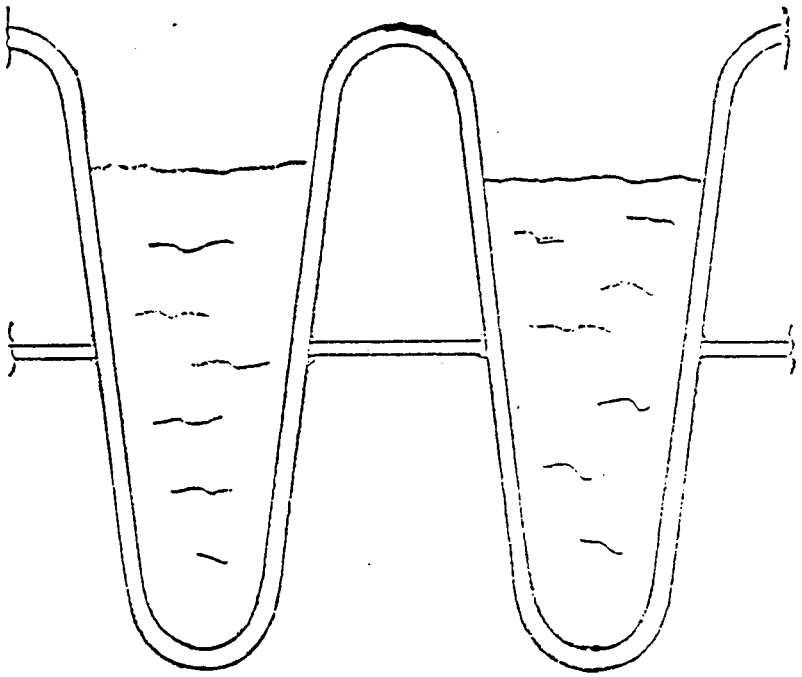

70% Fin Volume

Nodal Breakdown of Fin for Tip Temperature Model

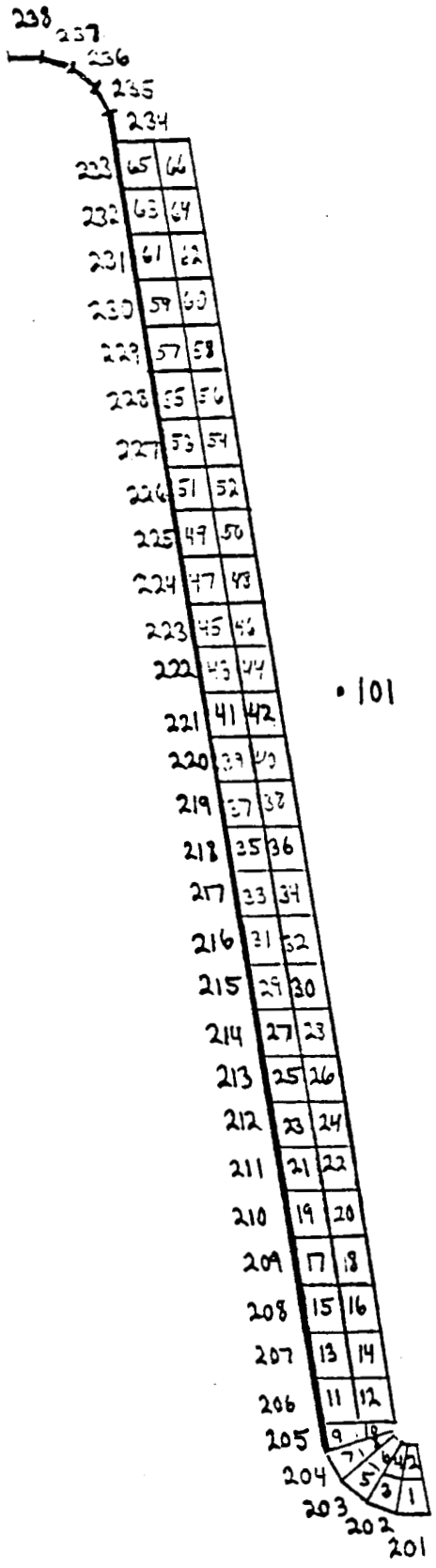

TABLE 3

RECEIVER PARAMETERS

Rcav(cm)	FH(cm)	Fin Thickness(cm)		Absorber Mass(kg)		Receiver Mass(kg)	
		Clamped	Simply Supported	Clamped	Simply Supported	Clamped	Simply Supported
26	5.75	.1022	.1252	56.6	69.2	149.1	161.7
34	5.0	.0910	.1114	59.1	72.4	152.4	165.7
40	4.5	.0827	.1013	60.3	73.8	154.1	167.6

TABLE 4

MODEL DESCRIPTION

Model	RCAV(cm)	FH(cm)	V-PCM(% of LP)	l(cm)	t(cm)	R	ε	View Factor	Flux(W/cm2) Tip	Flux(W/cm2) Fin	FD(fins/cm)	h(W/cm2°K)
TIP_1	34	5.0	70	5.42	.0910	2t	---	---	11.03	11.03	.425	.00562
TIP_2	34	5.0	100	5.42	.0910	2t	---	---	11.03	11.03	.425	.00562
TIP_3	34	5.0	70	5.42	.0910	2t	.3	1.00	11.03	11.03	.425	.00562
TIP_4	34	5.0	100	5.42	.0910	2t	.3	1.00	11.03	11.03	.425	.00562
TIP_5	34	5.0	70	10.84	.0910	2t	.3	1.00	11.03	11.03	.425	.00522
TIP_6	34	5.0	70	10.84	.0910	2t	.3	1.00	3.31	11.03	.425	.00522
TIP_7	34	5.0	100	10.84	.0910	2t	.3	1.00	11.03	11.03	.425	.00552
TIP_8	34	5.0	100	10.84	.0910	2t	.3	1.00	3.31	11.03	.425	.00552
TIP_9	34	5.0	100	10.84	.0910	3t	.3	1.00	11.03	11.03	.425	.00522
TIP_10	26	5.75	100	10.84	.1022	2t	.3	1.00	15.68	15.68	.404	.00537
TIP_11	40	4.5	100	10.84	.0827	2t	.3	1.00	8.83	8.83	.438	.00521

TABLE 5

MODEL TEMPERATURES

Model	Boundary Temperatures(^{0}K)		Gas Temperatures(^{0}K)		Absorber Temperatures(^{0}K)			
	Radiation	PCM	Inlet	Outlet	Node 238	Node 237	Node 227	Node 220
TIP_1	1122.	1121.	875.	942.	1245.	1245.	1194.	1171.
TIP_2	1122.	1121.	875.	939.	1218.	1217.	1176.	1162.
TIP_3	1122.	1121.	875.	941.	1228.	1227.	1185.	1167.
TIP_4	1122.	1121.	875.	939.	1207.	1206.	1171.	1160.
TIP_5	1122.	1121.	875.	984.	1248.	1248.	1204.	1185.
TIP_6	1122.	1121.	875.	969.	1170.	1170.	1160.	1152.
TIP_7	1122.	1121.	875.	980.	1222.	1221.	1186.	1176.
TIP_8	1122.	1121.	875.	967.	1159.	1159.	1152.	1148.
TIP_9	1122.	1121.	875.	994.	1258.	1257.	1203.	1191.
TIP_10	1122.	1121.	875.	980.	1270.	1269.	1213.	1197.
TIP_11	1122.	1121.	875.	980.	1199.	1198.	1173.	1165.

TABLE 6

MODEL ENERGY DISTRIBUTION

Model	Energy Absorbed by the Model(W)	Energy Convected to Gas(W)	Percentage of Absorbed Energy Convected to Gas(%)
TIP_1	70.3	46.2	65.8
TIP_2	70.3	44.2	62.8
TIP_3	67.7	45.5	67.3
TIP_4	68.3	44.2	64.7
TIP_5	134.1	75.2	56.1
TIP_6	91.7	64.9	70.8
TIP_7	135.7	72.5	53.4
TIP_8	92.3	63.5	68.8
TIP_9	163.6	82.1	50.2
TIP_10	202.	97.9	48.6
TIP_11	105.9	61.0	57.6

TRANSIENT THERMAL ANALYSIS

Transient Thermal Analysis Illustrates Advantages of Direct Absorption Concept II

Solar absorption tailoring alleviates dependency on low solid PCM conductivity during solar charge

- No voids (micro as in felt mesh containment approaches or macro as in IOC solar dynamic designs)
- Performs as high effective conductivity by melting uniformly throughout volume
- Some direct absorption on heat exchanger wall reduces droop around morning

Sanders
A Lockheed Company

SINDA TRANSIENT THERMAL ANALYSIS

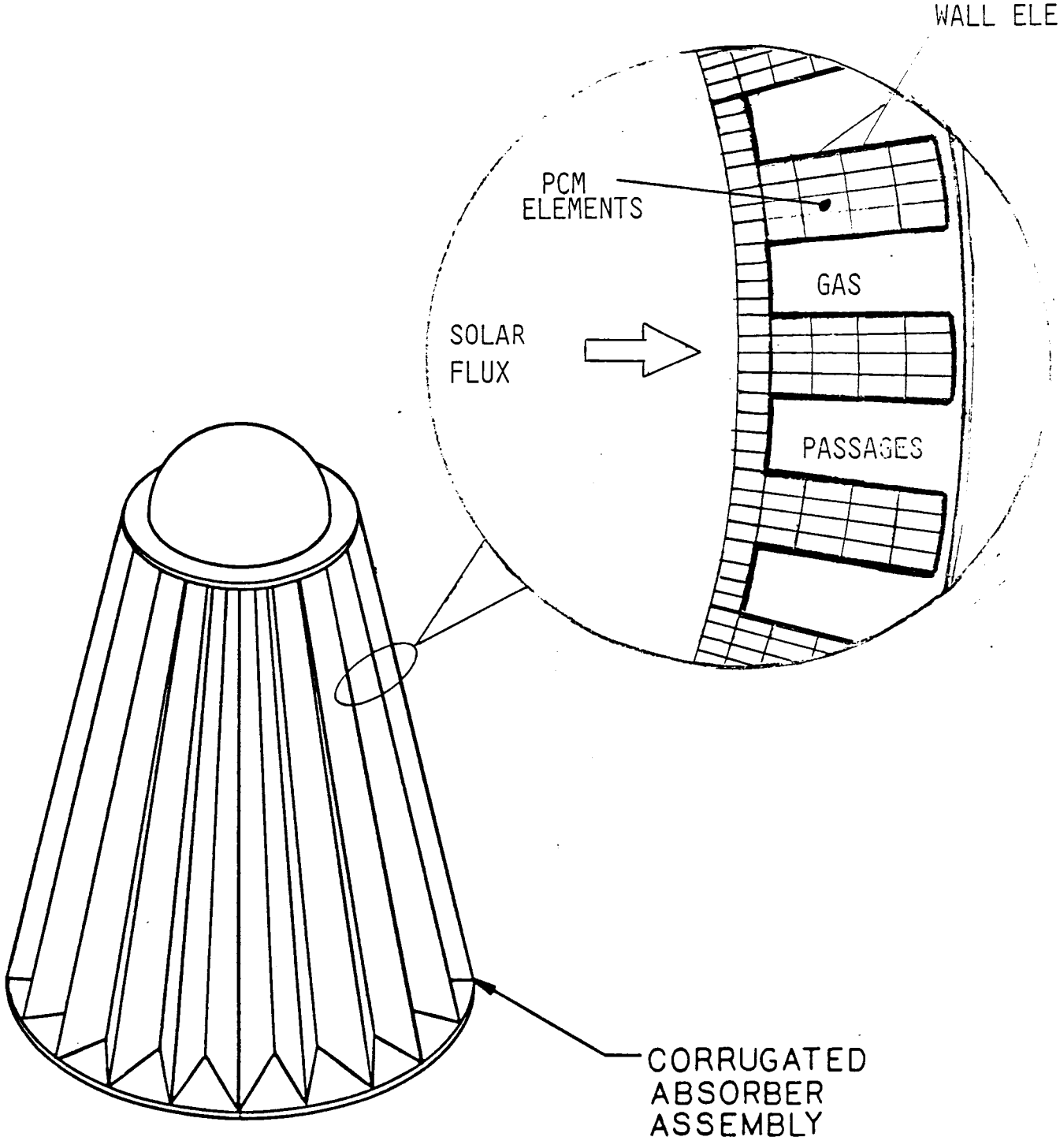

BRAYTON CONCEPT II:

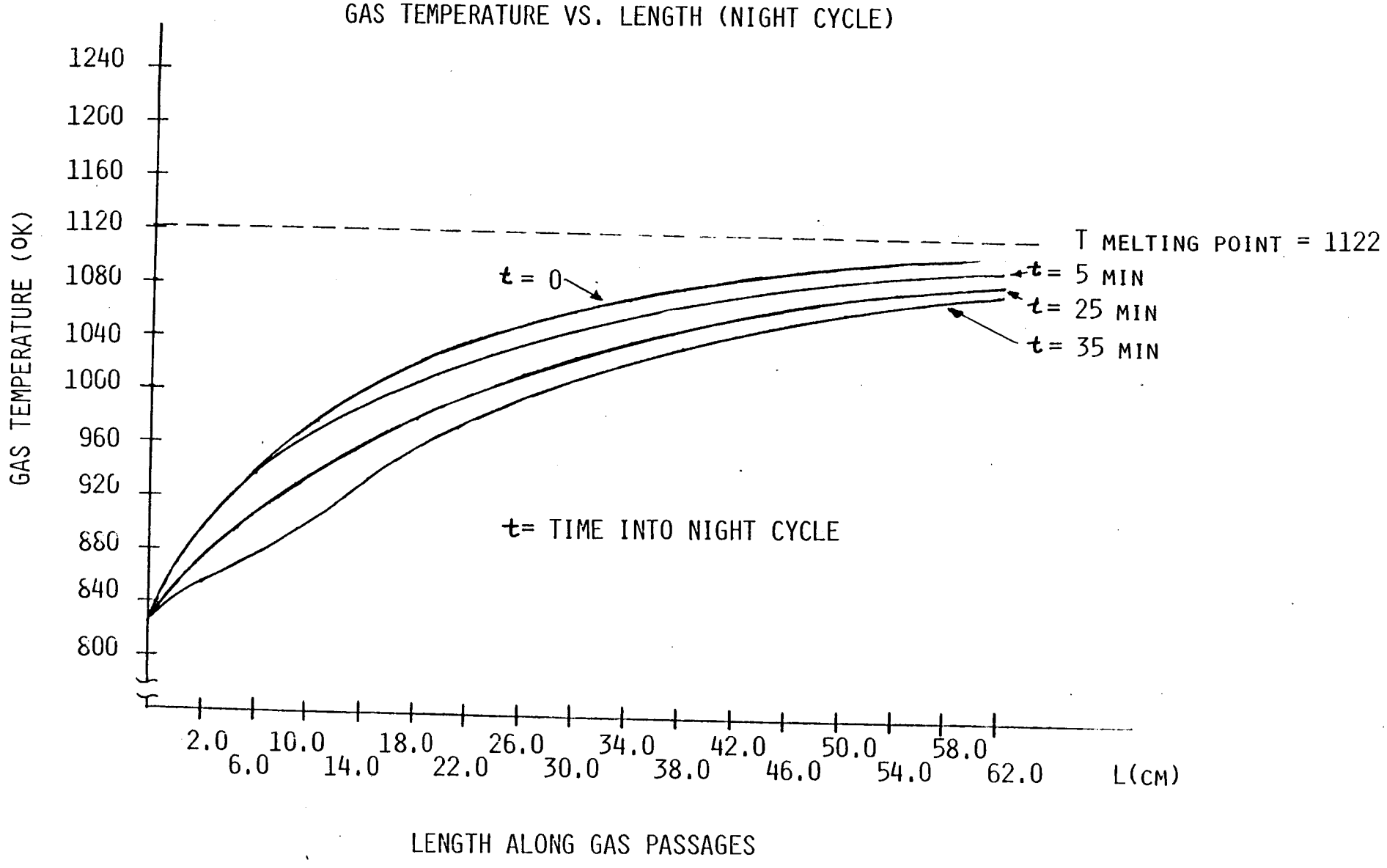

BRAYTON CONCEPT II:

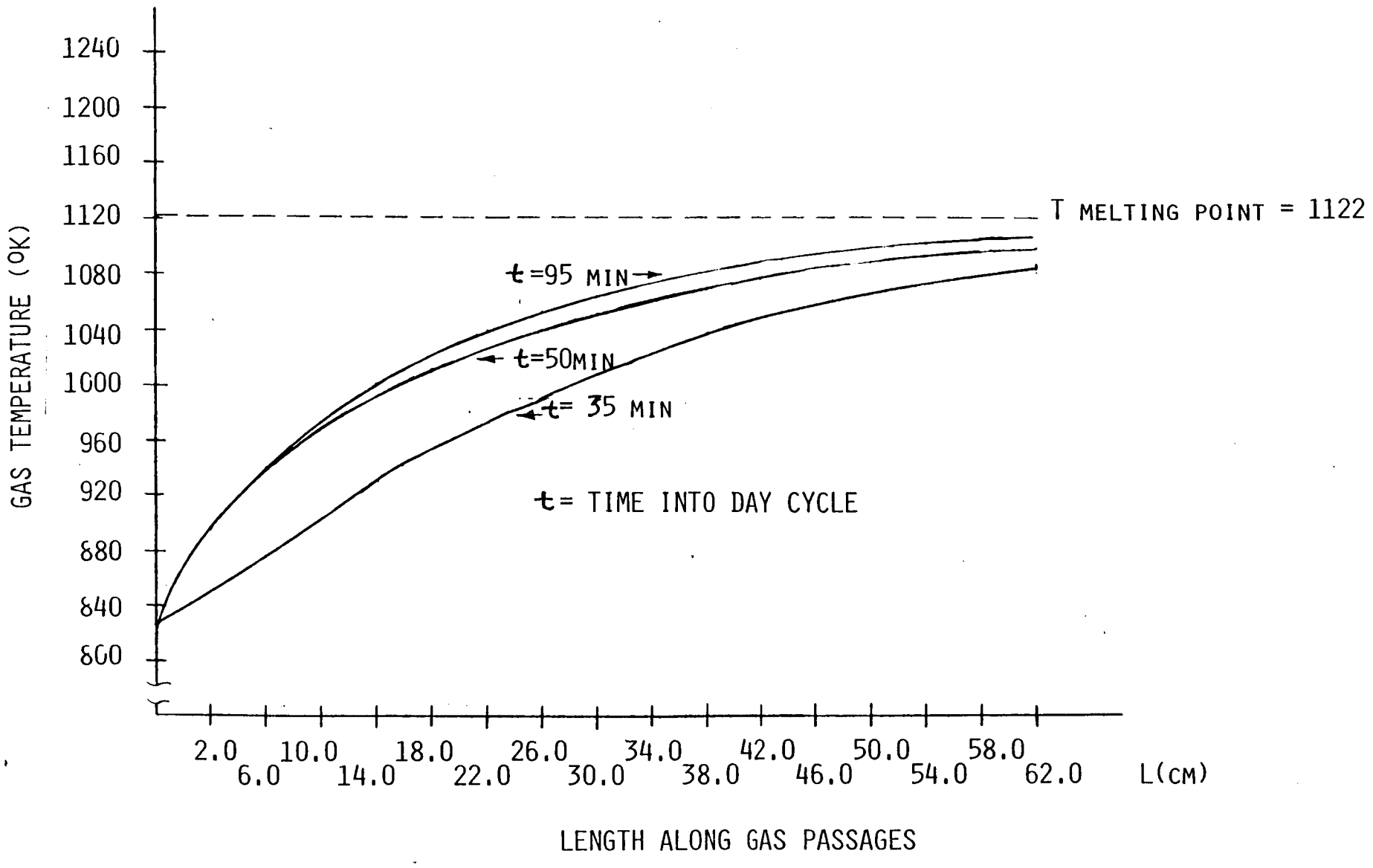

BRAYTON CONCEPT II:

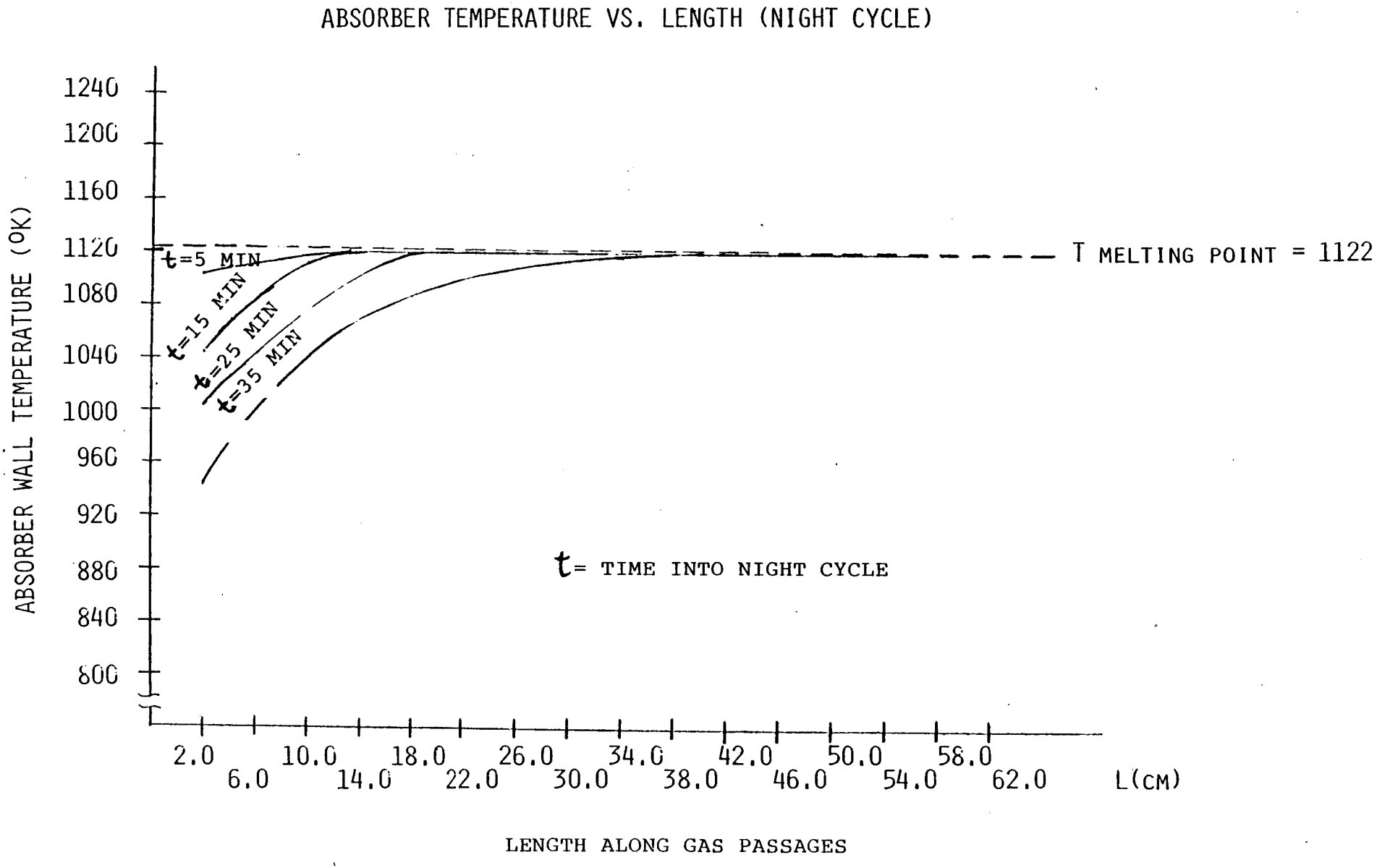

BRAYTON CONCEPT II:

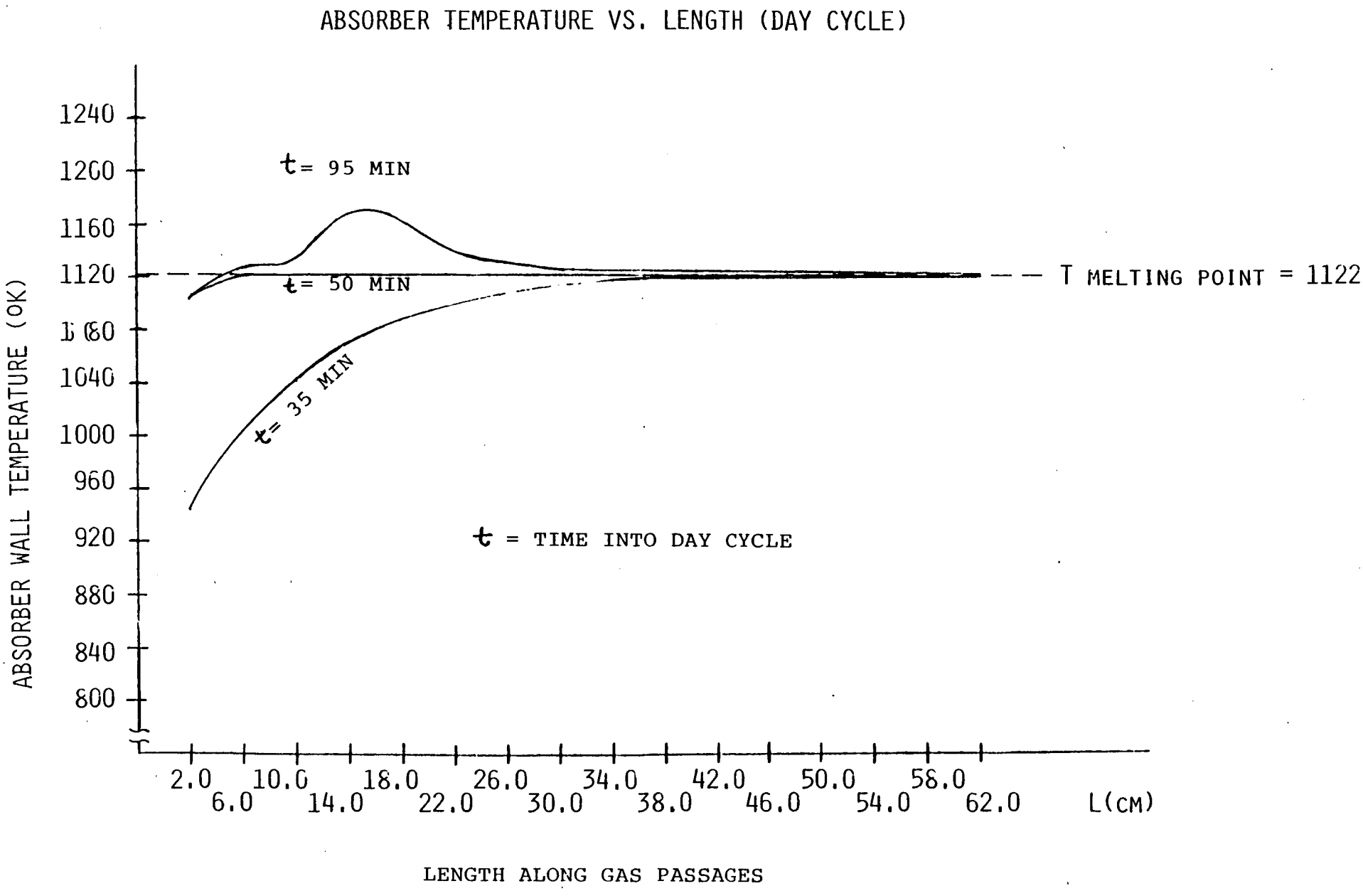

Steady State Thermal Loss from Exterior RSU Boundaries

- Geometry variation study using refractory batt type insulation has been conducted
- Model customized to allow for implementation of multifoil insulation when characteristics become available

Sanders
A Lockheed Company

SINDA FINITE DIFFERENCE NODE EXAMPLE FOR BRAYTON

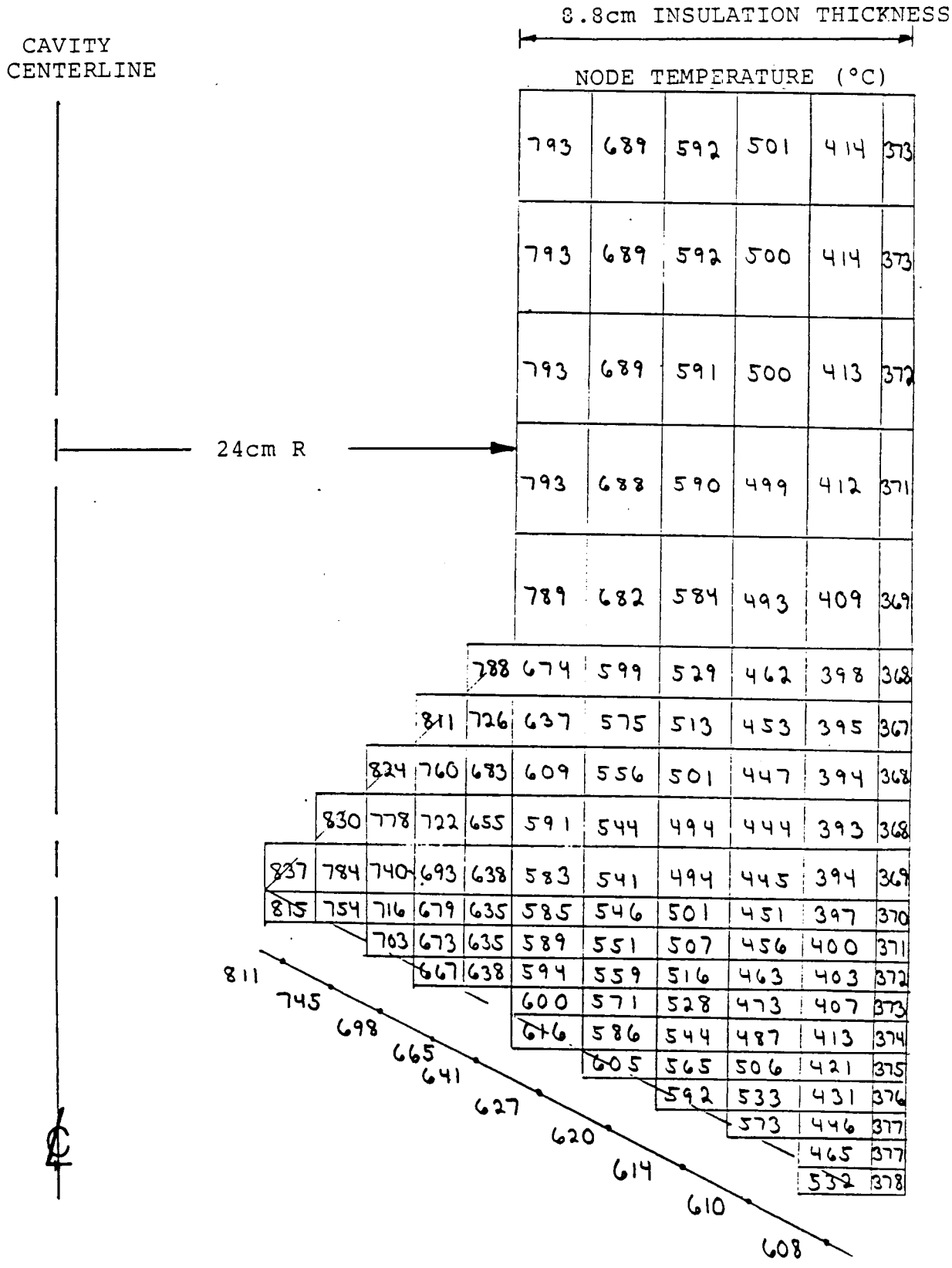

Exterior Envelope Heat Loss Parametric Study

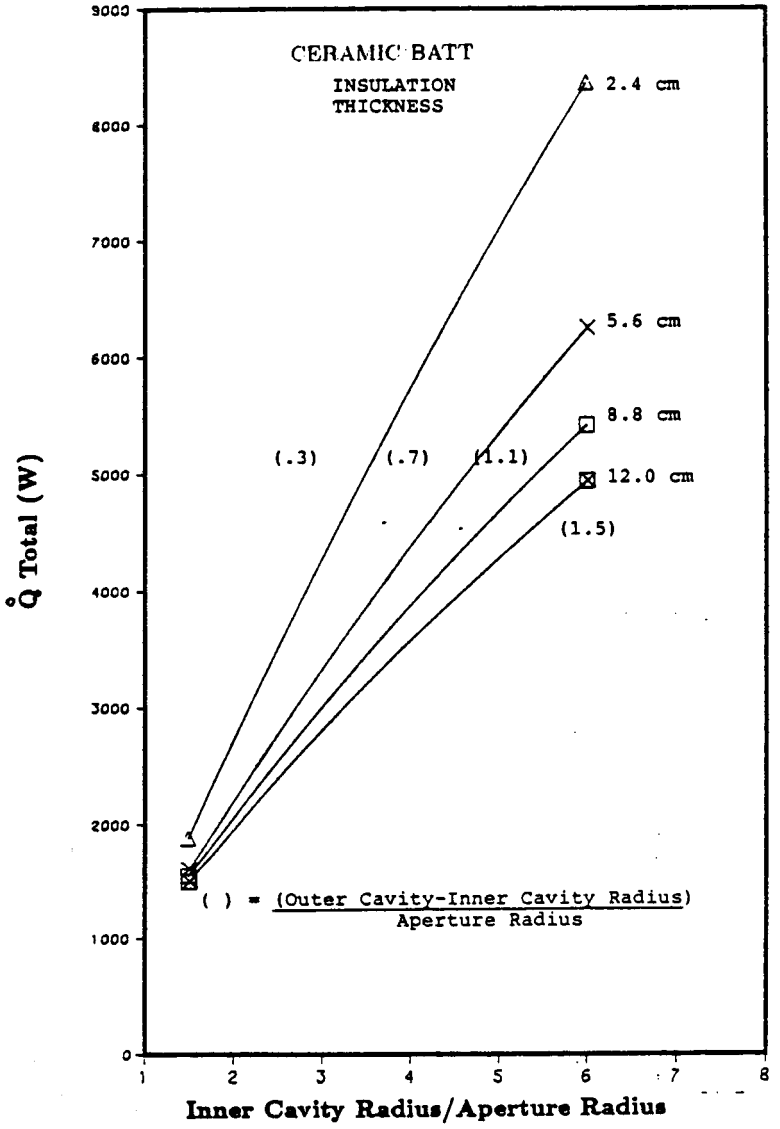

Results illustrate relatively thick layers of batt insulation relative to potential of multifoil types

Sanders
A Lockheed Company